Load Transfer and Creep Behavior of Pile Foundations in Frozen Soils

by

Abdulghader Abdulrahman

A thesis submitted to the Faculty of Graduate and Postdoctoral Affairs in partial fulfillment of the requirements for the degree of

Doctorate of philosophy

in

Civil Engineering

Carleton University

Ottawa, Ontario

©2019, Abdulghader Abdulrahman

Abstract

This study investigates the load transfer mechanism and creep behavior of concrete piles, open-ended steel pipe piles, helical piles, and grouted shaft helical piles installed in frozen ice-rich and ice-poor soils in field. Load transfer of these piles under unfrozen condition was also assessed and compared to those obtained in frozen conditions. The evolution of unfrozen water content and the associated thermally induced normal stress and adfreez strength of the pile-soil interfaces following to soil freeze-back after pile driving was also studied using laboratory experiments. The effects of strain rate on load carrying capacity of model steel piles in ice-poor and ice-rich soils were also investigated.

Laboratory results showed that the roughness factor “m” may not be considered constant for a given pile material but rather changed as a function of ground temperature. The temperature-dependency of the roughness factor was more pronounced for piles installed in ice-rich frozen soils. In addition, the roughness factor was significantly different for a given pile installed in different soil types. A frictional factor "n" analogous to the roughness factor "m" was introduced to correlate the frictional resistance of frozen soil to the frictional resistance of pile-soil interface. The freezing induced normal stress due to soil freeze-back around the piles was significant in ice-rich soils and minimal in ice-poor soils. The load carrying capacity of pile foundations in frozen ground was influenced significantly by the loading rate, showing lower values under slower loading conditions.

Modified forms of previously proposed theoretical models for predicting load carrying capacity and creep behavior of piles in frozen ground were introduced. The predicted capacity using the modified forms agreed well with the field observations of pile performance reported in

this study. The creep behavior of the test piles in frozen soils was dependent on the applied stress and frozen ground temperature. The pile creep rates increased when the frozen ground became warmer even under constant creep loading condition. The pile creep rates measured in the current study for conventional smooth-shafted piles compared well with the predicted creep rates from previously published pile creep models. An innovative design approach along with an improved graphical solution are provided in this study for predicting load carrying capacity and creep rate of helical piles in frozen ground at different exposure temperatures.

Dedicated to my dear parents, my lovely wife, my siblings, and my kids

Acknowledgements

I would like to express my respect and gratitude to my supervisor, Professor Mohammad Rayhani. His dedication, understanding, patience, and sympathy added considerably to my personal and professional attitudes. I appreciate his vast knowledge and skills in many areas (e.g., vision, ethics, interaction with students), and his outstanding inputs to this research and thesis. I would like to thank my thesis examination committee, Professor Guy Doré, Professor Sai Vanapalli, Professor Dariush Motazedian and Professor Paul Simms for taking the time reviewing and examining this dissertation. Moreover, I would like to thank all of my friends for their understanding and support. Special thanks go to our Civil Engineering laboratory technicians including Stanley Conley, Jason Arnott, Pierre Trudel, and Kenneth Akhiwumy whom their laboratory support and inputs to this research cannot be denied. Last, but not least, I would like to thank my wife "Hanan" for her understanding, love, and support during my PhD journey. Her dedication and encouragement were in the end what made this research work possible. My Father "Abdulrahman" and my mother "Amna" receive my deepest gratitude and love for their dedication and prayers.

Table of Contents

List of Tables

List of Illustrations

CHAPTER 1: INTRODUCTION

1.1 Overview

Permafrost, or perennially frozen ground, is the ground that remains in frozen condition (i.e., exists at or below 0°C) for two or more consecutive years. Permafrost is considered a critical component of the cryosphere and Arctic region influencing its ecosystems and hydrological systems and causing challenges for infrastructure development. Permafrost regions extend over 24% of the terrestrial surface of the Northern Hemisphere. Permafrost is often overlaid by a seasonally frozen ground known as active layer. The permafrost temperature and active layer thickness are two key indicators of thermal stability of permafrost conditions. Permafrost temperature at depth may vary within very narrow range and can indicate the long-term changes of its thermal regime. Temperature in active layer, in contrast, may fluctuate significantly due to variation in annual surface temperature. However, many observational field studies (e.g., Jorgenson et al. 2006; Frey and McClelland 2009) reported an unusual increase in the extent of permafrost degradation in permafrost regions including northern Alaska, northwestern Canada, northeastern Canada, Nordic region, and Siberia. This degradation was associated with the unusual warm temperatures witnessed since 1989.

Permafrost temperature in northwestern Canada in the central Mackenzie Valley has experienced overall warming temperature since the mid-1980s at Norman Wells and Wrigley locations, with less temperature increase recorded since 2000 (Figure 1.1, Table 1.1) (Smith et al., 2016). In colder permafrost of the northern Mackenzie, in contrast, greater recent warming has been observed at Norris Ck and KC-07 locations (Figure 1.1, Table 1.1) corresponding to relatively higher average air temperatures over the last decade (Smith et al., 2016).

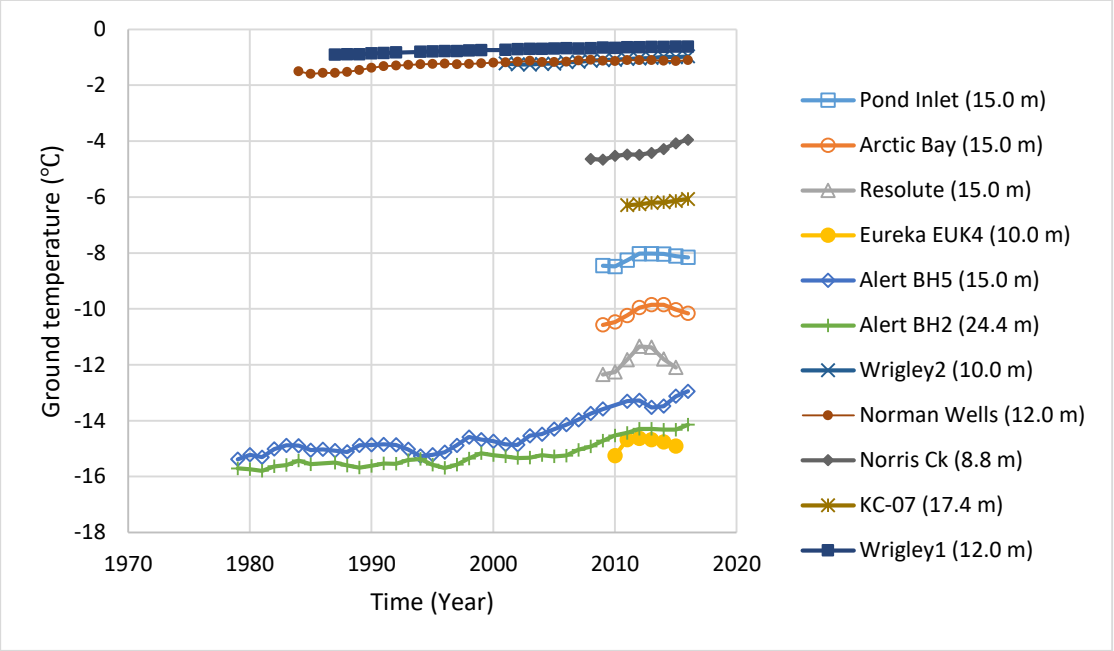

Figure 1. 1. Permafrost temperatures between 1978 and 2016 in various locations in Canada (after Smith et al., 2016).

In northeastern Canada, the mean permafrost temperatures at 25 m depth from ground surface at the Alert sites were within the highest recorded since 1978 (Figure 1.1) showing the most temperature increase between 2000-2010 (Smith et al., 2015). Since 2010, the permafrost temperature showed less variations coincided with a period of relatively colder surface air temperatures. Short period records have been obtained at the Resolute and Eureka locations in Queen Elizabeth Islands and in the Pond Inlet and Arctic Bay on Baffin Island exhibiting an overall warming of permafrost at 10-15 m depth since 2008 with little cooling since 2012. The difference between permafrost temperature in cold and warm permafrost regions is likely related to regional variation in ambient air temperatures. There has been a greater reduction in air temperature at Eureka and other locations farther south compared to Alert sites since 2012 (Figure 1.1). At the relatively shallow measurement depths, furthermore, variation in ground temperature has been greatly influenced by the seasonal variation in the air temperatures. Therefore, permafrost

temperature at shallower depths is more sensitive to shorter term fluctuations in air temperature. Table 1.1 presents the changes in the mean annual ground temperature of permafrost in Canada observed between 1978 and 2016.

Table 1. 1. Summary of changes in mean annual ground temperature of Canadian permafrost between 1978 and 2016 (after Smith et al., 2016).

Region	Sites	Entire Record	Since 2000
Northern Mackenzie Valley	Norris Ck (No), KC-07 (KC)	NA	+0.4 to +0.8
Baffin Island	Pond Inlet (PI), Arctic Bay	NA	+0.5 to +0.7
High Canadian Arctic	Resolute (Re), Eureka (Eu)	NA	+0.4 to +0.7
High Canadian Arctic	Alert (Al) @ 15 m	0.5	+1.2
High Canadian Arctic	Alert (Al) @ 24 m	+0.3 to +0.4	+0.7 to +1.0

The increase in mean annual ground temperature in permafrost region could also influence its extent. Jorgenson et al. (2006) conducted air photo analysis on photos taken in 1945, 1982, and 2001 to investigate possible changes in permafrost extend. Their results showed significant degradations of ice wedges that had been stable for 1000s of years. Lawrence and Slater (2005) discussed the evolution of permafrost extent in the Northern Hemisphere under global warming impact predicting present-day permafrost area as well as permafrost condition during the 21st century. The predicted permafrost area projections on the International Permafrost Association (IPA) map showed 25% reduction in the global permafrost extent occurred between 1900 and 2000. Dramatic permafrost degradation was also predicted for 2100 and anticipated to produce 15% discharge increase into the Arctic Ocean.

Recently, permafrost regions have become economically important following the explorations of enormous natural resources especially in the north circumpolar. This has been

followed by a vast economic boom occurred after the development of raw materials' extraction methods and ease of transportation to population centers and consumers. The economic development, however, has been accompanied with increase of population and expansion of infrastructure systems such as civil facilities, hydrocarbon extraction facilities, transportation networks, communication lines, and industrial projects. In addition to the considerable expenses that was attendant to the rapid and vast development, Williams (1986) and Smith and McCarter (1997) suggested that these expenses could be aggravated severely in both environmental and human terms by the effects of global warming on permafrost. The stability of civil structures supported by the conventional type of foundations situated on degradation prone permafrost could be challenging and worth studying.

There has been long debate about the most effective type of foundation technique that should be used to support structures situated on frozen ground in permafrost region and withstand the effects of the dramatic change in ground temperature. Most of the opinions suggest that the permafrost conditions (i.e., warm permafrost or cold permafrost) dictate the selection of the proper foundation type that should be used.

Because of their proven performance, pile foundations have since then become the most common type of foundations used to support structures and infrastructure in northern communities as reported in the Design Manual for New Foundations on Permafrost (Fish, 1983). Pile foundations are load bearing columns that can be installed deep into the ground and interact with the surrounding soil through their end bearings and skin friction to transfer the applied structural loads deep to a stronger and more stable ground layers. In frozen ground, adfreeze strength developed during the frost formation along the pile shaft can significantly enhance the pile capacity. The major research contributions to pile foundation engineering in cold region happened

between mid ‘70s to mid ‘80s of the last century. This was attendant to the high demand for reliable foundation techniques in cold region to accommodate for the rapid industry movement onto the northern grounds seeking raw petroleum materials (Arenson et al., 2015). The research activities during this period had led to the development of the until-nowadays used design specifications for pile foundations in cold region.

Performance of pile foundations in frozen grounds has long been evaluated in both field (e.g., Vialov 1959; Crory 1963; Johnston and Ladanyi 1972; Nixon 1988; Biggar and Sego 1993) and in laboratory (e.g., Parameswaran, 1978; Parameswaran 1979, Parameswaran 1981&1987; Sego and Smith 1989; Ladanyi and Theriault 1990). The design criteria for pile foundations in frozen ground was originally based on the short-term strength consideration (e.g., Vialov 1959; Crory and Reed 1965; Penner 1970; Penner and Irwin 1969; Penner and Gold 1971; Dalmatov et al. 1973). However, pile foundation design considering the solo role of strength consideration had become questionable especially in grounds that contain large amount of ice content. Frozen soils were accordingly classified into ice-rich and ice-poor soils, where ice-rich exhibiting a frozen bulk density less than 1.7gm/cm^3, while ice-poor soil shows higher frozen bulk density (Nixon and McRoberts 1976). Frozen soils behave differently compared to unfrozen soils where the former show visco-elastic-plastic behavior, while the latter exhibit elasto-plastic behavior. Materials with viscus behavior demonstrate creep upon exposure to loading, where creep is the plastic time-dependent deformation under a constant loading condition. At the early stage of developing the pile design methodologies, the principal of pile creep in frozen soils had not yet been distinguished as a major geotechnical concern. Johnston and Ladanyi (1972), however, advocated a design approach of pile foundations in frozen ground based on limiting deformations using data from field tests conducted on grouted anchors. Their approach allowed using field creep data to estimate

long-term adfreeze strength that would cause an allowable displacement (or creep) rate over the life time of structures, thus accommodating for the time-dependent behavior of frozen soils. Other researchers including Nixon and McRoberts (1976), Morgenstern et al. (1980), and Weaver and Morgenstern (1981) later suggested that the allowable pile load in ice-rich soils should be determined based on limiting deformation, while in ice-poor soils, the allowable pile load must satisfy both strength and deformation considerations. Limiting deformation, furthermore, was suggested to be governed by primary creep in ice-poor soils and secondary creep in ice-rich soils. Therefore, it was emphasized that ensuring tolerable pile displacements throughout the life of the structure is essential.

Ice-rich soils are susceptible to excessive thaw settlement because of their excessive ice contents. At the pile vicinity, excessive ice may also present due to migration of unfrozen water under effect of higher cryosuction close to the pile resulting in ice lenses and ice segregation (Zhang, Y. 2014). Many other factors control the formation of excess ice in permafrost such as thermodynamic and geological process which make the prediction of its extent and volume in the field complex (Bush et al.1998).

Different studies have shown the effect of temperature on the pile displacement and creep rates. Ladanyi (1995) reported 35% increase in the creep settlement for a pile exposed to constant axial load installed in an ice-rich silt when the ground temperature increased by 1°C. Nixon (1990a) developed a mathematical expression to predict creep settlement corresponding to permafrost warming. For a pile carrying 200 kN concentrated load and embedded 6m in frozen silty clay at a temperature of -1.3°C, an increase in creep settlement of 30% along 25 years was estimated if a warming rate of 0.1°C per year was applied. Nixon and McRoberts (1976) suggested using creep settlement criteria for pile design in ice-rich soils. However, pile design in ice-poor

soils should satisfy both settlement and ultimate capacity criteria. Due to the greater displacement required to mobilize end-bearing, it has been often reported negligible for piles in homogeneous frozen ground compared to the skin friction.

1.2 Problem Statement

Frozen ground could fail to maintain frozen condition in confrontation of global warming. In warm permafrost, a small temperature increase may be sufficient to cause extensive thawing. In cold permafrost, temperature increase by couple of degrees may result in significant increase in active layer depth (annual thaw depth), which can promote significant thaw settlement and increase the potential frost heave upon freezing. The impact of thaw settlement could be more significant for ice-rich soils where the resulting thaw settlement and loss of bearing capacity can cause inclusive damage to the structures (Esch and Osterkamp, 1990). The evolution of the adfreeze strength and creep behaviors corresponding to the thaw action is not well understood at temperatures close to the freezing point (greater than -3°C). Moreover, the design approaches for piles in ice and ice-rich soil were always derived using flow law models that incorporate creep parameters of crystalline ice due to the lack of reliable creep data on realistic ice-rich soils (Weaver and Morgenstern 1981). The model proposed by Nixon and McRoberts (1976), for example, was mainly built upon published creep data on ice and then was idealized to describe creep behavior in ice-rich soils claiming that this will be a conservative measure in the absence of reliable creep data on ice-rich soils. Nevertheless, ice-rich soils might behave differently compared to the ice due to the presence of unfrozen water in ice-rich soils even at relatively low temperatures. In addition, Weaver and Morgenstern (1981) revealed that the use of published creep data on ice were short of reliable information in the temperature range between 0 and -5°C. Most of the design approaches were often developed based on data collection and interpolations with limited comprehensive

study on performance of pile foundations in different types of frozen soils when exposed to different levels of temperature and stress conditions (e.g., Nixon and McRoberts 1976; Nixon 1978; Morgenstern et al. 1980; Weaver and Morgenstern 1981). Furthermore, the roughness factor "m" that used for predicating adfreeze strength of piles based on the strength parameters of the surrounding frozen soil has always been assumed as a constant value for a give pile material regardless to the different thermal regime and the type of the frozen soil. In addition, helical piles which have been recently used foundation technique in frozen ground, lack reliable design protocol in term of its load carrying capacity and creep deformation.

Information on the strength and creep behaviors of frozen soils and pile-soil interface will help determining the load-displacement relationship for piles installed in permafrost susceptible to degradation. Field pile load tests, field pile creep tests, and well-controlled laboratory experimental programs are, therefore, required to address these shortcomings.

1.3 Objectives

The purpose of this research is to complement the work of other researchers pertaining to the assessment of performance of pile foundations in frozen grounds. The research, more specifically, focuses on the influence of ground temperature change on the load carrying capacity and deformation behavior of pile foundations installed in warming frozen ground. various experimental programs were conducted at various levels of temperatures ranged from -10 to zero degrees Celsius with narrower thermal intervals selected closer to the freezing point. This was determined to cover the shortcomings in research documentations describing the behavior of frozen ground and piles in frozen grounds at relatively warm temperatures (close to zero degrees Celsius). The objectives of this research were addressed from different perspectives including field investigations and laboratory testing. The field experimental program was aimed at observing the

real-life performance of pile foundations when installed in frozen grounds. Field experiment enabled tracking the changes in creep behaviors and adfresze capacity of the test piles when an exaggerated thermal condition encountered such as moving gradually from frozen to completely unfrozen condition. The laboratory work, on the other hand, provided more effective means of testing at predetermined thermal and mechanical boundary conditions. It allowed for comprehensive characterizations of creep behavior of frozen soils as well as the frozen soil shear strength and how it correlated to the adfreeze strength of the pile-frozen soil interface. Two laboratory testing programs, therefore, were considered including small element interface tests and uniaxial creep tests of frozen soil samples.

These experimental analyses were conducted to achieve the objectives of this research by investigating:

- Reliability of the used roughness factor "m" in correlating pile adfreeze strength to the shear strength of the frozen soils. This laboratory investigation was conducted using small element interface testing utilizing direct shear test apparatus. The tests were carried out in a fully controlled environmental chamber. Unlike to the field work, the laboratory work enabled conducting the tests at the desired levels of temperatures (-10 to 0 degrees Celsius and at room temperature) and confining pressures (25 to 400 kPa) and using different soil types. This experimental investigation has provided important design guidelines of the proper roughness factor that should be used to predict load carrying capacity of the pile foundation installed in various types of frozen ground and in various ground temperature regimes.
- Creep behaviors of ice-poor and ice-rich frozen soils under combined effects of uniaxial compression loading and thermal exposure. This program setup is aimed at evaluating the

impact of warming action on the steady state creep rate of the frozen soils, establishing a creep power law using time and temperature dependent stress-strain curves, and obtaining the creep parameters needed for the flow law of piles in frozen ground. To do so, modified consolidation frames were placed inside the environmental chamber and used for conducting creep tests at various temperature and stress levels. As it has been indicated, greater attention was paid for testing at temperature slightly below zero to cover the shortcomings in information available for this thermal range.

- Load transfer mechanism and creep behaviors of pile foundations in warming frozen grounds. Through this experimental program, efforts were made to estimate the ultimate bearing capacity of different pile types installed in frozen ice-rich and ice-poor soils. The study evaluated the changes in adfreeze strength and creep behavior corresponding to the thaw action. Pile load tests were carried out on piles in unfrozen grounds and in frozen grounds to report the change in stress-displacement behavior of piles when the ground exposed to warming and changing from frozen to unfrozen condition. Pile creep test is also performed in field to obtained information about creep behavior of different pile types in frozen grounds. The result of this work highlighted the significant impact of permafrost degradation on the ultimate capacity and creep behavior installed in different types of froze grounds.

1.4 Thesis Layout

This thesis contains 8 chapters. Chapter 1 includes introductions to permafrost condition in Canada, pile foundation techniques in permafrost, advantages and possible problems along with the need for further investigations. Moreover, the objectives of the research along with the organization of the proposal are included. Finally, the associated journal and conference

publications are listed. Chapter 2 contains a comprehensive literature review that describes different pile installation techniques in frozen ground. In addition, it summarizes most of the design approaches, including analytical solutions and empirical equations, that are available in literature and have long been used for pile foundation design in frozen grounds. These design approaches were discussed in term of their background development and their use to predict either load carrying capacity or creep deformation of pile foundations in frozen grounds. Chapter 3 and Chapter 4 describe the experimental programs and the test results of the interface element tests conducted on ice-rich and ice-poor frozen soils respectively. Shear strength of ice-rich frozen clay and adfrezze strength of steel-frozen clay interface are discussed in Chapter 3, whereas, shear strength of ice-poor frozen sand and adfreeze strength of steel-frozen sand interface are presented in Chapter 4. Chapter 5 provides description of the field experiment and analyzes the field results of load carrying capacity of steel open-ended pipe pile, cylindrical concrete pile, and helical piles tested in frozen and unfrozen Leda clay. The results of this experiment are presented and thoroughly analyzed. Chapter 6 contains detailed description of the filed experiment of creep testing and load transfer testing of steel open-ended pipe piles, helical piles, and grouted shaft helical piles installed in sandy silt frozen soil. Chapter 7 details the development of a temperature-dependent creep model for pile foundations in frozen Leda clay. The model was developed based on the creep parameters of frozen Leda clay obtained from serios of uniaxial creep tests using modified Oedometer apparatus. Finally, recommendation for further investigations and the conclusions of this research study are summarized in Chapter 8.

1.5 Publications

1.5.1 Journal publications

- Aldaeef, A.A., and Rayhani, M.T., (2019). Interface Shear Strength Characteristics of Steel Piles in Frozen Clay under Varying Exposure Temperature, *Soils and Foundations*. (Tentative acceptance).
- Aldaeef, A.A., and Rayhani, M.T., (2019). Load Transfer and Creep Behavior of Helical Piles in Frozen Ground. *Journal of Geotechnical and Geo-Environmental Engineering (ASCE).* (Under review)
- Aldaeef, A.A., and Rayhani, M.T., (2019). Load Transfer and Creep Behavior of Open-ended Pipe Piles in Frozen and Unfrozen Ground. *Innovative Infrastructure Solutions.* (Submitted).
- Aldaeef, A.A., and Rayhani, M.T., (2019). Pile-Soil Interface Characteristics in Ice-Poor Frozen Ground under Varying Exposure Temperature. *Journal of* E*nvironmental Geotechnics. (*Submitted).
- Aldaeef, A.A., and Rayhani, M.T., (2019). Temperature-dependent Creep Model for Pile Foundation in Frozen Leda Clay. *Journals of Cold Regions Engineering (ASCE).* (Submitted)
- Aldaeef, A.A., and Rayhani, M.T., (2019). Load Transfer of Pile Foundations in Frozen and Unfrozen Soft Clay. *International Journal of Geotechnical Engineering*. (Under review)

1.5.2 Conference papers

- Aldaeef A.A., Rayhani M.T. (2019). Influence of Exposure Temperature on Shaft Capacity of Steel Piles in Ice-Poor and Ice-Rich Frozen Soils. In: El-Naggar H., Abdel-Rahman K.,

Fellenius B., Shehata H. (eds) *Sustainability Issues for the Deep Foundations. GeoMEast 2018. Sustainable Civil Infrastructures.* Springer, Cham.

- Aldaeef A.A., Rayhani M.T. (2018). Adfreeze Strength and Creep Behavior of Pile Foundations in Warming Permafrost. In: Abu-Farsakh M., Alshibli K., Puppala A. (eds) *Advances in Analysis and Design of Deep Foundations. GeoMEast 2017. Sustainable Civil Infrastructures.* Springer, Cham.
- Aldaeef, A. A. and Rayhani, M. T. (2018). Impact of Ground Warming on Pile-Soil Interface Strength in Ice-Poor Frozen Soils, *Proceed. of GeoEdmonton 2018*, Edmonton, Canada.
- Aldaeef, A. A. and Rayhani, M. T. (2017). Creep Behavior of Frozen Leda Clay under Combined Compression Stress and Thermal Exposure, *Proceed. of GeoOttawa 2017*, Ottawa, Canada.
- Aldaeef, A. A. and Rayhani, M. T. (2016). Evolution of Adfreeze Strength of Pile Foundations in Warming Permafrost, *Proceed. of GeoVancouver 2016,* Vancouver, Canada (Best Student Paper Award).
- Aldaeef, A. A. and Rayhani, M. T. (2015). Load Transfer of pile foundations in warming frozen ground. *Proceed. of the 7th Canadian Permafrost Conference*, (Paper #480), Quebec, Canada.

CHAPTER 2: LITERATURE REVIEW

2.1 Pile Foundation Techniques in Frozen Ground

Shallow and deep foundations both have been used to support structures and infrastructure systems in frozen ground and permafrost region, however, the amount of load and the type of soils determine what foundation type is more suitable. Shallow foundations are often used for light structures and relatively stable frozen ground. Deep foundation, on the other hand, are more commonly used to support heavy loads such as high-rise buildings and for structures sensitive to subsidence. Generally, foundation design and construction in frozen grounds are more complex than in temperate zone. Although, frozen grounds are stiffer than unfrozen grounds, provide larger bearing capacity, and exhibit less settlement, they may undergo secondary creep and apply frost heave to the foundation especially in frost susceptible soils. The construction in permafrost region including excavation, compaction, material transportation, and installation is more complicated and expensive compared to similar projects in warm regions, therefore, it is important to select a suitable type of foundation that will provide reliable performance, and can be easily handled and installed.

There have been different types of pile foundations used in permafrost. Some of these piles are conventional such as timber, steel pipe piles, steel H-piles, corrugated metal piles, prestressed precast concrete piles and cast-in-place concrete piles (Andersland and Anderson 1978), and others are less common such as helical piles and thread bar piles (Johnston and Ladanyi 1972). The selection of certain type of pile depends on different factors including the magnitude of the applied load, the soil type, permafrost temperature, construction and installation equipment, availability of materials, and the cost of transportation. The following sections provide a brief description of the most pile types and piling techniques used in permafrost region.

2.1.1 Timber piles

Timber piles are commonly used in northern region and considered the least expensive type of piles when they are locally available. Timber piles generally are tapered with larger diameter at the base to provide greater uplift resistance against frost heave (Crory 1966). They come in lengths ranging from 6 to 15 m, top diameters from 150 to 250 mm, and base diameters from 300 to 350 mm.). Timber piles are mostly manufactured from local materials including spruce, Douglas fir, or pine. They generally remain well preserved as long as embedded in permafrost, however, they may be exposed to deterioration and decay when active layer exists. Therefore, timbre piles are often treated with wood preservative products to extend their service life spans (Andersland and Ladanyi 2004). Nevertheless, some of these treatments may reduce the adfreeze bond at the pile-frozen soil interface. Timber piles provide good insulation properties thus do not disrupt the ground temperature. Although they provide a relatively high bond strength, timber piles have low structural capacity and may not withstand the mechanical driving into the frozen ground.

2.1.2 Steel piles

Steel piles are the most commonly used type of piles in frozen ground and permafrost region. They can be installed in both warm and cold permafrost. The pipe pile and H-steel piles are the most commonly used steel piles. Pipe piles are normally utilized when lateral load resistance is required and can be filled with concrete or sand to enhance their bearing capacity. For relatively warm permafrost, Open-ended steel-pipe and H-steel piles can be driven deep enough in frozen ground in order to develop sufficient adfreeze bond and provide high bearing capacity. In cold permafrost, closed-ended pipe piles may be installed in oversized predrilled holes where the gap between the pile wall and the cut hole is filled with sand-water slurry or grouted with concrete. Linell and Johnston (1973) stated that the part of steel piles embedded in permafrost are well preserved from

corrosion, however, small amount of corrosion was reported along the active layer depth. Steel pipe pile can be used as thermal pile by installing an exchange-heat tube inside them to maintain the thermal regime. Steel pile sections can be manufactured with special lugs on them (Andersland and Alwahhab 1982, 1983) or their surface may be corrugated (Thomas and Luscher 1980) to improve their overall bearing capacity.

2.1.3 Concrete piles

The relatively low tensile strength of the concrete material makes the precast and cast-in-place concrete piles not the ideal choice to be used in frozen ground and permafrost. Frost heave may apply significant tensile stress which most likely will generate cracks and respectively expose the steel rebar in concrete piles to corrosion (Andersland and Ladanyi 2004). Therefore, this type of piles is rarely used in North American permafrost practice, however, circular and square precast reinforced piles have been widely utilized in Siberia. They are installed in pre-thawed ground or predrilled holes where in the latter they are backfilled with slurry or grouted with concrete. The performance of precast concrete piles can be enhanced by exposing them to pretension stresses to minimize the impact of frost heave. The precast prestressed concrete piles also can be handled and transported more readily than precast concrete piles. Concrete piles can also be cast in place although they have been barely used in permafrost until recently due to a potential challenge of thermal degradation of frozen ground and freezing of fresh concrete. However, the development of a high-aluminous cement, that allows rapid grout curing and strength development at low temperatures as low as -10 ℃, makes cast-in-place piles more practical than before for the use in frozen ground and permafrost (Biggar and Sego 1990; Benmokrane et al. 1991).

2.1.4 Helical piles

Helical piles, known also as screw piles, consist of one or more circular helices welded to a solid or hollow shaft in a square or circular section. Helices diameters are either identical or tapered towards the pile tip. These helices are aimed at mobilizing larger soil resistance compared to conventional smooth-shaft piles. Helical piles have been widely used to support many types of structure and provide structural stability against axial compression, uplift tension and lateral static and dynamic loads. Helical piles are distinguished with their light weight, ease and speed of instillation, minimum soil disturbance, free vibration instillation and different instillation angles. This type of piles is installed into the ground by applying a mechanical torque through a drive head using hydraulic torque unit or handy equipment depending on the pile size and site conditions. During installation, the helices cut downward into the soil such that the shaft is pulling into the ground. Helical piles often equipped with 1.5 m or 3 m length shaft extensions that can be bolted to the leading shaft to increase the pile length in order to reach the desired bearing depth. Recently, helical piles have been proposed to be an alternative deep foundation to support structures on frozen ground in cold regions. They have been reported to minimize the impact of frost heave which commonly occurs to pile foundations situated within frozen ground. Unlike to helical piles in warm ground, the mechanism of load transfer and design requirements for helical piles in frozen ground are not well understood.

2.1.5 Summary and other piling techniques

Precast concrete piles are often prestressed to withstand handling stresses and tensile stresses developed during driving or resulted from frost heave. Cast-in-place concrete piles are not recommended for use in permafrost because of the required longer time for freeze-back and establishment of adfreeze strength due to the heat of hydration being released during concrete

curing. Pile sections can be modified to improve capacity: protruding spikes have been driven into the sides of timber piles, and steel pieces have been welded onto steel piles (Anderson and Alwahhab 1983; Crory 1966). The intent is to get higher pile capacity by forcing failure to occur in the frozen soil rather than along the pile surface. In practice, it is time consuming and costly to make such modifications, but pile capacities can be substantially increased (Andersland and Ladanyi 2004). High levels of adhesion can be attained using corrugated metal or other types of piles with irregular pile surfaces. Insulated or thermal piles can be used to maintain low permafrost temperature (Phukan 1980; 1985). It is common to insulate piles from structures to prevent heat transfer to the piles and ensure better longer-term thermal stability of the frozen ground around the piles. Thermal piles contain special thermal devices that are placed in a slurry within the piles. During the winter, heat flows from the permafrost to the atmosphere, but the reverse does not occur during the summer. Consequently, the temperature of the permafrost remains low so that pile adfreeze is maintained.

2.2 Pile Installation in Permafrost

The selection of pile installation technique in frozen ground is controlled by many factors including pile type, thermal condition of permafrost, time from installation to loading, equipment availability, and site accessibility (Nottingham and Christopherson 1983). Maintaining the coldness condition of permafrost and frozen grounds is essential. Therefore, pile installation in permafrost is favorably performed by means that would release the least amount of heat in order to ensure rapid and adequate adfreeze bond formation (Heydinger 1987). Conventional pile driving techniques will result in minimal heat production; however, it is not always possible to drive piles into permafrost. Several of pile installation techniques have been used to facilitate pile placement in different permafrost conditions.

Pile placement in permafrost is conducted through pre-thawing, driving, dry auguring, and/or boring. In the past, predrilled and slurry backfilled piles were exclusively used as a primarily piling techniques in permafrost. Early attempts for pile driving were conducted by the U.S. Army Corps of Engineers, oil companies and others with various level of successfulness. Although piles had been driven in permafrost since then, Nottingham and Christopherson (1983) criticized the methods used for driving suggesting that they were neither reliable nor economical. Therefore, predrilling and slurry backfilled pile placement had remained the most used installation technique and utilized for many projects such as the Trans-Alaska Pipeline and North Slope Oilfield. However, the disadvantages associated with predrilled slurry backfilled piles continued to inspire researchers to develop better techniques for pile driving in permafrost and frozen ground. Amongst these disadvantages are the need for large diameter auger equipment, equipment for pile placement and support, slurry preparation and pouring, haul and placement. Moreover, the slurry used for pile backfill was mainly produced using conventional cement mixture that cures slowly and respectively releases significant amount of heat during hydration. This may change the thermal condition of the regime and makes the immediate loading challenging. As a result, using slurry backfilled pile placement technique would require relatively longer time for freeze-back resulting in significant loading delays. In contrary, driven pile can be placed in two to three times faster rate, the installation requires less equipment and support, and can be loaded shortly after installation compared to slurry backfilled piles. However, some limitations associated with driven piles do exist including location tolerances and lack of refined driving equipment used to present.

Nowadays, pile driving in permafrost has become more reliable and economical after the driving equipment has become more refined and suitable for different site conditions and pile sizes (Nottingham and Christopherson 1983).

2.2.1 Driven pile placement methods

Steel piles, including pipe piles, H-shape and sheet piles, can be readily driven into frozen grounds using either impact hummers, vibratory hammers or sonic hammers, depending on soil conditions. US Army Engineer School (1985) stated that the impact driving is performed using one of three types of impact hammers: drop hammer, diesel hammer, and the pneumatic or steam hammer. Vibratory driving mechanism is not classified as impact hammers. These three techniques found to be efficient to drive H-piles and open-ended steel pipe piles to depths of 15 meter or more in frozen grounds that consist of silty sand or finer-grained soils at ground temperature warmer than -4°C. At lower temperatures, heavy pipe piles and H-piles can be used. When very stiff frozen soil exists, impact hammers and pile tip aids are needed (Nottingham and Christopherson 1983). Nottingham and Christopherson (1983) suggested that pile tips are highly recommended when using impact hammers even when easy driving is anticipated. This measure can prevent pile tip ovaling and flattening during impact driving into pilot holes. For driving in warmer frozen ground or driving in thermally modified pilot hole, vibratory hammers are preferable where no pile caps are required for protection against impact stresses. The vibratory hammers are clamped to the pile to enhance vibration and advance the pile into the ground. Observations have shown the deficiency of vibratory hammers in driving piles into strong frozen, hard layers, and predominantly coarse gravel frozen ground. However, it has been used for slow motion driving in warm frozen silts without using pilot holes. The steel types used for pile manufacturing, in addition, can indeed determine the type of hammer utilized. For example, Nottingham and Christopherson (1983) reported that the piles made of mild steel have not been reported to fracture while driving with impact hammers even in extreme cold environments. US Army Engineer School (1985) suggested that hammer energy should not be less than 25,000 foot-pounds to drive H-piles in frozen soil and

the H-pile should not be smaller than the HP 10 x 42. It was also stated that the freeze-back in most cases will be established within 15 to 30 minutes after driving. The following sections illustrate with more details the pile driving techniques used in cold region.

2.2.1.1 Impact hammers

Mechanism of Impact hammers mainly depends on periodic mass drops on the pile head to produce energy and enhance pile penetration (Nottingham and Christopherson 1983). In Alaska, the diesel hammers have been reported to be the most practical impact hammer compared to hydraulic and air impact hammers. The performance of diesel hammers is maximized by maintaining the hammer at warm temperature and providing some resistance to driving to ensure ignition. Diesel hammers have shown reliable and efficient driving when used for short piles or driving with pilot hole. In contrast, air hammers provide reasonably controllable driving, nevertheless, they may freeze up during cold weather if line defrosters or heaters are not provided. For relatively small piles such as in remote building foundations, hydraulic impact hammers are preferable. They are small, rapid-hitting devices that can be mounted on tracked vehicles for efficient and mobile machines. For reliable performance, hydraulic hammers require maintaining warm condition and, as any hydraulic system, their hydraulic fluids must maintain liquidity in cold weather. In terms of productivity, suitably selected impact hammers can make a penetration rate equal to 305 mm/min (one foot per minute) in fine-grained frozen soils. In dense granular frozen soils, the pile driving is aided by advancing a pilot hole in order to achieve a driving rate of 305 mm/min. The use of thermally modified pilot holes can further facilitate the pile driving to be five times the previous rate resulting in about 1525 mm per minute for most soil types and temperatures (US Army Engineer School 1985).

2.2.1.2 Vibratory hammers

Vibratory hammers are a recent improvement to pile-driving techniques. They are primary used in pile driving industry, especially for sheet pile installations. Vibratory hammers are operated by either hydraulic or electric supply and their mechanism is based on a principle which uses two counter-rotating eccentric weights (Nottingham and Christopherson 1983). Vibratory hammers consist of the vibrating unit which comprises of the rotating eccentric weights, the suspension system that insulate the vibratory motions from the lifting device, and the clamping system which connects the vibratory driver to the pile (US Army Engineer School 1985). The eccentric weights move in limited range and provide short strokes, less than two inches, thus, they generate high impulse rates reaching up to 2,000 pulses per minute. Their driving ability differs based on the vibrations and the weights of driver and pile. However, Nottingham and Christopherson (1983) stated that even the largest vibratory hammer would produce driving energy less or equal to a small impact hammer, nevertheless, they will perform the same should difficult driving be encountered such as in coarse granular or dense material. Vibratory hammers are more efficient for driving in fine-grained saturated soils or loose coarse-grained soils. Moreover, they are a good installation tool when used with thermally modified pilot holes. In permafrost condition, vibratory hammers have shown driving rates of less than 152.5 mm/min (0.5 feet/min) in warm fine-grained soils. The driving rate becomes significantly larger, up to 20 feet per minute, in most soils when the thermally modified pilot hole is utilized.

2.2.1.3 Sonic Hammers

Sonic hammers are similar in their mechanism to vibratory hammers, but differ in their driving rates. Sonic hammers manly depend on their high frequency in being a great driving tool, but at the present time they are costly, limited in availability and have many significant operational

problems, especially when used in cold weather. The driving rate, in most frozen fine-grained soils without pilot holes, using sonic hammer is comparable to the achieved driving rates when using vibratory hammers with the aid of thermally modified pilot holes. However, frozen granular soils are still a problematic condition for sonic driving hammers like other hammers, thereby; thermally modified pilot holes have been used to facilitate pile installation in such ground condition (US Army Engineer School 1985).

In summary, the three methods of pile driving have different installation accuracy in term of alignment. The designers recognize that placement tolerances are to be expected, thus, plans must be detailed accordingly. Impact hammers are allowed for horizontal tolerances of 560 mm (22 inches) while deviation from plumb may be up to 2 percent. Vibratory hammers can provide better installation accuracy because piles can be vibrated up and down the thawed pilot hole until desired tolerances are achieved which fall within a 12.7 mm (0.5 inch) vertical tolerance and virtually plumb. This adjustment procedure cannot be conducted for piles driven by impact hammers. However better installation accuracy can be obtained by drilling an accurate pilot hole, since the pile follows hole alignment during driving. During the pile installation, a small diameter weeping hole should be placed at the final ground line elevation to release the access pore water pressure and minimize the effect of water accumulation.

2.2.2 Predrilled pile placement methods

Piles can be installed in predrilled holes conducted by one of the drilling techniques including dry augering, boring, and steam/water thawing. The holes can be drilled undersized and wood or pipe piles are respectively driven into the holes. However, oversized holes are usually performed and a backfill material is placed around the pile and allowed to freeze back. Upon freezing, the backfill materials are aimed at transferring the imposed pile loads to the surrounding frozen soil. The

Backfills might consist of natural materials, such as sand and silt obtained from borrow pit or from the pile hole excavation, which is then mixed with water to make slurry backfill. Cement grout is also used as backfill materials for piles in permafrost. However, the use of sand-water mixture has become more common technique since it has shown a relatively higher pile capacity. Clay soils unlike to sand and silt are difficult to mix and blend, and when frozen they are not strong. US Army Engineer School (1985) suggested that water, gravel, unsaturated soil, or concrete should not be used for backfill in permafrost areas, while organic matter must not be used for slurry. Nottingham and Christopherson (1983), in contrast, reported using different types of natural backfill materials including silt-water slurry clay-water slurry, dry sand, and even water.

Backfilling is conducted by making the slurry with water, placing the slurry in lifts and applying vibration to eliminate void formation within the backfill. The oversized drilled holes must provide sufficient space between the pile and the cut to insure even and proper distribution of the slurry around the pile. The temperature of the slurry should be maintained near freezing point before pouring it into the hole in order to minimize freeze-back time, however, slurry should not contain any ice (US Army Engineer School 1985). Pile holes can also be accomplished oversized or undersized using steam or water thawed technique (Crory 1966). Natural freeze-back may not occur as rapid as desired; therefore, an artificial freeze-back is utilized by circulating a refrigerant below the subsurface in order to shorten freeze-back time. Artificial freeze-back could be necessary for certain projects such as pile placement in warm permafrost, pile group projects, or when a rapid loading is required before freeze-back could occur naturally. The next subtitles briefly discuss some of the mostly used pile hole drilling techniques in the cold region.

2.2.2.1 Dry augering method.

Dry augering is performed by utilizing a conventional power auger with specially designed bits for boring pile holes into permafrost. A typical auger can drill holes up to 610 mm (2 feet) in diameter at rates of about 305 mm per minute in frozen silt or clay, depending on ground temperature, size of equipment, and the type of drill bit. Holes up to 1220 mm (4 feet) or more in diameter can be advanced easily in such soils (US Army Engineer School 1985). Nottingham and Christopherson (1983) reported boring of test pile holes ranging in depth from 1830 mm to 6400 mm (6 ft to 21 ft) in permafrost performed using conventional power auger. The diameter of the reported holes ranged from 305 mm to 46 mm (1 ft to 1.5 ft). Dry auguring was reported to be effective for drilling pile pits when the frozen ground surface allows ready mobility and difficulty of using steam and water thawing is expected. However, dry augering is not an efficient technique in coarse frozen soils containing boulders.

2.2.2.2 Steam or water thawing

Frozen ground can be pre-thawed by steam points or water in preparation for pile installation in permafrost. Frozen soil can be thawed up to 4500mm or 6100mm (15 or 20 feet) using pressurized steam at 30 psi delivered through a 25.4 mm (1-inch) steel pipe followed by pile driving through the pre-thawed depth. Pressurized steam between 60 to 90 psi is needed for greater depths where a larger delivery pipes (2-inch) are used. Approximately, 0.4 to 0.56 cubic metre of steam are needed to advance 305 mm (1 foot) of penetration. Water jetting is used for pre-thawing when sandy type of soil is encountered. The pile is slightly hammered into the ground, and the steam aids the penetration while scaffolding or an A-frame is used to facilitate handling long sections of water jetting and steam-jetting pipes. When the final depth is reached, the steam or water point is kept in the hole to make the hole large enough to receive the pile. The US Army Engineer School

(1985) suggests that the steam or water point should be kept in place for ½ hour if the soil is sand and up to 3 hours if the soil is clay. Figure 2.1 shows the approximate shape of the hole thawed in sand-silt soil after 1½ hours of steam jetting. Upon thawing completion, piles are positioned and respectively driven by the usual methods of pile driving through the thawed ground. A series of piles may be set after three to four days of thawing. Timber piles are relatively lighter thus having a tendency to float when inserted into the thawed holes. Therefore, they must be held down in place or weighted until freeze-back is being established.

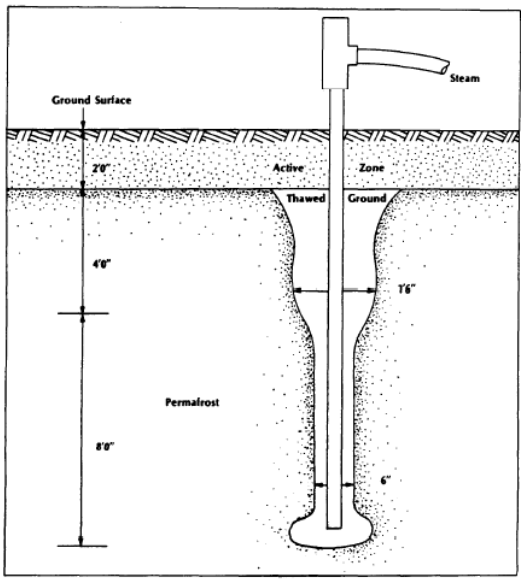

Figure 2. 1 Pile predrilling using stem jetting technique (after Andersland and Ladanyi 2004).

Although steam or water thawing is an efficient technique for making pile holes, it can produce significant amount of heat into the frozen ground and cause indefinite delay in freeze-back occurrence. Piles may develop inadequate bearing capacity, or undergo significant heave which may result in working the piles out of the ground and damaging supported structures. It has been reported that steam or water thawing is improper technique for pile installation in warm

permafrost that exposed to mean annual temperature greater than -6.5℃ (The US Army Engineer School 1985). The usage of this method maybe limited to colder permafrost only with special precautions to minimize heat input into the frozen ground if other techniques of installation cannot be used.

2.2.2.3 Boring

Ground boring is another technique used to perform pile pits by utilizing rotary or churned drilling or by drive coring using various bits and drive barrels. Frozen cuts are then removed by air, water, or mechanical systems. Boring procedures are the same as for dry augered holes. Nottingham and Christopherson (1983) reported piles installation using churn drilling and driving technique for open-ended standard steel pipes with 100 mm (4-in) outer diameters and embedment depths ranging from 3000 mm to 4800 mm (10 to 16ft). The pile installation procedure was initiated by churn drilling of a pilot hole with a slightly smaller diameter than the pile pipe diameter using a conventional churn drill chopping bit. The pilot holes were drilled to a shallower depth (3-ft) compared to the total embedment depths of the piles. The pipe piles then were firmly driven to the final depth without aid of pilot holes.

2.3 Design Approaches for Pile Foundations in Frozen Grounds

The principle of the design criteria for pile foundations in frozen soils was initially based on the allowable load carrying capacity obtained from the ultimate adfreeze strength of pile-soil interface (e.g., Vialov 1959; Crory and Reed 1965; Penner 1970, 1974; Penner and Irwin 1969; Penner and Gold 1971; Dalmatov et al. 1973). Johnston and Ladanyi (1972), in contrast, considered an allowable load carrying capacity that would cause an allowable displacement (or creep) rate over the life time of structures to accommodate for the time-dependent behavior of frozen soils. Other researchers including Nixon and McRoberts (1976), Morgenstern et al. (1980), and Weaver and

Morgenstern (1981) suggested to check both load carrying capacities and design based on the smaller value amongst them. Weaver and Morgenstern, (1981) added that the type of soil that constitutes the frozen grounds can influence the governing failure criterion. They stated that the failure criteria of piles in ice-rich soils may be primarily governed by creep settlement, while piles in ice-poor soils are governed by both bearing capacity and creep settlement failure criteria. Pile settlement under the design load may be governed by primary creep in ice-poor soils while in ice-rich soils primary and secondary creeps prevail. Pile settlement must not in all cases exceed the tolerable displacement limit along the design life of the supported structure.

The design protocol of pile foundations in frozen grounds, therefore, can be grouped under two categories. First category demonstrates the design approaches based on the ultimate bearing capacity, while the second category demonstrates the design approaches based on creep settlement.

2.3.1 Bearing capacity of piles in frozen grounds

Parameswaran, (1978) reported that ultimate bearing capacity of piles depends mainly on the shaft resistance along the permanently frozen depth. The strength gained from end bearing could be negligible for piles installed in ice-rich soils and may only be significant if the pile is situated on ice-poor frozen soils such as bedrock or granular soils (Crory 1963). The US Army/Air Force (1967) suggested that the end bearing capacity could be neglected from design considerations for piles with base diameter smaller than 150 mm regardless of the soil type. This was attributed to the greater displacement that is required for mobilizing the end bearing compared to the much smaller displacement needed to overcome the adfreeze bond along pile shaft.

An empirical equation proposed by Vialov (1959) was one of the earliest approaches for estimating long-term adfreeze strength of piles in frozen ground as a function of ground temperature. The equation was derived based on experimental data collected from full scale

loading tests on hand-driven timber piles into pre-steamed holes in silty sandy loam and argillaceous loam and written as follow:

$$\tau_{al} = \sqrt{1.65\,\theta} - 0.3 \qquad [2.\ 1]$$

where: τ_{al} is the long-term adfreeze strength (kgf/cm^2) and θ is the positive value of the temperature below the freezing point (℃). Later in 1963, Crory (1963) conducted a series of full-scale loading tests on 200 mm diameter steel pipe piles installed in predrilled frozen silty sand and shaft-grouted with silt-water slurry under an average ground temperature of -4℃ to 0℃. The study summarized the change in ultimate and sustained adfreeze strengths of the test piles as a function in ground temperatures. The results were demonstrated in a graphical illustration; however, they can be expressed in the following forms:

$$\tau_{ul} = (0.0176\,T + 0.154)\,T + 0.005 \qquad [2.\ 2]$$

$$\tau_{al} = (0.012\,T + 0.107)\,T + 0.002 \qquad [2.\ 3]$$

where, τ_{ul} and τ_{al} are the ultimate and sustained adfreeze strength (MPa)respectively; T is the positive value of the freezing temperature (℃).

Parameswaran (1978) examined the ultimate adfreeze capacity of model piles made of different materials. The piles were tested in frozen sand at temperature of -6.0℃. The results showed that wood piles exhibited the largest adfreeze capacity followed by concrete piles and then steel and coated piles. Accordingly, the surficial characteristic of the pile shaft became an important factor in predicted the adfreeze capacity of piles installed in frozen ground. Weaver and Morgenstern (1981) were first who used this concept when they correlated the long-term adfreeze strength (τ_{al}) to the long-term shear strength of the frozen soil (τ_{lt}) using a roughness factor "m" that characterizes the pile surface and other pile surficial variables such as impurities. The long-term adfreeze strength respectively was expressed in the following formula:

$$\tau_{al} = m\,\tau_{lt} \qquad [2.4]$$

The long-term shear strength of frozen soils (τ_{lt}) has often been expressed using Mohr-Coulomb failure criterion as follow:

$$\tau_{lt} = C_{lt} + \sigma_n \tan \emptyset_{lt} \qquad [2.5]$$

where: C_{lt} and $\emptyset_{lt}$ are the long-term strength parameters of frozen soils and σ_n is the normal stress acting on the pile shaft. In frozen grounds, Weaver and Morgenstern (1981) stated that the normal stress on the pile shaft is typically less than 100 kPa which may make the contribution of the frictional component to the total strength insignificant, thus, may be neglected. Therefore, the long-term shear strength of the frozen soil was reduced to:

$$\tau_{lt} = C_{lt} \qquad [2.6]$$

By substituting the equation [2.6] into equation [2.5], the long term adfreeze strength in [2.6] can be rearrange as follow:

$$\tau_{al} = m\,C_{lt} \qquad [2.7]$$

The roughness factor "m" was first extrapolated by Weaver and Morgenstern (1981) when data on shear strengths of frozen soils was compared to the data on pile-soil adfreeze strengths. A roughness factor of 0.7 was suggested for uncreosoted timber piles based on the ratio between adfreeze strength of timber piles in ice to the long-term shear strength of ice obtained from field and experimental data of Voitkovskii (1960) and Vialov (1959). A roughness factor of 0.6 was inferred for steel and concrete piles based on data from field experiments conducted by Johnston and Ladanyi (1972) and Crory (1963). Weaver and Morgenstern (1981) stated that the long-term adfreeze strengths of steel and concrete piles in the used data were not well defined, however, 0.6

represented the lower boundary and could still be acceptable for conservative pile design. Ladanyi and Theriault (1990) evaluated the soil-metal adfreeze bond at -2°C and reported that the long-term shaft resistance of piles in frozen ground does not solely depend on the long-term adfreeze, but also on the long-term friction angle at the interface, and respectively on the total normal stress. Therefore, they improved the Weaver and Morgenstern's (1981) equation by adding the contribution of the long-term friction angle of frozen soil and proposed the following formula:

$$\tau_{al} = m\, C_{lt} + \sigma_{n_{total}} \tan \emptyset_{lt} \qquad [2.8]$$

Interestingly, the experimental results from Ladanyi and Theriault (1990) showed not only the frictional resistance was dependent on normal stress but the roughness factor too. For steel-frozen sand interface, the roughness factor increased from 0.1 to 0.3 when the confining pressure was increased from 100 kPa to 1100 kPa but never reached the value of 0.6 that had been suggested by Weaver and Morgenstern (1981). Although Ladanyi and Theriault (1990) were not confident of using their short-term study to argue about the roughness factor validation and suggested more investigations, continuation of using constant roughness factors as proposed by Weaver and Morgenstern (1981) may have become questionable.

There are some uncertainties associated with the suggested roughness factors as they were extrapolated form very limited field and laboratory data that lacked important information about the frozen grounds and the piles in certain conditions. The used data from Johnston and Ladanyi (1972) and Crory (1963), for example, were obtained from their field studies on adfreeze strength of steel rods and steel pipe piles respectively, with no record of experiments on concrete piles. It is not clearly shown that the adfreeze strength of piles and shear strengths of frozen soils were obtained at identical conditions (i.e., pile material, soils type, stress history, and thermal boundary)

that allows for reliable comparisons and accurate estimation for roughness factors. The roughness factor for a steel pile in frozen sand, for instance, could be different from the one in frozen clay or silt. It could also be different for two identical steel piles embedded in the same soil type but exposed to different ground temperatures or installed at different depths. The soil to soil interaction behavior may be different from pile to soil interaction characteristics which may result in different responses at different exposure conditions, thus leading to different roughness factors. Therefore, roughness factor needs to be assessed to obtained more reliable predictions of adfreeze strength of pile-soil interfaces.

In addition to these limitations, these design approaches may not be able to capture the load transfer mechanism of piles other than smooth-shafted piles. Helical piles, for example, have long been used in frozen ground for different applications including boardwalks, utilidors, fence posts, light posts, etc. However, unlike to smooth-shafted piles, their design protocol in frozen grounds is still not well established. In unfrozen grounds, helical piles have been designed based on either Individual Plate Bearing (IPB) or Cylindrical Shear Model (CSM). The ultimate load carrying using IPB model is the summation of the bearing capacity of each individual helix in addition to skin friction along the section of pile shaft between the helices and between the ground surface and the top helix (Narasimha Rao et al. 1993; Mitsch and Clemence 1985). The ultimate load carrying capacity of using CSM, in comparison, is calculated as the skin friction acting along a cylinder of soil circumscribed between the top helix and the bottom helix plus the skin friction acting along the shaft between the ground surface and the top helix. The bearing capacity of the upper helix in pull-out loading and of the lower helix in compression loading is also considered.

It is very important to understand the governing failure mode of pile foundations in frozen ground before providing any solution that can predict the ultimate capacity of the piles in frozen

medium. For helical piles in unfrozen grounds, Chance Co. (1996) adapted a modified bearing capacity formulation based on the IPB model to estimate the bearing capacity of the helix as follow:

$$Q_{base} = \frac{\pi(D^2-d^2)}{4}\left[9\ \mathrm{C} + q\ N_q\right] \qquad [2.\ 9]$$

where: D and d are the diameters of the helix and pile shaft respectively; C is soil cohesion strength; Nq is bearing capacity factor from Meyerhof's chart and based upon an internal friction angel; q is overburden pressure at the helix depth.

For helical piles in unfrozen cohesive soils, two formulations were derived by Tappenden and Sego (2007) adopting the IPB model to estimate the ultimate bearing capacity resulted from helix bearing (Eq. 8) and pile shaft friction (Eq. 9) under pull-out loading condition as follows:

$$Q_{base} = \frac{\pi(D^2-d^2)}{4}\left[N_c\ \mathrm{C_u} + \gamma'\ H\right] \qquad [2.\ 10]$$

$$Q_{shaft} = \pi.\ d.\ H_{eff}.\ \mathrm{C_u}.\ \alpha \qquad [2.\ 11]$$

where: Nc is the bearing capacity factor for cohesive soil; Cu is the undrained shear strength of cohesive soil; γ' is the effective unit weight; H is the depth of the helix from ground surface; H_{eff} is the effective depth of the pile shaft; and α is the adhesion factor. For the uplift loading condition, Nc is to be determined from the following Equation:

$$N_c = 1.2\left(\frac{H}{D}\right) \leq 9 \qquad [2.\ 12]$$

The Cylindrical Shear Model (CSM) is usually adopted for multi-helix helical piles when the helices are spaced closely, thus, the shaft resistance is enhanced by the contribution of the friction along the confined cylinder of soil between the top and bottom helices of the helical pile

in addition to the upper or lower helix bearing based on the loading condition. Using CSM in cohesive soils, Tappenden and Sego (2007) proposed the following equation for predicting the cylindrical shear capacity:

$$Q_{cyl} = \pi . d . \mathrm{C_u} . \alpha . (H_n - H_1) \quad [2.13]$$

where: H_n and $H_1$are depths of the lowermost helix and the uppermost helix below the ground.

In frozen soils, however, there have been no specific formulations for estimating ultimate capacity of helical piles based on adfreeze strength of pile-soil interface. Johnston & Ladanyi, (1974) suggested that the performance of helical piles would be similar to those exhibited by deep circular footings which usually attain their ultimate bearing capacity only after a large displacement proportional to the footing diameter (D). This was also reported by Hanna and Carr (1971) when a pile displacement up to 20%D was necessary to attain the ultimate capacity of a 38-mm diameter helical pile in sand. Similarly, Bhatnagar (1969) found that for a 75-mm diameter plate anchor in silty clay, a displacement equal to 50%D was needed to fully mobilize the anchor. In contrast, Johnston & Ladanyi, (1974) argued that much smaller displacements would be required to mobilize the ultimate shear strength at the pile-soil interface, for example, on the lateral surface of grouted rod archers or other smooth-shafted piles. As such, Johnston & Ladanyi, (1974) proposed a pile creep model to predict the allowable displacement of helical piles in frozen grounds under the design loads. This model will be discussed in details in the following section.

2.3.2 Deformation behaviors of frozen grounds and piles in frozen grounds

One of the first attempts to comprehend upon creep behavior of frozen soils was by Glen (1952, 1955). His studies were performed in laboratory to evaluate the temperature-dependent creep

behaviors of randomly oriented polycrystalline ice. He reported three different stages that distinguished the deformation behavior of ice samples under compression stress. The first stage occurred right after the load application and was featured by a small instantaneous elastic deformation recorded at the loading outset. In the second stage, the ice sample continued to deform at a slower rate that tended to decrease with time forming a transient stage. A secondary creep was eventually observed and featured the third stage where a steady state creep rate was usually obtained. The samples were also reported to experience reacceleration after showing a steady state when subjected to a very high pressure and the ice ultimately experiencing failure. Since the ice is a crystalline material, its deformation was modeled using similar creep theories for metals (Hult 1966; Odquist 1966). Glen (1952, 1955) adopted this phenomenological model and proposed the following creep law to describe the flow of polycrystalline ice in simple compression:

$$\epsilon_z = A\,\sigma^n \qquad [2.14]$$

Where ϵ_z denotes axial strain rate; σ denotes axial stress; A is constant for a given temperature and ice type; n is an experimentally derived exponent. Schreve and Sharp (1970) conducted survey study on several boreholes in the Blue Glacier and reported reasonable correspondence between the field data and a flow law of the form suggested by Glen (1955).

The log-log plot of strain ϵ_z versus stress σ, yielded an exponent "n" approximately equal to 4. However, a slight curvature started to form when the applied stress became relatively higher indicating that greater exponent values could be observed at higher stress levels. Although steady-state conditions were apparently established in few of Glen's (1955) tests, Morgenstern et al. (1980) believed that this early work provided a remarkable reference for the abundant number of studies that followed. A smaller exponent “n” of 1.8 was reported by Mellor and Testa (1969b) when conducted long-term, low-stress tests at -2°C and defined a power law relationship. They

later combined these results with others (Mellor and Smith 1967; Mellor and Testa 1969a) to propose a power law relationship that represented a much wider range of stresses.

Mellor and Testa (1969a) evaluated the impact of temperature on the steady-state creep rates, and reported that the apparent viscosity of ice decreases with increasing temperature. Creep measurements by Butkovich and Landauer (1959, 1960) showed linear viscous behavior dominated for low stresses and temperatures near the freezing point. For temperature colder than - 1°C and stresses higher than 43 kPa, Voitkovskii (1960) reported non-linearly viscous behavior for polycrystalline ice using both torsion and simple shear tests.

Barnes et al. (1971) suggested that the total creep strain of polycrystalline ice would be the resultant of the elastic, transient strain and the steady-state creep strain and can be expressed in the following form.

$$\epsilon = \epsilon_o + B\, t^{\frac{1}{3}} + \epsilon_s t \qquad [2.15]$$

where: ϵ_o denotes the instantaneous elastic strain; B denotes an appropriate constant for transient creep; ϵ_s denotes the steady-state creep rate; t is time.

Barnes et al. (1971) believed that the proposed equation could be used to extract steady-state creep rates from short-term, low-stress tests, given that transition process would occur during the tests. This method was used to estimate secondary creep rates over a wide range of temperatures and stresses.

In 1973, Colbeck and Evans conducted a comprehensive research to investigate creep rate of ice at the pressure melting point. The results were used to constitute the following flow law equation:

$$\epsilon = A\sigma + B\sigma^3 + C\sigma^5 \qquad [2.16]$$

where: A, B, and C are material and temperature dependent parameters.

Morgenstern et al. (1980) suggested that strain rates estimated by Colbeck and Evans (1973) were one order of magnitude higher compared to Mellor and Testa (1969b) under similar stresses. However, given the small total creep strains and relatively short test durations (200 hrs. maximum) reported in Colbeck and Evans (1973) study, Morgenstern et al. (1980) proposed that true steady-state conditions may not have been achieved; thus, the results of Colbeck and Evans' (1973) study should be used with caution.

Observation of creep movement of ice bodies under the effect of their self-weight gravity stresses have led to establishing different constitutive models and deriving different flow laws of ice. Meier (1960) utilized both vertical and transverse velocity profiles recorded on the Saskatchewan Glacier and proposed a flow law for glacier ice at temperatures close to the melting point that can be best described by the form:

$$\epsilon = B\sigma + A\sigma^{n} \qquad [2.17]$$

where: A and B are material dependents for a given temperature and ice type. The multiaxial creep law proposed by Meier (1960) utilized the Glen's (1955) simpler power law at lower stresses and another component that account for viscous strain. Morgenstern et al. (1980) emphasized that, at low stresses, a considerable error may be encountered when analyzing Meier's (1960) field data. This was further confirmed by the Meier's (1960) expression of uncertainty and by the significant scatter evident in his field data. Paterson and Savage (1963) and Budd (1969) analyzed data collected from the Athabasca Glacier boreholes and Tuto ice ramp in Greenland respectively. Their results showed a general agreement with Meier's (1960) results, but also exhibit significant scatter in the low-stress region and all subject to the same interpretive difficulties.

Another interpretation analysis was conducted by Raymond (1973) utilizing field data from several glaciers and using a three-dimensional velocity distribution. This study supports the

validity of extrapolating a simple power law for low shear stresses (effective shear stress, 0 - 90 kPa). The uncertainty that accompanies data interpretation was reduced by Thomas' (1971, 1973a, b) proposal which considers the deformation behavior of floating ice shelves. In 1973, Thomas derived equations to estimate the creep of an ice shelf, and respectively used the equations to interpret deformation data obtained from several locations in the Arctic and Antarctic (Thomas 1973b). He reported good agreement between field measurements and an extrapolation of test results from a previous laboratory study on creep conducted at higher stress levels (Barnes et al. 1971). This finding was believed to provide an important extension to the application of the flow law for ice at low stresses. Thomas (1973b) suggested that the Glen's form with an exponent n = 3 could be applicable to adequately describe the creep behavior of ice shelves over the stress range of 60-1500 kPa, and could also be extended to stresses less than 20 kPa considering average temperatures ranging from -6 to -16°C. Morgenstern et al. (1980), however, stated that it remains not well defined whether this flow law is valid at temperatures closer to the freezing point or not.

When a plastic material is subjected to a constant load, it deforms continuously. The initial strain is roughly predicted by its stress-strain modulus. The material will continue to deform slowly with time indefinitely or until rupture or yielding causes failure. In general, the creep response of the frozen soil under the applied load can occur in one of three ways depending on the ice content, stress level, and ground temperature. These stages are known as primary creep, secondary creep, and tertiary creep rate (Nixon and McRoberts 1976). In primary creep, the creep rate is continually decreasing, in the secondary stage the creep rate is constant, and in the tertiary creep phase the creep rate continually increases.

Although some studies reveal that frozen soils exposed to high stresses may undergo all three stages of the classical creep successively, soils tested at low stresses, however, mostly show either primary creep or a short period of primary creep followed by a secondary creep behavior.

Nixon and McRoberts (1976) developed analytical solution to predict axial strain of frozen soils using published creep data obtained from uniaxial creep test conducted on ice. The reason behind using creep data for ice was the lack of creep data for frozen soils at the stress level of interest which has been defined to be between 0 and 138 kPa as per typical foundation loads. The data was plotted in a log-log scale (Figure 2.2) and power law fitting curves were used to describe creep parameters for a range of temperature from 0 to -11°C. Accordingly, the following formula was proposed:

$$\epsilon_z = B_1 \, \sigma_z^{n_1} + B_2 \, \sigma_z^{n_2} \qquad [2.18]$$

where: $B_1, B_2, n_1,$ and n_2 are temperature dependent fitting parameters, and σ_z is the applied axial stress.

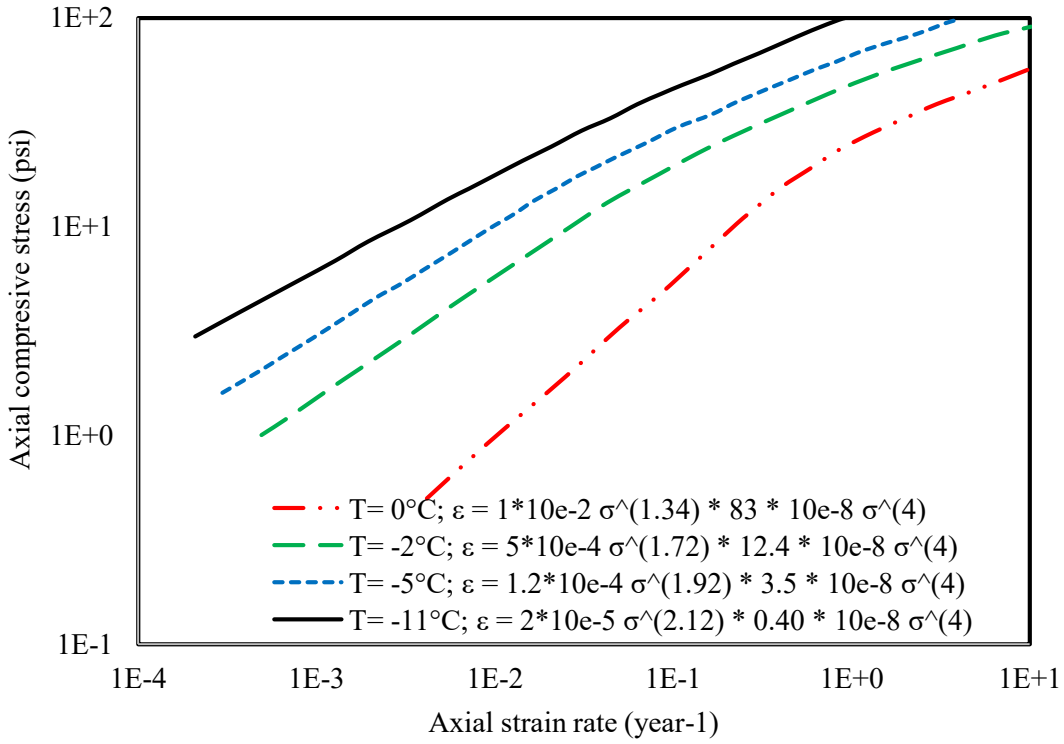

Figure 2.2 Axial stress versus axial strain for ice (after Nixon and McRoberts 1976).

By plotting the fitting parameters versus (T+1) on a double logarithmic graph as in Figure 2.3 and Figure 2.4, the authors were able to provide approximate correlations to predict the fitting parameters for a given temperature as follow:

$$B_1 = 8E^{-3}\,(T+1)^{-2.37}$$

$$B_2 = 1E^{-6}\,(T+1)^{-1.9}$$

$$n_1 = 1.35\,(T+1)^{0.2}$$

$$n_2 = 4$$

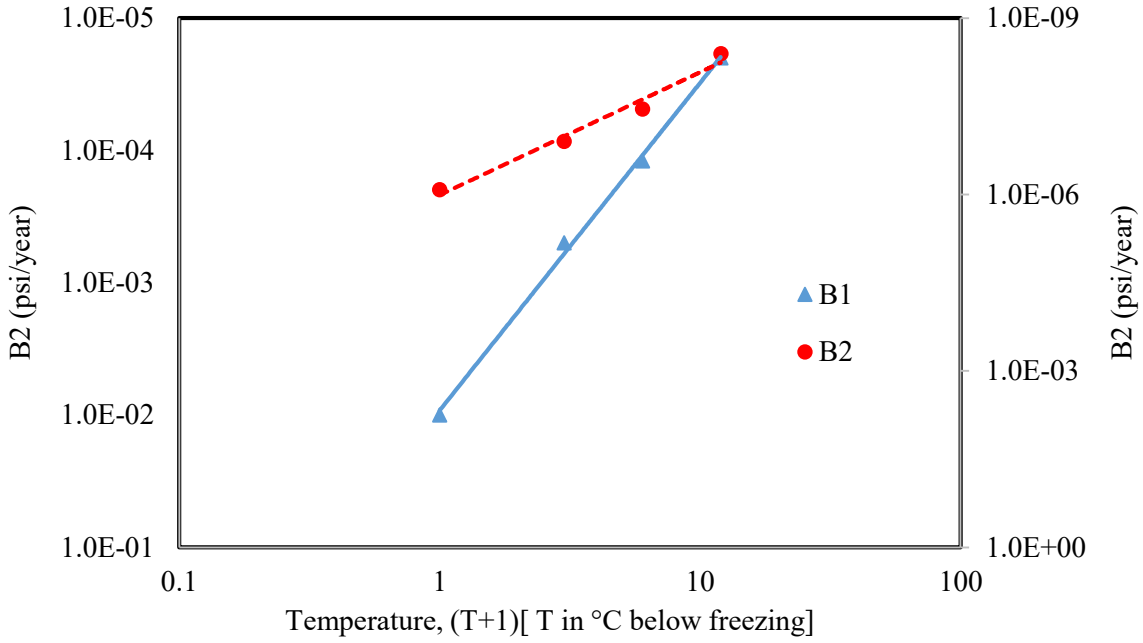

Figure 2. 3 Temperature dependent parameters for flow low of ice (after Nixon and McRoberts 1976).

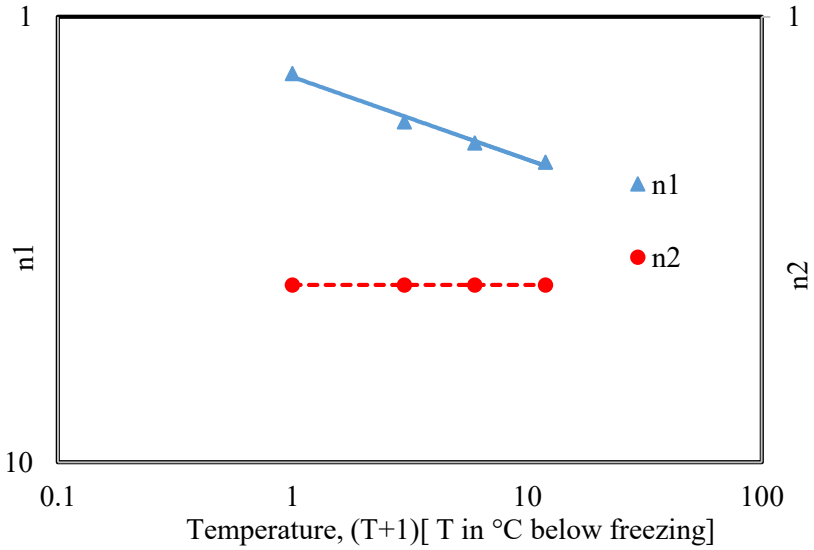

Figure 2. 4 Variation of the exponent "n" with temperature (after Nixon and McRoberts 1976).

where: T is the temperature below the freezing point. By substituting these parameters in the axial strain equation, the following formula is obtained:

$$\epsilon_z = 8E^{-3}\,(T+1)^{-2.37}\;\sigma_z^{1.35\,(T+1)^{0.2}} + 1E^{-6}\,(T+1)^{-1.9}\,\sigma_z^4 \qquad [2.19]$$

The creep parameters for ice and ice-rich soils at various freezing temperature were also summarized by Nixon and McRoberts (1976) and presented here in Table 2.1.

Table 2. 1. Creep parameters for ice and ice-rich soils (Nixon and McRoberts 1976).

Temperature (℃)	B_1 (psi^{-1}. year $^{-1}$)	n_1	B_2 (psi^{-1}. year $^{-1}$)	n_2
0.0	1.0E-2	1.34	83E-8	4.0
-2.0	5.0E-4	1.72	12.4E-8	4.0
-5.0	1.2E-4	1.92	3.5E-8	4.0
-11.0	2.0E-5	2.12	0.4E-8	4.0

Nixon and McRoberts (1976) emphasized that the proposed solution was formed based on available creep data on ice and should be modified accordingly as more creep data on frozen soils becomes available. They, later, used the ice creep law described in equation [2.9] to predict the normalized steady state creep rate of piles displacement rate $\frac{u_a}{a}$ in frozen ground based on the applied shaft shear stress (τ_a) and the following equation was proposed:

$$\frac{u_a}{a} = \frac{3^{\frac{n_1+1}{2}}\,B_1\,\tau_a^{n_1}}{n_1-1} + \frac{3^{\frac{n_2+1}{2}}\,B_2\,\tau_a^{n_2}}{n_2-1} \qquad [2.20]$$

where: u_a is the steady pile displacement rate, τ_a is the applied shaft shear stress in terms of the pile radius (a), and B and n are the temperature dependent parameters determined from uniaxial creep data for the frozen soil in question.

Morgenstern et al. (1980) improved the axial strain model proposed by Nixon and McRoberts (1976) by including additional creep data on ice and came up with different temperature-dependent parameters B and n. However, the stress-strain relationship on the log-log scale was found linear unlike to the nonlinear relationship reported by Nixon and McRoberts (1976). The creep parameters from Morgenstern et al. (1980) are summarized in Table 2.2.

Table 2. 2. Creep parameters for ice and ice-rich soils (Morgenstern et al. 1980).

Temperature (°C)	B (psi^{-1}. year $^{-1}$)	n
-1.0	4.5E-8	3
-2.0	2.0E-8	3
-5.0	1.0E-8	3
-10.0	5.6E-9	3

These parameters were then used to develop a new flow law for piles in ice or ice-rich soils. This model is believed to capture substantially slower strain rates at a given stress and results in much smaller predicted settlement for a pile under a given load. The new flow law model was given the following format:

$$\frac{u_a}{a} = \frac{3^{\frac{n+1}{2}}\ B\ \tau_a^n}{n-1} \qquad [2.21]$$

The two pile creep models proposed by Nixon and McRoberts (1976) and Morgenstern et al. (1980) are used to constructed a graphical illustration of the correlation between the normalized creep rate (h^{-1}) and the applied shaft stress (kPa) and presented in Figure 2.5.

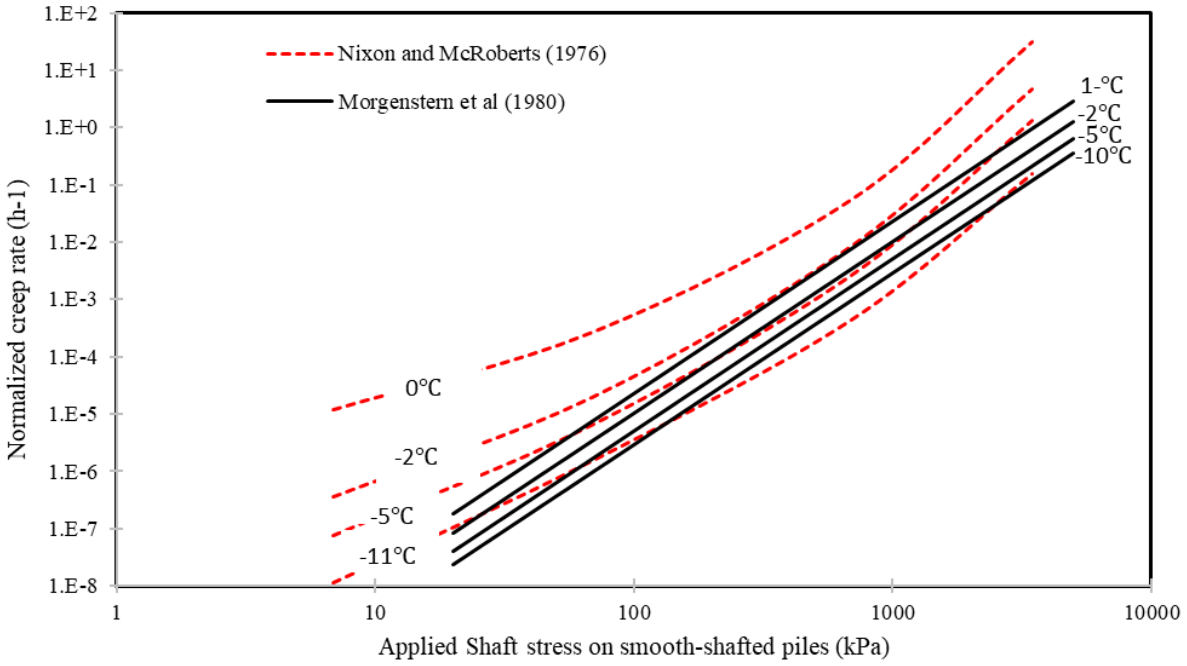

Figure 2. 5. Summary of pile creep models proposed by Nixon and McRoberts (1976) and Morgenstern et al. (1980).

Weaver and Morgenstern (1981) conducted a comprehensive research on the pile performance in permafrost and stated that pile design in ice-rich soils should be governed by settlement while pile design in ice-poor soils should satisfy both strength criteria and settlement. Therefore, they proposed a creep law for ice-poor soils taking into account the effect of confining pressure on the primary creep as follow:

$$\epsilon_1 = D(\sigma_1 - j\sigma_3)^c \, t^b \qquad [2.\ 22]$$

where

$$j = \frac{(1 + \sin \emptyset)}{(1 - \sin \emptyset)}$$

$$D = \left[\frac{1}{w(\theta + 1)^k}\right]^c$$

$\emptyset$ is the internal friction angle, t is the time elapsed after the application of the load (h), θ is the temperature below the freezing point of water (℃) and w, b, c, k are material dependent parameters.

The authors later used the creep law model of the ice-poor soils to derive flow law model for piles in ice-poor condition and proposed the following equation

$$\frac{u_a}{at^b} = \frac{3^{\frac{c+1}{2}}\ D\ \tau^c}{c-1} \qquad [2.23]$$

The creep behavior of pile foundations in frozen soils is also affected by thaw settlement. Different studies have shown the effect of temperature on the pile creep and creep rate. Ladanyi (1995) predicted 35% increase in the creep settlement for a pile exposed to constant axial load installed in an ice-rich silt when the ground temperature increased by 1°C. Nixon (1990a) developed a mathematical expression to predict creep settlement corresponding to permafrost warming. For a pile carrying 200 kN concentrated load and embedded 6m in frozen silty clay at a temperature of -1.3°C, a creep settlement increase of 30% along 25 years was estimated when a warming rate of 0.1°C per year was applied.

One of the earliest studies that physically modeled the behaviors of pile creep in frozen soils was conducted by Parameswaran (1979). Model piles made of wood, concrete, and steel, having different surface roughness were tested in ice-poor soils namely sand and silty sand utilizing cold room facility for freezing. Pile creep was measured at a temperature of -6°C under different axial compression pressures. The observed pile displacement in frozen ice-poor complied with the power law creep rate that was directly related to the applied shear stress at the pile-soil interface. The recorded creep behavior was found to be similar to high temperature steady state creep of viscoelastic materials. The results of this experiment were favorably in agreement with

those obtained by Ladanyi (1972) from field tests on piles tested at Gillam and Thompson, Manitoba when the values for the exponent "n" on a log-log plot of stress vs. creep rate were compared.

In the same study, Parameswaran (1979) evaluated the effect of permafrost freezing on creep behavior of piles in ice-poor soils. The researcher lowered the test temperature from - 6 to -10°C and observed the corresponding creep behavior under the new thermal condition. The result showed a reduction in the steady state creep rate of the pile by almost an order of magnitude after 24 hours' exposure to -10°C. Later, the temperature was brought back to -6°C to evaluate the effect of permafrost warming. The creep rate increased and steadied at a rate lower than the original rate before freezing (Figure 2.6). The small hesitate in the creep rate was attributed to the large portion of unfrozen water content underwent freezing as the temperature lowered from - 6 to - 10°C and remained partially unrecovered after warming.

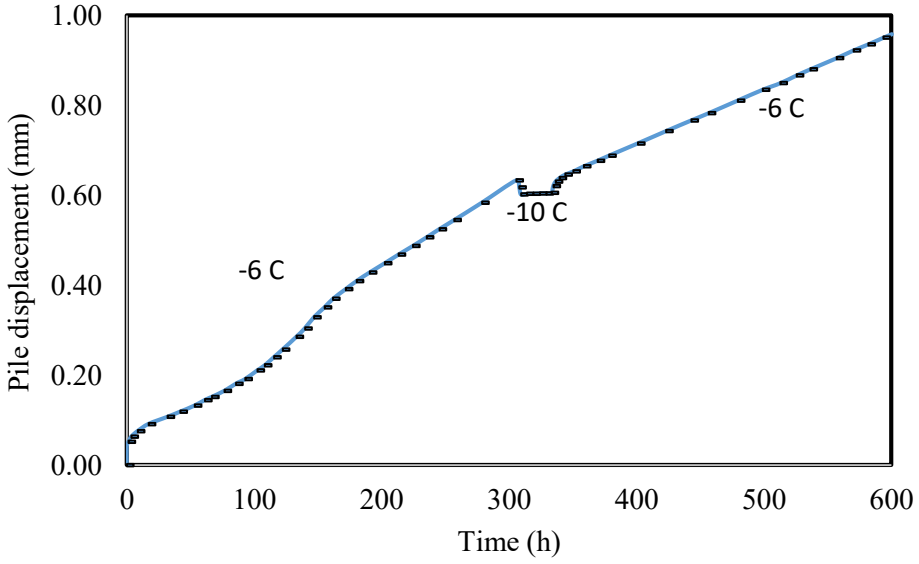

Figure 2. 6 Impact of thermal change on creep rate of a model pile in frozen soil (after Parameswaran 1979).

Using creep data from pull-out tests conducted on single helix helical piles in frozen silty clay, the authors derived the following equations to estimate pseudo-instantaneous displacement and the creep rate of the helical pile respectively:

$$F(q_{net}) = s_i = s_c^i \frac{C(q_{net}+\gamma D)}{q_{as}^i-(q_{net}+\gamma D)} \qquad [2.24]$$

$$G(q_{net}) = s^{\cdot} = s_c^{\cdot} \frac{C^-(q_{net}+\gamma D)}{q_{as}-(q_{net}+\gamma D)} \qquad [2.25]$$

In these two equations, $F(q_{net})$ and $G(q_{net})$ are the pseudo-instantaneous displacement and the creep rate respectively, and s_c^i and $s_c^{\cdot}$ are arbitrary constants. The other four parameters, C, q_{as}^i, C^-, and q_{as}, could be determined by plotting the field data for pseudo-instantaneous displacement and creep rate for each creep stage in a linearized stress-strain plot format. Subsequently, the time required (t_{req}) to reach the measured allowable displacement (S_{all}) is then estimated using the following form:

$$t_{req} = \frac{S_{all}-F(q_{net})}{G(q_{net})} \qquad [2.26]$$

The observations made by Johnston & Ladanyi, (1974) supported the previous hypothesis and concluded that helical piles in frozen grounds tended to exhibit large displacement before reaching their ultimate pull-out capacity. In fact, helical piles experienced significant displacement rates under relatively small uplift pressures resulting in very quickly reaching the maximum allowable deformation.

2.4 Freezing Induced Normal Stress in Frozen Grounds

Pile foundation in unfrozen saturated soils are exposed to normal stress from overburden pressure which can be easily calculated from the saturated unit weigh of the soil. Normal stress may increase

right after pile driving due to the increase in pore water pressure. However, the mobilized normal stress is expected to relax upon pore water pressure dissipation within few hours to few days based on the type of the surrounding soil (i.e., coarse-grained soil or fine-grained soil). In unsaturated expansive clay, normal stress may increase following to water infiltration because of swelling pressure (Puppala and Cerato 2009; Nelson et al. 2015), thus, pile foundation in such soils may experience increase in normal stress exerted on their shaft. The topic of normal stress and swelling pressure in unfrozen grounds is well-established and extensively investigated by many researchers including Richards and Kurzeme (1973), Sudhindra and Moza (1987), Moza et al. (1987), Puppala and Cerato (2009), and Nelson et al. (2015). However, in frozen grounds, normal stress is still widely undefined especially following to pile installation.

Weaver and Morgenstern (1981) stated that the normal stress exerted on the pile shaft in frozen grounds is typically less than 100 kPa and may be neglected. However, Ladanyi and Theriault (1990) reported that the normal stresses in frozen soils may become greater than the initial state following to pile installation. This mobilized stress happens due to the frost heave associated with slurry refreezing or soil freeze-back around the pile and may not relax in short time because of the extremely low permeability at the pile-frozen soil interface. However, the magnitude of normal stress increase following to soil freeze back is still widely unknown and received scant attention.

Practically, installation of pile foundations in frozen grounds could induce normal stress increase at any depth along the pile shaft. This happens following to slurry refreezing around piles installed in oversized holes, or by soil freeze-back occurrence after direct pile driving in pre-thawed frozen ground or in a slightly undersized hole. The process of freezing induced normal stress and the stress distribution around the pile after driving in pre-thawed frozen ground is illustrated in the conceptual model in Figure 2.7.

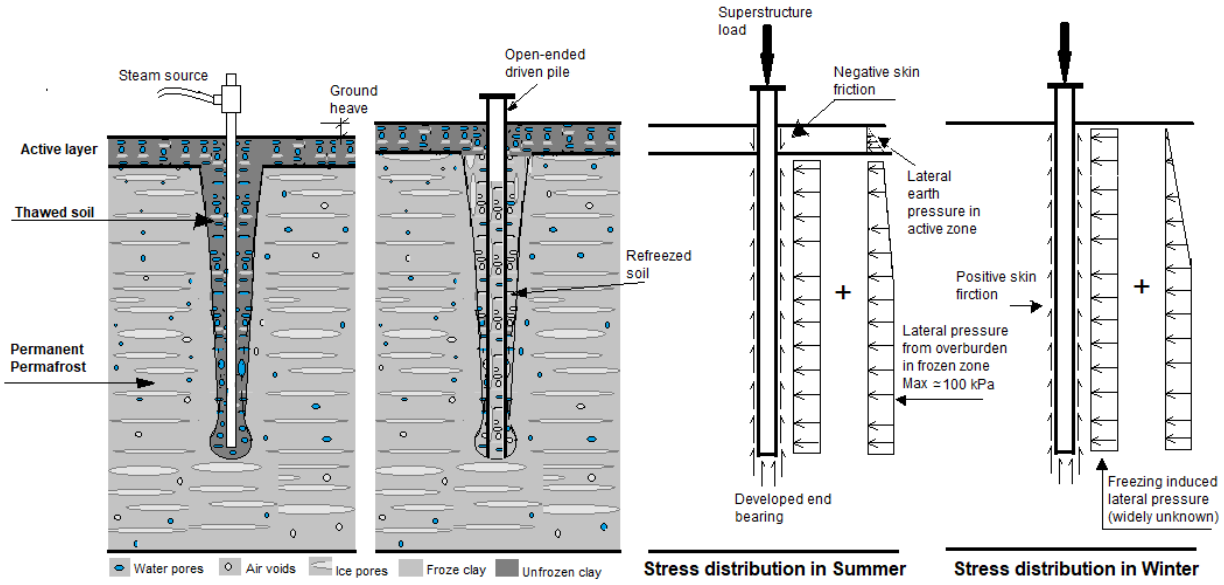

Figure 2. 7 Pile installation in pre-thawed soil and normal stress distribution from overburden and freeze-back pressure.

Frozen ground is first melted to a desired depth using steam or hot water jet. Subsequently, the pile is driven into the melted soil and usually loaded on the head to minimized vertical jacking associated with frost heave during the process of soil freeze-back. Melted soil will start to freeze and may acquire significant freezing condition within hours to few days (Johnson & Buska, 1988). As the soil is frozen-back, its volume increases due to the phase transformation of water from liquid to ice. The volume growth of the refrozen soil is likely to be restrained by the surrounding frozen boundary, thus, enhancing normal stress around the pile shaft which respectively contributes to a greater skin friction. Ladanyi (1988) theoretically showed that the mobilized lateral pressure due to pile installation in ice-rich soils may relax within 24 hrs. falling to less than 1% of the before-installation lateral pressure. Nevertheless, a rapid dissipation of the mobilized lateral pressure may not occur in frozen soils because of their extremely low permeability and long consolidation time that could be longer than the service life of the structure. This was shown in Johnson & Buska, (1988) where a pile shaft strain associated with freezing induced normal stress gradually increased from Oct. 1983 to Feb. 1984 and declined to zero when the soil entirely melted in May 1984. The dissipation of the freezing induced normal stress was mainly due to the melting of the seasonally frozen active layer. Given that piles

are often driven deep enough into the permanent frozen ground; the induced normal stress may not relax in a short time. Therefore, including the contribution of freezing induced normal stress acting on the pile shaft could be important for pile design and installation in permeant frozen ground in term of accurately estimating ultimate bearing capacity and frost heave.

Measurement of the freezing induced normal stress in frozen ground may be complicated and lack of standard testing techniques. Unlike frozen ground, determination of the normal swelling pressure in unfrozen soils is available through both laboratory and in-situ techniques. Review of some recently developed measuring techniques of swelling pressure in unfrozen soils may help determine their applicability for freezing induced normal stress testing.

2.4.1 Laboratory testing technique for swelling pressure in unfrozen soils

One of the commonly used testing techniques for measuring normal swelling pressure in unsaturated unfrozen soils is the modified Oedometer apparatus (Ofer 1981; Saba et al. 2014). The Oedometer cell in the conventional Oedometer apparatus was modified to provide measurements of swelling pressure through implemented strain gauges (type A Oedometer) (Figure 2.8a) or directly through implemented pressure cells and transducer (type B Oedometer) (Figure 2.8b).

The type A Oedometer consists of strain gauges placed on the outer surface of the ring through which the radial deformation of the ring is measured. The type A Oedometer is also equipped with a T5 type of tensiometer inserted into the soil sample through the bottom of the apparatus. The T5 tensiometer is meant for the measurement of soil suction. The layout of Oedometer type B is similar to Oedometer type A except for the oedometer ring. The inner side of the Oedometer ring is equipped with a rubber membrane to allow for the control and measurement of radial pressure and deformation via a pressure cell. The space between the ring and the membrane is filled with a fluid. this modification makes the working mechanism of Oedometer type B is similar to those in a triaxial apparatus.

The working mechanism of the modified Oedometer apparatus could be effective in determining the normal swilling pressure for unfrozen soils. However, measuring the freezing induced normal stress in

frozen soils using this type of apparatus may be challenging. For frozen soils, the use of T5 tensiometer may not be possible due to the expected fracturing that would happen to the ceramic tip as the liquid water transforms to ice. In type A Oedometer, a dummy strain gauges must be implemented to account for the temperature-induced apparent radial strains that would occur due to the exerted thermal stress. In type B Oedometer apparatus, On the other hand, the fluid in the space between the ring and the membrane may freeze as the temperature drops below the freezing point. This problem may be address by using antifreeze fluid, however, at very low freezing temperature, antifreeze fluid may be still not effective.

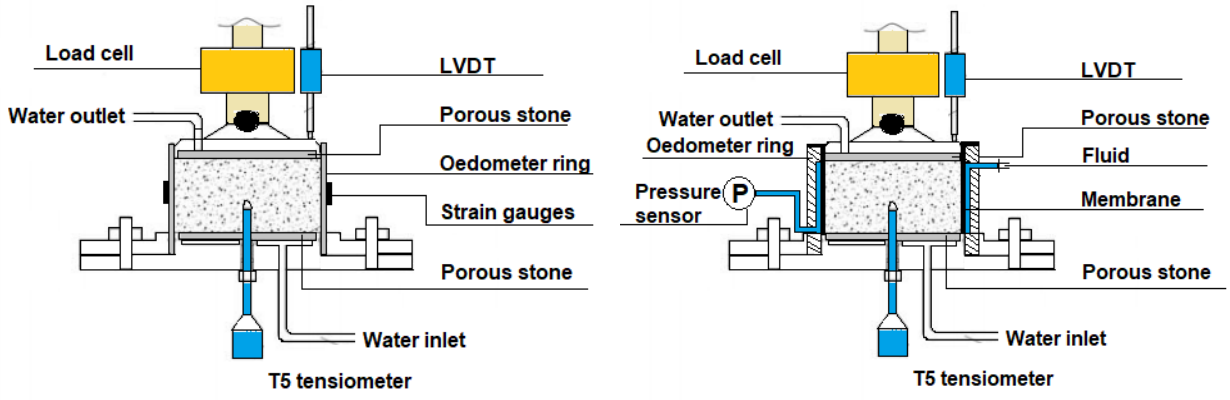

a. Type A Oedometer (modified after Ofer 1981)

b. Type B Oedometer (modified after Saba et al. 2014)

Figure 2. 8. Illustration of different designs of the modified Oedometer apparatus for swelling pressure measurement.

The measurement of the freezing induced normal stress around pile foundation in frozen ground may still be challenging utilizing the modified Oedometer apparatus. The fabrication of the apparatus and the small size of the test samples make it difficult for such measurement to be captured using such laboratory experiment. Therefore, irregular laboratory set up may be required to conduct such experiment., large scale laboratory testing, and more preferably, field testing program and instrumentations may be required for more reliable measurement of the freezing induced normal stress around pile foundation.

2.4.2 Field measurement of freezing induced normal stress

Few attempts were conducted in the past and reported in literature for measuring normal stresses in frozen soils and their contribution to ultimate shear strength of frozen soils and to ultimate adfreeze strength of pile-soil interface. For example, Johnson & Buska, (1988) conducted a well-instrumented field experiment for measuring frost heave force, adfreeze strength of piles, and freezing induced normal stress acting on pile shaft using electric strain gauges along pipe pile and H-pile installed in Fairbanks silt. The strain gauges were mounted along the centerline on both sides of the web for the H-pile and on radially opposite sides of the pipe pile. Strain gauges installed horizontally with respect to the axial direction were interspersed between the axially oriented gauges along the shaft of the instrumented sections. These gauges were utilized to measure transverse strains in the piles and to estimate the magnitude of freezing induced normal compressive stresses in the soil acting on the piles. To account for the temperature-induced apparent strains, dummy strain gauges mounted on thin metal plates with the same thermal expansion properties as the piles were used with one end fixed to the pile to ensure that the gauge-shim system was unstressed (Figure 2.9). Dummy gauges were wired to active gauges to cancel temperature induced apparent strain. The gauges were coated with a waterproof coating and polyurethane foam to provide corrosion protection and insulation.

Johnson & Buska, (1988) reported maximum frost heave forces of 800 kN and 1100 kN subjected to H-pile and steel pipe pile backfilled with silt slurry. The associated adfreeze strength was reported as 214 kPa and 972 kPa respectively. Total normal stress including the freezing induced normal stress acting on the pile shafts were estimated from the transverse strain gauge readings and found to be one third of the adfreeze strength, recording a maximum value of 370 kPa observed on the pipe pile shaft. Similar forces/stresses were recorded over three consecutive winters, i.e., 1983, 1984, and 1985, at relatively shallow depths ranged from 1.4 to 2.2 meters from the ground surface (within the active layer).

Given the relatively shallow depth of instrumented suction of around 3.0 m, the normal stress from the overburden pressure could be minimal compared to the total measured normal stress. The majority of the measured total stress seemed to be resulted from the freezing induced normal stress which in this case

may not be less than 300 kPa. This high magnitude of the freezing induced normal stress suggested that a future design approaches of ultimate adfreeze capacity need to account for such contribution.

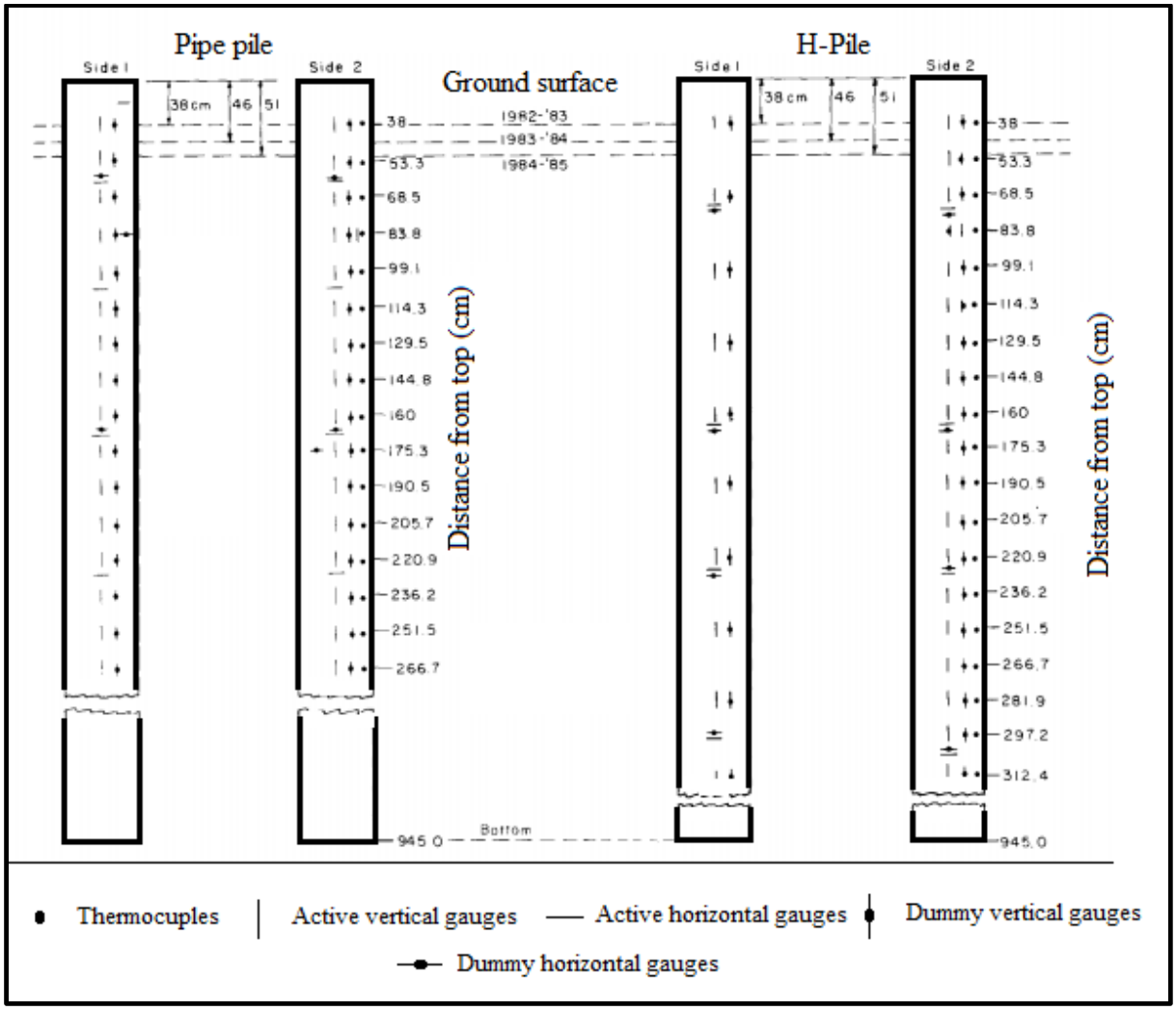

Figure 2. 9. Field instrumentation for measuring frost heave, adfreeze strength and normal stress (modified after Johnson & Buska, (1988).

2.5 Summary

Based on the information available in the literature, the design approaches for piles in frozen ground are derived to address adfreeze strength and creep behavior of piles based on shear strength and creep behavior of the frozen soils. However, roughness factor "m" that correlates adfreeze strength of piles to shear strength of frozen soils needs to be reevaluated using well-controlled

experiment. Moreover, the creep models for designing pile foundations in frozen ground were often derived using flow law models that incorporate creep parameters of crystalline ice, with very limited creep data on frozen soils. The model proposed by Nixon and McRoberts (1976), for example, was mainly built upon published creep data on ice and then was idealized to describe creep behavior of ice-rich soils claiming that this will be a conservative measure in the absence of reliable creep data on ice-rich soils. Nevertheless, ice-rich soils might behave differently compared to the ice due to the presence of unfrozen water content in ice-rich soils even at relatively low temperatures. In addition, Weaver and Morgenstern (1981) revealed that the use of published creep data on ice were short of reliable information in the temperature range between 0 and -5°C. The average temperature of most of Canadian permafrost falls below -3°C, therefore, it is important to understand the behavior of frozen soils at this level of temperature and predict the behaviors of pile foundation in such thermal boundary condition.

This research is aimed at complementing the previous work done by other researchers to investigate the performance of pile foundations in warming permafrost. Strength and deformation characteristics were tested for different types of frozen soils including undisturbed Leda clay and remolded Ottawa sand. The tests were conducted at various temperatures including temperatures slightly below the freezing point. The goal is to develop temperature dependent solutions that can predict bearing capacity and creep rate of piles installed in warming permafrost.

CHAPTER 3: INTERFACE SHEAR STRENGTH CHARACTERISTICS OF STEEL PILES IN FROZEN CLAY UNDER VARYING EXPOSURE TEMPERATURE

3.1 Introduction

Load carrying capacity of pile foundations installed in ice-rich soil is important not only in naturally frozen ground such as in cold regions but it is of interest for pile foundations used in artificial frozen ground. Although the performance of pile foundations in ice-rich soils may be governed by time dependant creep deformation, their load carrying capacity based on ultimate adfreeze strength may still be critical for temporary structures and mobilized camps. It is also important for any type of structures situated on warming frozen ground. As the available design approaches have limited accountability for effects of temperature on the predicted adfreeze strength of pile foundations, this chapter was aimed at studying the impact of changing ground temperature on the roughness factor “m” used mainly to predict adfreeze capacity of pile foundations based on shear strength of the surrounding ice-rich soils. Thus, complementing other previous research efforts for developing a sound design method for pile foundations in ice-rich soils.

This chapter, therefore, summarizes results from experimental programs dedicated to evaluate the thermal exposure impact on shear strengths of ice-rich soil and shaft resistance of steel piles in ice-rich soils. Several direct shear tests were conducted inside a temperature-controlled environmental chamber to measure cohesion and friction angle of frozen soil, steel-soil adhesion, and steel-soil friction angle at different temperature and normal stress levels. The roughness factor "m" was accordingly re-evaluated under different thermal boundaries and loading

conditions. Moreover, this chapter discusses the contribution of frictional resistance to the shaft capacity of steel piles in ice-rich soils. The effects of shear rate on shear strengths of ice-rich soil and shaft resistance of steel piles in ice-rich is also evaluated. Th evolution of thermally induced normal stress acting on pile shaft for pile foundations installed in ice-rich soils is carefully assessed. This is studied by employing a laboratory physical model that enabled measuring the induced normal stress directly through a load cell positioned on the side of the soil sample that encircled a steel model pile simulating the testing mechanism of modified type B Oedometer. The development of unfrozen water content during freezing is also observed and reported.

3.2 Test Materials

3.2.1 Soil material

A marine soil known as Leda clay was used in this experiment to represent the ice-rich frozen materials. The clay soil was sampled intact from the Navan Landfill site in Ottawa, Ontario. The soil samples were collected undisturbed in 200-liter steel barrels that were carefully pushed into the natural Leda clay forms using a backhoe (Figure 3.1). Before sampling, the bottoms of the barrels were drilled at their centres to generate holes which would enable the air to escape while pushing the barrels into the soil. The inside surface of the barrels was coated with a thin layer of wax followed by another layer of lubricant to facilitated soil sampling. The top 500 mm of the clay soil in the field was removed and the open sides of the barrels were then placed on the exposed clay soil. The barrels were then gently pushed into the soil using backhoe until the soil reached the bottoms of the barrels. The soil surrounding the barrels was then excavated and the barrels were lifted up and unloaded from the backhoe and put on their bases. After sampling, the top of the clay sample was trimmed, waxed, and sealed with airtight plastic sheet followed by a steel led to ensure

maintaining the natural water content of the collected samples. The barrels were then loaded on a truck using a loader and tightened enough to prevent falling or movement during transporting to the laboratory.

Figure 3. 1. Soil sampling at the Navan landfill site in Ottawa.

The basic geotechnical properties of Leda clay including particle size distribution, Atterberg limits, bulk density, and the natural water content were examined (Table 3.1). Particle size distribution and clay contents of Leda clay were determined using sieve analysis and hydrometer tests in accordance with ASTM D422-63. The liquid limit of the soil was 51% while the plasticity index was 24% based on Atterberg limit test results (ASTM D4318-10). The average bulk density and water content of the test soil were 1.62 Mg/m^3 and 75% respectively. Hydraulic conductivity of the clay sample was also measured following the Falling Head testing technique and using a Rigid-Wall mold (ASTM D5856-95, 2007) equipped with a rubber membrane to minimize side-wall leakage (Table 3.1).

Table 3. 1. Physical and hydraulic properties of the test soil.

Characteristic	USCS	$w_{i_{ave}}$ (%)	LL (%)	PI	$\rho_{b_{ave}}$ (Mg/m^3)	%clay	Activity	k (m/s)
Physical & hydraulic Properties	CH	75	51	24	1.624	71	0.34	5.9E-10

A chemical analysis was also performed on the extracted pore waters obtained by squeezing the soil samples under very high pressure. Cation concentrations including potassium, calcium, and magnesium ions were determined in the pore water (mg/l), while sodium concentration was measured based on acid extractable sodium ions (mg/kg). Cation exchange capacities (CEC) were determined and the results presented in Table 3.2.

A random X-ray powder diffraction analysis was carried out to determine the mineralogical composition of Leda clay. Semi-quantitative analysis was conducted on the X-ray results to measure the clay mineral components. The abundant clay mineral found in this Leda clay soil was illite comprising 83%. The remining mineral portion was kaolinite and chlorite with amounts of 11% and 6% respectively. The results indicated no evidence of having any expandable clay minerals (here defined as vermiculite, montmorillonite, or interlayered illite/ smectite) in the test soil (Table 3.2).

Table 3. 2. Chemical and mineralogical properties of the test soils.

Characteristic	Sodium (mg/kg)	Potassium (mg/l)	Calcium (mg/l)	Magnesium (mg/l)	(CEC)* meq/100g	Illite	Chlorite	Kaolinite
Chemistry and Mineralogy	1700	15	83	40	18	83	6	11

*Cation exchange capacity.

3.2.2 Characteristic of the model pile material

Structural steel specimens are used in this study to represent the pile material for pile-soil interface tests. Steel is a common pile material used in cold region for manufacturing steel pile in various geometries including pipe piles, H-section piles, and helical piers. For relatively warm permafrost, Open-ended steel-pipe and H-steel piles can be driven deep enough in permafrost in order to develop sufficient adfreeze bond and provide high bearing capacity. In cold permafrost, closed-ended pipe piles may be installed in oversized predrilled holes and backfilled with sand-water slurry or grouted with concrete. Pile installation in pre-thawed permafrost using steam or hot water is widely used for H-pile and pipe piles (Kitze, 1957).

In this experiment, a steel plate of 90 mm by 90 mm was used to simulate the shaft surface of a typical steel pile. It was machined to couple with the upper half of the direct shear box and provide a steel-soil interface area of 60 mm by 60 mm. The total and the average surface roughness values for this particular type of steel were measured by a FARO arm measuring device and reported to be 9.7 μm and 11.3 μm respectively (Giraldo and Rayhani 2013). The steel plate was equipped with a copper-constantan thermocouple inserted in a 1.0 mm diameter hole predrilled underneath the upper surface of the plate. A 1 mm diameter window was made in the middle of the steel plate such that the sensing end of the thermocouple be in contact with the soil sample in order to track the temperature change at the steel-soil interface (Figure 3.2).

3.3 Test Equipment

The roughness factor represents the ratio between pile-soil adhesion strength and cohesion strength of frozen soils. Obtaining this factor, thereby, would require using a representative cold environment and a suitable testing technique. This experimental investigation was carried out in a walk-in environmental chamber that enabled cooling to the desired freezing temperature through

an automatic temperature controlling system. Although the temperature in the environmental chamber fluctuated within ± 0.5 ℃, the temperature fluctuation within the test samples was ± 0.1 ℃ as tracked by the thermocouples.

For evaluating the adfreeze shear strength and shear strength of frozen clay, a modified direct shear test apparatus was employed in accordance with ASTM D3080/D3080M-11 and ASTM D5321-12. The apparatus consists of conventional and modified shear boxes designed to mount on a shear-rate controlled testing frame (Fig. 2a&2b). The conventional shear box, which was used to test the shear strength parameters of frozen clay, consists of two attachable hollow square parts designed to confine the test sample within the hollow space and machined to facilitate shearing along a predefined horizontal plane. The modified shear box, in contrast, was used to test the steel-soil adfreeze shear strength. It consists of a lower solid square steel plate machined to couple with the upper hollow square part of the shear box such that a steel-soil interface element is produced to simulate pile set up in the field and facilitate shearing along the line of the interface.

The direct shear test apparatus was placed inside the walk-in environmental chamber to enable shear testing at various temperatures below freezing point. The testing mechanism of the apparatus depends on imposing a constant horizontal shear velocity on the test sample while continually recording the shear force, the horizontal shear displacements, and the vertical displacements. The displacements were measured through Linear Variable Differential Transducers (LVDTs) to an accuracy of 0.001 mm. The desired normal pressure was applied using a dead load subjected vertically to the top of the soil sample through a steel bearing arm. The test data was recorded in a frequency of one data point per second using a data acquisition system and plotted instantaneously on a LabVIEW platform.

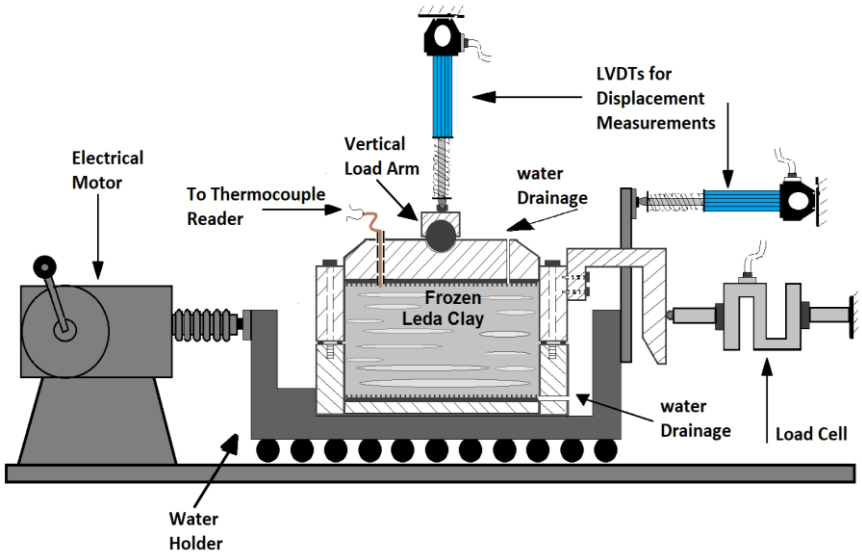

a. Conventional shear box apparatus

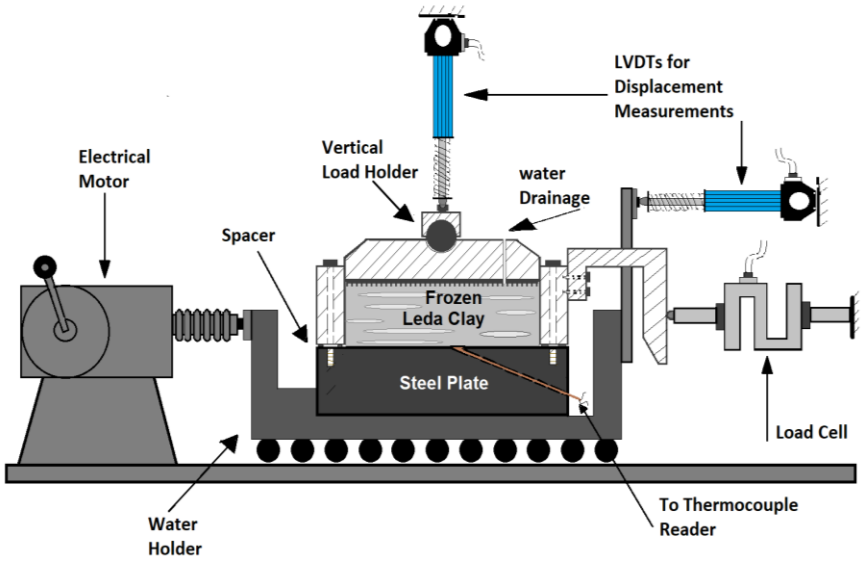

b. Modified shear box set up

Figure 3. 2. Conventional and modified shear box assembly for shear strength testing.

3.4 Sample Preparation

All test samples were obtained from Leda clay soil in the 200-liter steel barrels. Shelby tube sampler with an inner diameter of 101.6 mm was used for soil coring from the barrel. The soil was then extracted from Shelby tube using a mechanical extruder and cut into two different heights;60

mm for frozen soil testing and 30 mm for steel-soil interface testing. For frozen soil testing, the 60 mm-height cylindrical specimens were trimmed to a square shape of 62 mm x 62 mm. The upper hollow square part of the shear box was oiled and gently pushed through the clay specimen followed by the lower part until the soil reached the base of the lower part of the shear box and the two parts of the shear box came in contact. The two parts were then tightened to each other using steel screws followed by trimming the top of the clay specimen to the final height. A similar procedure was followed for preparing the interface samples where the upper hollow square part of the shear box was oiled and gently pushed through the 30mm-height clay specimen. The upper part of the shear box with the contained soil specimen was then placed on top of the steel plate and tightened to each other using two steel screws. The soil specimen in the upper part of the shear box was then gently pushed back against the steel plate to ensure full contact between the soil and the steel plate. The top of the soil specimen was then trimmed to the final height. The final dimensions of the clay specimens used for shear strength testing of frozen clay was 60 mm by 60 mm by 50 mm compared to the specimen's dimension of 60 mm by 60 mm by 25 mm used for adfreeze strength testing of steel-soil interface. The initial bulk density, initial gravimetric water content, and the ultimate shear strength for each test sample is presented in Table 3.3.

Table 3. 3. Summary of initial bulk density and initial gravimetric water content along with ultimate frozen shear strengths at various test conditions.

T (°C)	σ_n (kPa)	Clay soil specimens ($11x10^{-3}$ mm/min)			Soil-steel interface specimens ($11x10^{-3}$ mm/min)			Soil-steel interface specimens ($2.08x10^{-3}$ mm/min)		
		$\rho_{b\,i}$ (Mg/m^3)	w_i (%)	τ_{ult} (MPa)	$\rho_{b\,i}$ (Mg/m^3)	w_i (%)	τ_{ult} (MPa)	$\rho_{b\,i}$ (Mg/m^3)	w_i (%)	τ_{ult} (MPa)
	25	1.621	76.3	1.97	1.634	75.8	1.90	-	-	-
	50	1.625	75.2	2.04	1.628	74.0	1.927	-	-	-
-10	100	1.619	76.8	2.10	1.628	76.5	2.08	-	-	-
	200	-	-	-	1.624	74.2	2.36	-	-	-
	400	1.622	74.9	2.40	-	-	-	-	-	-
-7	25	-	-	-	1.627	77.0	1.356	-	-	-

	50	-	-	-	1.622	75.1	1.45	-	-	-
	100	1.626	75.1	1.561	1.617	76.9	1.50	-	-	-
	200	1.624	74.0	1.60	1.625	73.8	1.80	-	-	-
	400	1.618	76.5	1.791	-	-	-	-	-	-
	25	1.631	74.8	1.10	1.623	76.5	0.833	1.621	78.1	0.588
	50	-	-	-	1.629	74.4	0.90	1.630	75.8	0.67
-4	100	1.624	73.3	1.172	1.624	77.1	0.952	1.628	76.0	0.75
	200	1.619	76.8	1.278	1.631	75.9	1.181	-	-	-
	400	1.627	75.9	1.30	-	-	-	-	-	-
	25	1.617	76.1	0.71	1.632	75.1	0.556	1.624	75.6	0.359
	50	-	-	-	-	-	-	1.625	74.9	0.308
-2	100	1.622	73.6	0.833	1.629	73.8	0.611	1.629	73.8	0.408
	200	1.621	77.3	0.833	1.622	76.2	0.736	-	-	-
	400	1.625	75.4	0.92	-	-	-	-	-	-
	25	1.628	74.2	0.653	1.620	74.8	0.436	-	-	-
	50	1.624	74.0	0.70	-	-	-	-	-	-
-1	100	1.632	74.7	0.683	1.627	75.0	0.522	-	-	-
	200	1.621	74.9	0.744	1.631	75.9	0.597	-	-	-
	400	-	-	-	-	-	-	-	-	-
	25	1.626	73.1	0.40	1.616	76.4	0.236	1.631	73.7	0.142
	50	-	-	-	-	-	-	1.625	74.5	0.159
0	100	1.627	77.6	0.431	1.627	75.2	0.264	1.626	73.1	0.199
	200	1.627	76.3	0.472	1.623	75.9	0.355	-	-	-
	400	-	-	-	-	-	-	-	-	-

The shear box was then mounted on the direct shear test apparatus inside the environmental chamber which was always pre-set to the desired testing temperature before the placement of the test samples inside the chamber. Right after sample placement on the direct shear test frame, the desired normal pressure was applied. This allow for simultaneous consolidation and freezing of the test samples under the desired freezing temperature and normal pressure. The simultaneous action of consolidation and freezing of the test specimens was aimed at producing uniform element test specimens by minimizing formation of ice lenses, and thus reducing inhomogeneity (Wang et al. 2017). The absence of confining pressure during freezing, in particular under slow rate, could lead to formation of small ice lenses that may reduce the uniformity of the test specimens (Viggiani

et al. 2015; Wang et al. 2017). Simultaneous application of normal stress and freezing action in this experiment is also similar to the condition occurred in field following to pile driving in undersized predrilled holes or in pre-thawed soils in cold frozen ground as well as in the case of direct pile driving in warm frozen ground. The ambient temperature in these cases varies based on the present ground temperature and frozen ground condition (i.e., cold or warm). Pile driving in undersized predrilled holes or directly in warm frozen ground is expected to increase the normal stress subjected to the pile shaft from the surrounding soil and generate heat in the pile vicinity. The heat release may cause the frozen ground to melt around the pile. However, freeze-back action would occur due to the present freezing temperature of the frozen ground as well as the thermal conductivity of the steel pile which would transmit the cold air temperature to depth. Thereby, freezing and consolidation are expected to happen simultaneously in the field setting too. In this experiment, complete consolidation may not have been achieved giving the relatively rapid occurrence of sample freezing. Nevertheless, this scenario is expected to occur in field as well. Stress relaxation around the pile in field may, therefore, happen during the process of complete consolidation considering the long-term effects. However, normal stress change in frozen ground following to pile setup is remained widely undefined and still a concern to the engineering community. Although one-dimensional freezing action is expected to happen in field, simulating this field condition was challenging in this experiment. The main difficulties were associated with the limited space around the test sample and the standard instrumentation fabrications of the test apparatus that prevented adopting a reliable measure for imposing 1-D freezing action. Given these limitations, the test samples in this experiment were exposed to freezing from all around. Nevertheless, the soil in field may still experience freezeback from more than one direction post pile installation. Two-way freezing action could be enhanced by the superior thermal conductivity

of the steel pile at one side and the presence of frozen soil in the vicinity of the pile on the other side. Therefore, this experiment is believed to capture many aspects of pile foundations in field.

3.5 Test Procedure

3.5.1 Shear strength testing

A total number of 68 shear tests were conducted in this study to evaluate shear strength of frozen clay and the adfreeze strength of steel-clay interface. Out of the 68 test, 22 tests were used for test-retest reliability assessment and to ensure test repeatability. All tests were conducted following similar procedure. After placing the test sample inside the environmental chamber, it was left for 24 hrs. to acquire thermal and volumetric equilibrium under the desired temperature and normal stress. After 24hrs., the two steel screws were removed to allow for the two parts of the shear box to freely slide on each other along the line of the interface. The shear load was subsequently subjected to the lower part of the shear box/steel plate while the upper part of the shear box was restrained by the load cell for measuring the shear resistance. The shear load was applied at a constant shear rate of 0.011 mm/min (i.e., 16.3 mm/day). This shear rate was adopted from the similar study performed by Ladanyi and Theriault (1990) on ice-poor frozen sand. Using similar shear rates to those reported in literature and applied on different test materials may be useful in discovering the differences in the shear behaviors of various types of frozen grounds. However, other sets of steel-frozen clay interface samples were sheared at slower shear rate of 0.00208 mm/min (3 mm/day) to examine the effect of different shear rates on the ultimate interface shear strength of steel piles in ice-rich clay. The shear tests were conducted at various levels of temperatures including -10°C, -7°C, -4°C, -2℃, -1.0°C and 0°C. At each temperature, the peaks

of shear strengths and interface adfreeze strengths were determined under various normal stresses including 25 kPa, 50 kPa, 100 kPa, 200 kPa, and 400 kPa.

3.5.2 Determination of unfrozen water content and thermally mobilized horizontal stress

Interface shear strength of pile foundations in frozen ground is highly influenced by the amount of unfroze water content. Ice-rich soils would often preserve considerable unfrozen water volume even at relatively low levels of freezing temperature. Unfrozen water content at the pile vicinity could further increase following to pile driving either by using pre-thawing or predrilling driving techniques. The increase of unfrozen water content (UWC) in the region near to pile shaft could minimize the adfreeze strength of the pile-soil interface and reduce the pile's load carrying capacity. However, the surrounding soil is expected to acquire sufficient freezeback within hours to days. This can enhance the adfreeze strength of the pile-soil interface as well as the normal stress due to frost heave. In this study, a physical model was developed to study the evolution of UWC during the process of soil freezing around a steel model pile. The physical model was also set to provide measurements of the normal load that could be generated and subjected to the pile shaft as a result of soil freezing. The physical model consisted of a rectangular steel box that had a length of 400 mm, a width of 100 mm, and a height of 350 mm. The box had two steel partitions that divided the box into three rooms. The meddle room contained the test soil and the pile, while the side rooms where designed to contained fiberglass for providing thermal insulation in addition to a layer of Styrofoam placed at the bottom of the box. This measure was conducted to enhance 1-D downward freezing action. One of the side room, furthermore, contained steel spacers to restrain the steel partition from horizontal movement that may follow soil freezing. The other side room contained a load cell on which the other steel partition was let to bear to measure the exerted horizontal load following to freezing (Figure 3.3).

A block of undisturbed Leda clay soil was broken to small chunks and compacted in four layers within the middle room resulting in final soil sample dimensions of 200 lengths, 100 mm width, and 200 mm height. The model pile was then driven into the compacted clay and bear on the bottom of the steel box. The model pile was a steel tube with outer diameter of 5 mm and height of 350 mm equipped with a pile cap fixed to the steel box to prevent the upward pile heave during freezing.

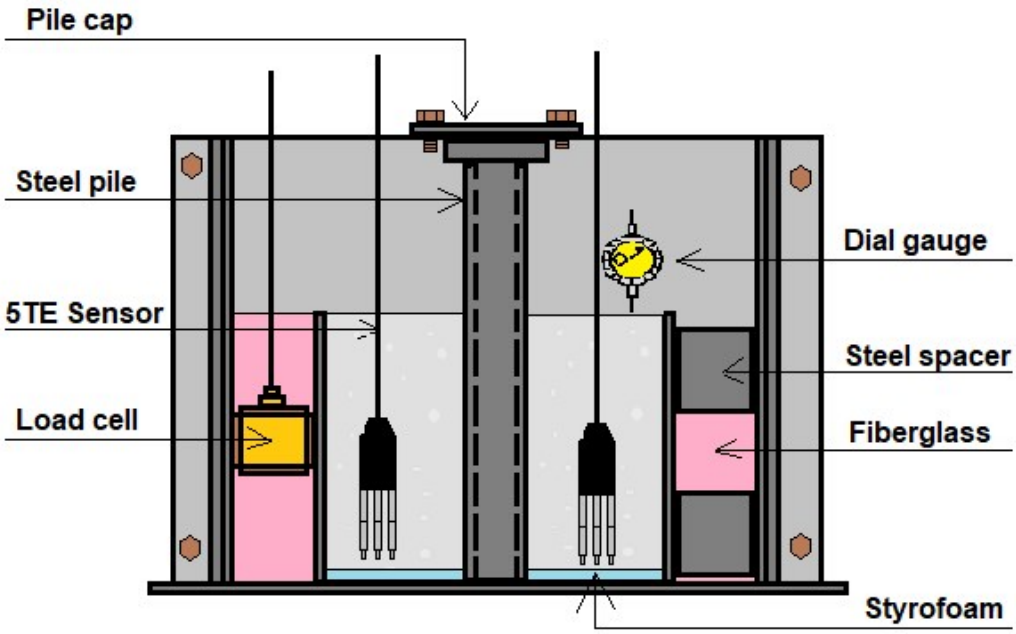

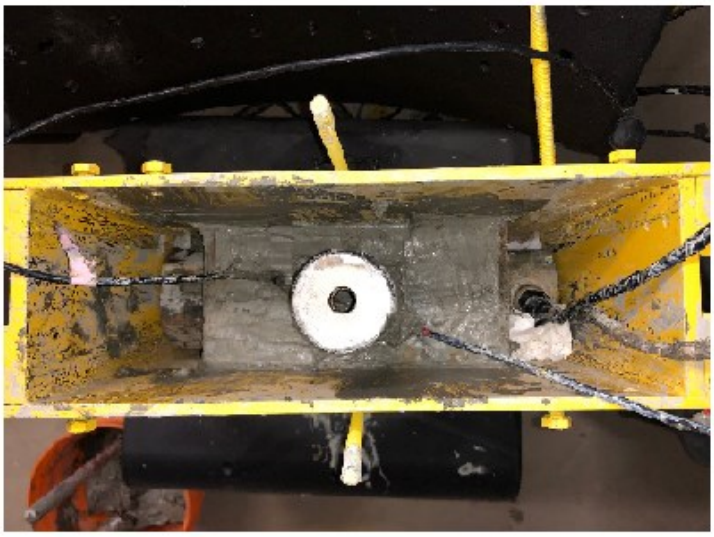

Figure 3. 3. Physical model for measuring unfrozen water content and freezing force acting on pile surface.

The Unfrozen water content was measured at distances of 20 mm and 50 mm from the pile shaft using 5TE sensors which monitor the bulk electrical conductivity (EC), volumetric water content (VWC), and soil temperature. The load cell and 5TE sensors were connected to a PC unit through a data acquisition system to record changes in unfrozen water content and development of the horizontal load associated with soil freezing. The instrumented cell was then placed inside a refrigerator and exposed to thermal loading at freezing rate of -0.06 ℃/min. After recording the maximum freezing stress and the minimum unfrozen water content, the test cell remained under the same freezing conditions for additional 72 hrs. to observe any stress relaxation. A pull-out load test was then conducted on the model pile to determine its ultimate shaft capacity of -7 ℃.and compare it to those obtained from steel-frozen soil element test recorded at the same temperature.

3.5.2.1 Specifications and calibration of 5TE sensor

The 5TE probe uses an electromagnetic field to measure the dielectric permittivity of the surrounding medium. The sensor can provide measurements of electrical conductivity (EC), volumetric water content (VWC), and temperature. As per the manufacturer's specification, the sensor can provide reliable measurements when the temperature is in the range of -40 to 50.0°C. Before using the 5TE sensors in this experiment, the sensors were calibrated by establishing correlation between the directly measured VWC and the sensor-measured VWC following the calibration procedure outlined by Starr and Palineanu (2002). The calibration was conducted as follow:

a- A 1000 ml cylinder and 500 ml PVC column were prepared.

b- Five clay samples were air-dried to different gravimetric water contents.

c- The volume of the 5TE sensor was determined by advancing it in a 1000 ml cylinder that was half full of water. The volume of the sensor would be equal to the increase in water level in the cylinder (Figure 3.4).

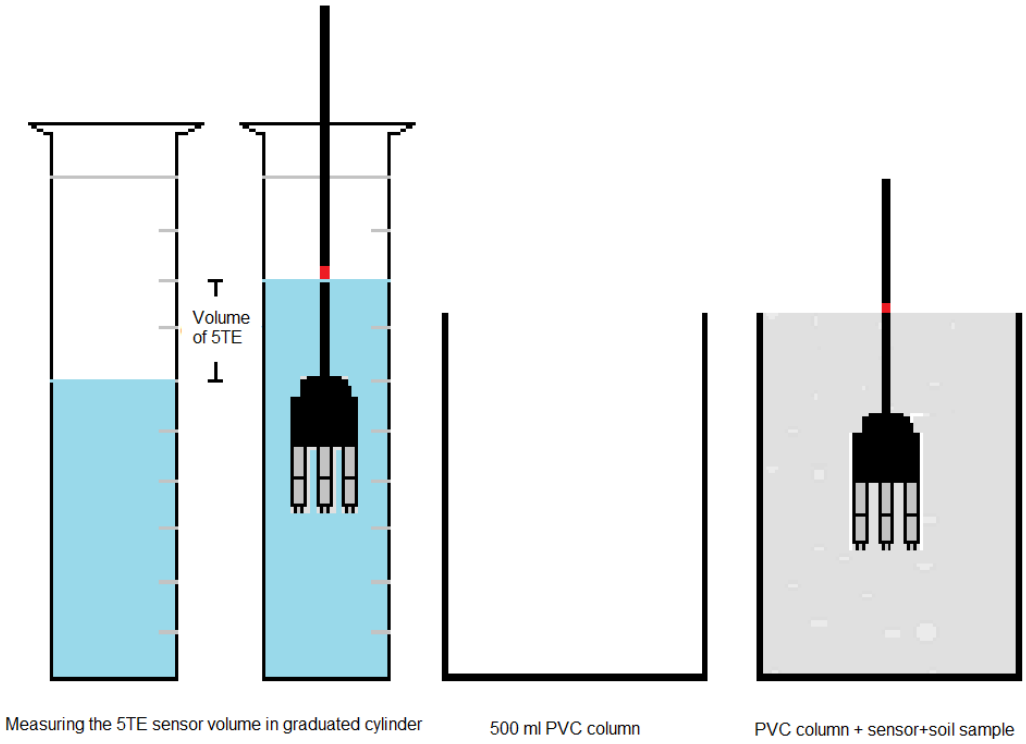

Figure 3. 4. Soil-specific calibration procedure of 5TE sensor.

d- The masses of the sensor and the empty PVC column were also determined to an accuracy of 0.1g using laboratory scale.

e- One of the clay samples was then compacted into the column to an arbitrary density followed by inserting the 5TE sensor into the soil sample. The soil was compacted carefully around the cable and leveled to the top of the PVC column to eliminate any voids.

f- The total mass of soil sample, PVC column, and the sensor were recorded along with the VWC reading from 5TE.

g- A representative specimen was taken from the soil in the PVC column for determination of gravimetric water content using oven-dried method. Once the gravimetric water content was known, the water mass and respectively water volume contained within the soil sample in the PVC column could be determined.

h- The VWC was then directly calculated as the volume of water within the soil sample in the PVC column divided by the total volume of the sample in the PVC column; where the total volume of the sample would be equal to the volume of the PVC column minus the volume of the 5TE.

i- The steps from e to h were repeated for the other four clay samples. The directly measured VWCs were then plotted against the sensor-measured VWCs as shown in Figure 3.5.

j- The UWC obtained from the 5TE for the frozen samples at various freezing temperature was then corrected using the calibration equation as follow:

$$VWC_{corrected} = 1.6496 * VWC_{5TE} - 0.0605 \qquad [3.\ 1]$$

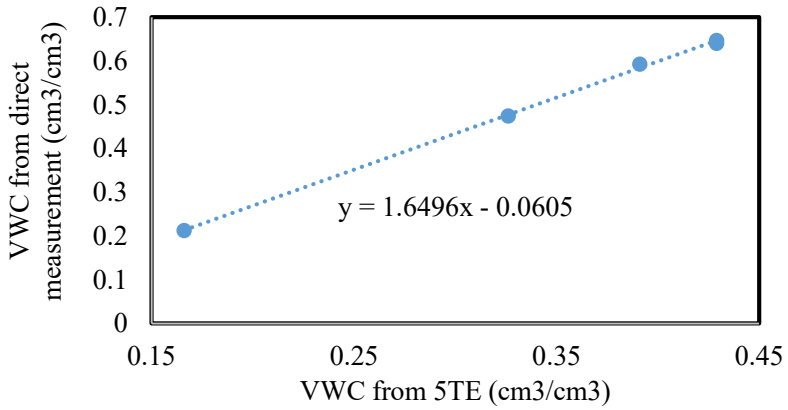

Figure 3. 5. Soil-specific calibration curve line.

3.6 Results

3.6.1 Shear strength of frozen Leda clay

Stress-displacement curves for the frozen Leda clay samples tested at various temperatures and under various confining pressures were constructed and presented in Figure 3.6. Peak strengths were typically observed at shear displacement ranged from 0.36 mm to 2.4 mm representing shear strain range of 0.6% to 4.0%, respectively. The variation of shear displacement at peak is mostly associated with the test temperature where soil samples tested at higher freezing temperatures failed at lower shear displacement. As the test temperature was decreased, however, the shear displacement at failure respectively increased. Most of the shear tests were continued after the failure up to 10% strain (6 mm displacement) in attempt of characterizing the residual shear strength.

Frozen soils tested at temperatures lower than -4.0°C always showed a brittle failure mode demonstrated by the significant strength losses recorded right beyond the peaks. As the test temperature became higher than -4.0°C, however, the samples started failing in plastic manner exhibiting less catastrophic failure with relatively less difference between the peak and residual strengths.

In this experiment, temperature has shown substantial effects on strength behavior of frozen clay. The soil tested at -10°C under a normal stress of 25 kPa, for example, showed a peak strength around 2 MPa, however, its strength under the same normal stress but at the freezing point temperature, underwent significant reduction demonstrating an ultimate capacity of around 0.45 MPa. This thermal change decreased the shear strength of the frozen clay by almost 4.5 times, causing a strength reduction of 78%. The strength loss corresponding to the applied warming

action could be attributed to the decrease in adfreeze bond due to the reduction in the ice content and increase in unfrozen water content.

3.6.2 Shear strength of steel-soil interface

The steel-soil interface testing program was aimed at studying the strength behavior of pile foundations in frozen clay. Results from this experiment followed a similar pattern exhibited by the frozen clay with minor differences (Figure 3.7). The interface peak strengths, for instance, were measured usually at slightly smaller shear displacement compared to the frozen soil tests recording displacement values ranged from 0.18 mm and 2.1 mm. This shear displacement range corresponded to a horizontal shear strain of 0.3% to 3.5%respectively. As in frozen clay, a higher displacement at peak was recorded for the interface tests conducted at lower freezing temperatures. This usually would refer to a higher ice bond that needed greater energy to be overcome. The brittle behavior dominated most of the interface tests and was more pronounced compared to those witnessed during frozen clay testing. Subsequently, interface samples showed immense strength reductions right after the peak and demonstrated very small residual strengths. Interface tests conducted at 0°C, however, showed less intensive brittle failures and recorded smooth transition toward plastic behavior.

Freezing temperature often shows proportional correlation to the ice content and ice bonding concentration, thus to peak strength too. This could be the reason for higher peak interface strengths witnessed at lower freezing temperature. At a normal stress of 25 kPa and a test temperature of -10°C, interface peak strength was around 1.9 MPa, however, the strength under a similar normal stress but at temperature of 0°C, underwent significant reduction demonstrating ultimate capacity of around 0.25 MPa. This thermal change led to weakening shear strength of the

steel-soil interface by more than 7.5 times, causing a strength reduction of almost 85%. This, indeed, highlighted the significant impact of thermal change on ultimate bearing capacity of steel piles in frozen grounds. Although such dramatic temperature increase may not be encountered especially when considering macroscale level (i.e., global warming effects), it may happen in the microscale level due to different causes including improper thermal insulation measures and/or induced warming duo to improper pile installation techniques.

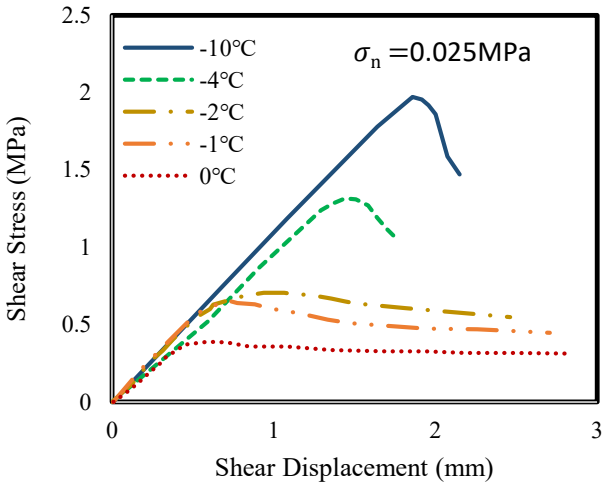

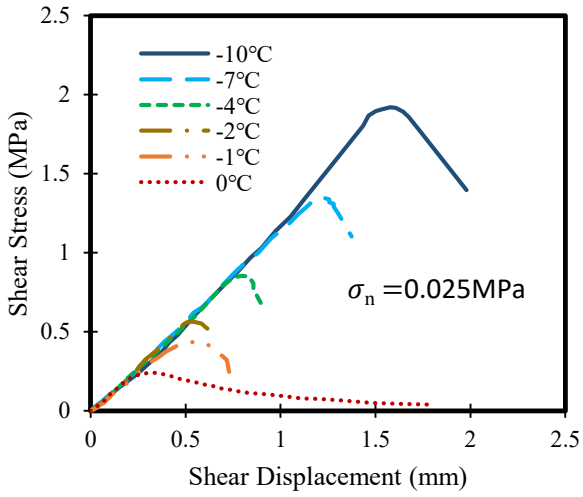

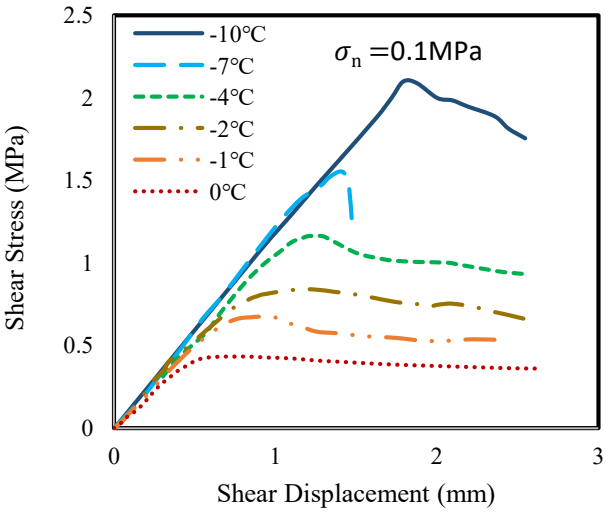

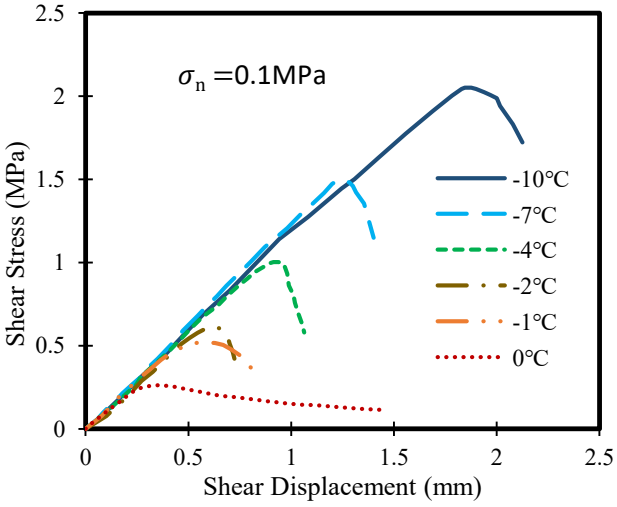

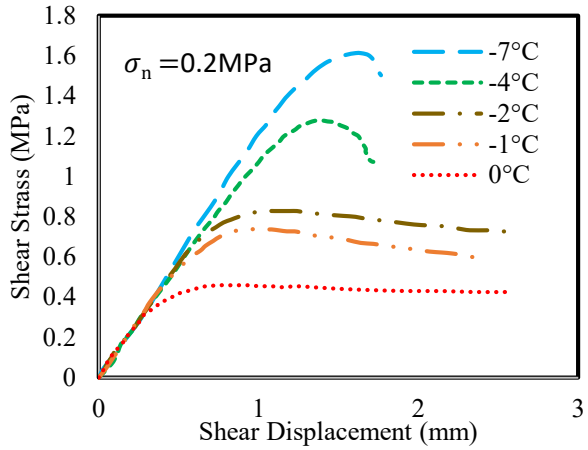

Figure 3. 6. Stress-displacement curves for frozen clay at different temperatures and normal stresses.

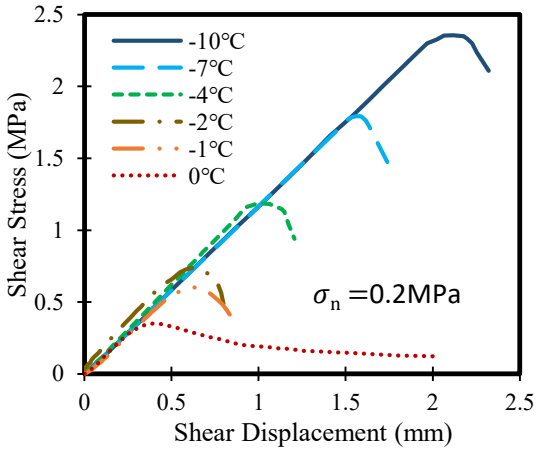

Figure 3. 7. Stress-displacement curves for steel-soil interface at different temperatures and normal stresses.

The stress-displacement curves for steel-soil interface specimens tested under a slower shear rate of 3 mm/day were illustrated in Figure 3.8. The results followed a typical trend of steel-soil interface behavior similar to those observed at the higher shear rate (16.3 mm/day) and reported in Figure 7. However, the magnitudes of the peak strengths and displacements at failure were significantly smaller under the slower shear rate. The peak shear strength recorded under the slow shear rate of 3 mm/day was almost 25-50 % less than those measured under the fast shear rate of 16.3 mm/day. For example, the interface samples tested under normal stress of 100 kPa showed peak strengths of 0.952 MPa, 0.61 MPa, and 0.263 MPa at -4.0°C, -2.0°C and 0°C when sheared at 16.3 mm/day. In contrast, under the shear rate of 3 mm/day and same normal stress, the peak strengths were recorded at 0.75 MPa, 0.408 MPa, and 0.20 MPa for the same temperature levels of -4.0°C, -2.0°C and 0°C. The interface samples also failed at smaller peak displacements when tested under the slower shear rate. The displacement at failure for the samples tested under 100 kPa, -4.0°C, and 16.3 mm/day failed at 9.5 mm horizontal displacement compared to 0.81 mm horizontal displacement at failure recorded when shearing at 3 mm/day.

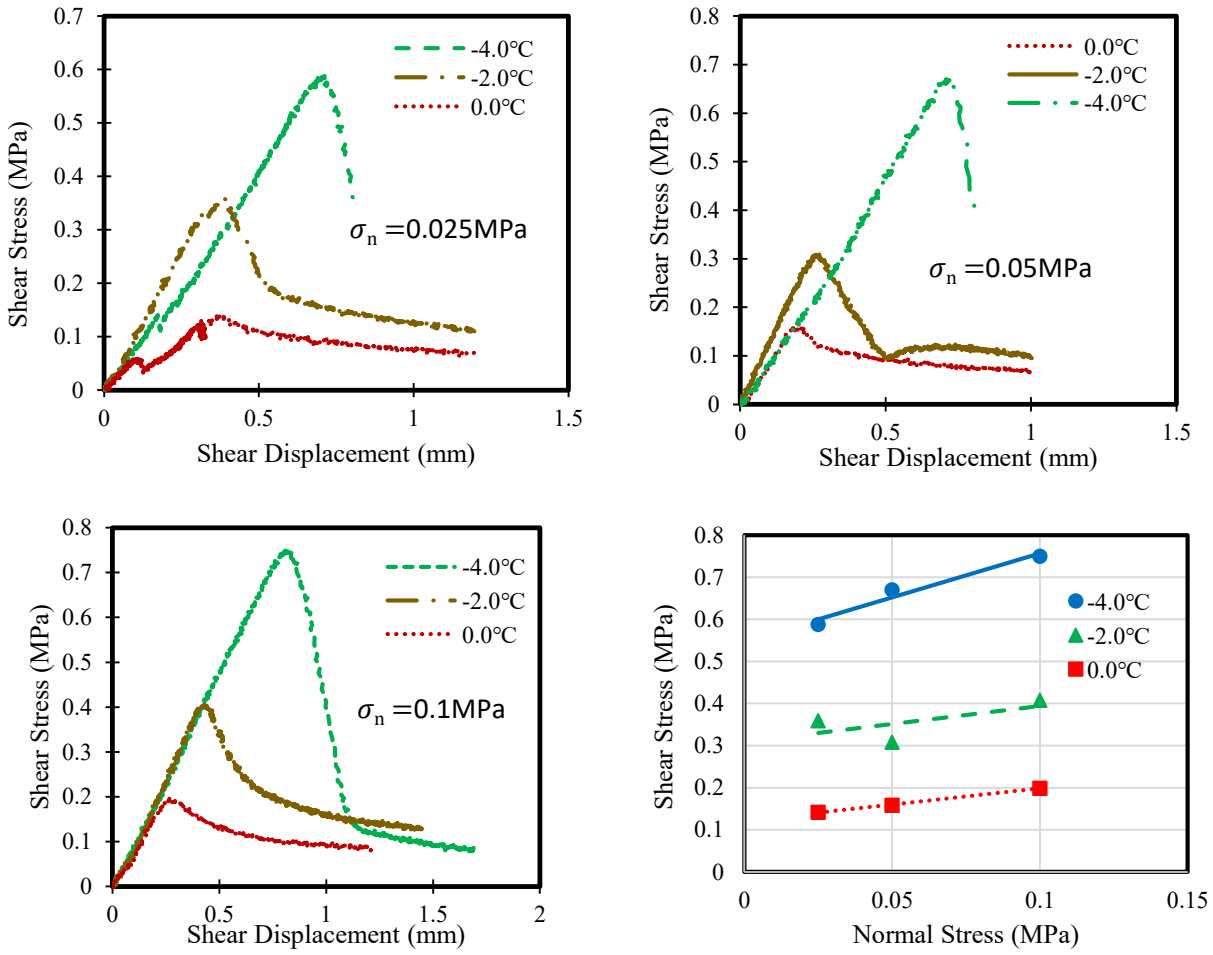

Figure 3. 8. Stress-displacement curves and failure envelopes pile-soil interface sheared at slow shear rate of 3 mm/day.

3.7 Analysis and Discussion

The results obtained from this study were used to develop better understanding on performance of pile foundations in frozen ice-rich soils. One main goal of the study was to evaluate the possible variation of the roughness factor corresponding to thermal change. Confining pressure acting on pile shaft could be another important aspect to address through this study. The attempts, in particular, could be toward quantifying the contribution of frictional resistance to the ultimate shaft capacity of the piles by bringing together the results from this study along with the hypotheses

available in literature about frictional resistance and lateral earth pressure in frozen soils. A correlation between ground temperature and ultimate shaft capacity of pile foundations can be established and introduced in forms of graphical and/or empirical equations.

3.7.1 Effect of ground temperature on the surficial roughness factor "m" of steel piles in frozen clay

Regardless to ground temperature and soil type, a constant roughness factor of 0.6 has long been used to correlate adfreeze strength of steel and concrete piles to the long-term shear strength of the surrounding frozen soil. In this section, efforts are made to evaluate the suitability of this assumption by comparing the peak shear strength of frozen Leda clay with the peak adfreeze strength of steel-clay interfaces at various temperature levels. Using Mohr Coulomb failure criterion, peak strengths versus confining pressures at different freezing temperatures were plotted for frozen clay and steel-frozen clay interfaces (Figure 3.9). Table 3.4 presents the strength parameters for the frozen clay soil and the pile-soil interface tests.

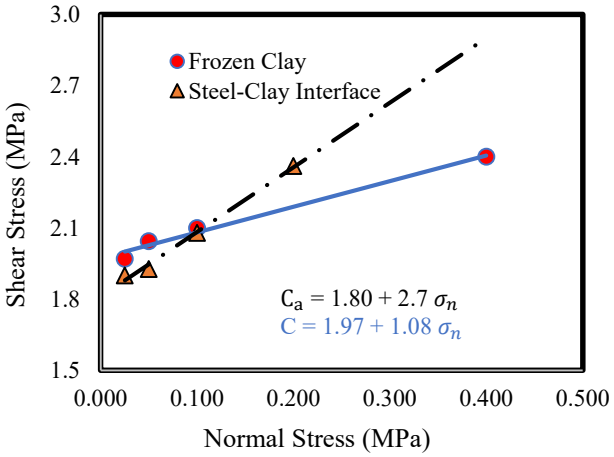

a. T = -10 °C

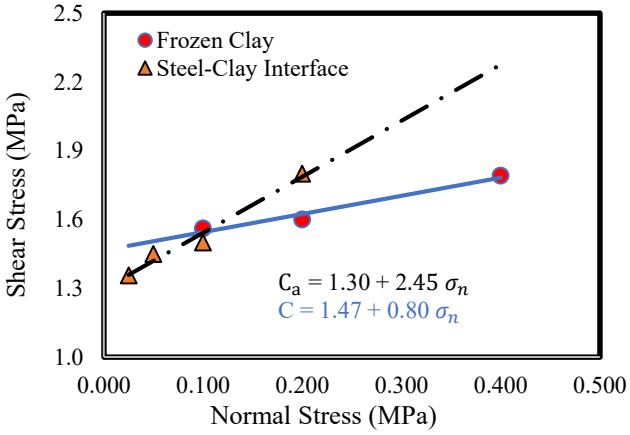

b. T = -7 °C

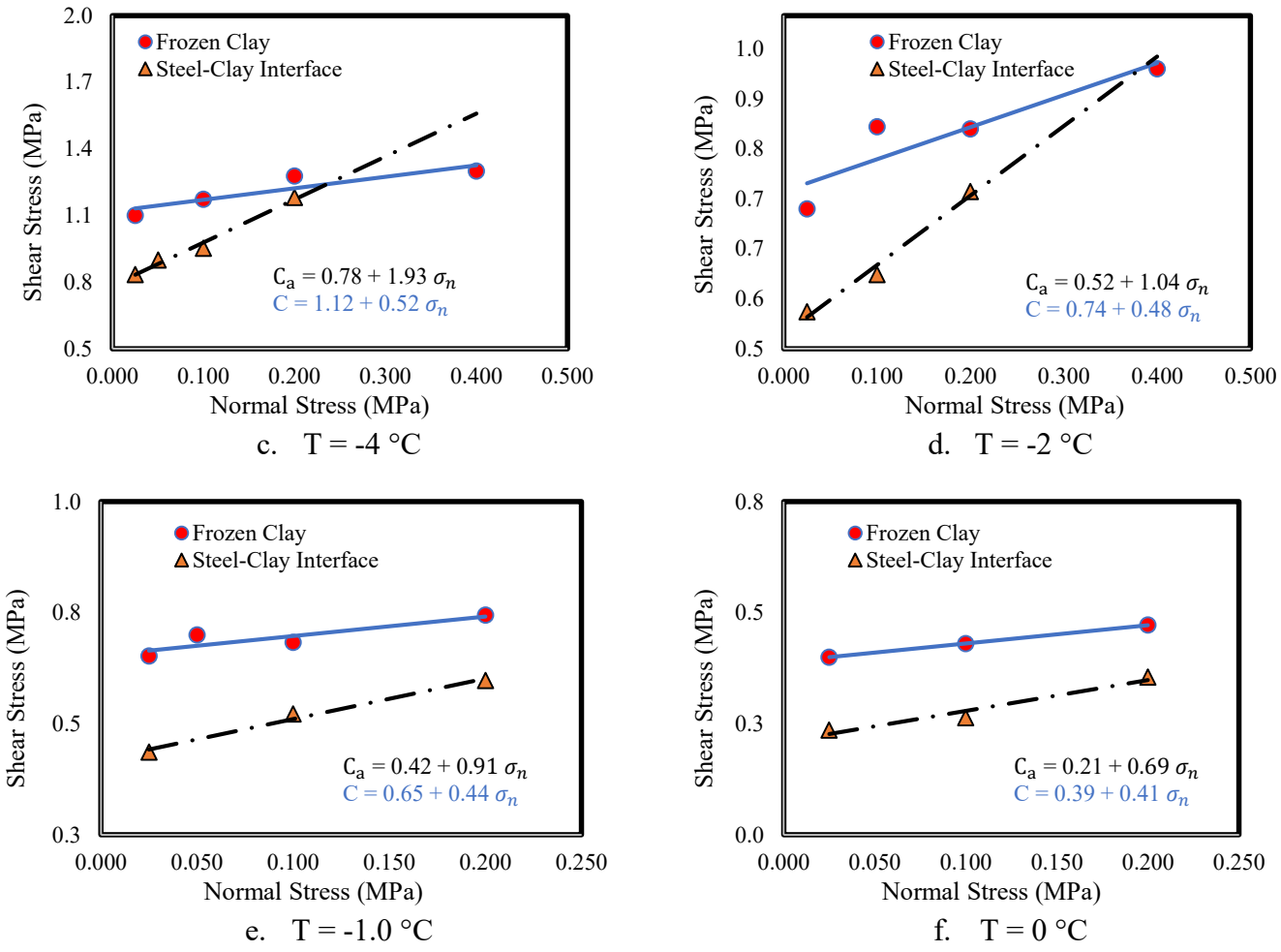

Figure 3. 9. Mohr-Coulomb envelop for frozen clay and steel-soil interface at various freezing temperatures.

For each test temperature, the intercept of the failure envelops of frozen clay samples and steel-pile interface elements with the vertical axis defines the cohesion and adhesion strengths respectively.

Cohesion strength of frozen clay was always higher than the adfreeze strength of the pile-soil interface. This could be attributed to the one-way drainage path formed within the pile-soil interface element. The one-way drainage path is enhanced by the existence of the impermeable steel plate which represent pile foundation in practice. The one-way drainage path may have delayed the movement of unfrozen water away from the shear plane during consolidation and

refreezing. This as a result, may have contributed to a higher inter-particles unfrozen water content compared to the case of clay samples where a two-way drainage path exists. The accumulation of unfrozen water content at the pile shaft would, therefore, lessen the ultimate water potential (Cryosuction) and, subsequently, decrease the ice bonding at the pile shaft.

The combination of soil to soil cohesion and the ice bonding exerted within the frozen clay compared to the ice bonding alone at the pile-soil interface could be another contributing factor that resulted in a greater frozen soil cohesion strength compared to pile-soil adhesion.

Table 3. 4. Strength parameters, roughness factor, and frictional factor at different freezing temperatures.

T °C	Clay-clay interface		Steel-soil interface		m, $\left(\frac{C_a}{C}\right)$	n, $\left(\frac{\tan\delta}{\tan\emptyset}\right)$
	C (MPa)	$\tan(\emptyset)$	C_a (MPa)	$\tan(\delta)$		
-10.0	1.97	1.08	1.8	2.7	0.91	2.50
-7.0	1.47	0.8	1.3	2.45	0.88	3.06
-4.0	1.12	0.52	0.78	1.93	0.70	3.71
-2.0	0.74	0.48	0.52	1.04	0.70	2.17
-1.0	0.65	0.44	0.42	0.91	0.65	2.07
0.0	0.39	0.41	0.21	0.69	0.54	1.68

Both the cohesion and adhesion strengths experienced dramatic reduction as the exposure temperature increased toward freezing point. This is possibly due to the reduction in ice content and the increase in unfrozen water content as the temperature increased. adhesion strength, however, underwent more pronounced degradation compared to cohesion strength of frozen soil at any given temperature. This may be attributed again to the one-way drainage effects which contributed to more unfrozen water accumulation as the temperature increased. This, therefore, has resulted in lowering the roughness factor to its minimum value of 0.54 when the temperature

reached the freezing point. The correlation between roughness factor and the ground temperature plus the unity (T+1) of ice-rich soil was established and presented in Figure 3.10.

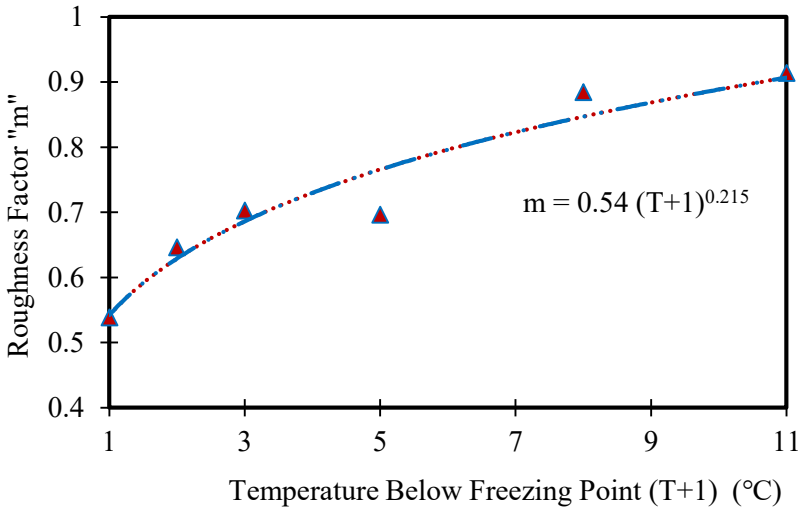

Figure 3. 10. Relationship between roughness factor "m" and ground temperature.

Theoretically, roughness factor may not be considered constant based on this graphical demonstration but rather varies exponentially from 0.54 to 0.91 corresponding to ground temperature reduction from 0°C to -10°C respectively. Practically, however, the assumption of using a constant value of 0.6 may still be valid and considered conservative as long as the ground temperature is lower than -1°C. For frozen ice-rich soils exposed to higher ground temperature, the roughness factor could not be more than 0.5. For precise estimation, however, the adhesion strength of steel piles in frozen ice-rich soils could be expressed as a function in temperature and cohesion strength of frozen clay using the following equation:

$$C_a = 0.54\ (T + 1)^{0.215}\ C \qquad [3.2]$$

where, C and C_a are cohesion strength of the frozen soil and adhesion strength of the pile-soil interface element at a frozen ground temperature (T), respectively. The frozen ground

temperature is substituted in the equation as a positive degree Celsius value. It is worth to mention that the cohesion strength was not denoted with long-term strength symbol because in this experiment only short-term strengths were obtained. However, the cohesion and adhesion strengths were normalized to each other with respect to time by the roughness factor "m". Thus, this equation is believed to be valid for correlating cohesion strength of frozen soil to adhesion strength of pile-soil interface for both short and long-term scenarios.

3.7.2 Effects of normal stress on s shaft resistance of steel piles in frozen clay.

In the current study, and from Fig. 6, the inclination in coulomb failure envelops indicates higher strengths for frozen soils and steel-soil interface samples as the normal stress becomes greater. This confirms the contribution of the frictional resistance to the ultimate strength for both frozen clay and shaft resistance of steel piles in frozen clay. Frozen clay showed decreased friction angles ($\emptyset$) with increasing temperature recording 45^{o} at -10°C and around 12^{o} at 0°C. Steel-soil interface friction (δ), on the other hand, followed similar pattern however with higher values at any given temperature exhibiting 70^{o} at -10°C and around 32^{o} at 0°C (Figure 3.11a).

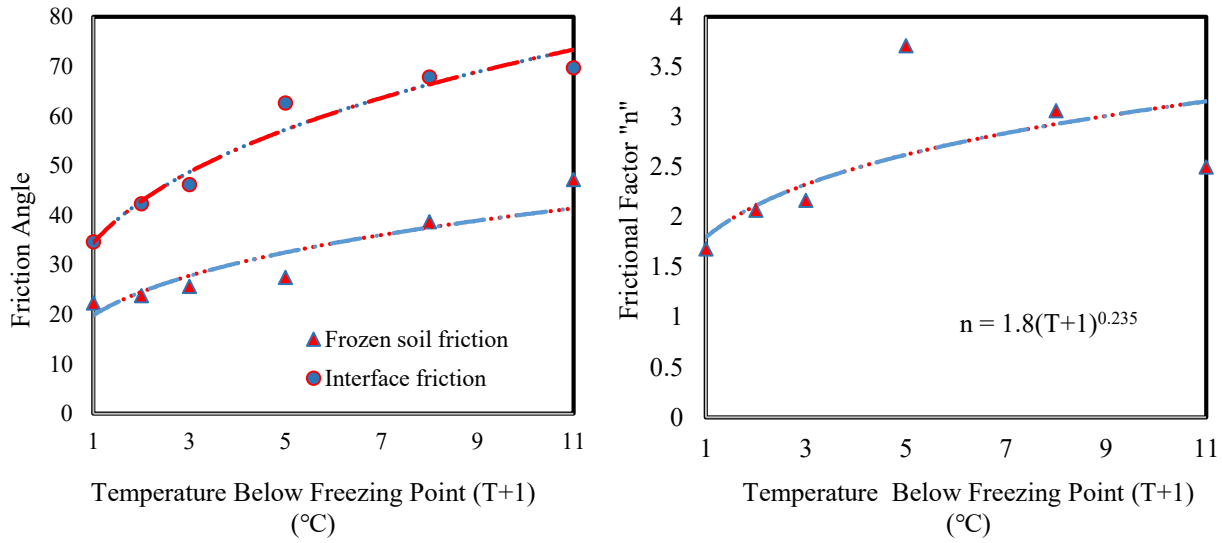

Figure 3. 11. (a) Variation of soil friction angle and pile-soil friction angle with temperature (b) surficial frictional factor at different temperature.

Friction resistance is predominantly due to soil particles interlock force which increases with increasing normal stress. Fractured ice crystals, moreover, contributes to the overall frictional resistance. At lower temperatures, therefore, higher friction angles were recorded due to a higher ice content. At temperatures lower than -1°C, increasing normal stress was reported to slightly increase unfrozen water content due to the pressure melting effect (Jones 1982). The increase in unfrozen water content would still be small to reduce the adhesion and cohesion strengths as temperature drops. However, the slight increase in unfrozen water content was rather stated to bring the soil particles closer resulting in higher frictional resistance. Because of the one-way drainage path system for pile setup, higher unfrozen water could accumulate at the predefined shear plane after soil refreezing around piles compared to the two-way drainage path formed in frozen soils. Thus, higher frictional resistance and lower adhesion strength was recorded at the pile-soil interface compared to the friction angle and cohesion strength in frozen soils at any given

temperature. The obtained results from the current experiment complies to the abovementioned philosophy which was first proposed by Williams and Smith (1991). This is also experimentally demonstrated in this study.

The obtained results from this study also support another statement made by Ladanyi and Theriault (1990) which suggests that the ultimate shaft capacity of piles may not only result from adhesion strength but from interface frictional resistance too. Therefore, the contribution of frictional resistance should be implemented into the general equation used to estimate the shaft resistance of steel piles in frozen clay. And, since the normal stress resulted in larger interface friction compared to friction angle of frozen soils, a frictional factor "n" similar to the roughness factor "m" can be introduced to express the ratio (tan δ) to (tan $\emptyset$) with respect to temperature. The frictional factor "n" versus temperature is presented in Figure 3.11b. Although the data showed a scattered pattern, an exponential correlation could be proposed to express the variation of the frictional factor "n' with temperature plus unity (T+1) as follow:

$$n = 1.80\ (T + 1)^{0.235} \qquad [3.3]$$

If the friction angle of frozen soil ($\emptyset$) is determined at any ground temperature (T) in the range from 0°C to -10°C, the frictional resistance of steel piles installed in this frozen soil can then be expressed as

$$\tan(\delta) = 1.80\ (T + 1)^{0.235} \tan(\emptyset) \qquad [3.4]$$

Based on equation [3.4], the normal stress acting on steel piles in frozen clay could exert a frictional resistance that is at least 1.8 times greater than the frictional resistance exerted by frozen clay. This finding supports the hypothesis proposed by Ladanyi and Theriault (1990) which states that the horizontal stresses in frozen soils become greater than the initial state following to pile installation. This mobilized stress happens due to the frost heave associated with slurry refreezing

or soil freeze-back around the pile. However, the magnitude of the freezing induced normal stress and the time required for normal stress relaxation is still widely unknown and need more investigation preferably using field set up.

3.7.3 Evolution of unfrozen water content and normal stress at pile-soil interface during freezing

Installation of pile foundations in frozen ground could induce an increase in normal stress at any depth along the pile shaft. This happens following to slurry freezing around piles installed in oversized holes, or by soil freeze-back occurrence after driving a pile directly in frozen ground or in a slightly undersized hole. The magnitude of horizontal stress acting on pile shaft from overburden pressure and/or slurry refreezing or soil freeze-back is still widely undefined. When an over-sized pre-drilling installation technique is used, horizontal stress from overburden pressure on pile shaft could be minimum and may not exceed 100 kPa (Ladanyi and Theriault 1990), However, induced horizontal stress from slurry refreezing or soil freeze-back may enhance the total normal stress acting on pile shaft

Ladanyi and Theriault (1990) theoretically showed that the mobilized normal pressure due to pile installation in ice-rich soils would dissipate within 24 hrs. falling to less than 1% of the before-installation lateral pressure. Nevertheless, a rapid dissipation of the mobilized lateral pressure may not occur in frozen soils because of their extremely low permeability and long consolidation time that could be longer than the service life of the structure. Therefore, Ladanyi and Theriault (1990) suggested that lateral stresses around a pile in frozen ice-rich soil would unlikely fall below the total lateral stress in the ground. Subsequently they proposed that the ratio between total lateral stress acting on the pile shaft to the total vertical stress could vary from k_0

for dense frozen soils to 1 for ice-rich soils and crystalline ice. To investigate this hypothesis, the UWC and the freezing induced normal were measured and discussed.

Figure 3.12a shows the change in volumetric unfrozen water content (UWC) of the frozen sand, with respect to its initial UWC value of 0.72 m^3/m^3, near the pile-soil interface and in a region far from the pile following freezing. Unfrozen water content followed a typical trend of reduction corresponding to soil freezing below zero degree Celsius. The amount of UWC at temperatures higher than -5.0°C, however, was greater near the pile-soil interface compared to the UWC observed farther from the pile. This could be attributed to the quicker response to thermal change exhibited by the steel pile compared to frozen soils which could cause a faster freezing rate at the pile-soil interface. As a result, a larger cryosuction may have developed near the pile and lead to migration of unfrozen water toward the pile shaft. The rapid declining rate of UWC in the soil far from the pile (Figure 3.12a) could refer to the unfrozen water migration from this region toward the pile-soil interface under the influence of possibly larger cryosuction. A greater inter-particles UWC, therefore, generated adjacent to the shear plane at pile-soil interface. As the temperature becomes colder than -5.0°C, the UWC near the pile became lower than the UWC far from the pile which could be due to the extreme coldness developed near to the pile because of the superior thermal connectivity of the steel. This coldness may with time have overcame the resistivity of UWC to freezing resulted eventually in smaller amount of UWC near to the pile compared to the native clay soil.

The ratio between the change in unfrozen water content at the pile-soil interface and in a region far from the pile are plotted against temperature in Figure 12b. On the same plot, the change in roughness factor “m” is also presented. The results showed that the ration between UWC near the pile surface and far from the pile shoed a reduction trend as the temperature decreased referring

to decreasing the difference between UWC at the two locations as the temperature was reduced. These results explain the lower adfreeze strength of the pile-soil interface compared to the shear strength of frozen soil. It also explains the lower roughness factor corresponding to lower exposure temperatures which could be attributed to the lower UWC ratio at lower temperature (Figure 3.12b). Although, the UWC near the pile became smaller than the UWC far from the pile when the temperature dropped below -5.0°C, the pile-soil dfreeze strength was still smaller than the shear strength of the frozen clay yielding roughness factor slightly less than the unity. This could be attributed to the different interface characteristic at the shear plane where the strength of the native clay would always be greater than the strength of a pile inserted in the same soil due to the smooth surface characteristic of the pile compared to the soil to soil interaction at the shear plane within the clay soil.

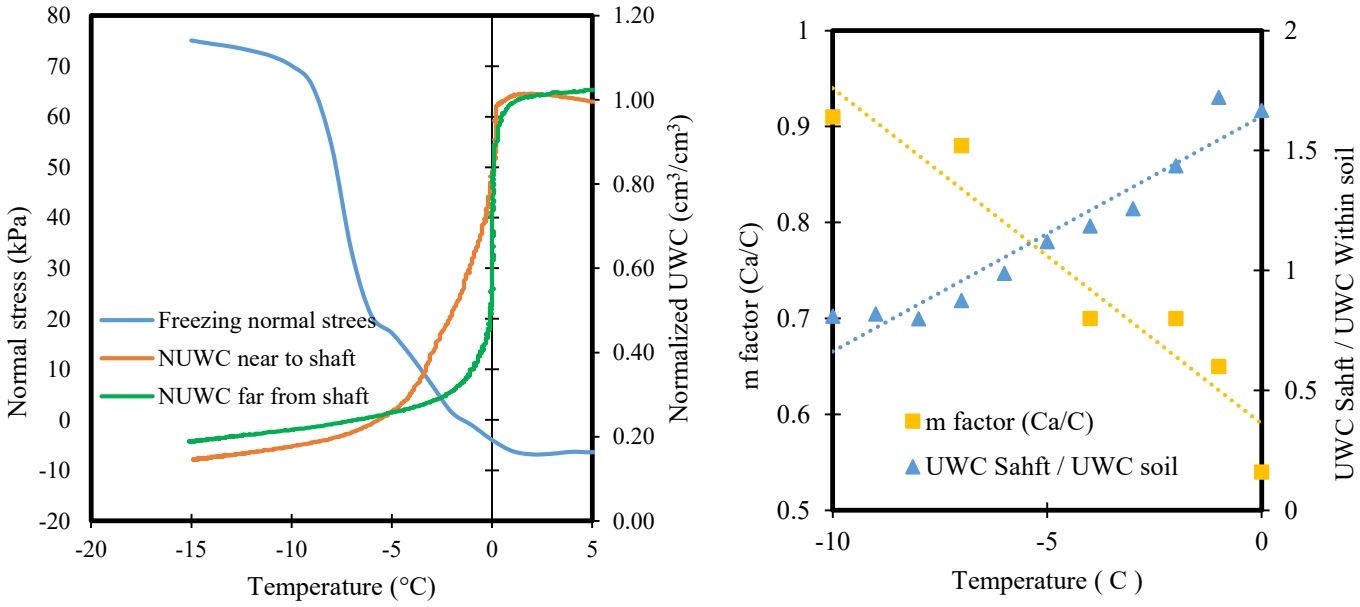

Figure 3. 12. (a) Unfrozen water content at pile shaft and within the soil, (b) variation of roughness factor and UWC ratio with temperature.

As the liquid water transforms to ice within the soil, the ice content increases, the unfrozen water content and permeability decrease, and frost heave develops. Figure 12a illustrates the variation of the exerted normal stress subjected to the pile shaft as a function of temperature and UWC. Before the freezing point, the normal stress experienced a slight reduction of about 7 kPa which could be attributed to soil consolidation around the pile. However, and as the temperature drops below zero-degree Celsius, the UWC decreases and normal stress dramatically builds up recording a maximum absolute increase of 76 kPa when the temperature reaches around –10.0°C. As the temperature was further dropped, the increase in normal stress became nominal reaching and absolute value of 84 kPa at -15°C. This agreed well with the reduction trend of UWC which was at max up to -5.0°C followed by a slight declining corresponding to further temperature reduction. The set up was lift inside the experimental fridge at -15°C for 72 hrs. to examine the possible occurrence of stress relaxation. However, the developed freezing normal stress, unlike to sand, remained constant and did not relax within the observation time.

The increase in normal stress is mainly attributed to the volume expansion of liquid water as it transforms to ice. The increase in normal stress corresponded well to the reduction in unfrozen water content referring to a strong correlation between the two measurements. The freezing induced normal stress in clay soil was larger than those recorded in ice-poor sand soil which was around 7 kPa only. This may be attributed to the large void space usually exists within the granular medium such as in sand, which would accommodate for most of the volume increase following to water freezing, thus, resulting in lower freezing induced normal stress. The observed freezing induced normal stress around a pile inserted in clay soil would be in the same magnitude compared to normal stress from overburden pressure for a typical pile length of 10 m and frozen bulk unit weight of 15 kN/m^3. Therefore, it would be very important to account for the contribution of

freezing induced normal stress for piles in ice-rich but it seems to be less important when having piles in ice-poor soils.

3.7.4 Influence of pile loading rate on adfreeze strength under varying temperature exposure

Shear strength of frozen soils and adfreeze strength of piles in frozen soil are influenced by strain rate. Parameswaran (1978), for example, showed that the peak yield adfreeze strength increased approximately linearly with increasing strain rate following a power law trend on log-log scale and could be expressed as following:

$$\tau_a \sim i^m \qquad [3.5]$$

where: (i) is the strain rate and (m) is the strain exponent.

The strain exponent from Parameswaran's (1978) experiment varied with pile surface materials and was reported as 0.1035 for unpainted steel and 0.2161 for concrete piles. However, the dependence of ultimate strength of piles on strain rate in frozen soils has often been reported at a given freezing temperature. Nevertheless, the influence of strain rate on ultimate capacity of piles may differ over a wide range of ground temperature due to the potential difference in unfrozen water content and change in viscus behavior of ice matrix. Williams and Smith (1991) suggested that frozen soil would exhibit higher strength when exposed to fast loading due to the undrained condition that would be respectively imposed. Undrained condition associated with fast loading would limit the dissipation of the inter-particle unfrozen water content resulting in excess pore water pressure, thus, yielding a higher total shear strength of frozen soil. Xu et al. (2017), more recently, reported higher yield and peak stresses for frozen clay soil samples tested under faster strain rates attributing that to the different stress distribution in the test sample under different strain rates.

Figure 3.13a compares the ultimate adfreeze capacity of steel-pile interface determined under a fast shear rate of 0.0113 mm/min and a slow shear rate of 0.00208 mm/min. The result shows that the adfreeze strengths measured under the faster were always greater than those measured under slow strain rate. This confirms the conclusion made by other researchers. Based on the conclusion proposed by Xu et al. (2017), shear testing under slower strain rates would require longer testing period which allows for more uniform stress distribution within the test samples causing the external load to be carried equally by the different matrices (i.e., ice, soil grains, and unfrozen water). As a result, soil samples tested under slower strain rates would deform uniformly and experience local failure, thus less likely to reach their peak stresses. In contrast, soil samples that are tested under higher strain rates would experience non-uniform stress distribution where the stresses usually are localized in parts of the sample and cause localized deformation. Therefore, only a portion of the sample carries most of load resulting in rapidly reaching its peak stress followed by brittleness failure occurrence. The non-uniform deformation would often limit the development of the plastic deformation inside the sample and lead to higher yield and peak stress under rapid strain rate condition.

To comprehend upon the role of temperature in controlling the effects of strain rate on the ultimate adfreeze strength of steel-soil interface, the ratio between ultimate adfreeze strength determined at the high strain rate and the ultimate adfreeze strength determined at the low strain rate is plotted against the freezing temperature and presented in Figure 3.13b. As noted, this ratio decreases in logarithmic trend with decreasing ground temperature varying from 1.72 at 0°C to 1.44 at -4.0°C. This refers to more pronounced effects of strain rate on ultimate adfreeze strength of pile foundations in frozen grounds that experience warm freezing temperature such as warm permafrost. This observation highlights the important role that the ground temperature plays in

controlling the response of pile foundations under different loading type in frozen ground. The warmer frozen ground would perhaps contain higher unfrozen water content and lower ice content than the frozen grounds that exist at very cold temperature. The high quantity of unfrozen water in warm frozen ground would make a higher chance for the stress to be localized in the pore water, therefore, resulting in greater excess pore water pressure under higher strain rates compared to the same sample that is tested under slower strain rates. As the test temperature decreases, ice content would respectively increase which would make the load to be more likely to localize in ice pores. Because of its higher viscosity, crystalline ice is less sensitive to shear strain compared to liquid water. Although, ice would carry greater load compared to liquid water, its load carrying characteristic would be less different under different strain rates at the same level of temperature, thus yielding slightly different load capacity if slow or high strain rates are applied. As the ground temperature decreases, Furthermore, and becomes significantly colder, the unfrozen water content would also become significantly smaller, thus excess pore water pressure would be also small at any strain rate resulting in smaller difference between the ultimate capacity of piles under fast and slow loading conditions. The short-term bearing capacity of pile foundations in frozen ground and under fast loading condition may not only be due to interface adfreeze and frictional resistances but the contribution of excess pore water pressure and stress localization too. Thereby, knowledge about long-term strength and creep behavior are always desired before designing pile foundations in frozen ground. Moreover, determining the design load of piles considering their ultimate load capacity at a given strain rate would require sufficient knowledge of the temperature regime and unfrozen water content of the surrounding soils for accurate estimation of load capacity and deformation predations.

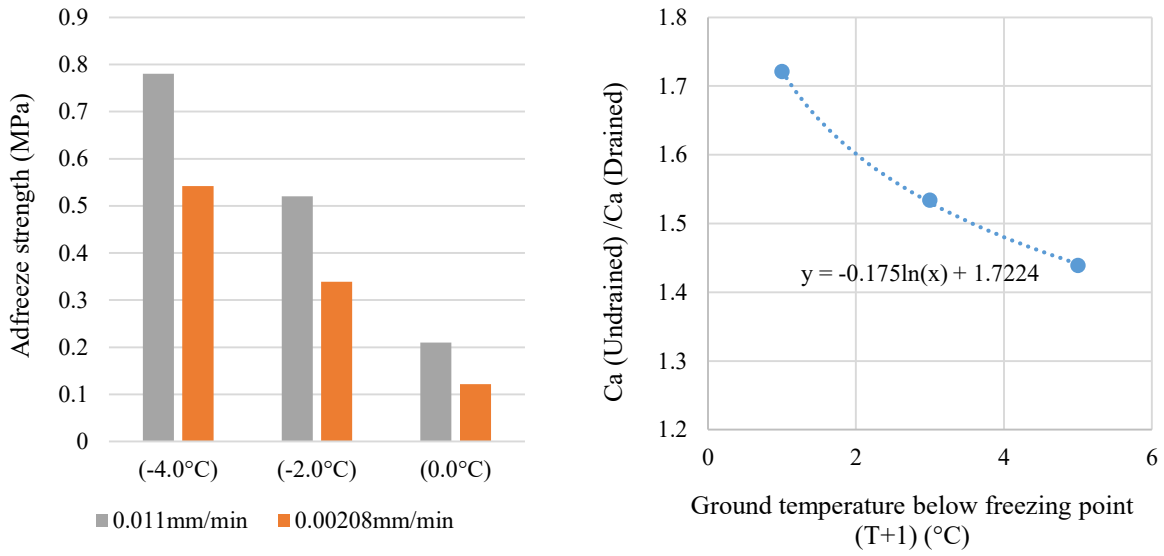

Figure 3. 13.(a) Adfreeze strength of steel-soil interface at different strain rates and temperatures, (b) Variation of the ration between undrained and drained adfreeze strength with freezing temperature

3.7.5 Comparison of ultimate capacities from interface element tests and model pile test

The pull-out capacity of the model steel pile embedded in the steel box was determined at -7°C and compared with those obtained from two steel-soil interface element tests for the purpose of validation and repeatability screening. The element tests showed very good repeatability exhibiting peak strengths of 1350 kPa 1310 kPa at the respective displacements of 1.26 mm 1.18 mm (Figure 3.14). The stress-displacement curve obtained from model pile test under pull-out capacity agreed well with those determined from element tests, however, the model pile showed slightly less peak strength recording 1156 kPa at an axial displacement of 0.82 mm. The slightly lower ultimate capacity from the model pile compared to the element tests could attributed to the lower normal stress subjected to the pile shaft in the box comparing to 25 kPa normal stress imposed on the element test samples. An ultimate capacity (Ca) of 1300 kPa was obtained from element tests at zero normal stress estimated based on Mohr-Coulomb lines as reported in Table 3.4. However, this value is still slightly greater than the ultimate capacity of the model pile,

nevertheless, the deviation between the two measurement fall within 10%. These results show the capability of the interface element tests in capturing the behavior of steel piles in ice-poor soils. The good repeatability observed from the element tests also supports the validity of the reported results in the current study.

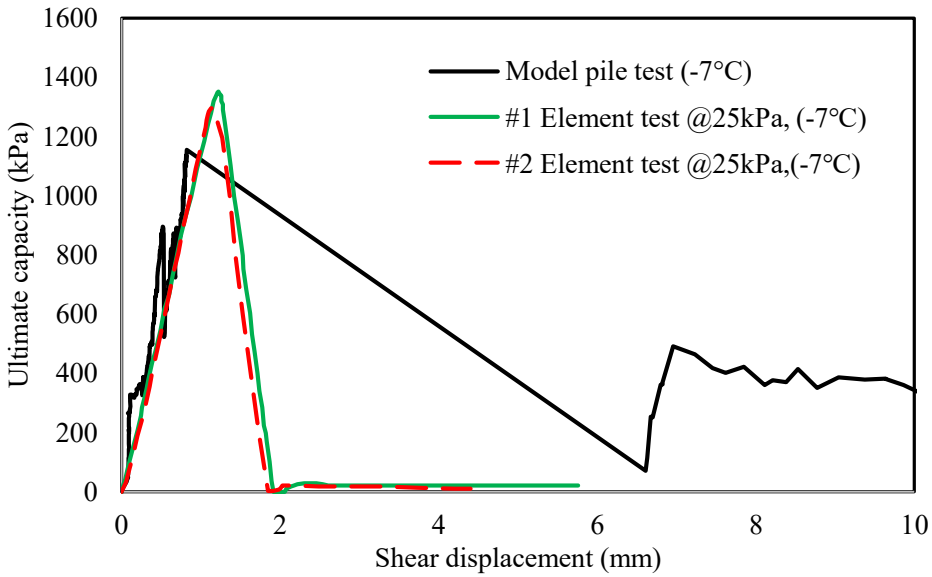

Figure 3. 14. Stress-displacement curves from model steel pile and steel-soil interface element tests.

3.7.6 Theoretical estimation of ultimate shaft capacity of steel piles in frozen clay

Results from the current study confirm that using a constant roughness factor for predicting adfreeze strength of steel piles in frozen ice-rich soils, as it was adopted in previous design methods, could be very conservative especially if the ground temperature is colder than -2°C. Load carrying capacity of pile foundations in practice depends on shear strength parameters of the soil as well as ground temperature and loading rate. In this study, the shear strength parameters of the clay, the roughness factor, and frictional factors were used to develop an empirical equation for predicting ultimate shaft capacity of steel piles in frozen clay. The solution correlates the shear strength of frozen clay to the interface shear strength of steel piles through the modified roughness

factor (m) and the introduced frictional factor (n). The ultimate shaft capacity is predicted based on the combination of pile-soil adhesion strength and the interface frictional resistance both as a function of freezing temperature and strength parameters of frozen clay as follow:

$$\tau_a = 0.54\ (T+1)^{0.215}\ C\ + 1.80\ (T+1)^{0.235}\ \sigma_n\ \tan(\emptyset) \qquad [3.6]$$

where, τ_a is adfreeze strength of steel piles in frozen clay at temperature (T), σ_n is total normal stress (kPa), C and $\emptyset$ are the cohesion strength (kPa) and the internal friction angle of the frozen clay at temperature (T), and T is ground temperature as a positive degree Celsius value. For low permeable frozen clay, the total normal stress is a resultant of overburden pressure and the refreezing-induced normal stress. Therefore, the equation [3.6] can be rewritten as follow:

$$\tau_a = 0.54\ (T+1)^{0.215}\ C\ + 1.80\ (T+1)^{0.235}\ (\sigma_{n_{overburden}} + \Delta\sigma_n)\ \tan(\emptyset) \qquad [3.7]$$

where: $\sigma_{n_{overburden}}$ and $\Delta\sigma_n$ are overburden pressure and the refreezing-induced normal stress respectively.

3.8 Conclusions

A comprehensive experimental program has been carried out to investigate the performance of steel piles in ice-rich clay soils. The following conclusions could be drawn:

1- The ultimate shaft capacity of steel piles can be correlated to the shear strength of frozen clay using two surficial factors; roughness factor (m) and frictional factor (n).

2- The roughness factor "m" is found to vary with not only the pile materials (e.g., steel, concrete, timber), but also with ground temperature and stress condition. This was attributed to the higher unfrozen water content accumulated at the vicinity of the pile-soil interface compared to a region far from the interface and maybe linked to the different thermodynamic aspects between steel pile and clay soil.

3- A frictional factor “n” representing the ratio between the pile-soil interface frictional resistance and the frictional resistance of the frozen clay, is introduced in this study. The frictional factor decreases with increasing freezing temperature, but it is always greater than the unity and indicates a higher steel-soil frictional resistance at any given temperature compared to the frictional resistance of the frozen clay.

4- UWC decreases as the temperature drops below freezing point leading to dramatical normal stress increases recording a maximum absolute value of 76 kPa in ice-rich soil when the temperature reaches around –10.0°C. As the temperature was further dropped, the increase in normal stress around the pile in ice-rich soil became nominal reaching and absolute maximum value of 84 kPa at -15°C. This agreed well with the reduction trend of UWC which was at max up to -5.0°C followed by a slight declining corresponding to further temperature reduction. after 3 days of observation, the induced normal stress maintained its value without experience any stress relaxation.

5- Adfreeze strength of pile foundation can be significantly affected by the strain rate. Piles that are loaded under a rapid loading condition would most likely to exhibit greater adfreeze strength. The higher adfreeze strength could be attributed to the stress localization and possibly the higher excess pore water pressure under faster strain rate. However, longer term adfreeze strength after a rapid loading condition may experience relaxation over the time due to the time-dependent behavior of frozen grounds.

6- An empirical equation is provided for predicting shaft resistance of steel piles in frozen clay soils. This equation would be more comprehensive upon obtaining information about refreezing-induced normal stress and normal stress from overburden pressure in frozen ice-rich clay soils.

CHAPTER 4: PILE-SOIL INTERFACE CHARACTERISTICS IN ICE-POOR FROZEN GROUND UNDER VARYING EXPOSURE TEMPERATURE

4.1 Introduction

Pile foundations in ice-poor frozen soils are often designed to satisfy both strength and deformation considerations. Following the strength criterion, the allowable bearing capacity of friction piles in frozen ground is estimated based on adfreeze strength of the pile-soil interface. The adfreeze strength has often been estimated as a fraction of the shear strength of the surrounding frozen soils using a surface roughness factor "m". The roughness factor is usually considered constant and used to describe adfreeze strength for piles in any frozen ground regardless of the temperature regime, the normal stress condition, and the type of frozen soil (i.e., ice-rich or ice-poor).

The current study summarizes results from an experimental program set to evaluate factors controlling pile-soil interface strength at various scenarios of freezing temperatures and normal stress conditions for steel piles in ice-poor frozen soils. The investigation was conducted in a walk-in environmental chamber using conventional and modified direct shear apparatuses as well as model pile testing. A frictional factor was also introduced to represent the contribution of frictional resistance at the pile-soil interface based on friction angle of frozen soils. The increase in normal stress subjected to the pile shaft following to soils freezing was also measured and correlated to ground temperature and unfrozen water content. A model pile was also tested and used to validate the results obtained from the interface element test.

4.2 Physical Properties of the Test Soil and Steel Interface

The test soil used in this research is classified as poorly graded non-plastic sand in accordance to the USCS classification system (ASTM D2487, 2005). The maximum dry density (ρ_d max) and optimum moisture content (w_{opt}) were measured at 1.850 Mg/m^3 and 10% respectively according to Standard Proctor test (ASTM D698, 2005). The particle size distribution for the soil was determined in accordance with ASTM D422, (2005). The soil contained approximately 5% fines passing through 0.075 mm sieve.

For pile-soil interface testing, steel plates were used to simulate the shaft surface of a typical steel pile. Steel piles are commonly used in permafrost region with different geometries including pipe piles, H-section piles, and helical piers. The interface test specimens were 90 mm by 90 mm square steel plates with a thickness of 25.4 mm, machined to couple with the upper half of the shear box in the direct shear test apparatus and provide a soil-steel interface area of 60 mm by 60 mm (Figure 4.1b). The total and the average surface roughness values for this particular type of steel were measured by a FARO arm measuring device and reported to be 9.7 μm and 11.3 μm respectively (Giraldo and Rayhani 2013). The steel plates were equipped with thermocouples that were inserted in tiny holes underneath the upper surface of the plates in order to track the temperature change at the steel-soil interface.

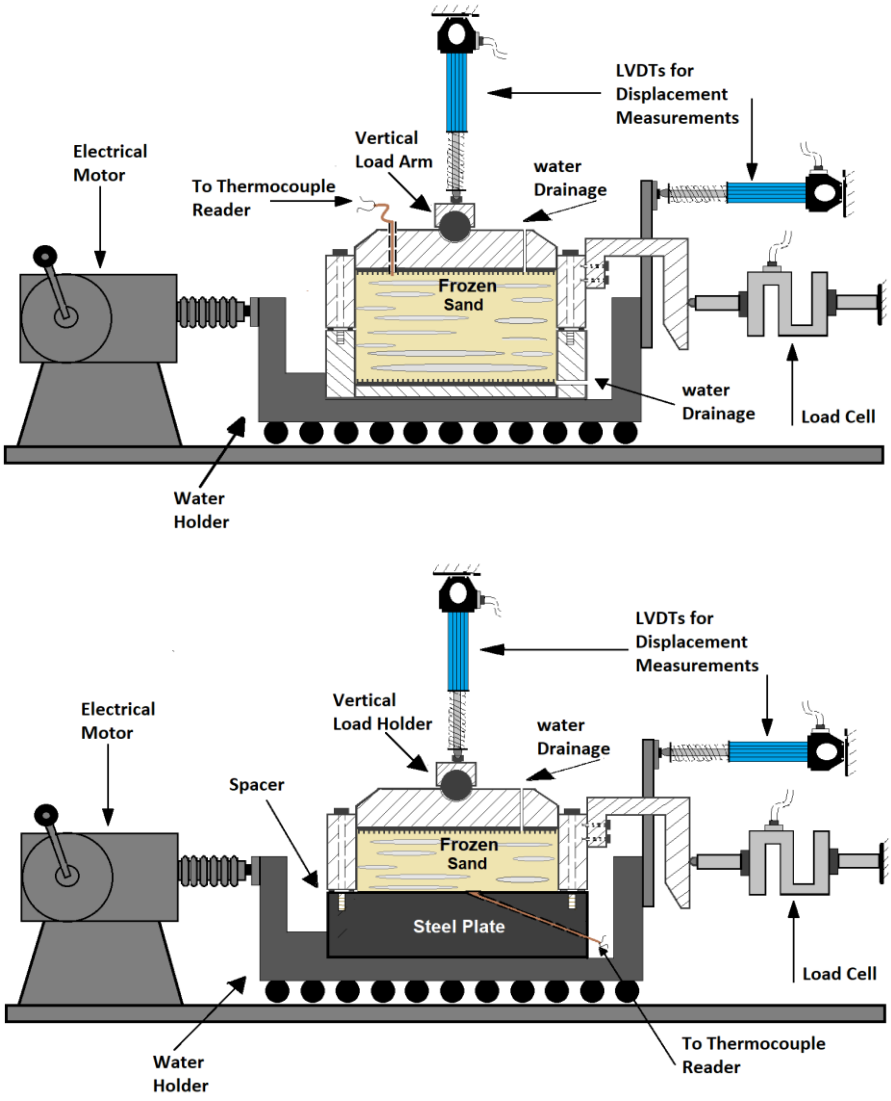

Figure 4. 1. Conventional and modified shear box for the interface test.

4.3 Experimental Program

4.3.1 Test equipment

All shear strength tests were conducted using a direct shear test apparatus in accordance to ASTM D3080/D3080M-11 and ASTM D5321-12. The apparatus was placed inside a fully controlled environmental chamber to enable testing at various freezing temperatures. The direct shear test

apparatus consists of an electrical motor that enables applying a constant shear rate to the lower part of the shear box, while the upper part is attached to a digital load cell that restrains its movement parallel to the shear plane. The apparatus is featured with a gearbox that controls the motion of the electrical motor and enables adjustment of the shear velocity. The horizontal and vertical displacements are measured through a Linear Variable Differential Transducers (LVDT) connected to a digital logging station using LabView software. The apparatus frame facilitates applying normal stress to the top of the test specimen by incorporating a steel bearing arm.

For frozen sand testing (soil-soil interface testing), a regular coupling shear box was used. This shear box had inner plan-view dimensions of 60 mm by 60 mm and depth of 40 mm (Figure 4.1a). For steel-frozen soil interface testing, on the other hand, a modified shear box was utilized to simulate pile-soil interface characteristics (Figure 4.1b).

4.3.2 Test sample preparation

The sand soil was prepared at a bulk density corresponding to its field capacity moisture content. This bulk density was determined by pouring the sand-water slurry into a known volume container and permitting water drainage and soil settling under gravity. When water flow stopped, the known volume soil sample was then weighed, and its density was determined which found to be 2.060 Mg/m^3 at a field capacity moisture content of 13.5%. To prepare the test specimens, dry sand was hydrated to the predefined field capacity moisture content and compacted to the corresponding density into the regular or modified shear box depending on the test type (i.e., frozen soil testing or steel-soil interface testing). The shear box was then mounted on the direct shear test apparatus and the desired normal stress was respectively applied simultaneously with setting the temperature

of the chamber to the desired level. All samples were left for 24 hrs. in the cold room before shear testing to allow for consolidation and freezing. The simultaneous action of consolidation and freezing of the test specimens was aimed at producing uniform element test specimens by minimizing formation of ice lenses, and thus reducing inhomogeneity (Wang et al. 2017). The absence of confining pressure during freezing, in particular under slow rate, could lead to formation of small ice lenses that may reduce the uniformity of the test specimens (Viggiani et al. 2015; Wang et al. 2017). Simultaneous application of normal stress and freezing action in this experiment is also similar to the condition occurred in field following to pile driving in undersized predrilled holes or in pre-thawed soils in cold frozen ground as well as in the case of direct pile driving in warm frozen ground. The ambient temperature in these cases varies based on the present ground temperature and frozen ground condition (i.e., cold or warm). Pile driving in undersized predrilled holes or directly in warm frozen ground is expected to increase the normal stress subjected to the pile shaft from the surrounding soil and generate heat in the pile vicinity. The heat release may cause the frozen ground to melt around the pile. However, freeze-back action would occur due to the present freezing temperature of the frozen ground as well as the thermal conductivity of the steel pile which would transmit the cold air temperature to depth. Thereby, freezing and consolidation are expected to happen simultaneously in the field setting too. In this experiment, complete consolidation may not have been achieved giving the relatively rapid occurrence of sample freezing. Nevertheless, this scenario is expected to occur in field as well. Stress relaxation around the pile in field may, therefore, happen during the process of complete consolidation considering the long-term effects. However, normal stress change in frozen ground following to pile setup is remained widely undefined and still a concern to the engineering community.

4.3.3 Test procedure

4.3.3.1 Shear strength testing

The shear tests were conducted under controlled strain rate where the shear load was applied at a constant shear velocity of 0.0113 mm/min (16.3 mm/day). The shear tests were conducted at different temperature levels including -10℃, -7℃, -4℃, and -1℃, with an accuracy of $\pm$0.5℃. At each temperature, shear strength was determined under different normal stresses including 25 kPa, 50 kPa, 100 kPa, and 200 kPa. To examine the effect of shear rate on the ultimate interface shear strength, another set of steel-soil interface specimen was tested under slower shear rate namely 0.00208mm/min (3mm/day) and their ultimate interface shear strengths were compared with the specimens tested at the higher shear rate.

4.3.3.2 Determination of unfrozen water content and thermally mobilized horizontal stress

Direct installation of piles in frozen ground using conventional driving technique could be difficult especially when encountering ice-poor soils. The common practice, therefore, is to either pre-thaw or pre-drill the frozen ground to facilitate pile driving. However, the shear strength of the pile-soil interface would depend highly on the degree of freeze-back of the pre-thawed soil or the backfill. The increase of unfrozen water content (UWC) in the region near to the pile could diminish the adfreeze strength of the pile-soil interface and reduce the pile's load carrying capacity. In this study, a physical model was developed to study the evolution of UWC during the process of soil freezing around a steel model pile. The physical model was also set to provide measurements of the normal load that could be generated as a result of soil freezing and subjected to the pile shaft. The physical model consisted of a rectangular steel box with inside dimensions of 400 mm length, 100 mm width, and 350 mm height. The box had two steel partitions that were set to contain the test soil

and the pile. One partition was restrained from horizontal movement by two steel spacers while the other was free to move in horizontal direction and bear on a load cell (Figure 4.2).

The soil sample within the partitions had dimensions of 200 lengths, 100 mm width, and 200 mm height. The model pile was a steel tube with outer diameter of 5 mm and height of 350 mm equipped with a pile cap fixed to the steel box to restrain the pile from heaving upward during freezing. The model pile was placed in the center of the box and the sand was then compacted around the pile at its field capacity moisture content and the associated density following the same procedure for preparing the test samples for shear strength testing. Before placing the pile and the soil in the box, layers of Styrofoam and fiberglass were placed at the base and along the sides of the box to provide thermal insulation and allow 1-D downward freezing action.

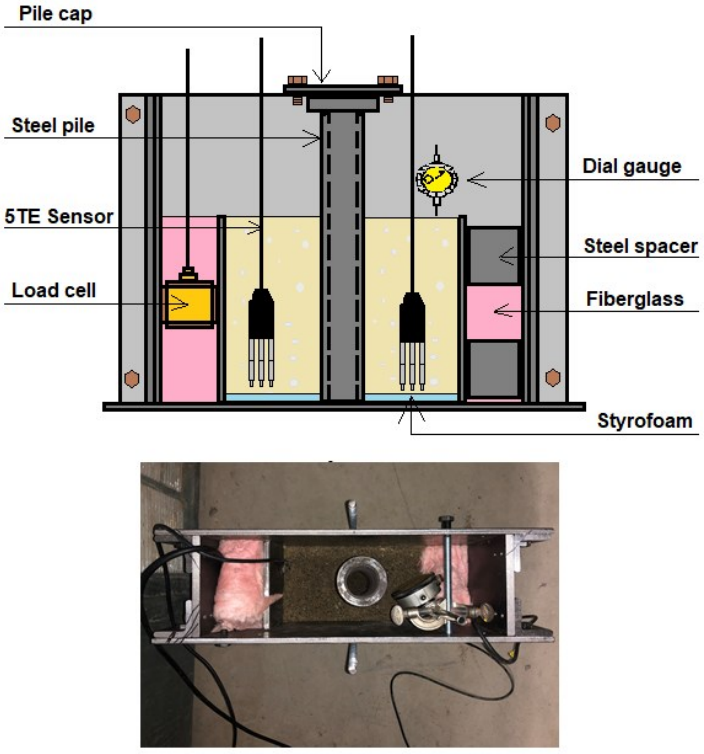

Figure 4. 2. Physical model for measuring unfrozen water content and freezing force acting on pile surface.

The Unfrozen water content was measured at distances of 20 mm and 50 mm from the pile shaft using 5TE sensors which monitor the bulk electrical conductivity (EC), volumetric water content (VWC), and soil temperature. The load cell and 5TE sensors were connected to a PC unit through a data acquisition system to record changes in unfrozen water content and development of the horizontal load associated with soil freezing. The instrumented cell was then placed inside a refrigerator and exposed to thermal loading at freezing rate of -0.06 ℃/min. After recording the maximum freezing stress and the minimum unfrozen water content, the test cell remained under the same freezing conditions for additional 72 hrs. to observe any stress relaxation. A pull-out load test was then conducted on the model pile to determine its ultimate shaft capacity of -7 ℃.and compare it to those obtained from steel-frozen soil element test recorded at the same temperature.

Soil-specific calibration of the 5TE sensor was conducted following to the calibration procedure outlined in Section 3.5.2.1. The calibration results are presented in Figure 4.3 where a calibration equation could be written as follow:

$$\mathrm{VWC_{corrected}} = 1.5801 * \mathrm{VWC_{5TE}} - 0.0367 \quad [4.\ 1]$$

The UWC obtained from 5TE for the frozen sand at various freezing temperatures was then corrected using the calibration equation listed above.

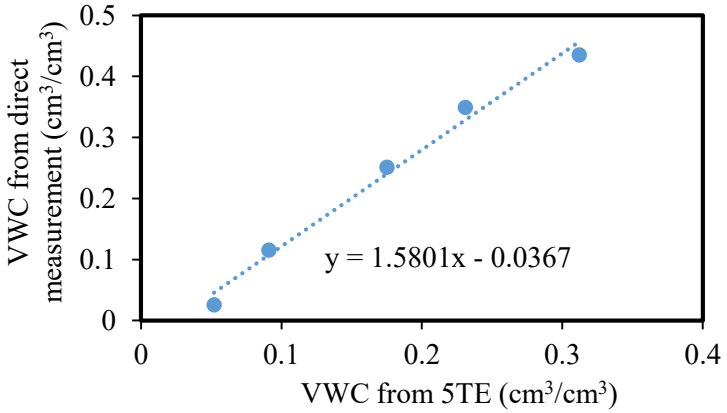

Figure 4. 3. Soil-specific calibration curve line.

4.4 Results

4.4.1 Shear strength behavior of frozen sand

Stress-displacement curves at different temperatures and normal stresses for frozen sand are illustrated in Figure 4.4. The peak strength was typically observed at shear displacement between 0.9 mm and 2.4 mm. The differences in shear displacement at peaks could be linked to the effect of test temperatures where soil samples tested at higher freezing temperatures failed at lower shear displacement. As the test temperature decreased, however, the shear displacement at failure respectively increased. Most of the shear tests were continued after the failure up to at least 10% strain (6 mm displacement) in an attempt of characterizing the residual shear strength. Beyond the peak, most of the test specimens showed a sudden strength reduction followed by a stage of strain hardening that continued up to displacement of 4 mm and was more pronounced for specimens tested at higher exposure temperatures. After this stage, all test specimens exhibited brittle failure recording very small residual strengths of about 10% their peak strengths. Residual strength was proportional to the applied normal stress where larger residual strength was observed for specimens tested under a higher normal stress (see Figure 4.4). Brittle behavior was more pronounced for samples tested under lower test temperature and normal stress, recording larger post-failure strength reductions.

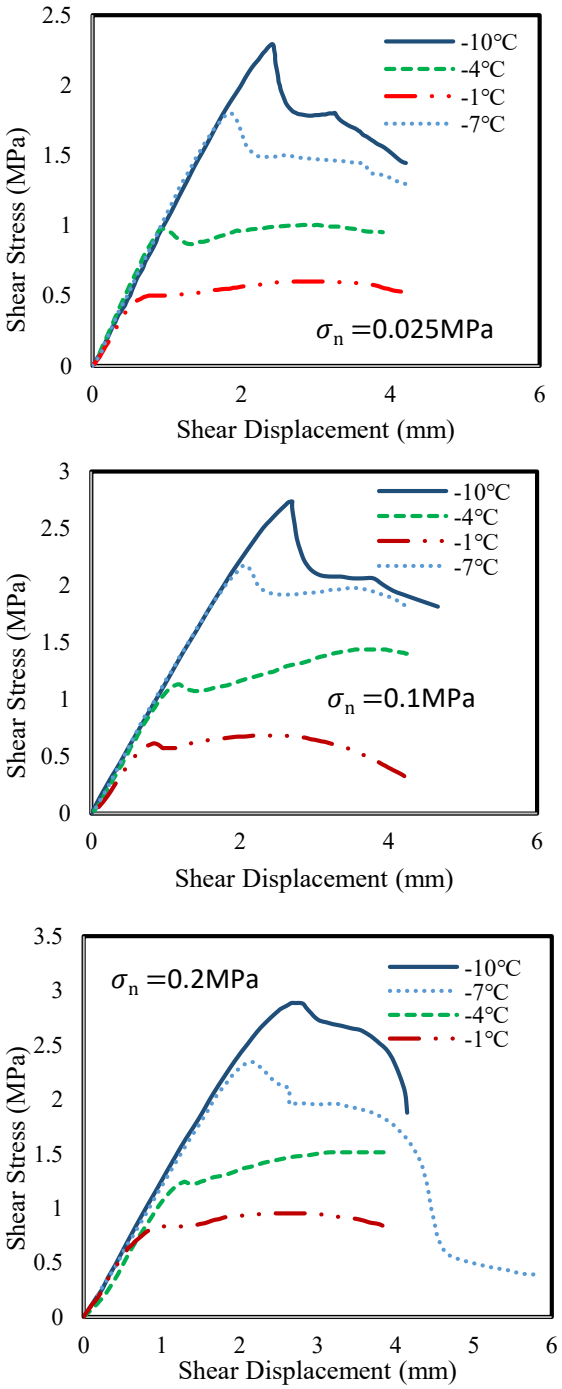

Figure 4. 4. Stress-displacement curves for frozen sand at different temperatures and normal stresses.

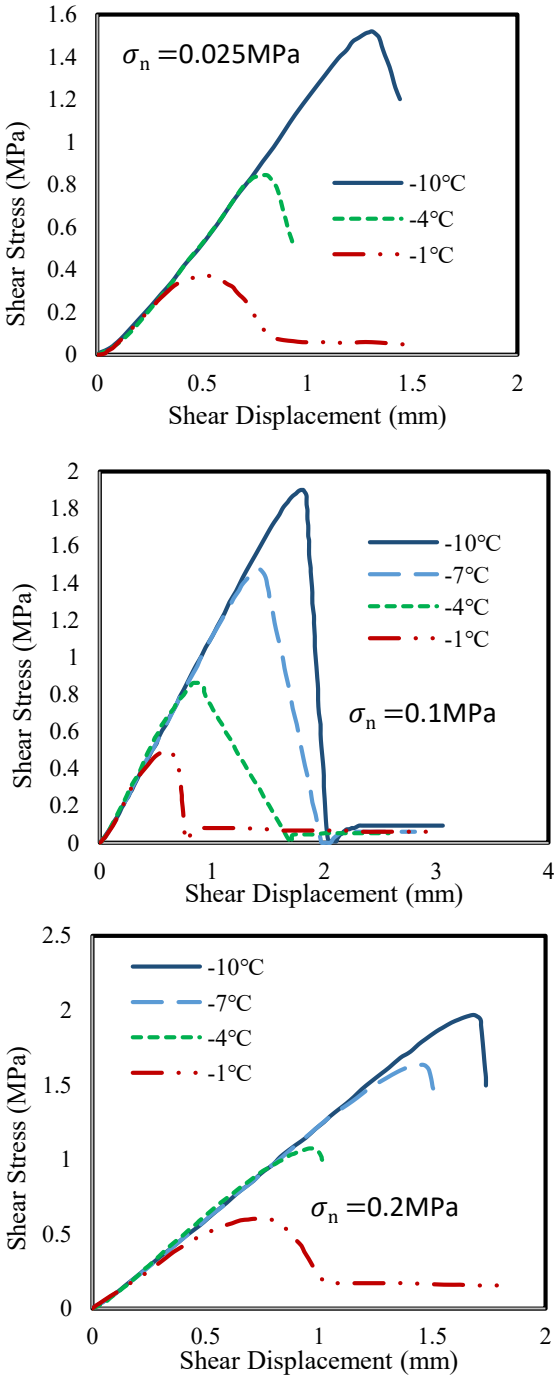

Figure 4. 5. Stress-displacement curves for pile-frozen sand interface at different temperatures and normal stresses.

In this experiment, temperature has shown significant effects on shear resistance of frozen sand. For instance, the specimen tested at -10°C and under a normal stress of 25 kPa, showed a

peak strength of around 2.3 MPa, however, its strength under similar normal stress but at -1°C was 0.5 MPa demonstrating a large strength reduction. This thermal change decreased the shear strength of the frozen sand by almost 5 times, causing a strength reduction of 78%. The strength loss corresponding to the applied warming action could be attributed to the decrease in adfreeze bonding due to reduction in the ice content and increase in unfrozen water content.

4.4.2 Shear strength behavior of steel-sand interface

Interface testing program was intended to characterize the strength behavior of steel-frozen sand interface simulating frictional steel piles in frozen ice-poor soils. The stress-displacement curves for the interface specimens followed similar patterns exhibited by frozen sand but with lower stress-displacement values at peaks (Figure 4.5). The peak interface strengths, for example, were usually recorded at displacement values between 0.6 mm and 1.8 mm depending on test temperature and the applies normal stress. Similarly, a higher displacement at peak was recorded for the interface tests conducted at lower freezing temperatures and under higher normal stresses. This usually would refer to a higher ice bonding potential and larger frictional resistance which requires greater energy to be overcome. The brittle behavior dominated most of the interface tests and it was more pronounced compared to the frozen sand tests. Subsequently, interface samples showed considerable strength reductions right after the peak shear stress and demonstrated very small residual strengths. Interface tests conducted at -1°C, however, showed relatively less brittle behavior.

The interface test results showed inverse correlation between the peak interface strength and freezing temperature. This was evident from the higher peak interface strengths witnessed at lower freezing temperatures. For example, at a constant normal stress, interface peak strength at a temperature of -10°C was around 2.2 MPa, however, the strength under a similar normal stress

but at a temperature of -1°C, underwent a significant reduction demonstrating an ultimate resistance of around 0.35 MPa. This thermal change led to weakening shear strength of the steel-soil interface by almost 85%. This, indeed, highlights the significant effect of thermal change on the ultimate capacity of steel piles in frozen ground. Although, such dramatic temperature increase may not be encountered especially when considering macroscale level (i.e., global warming effects), it may happen in the microscale level due to different causes including improper thermal insulation measures and/or induced warming duo to improper pile installation techniques. In discontinues permafrost zone, change from frozen to unfrozen condition is more likely to happen as the ground exists at relatively warm temperature.

The stress-displacement curves for steel-soil interface specimens tested under a slower shear rate of 3 mm/day were illustrated in Figure 4.6. The results followed a typical trend of steel-soil interface behavior similar to those observed at the higher shear rate (16.3 mm/day) and reported in Figure 4.5. However, the magnitudes of the peak strengths and displacement at failure were relatedly smaller under the slower shear rate. The peak shear strength at the slow shear rate of 3 mm/day was almost 45-55 % less than those measured under the fast shear rate of 16.3 mm/day. For example, the specimens tested under normal stress of 100 kPa showed peak strengths of 1.89 MPa, 0.816 MPa, and 0.467 MPa at -10°C, -4°C and -1°C when sheared at 16.3 mm/day. In contrast, under the shear rate of 3 mm/day and same normal stress, the peak strengths were recorded at 1.03 MPa, 0.36 MPa, and 0.20 MPa for the same temperature levels of -10°C, -4°C and -1°C. The specimens also failed at smaller strains when tested under the slower shear rate. The displacement at failure for the specimen tested under 100 kPa, -10°C, and 16.3 mm/day was 1.8 mm compared to 1.3 mm shear displacement at failure recorded when shearing at 3 mm/day.

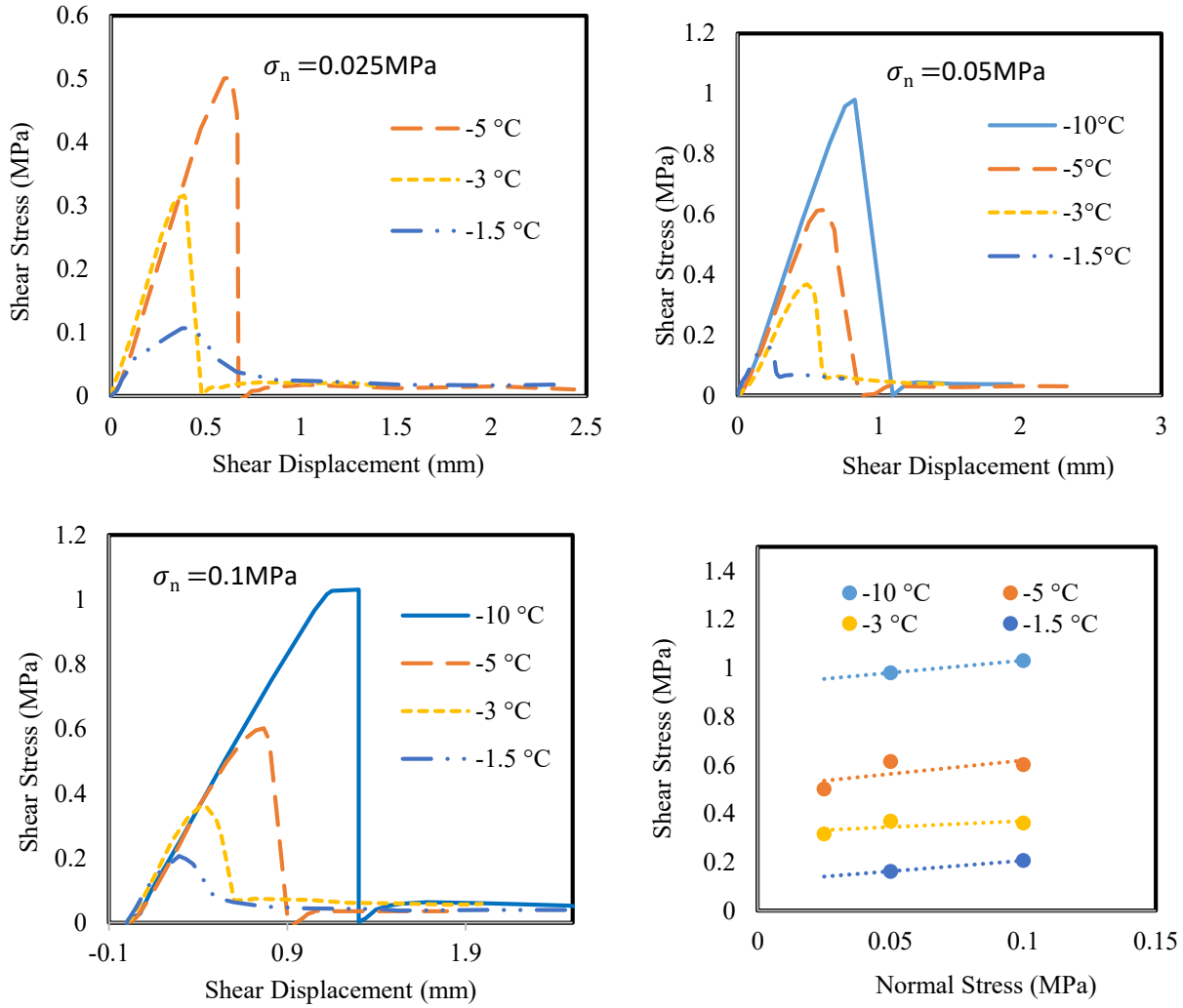

Figure 4. 6. Stress-displacement curves and failure envelopes pile-soil interface sheared at slow shear rate of 3 mm/day.

4.5 Discussion

4.5.1 Evaluation of roughness factor "m" for steel piles in frozen ice-poor soil

The load carrying capacity of pile foundations has been often calculated based on bearing capacity of the surrounding soil after by the use of a reduction factor. In unfrozen ground, for example, α – method is one of the common approaches used for designing piles in cohesive soils when an undrained condition is prevailed. α is a reduction factor that correlates shaft resistance of the pile to the undrained shear strength and can vary between 0.5 and 1.0 based on the ratio of the undrained

shear strength to the effective vertical stress. In frozen soils, adfreeze strength dominates the ultimate capacity of the pile foundation, thus, a surface roughness factor "m" analogous to the reduction factor " α" has been used to estimate the shaft resistance of piles. However, "m" has been often used as a consistent value for each pile material with no sensitivity to ground conditions. In this section, efforts were made to evaluate the suitability of this assumption by comparing peak cohesion of frozen ice-poor sand with peak adfreeze strength of steel-frozen sand interfaces at different temperature levels and normal stresses.

Using Mohr-Coulomb criterion, peak shear strengths versus normal stresses at different freezing temperatures were plotted for both the frozen sand and steel-soil interface and illustrated in Figure 4.7. The strengths of frozen soil as well as that of the interface samples were resultant of cohesion/adfreeze and frictional resistance. At each temperature level, peak cohesions and peak adfreeze strengths were measured at the intercept of the Mohr-Coulomb failure envelop with the vertical shear stress axis. These values along with the corresponding test temperatures, and the respective roughness factors "m" are all presented in Table 4.1.

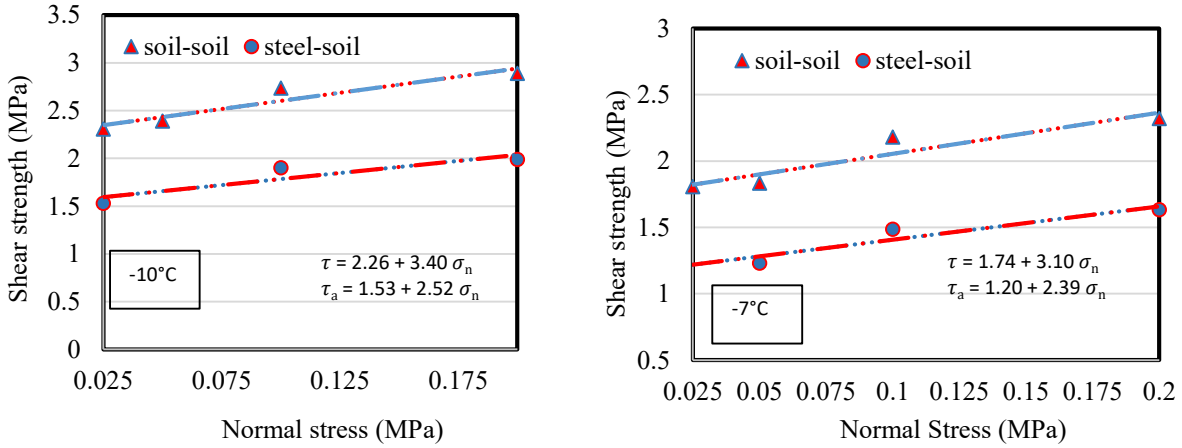

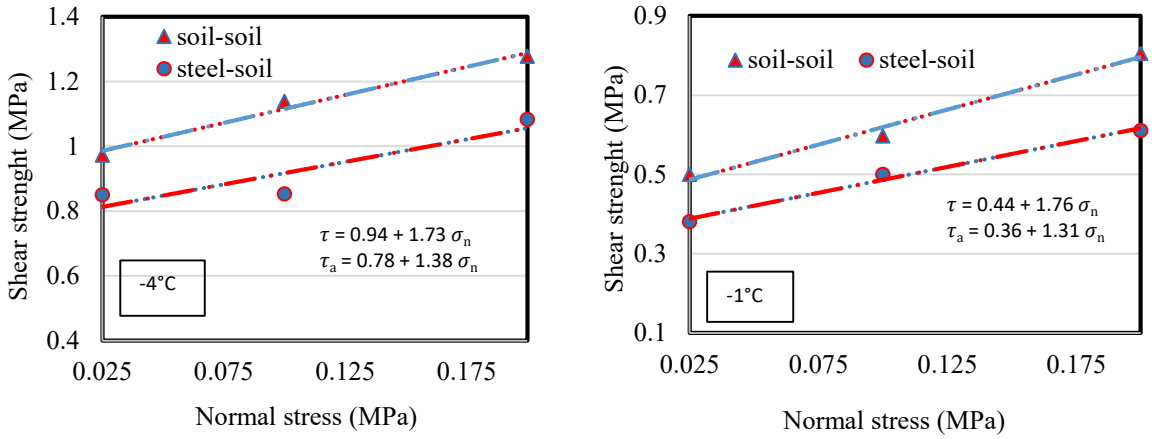

Figure 4. 7. Shear strength parameters of frozen sand and pile-soil interface under different exposure temperatures

At any given temperature, cohesion strength of frozen sand "C" was always higher than the adfreeze strength of the pile-soil interface "C_a". Since the sand is cohesion-less, the adfreeze strength would be probably due to existence of ice content at the pile-soil interface. Therefore, the higher cohesion strength of frozen sand compared to the adfreeze strength of pile-soil interface could be attributed to either higher ice content and/or lower unfrozen water content. Given its higher thermal conductivity, the steel pile would exhibit lower temperature at any time during the process of freezing compared to sand. Therefore, thermal gradient would exist while freezing and causes the free water to flow from higher to lower temperature region under water potential force effects (cryosuction). Furthermore, the quicker response to thermal change exhibited by the steel pile would also cause a faster freezing rate at the pile-soil interface. These factors would possibly result in greater volume of inter-particles unfrozen water contents adjacent to the shear plane at pile-soil interface compared to the soil region farther from the interface. This has, potentially, caused the lower steel- soil adfreeze strength compared to the cohesion strength of frozen sand.

Cohesion and adfreeze strengths both experienced dramatic reduction as the exposure temperature increased toward freezing point. This possibly was due to degradation of the ice bonding following to the reduction in ice content and the increase in unfrozen water content as the temperature warms up. However, the ratio between adfreeze and cohesion strength at different temperatures varied within a small margin

represented by the roughness factor "m" shown in Table 4.1. The correlation between roughness factor and the ground temperature (T) was established and presented in Figure 4.8.

Table 4. 1. Roughness factor "m" and frictional factor "n" for pile-soil interfaces in ice-poor soils

T °C	Soil-soil interface		Pile-soil interface		m	n
	C (MPa)	tan(Ø)	C_a (MPa)	tan(δ)		
-10.0	2.26	3.40	1.53	2.52	0.67	0.74
-7.0	1.74	3.10	1.20	2.39	0.69	0.77
-4.0	0.94	1.73	0.78	1.38	0.83	0.79
-1.0	0.44	1.76	0.36	1.31	0.82	0.74

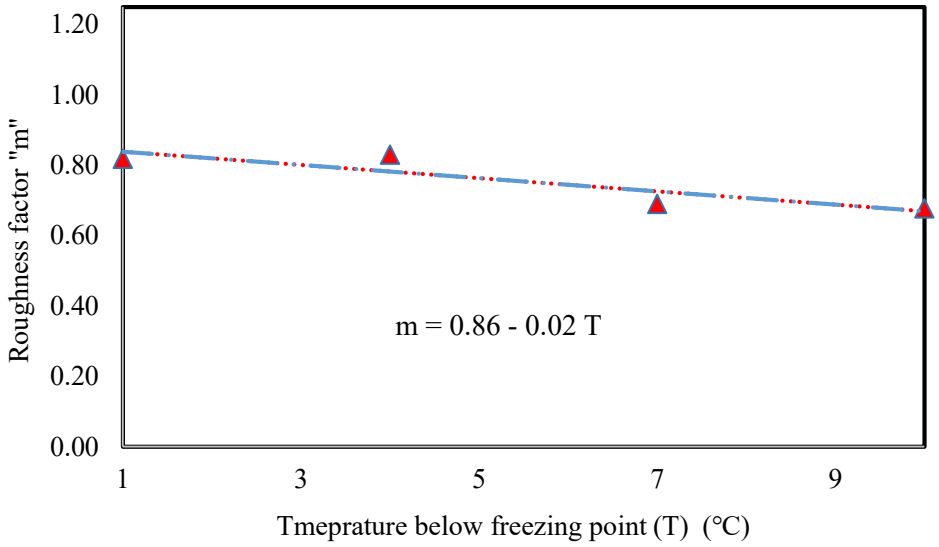

Figure 4. 8. Variation of roughness factor with ground temperature

The graphical demonstration in Figure 4.8 shows a reduction trend of the roughness factor corresponding to temperature reduction. However, this reduction is very small compared to the relatively large thermal change from -10°C to -1.0°C. A minimum roughness factor value of 0.68 was recorded at -10°C and under all other test circumstances it has never dropped to 0.6. Therefore,

these findings show that using a constant roughness factor of 0.6, as suggested by Weaver and Morgenstern (1981), could be considered conservative for the examined soil, pile material, and the test temperature.

4.5.2 Contribution of frictional resistance to the ultimate shaft capacity of steel piles in ice-poor soils.

The shaft resistance of steel piles in frozen sand is not solely dependent on adfreeze strength but also on frictional resistance and, thus, on the applied normal stress. Generally, at high strain rates, a higher strength corresponding to higher confining pressures in frozen soils is expected. At low strain rates, however, less strength increase was reported with increasing confining pressure (Jones, 1982). This was attributed to plastic deformation and predominant cohesive strength demonstrated at low strain rates.

In the current study, Mohr-Coulomb's failure envelops in Figure 4.7 show inclination indicating higher ultimate capacities for frozen sand and steel-soil interface samples tested under higher normal stresses. This confirms the contribution of frictional resistance to the ultimate strength for both frozen sand and frictional piles in frozen sand. The frozen sand, in addition, showed reduction in friction angles ($\emptyset$) with increasing temperature recording 74^{o} at -10°C and about 60^{o} at -1.0°C. Steel-soil interface friction (δ), furthermore, followed a similar reduction pattern but with lower values at any given temperature exhibiting 67^{o} at -10°C and about 54^{o} at -1.0°C (Figure 4.9).

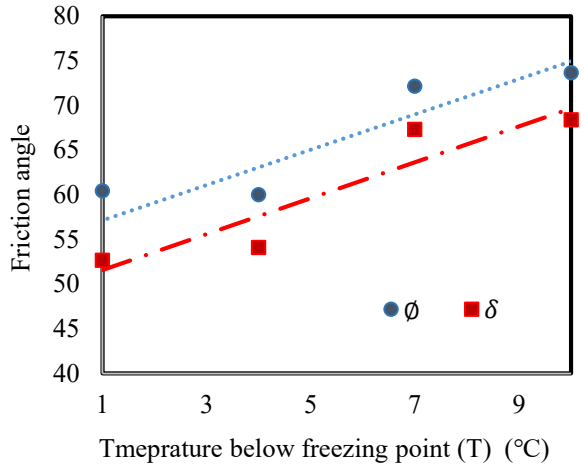

Figure 4. 9. Friction angles and interface frictions at different ground temperatures

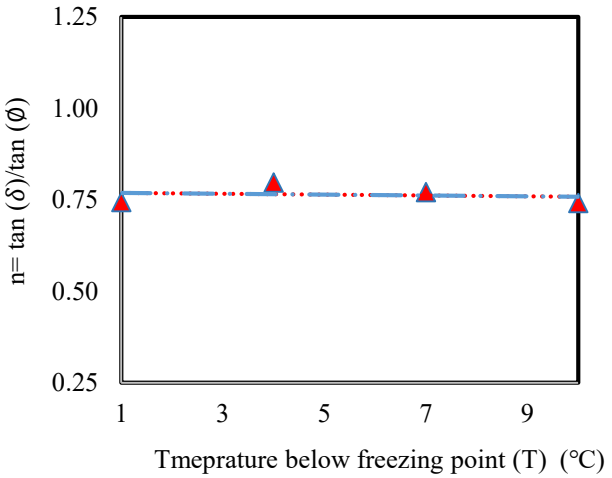

Figure 4. 10. Variation of frictional factor with ground temperature for steel piles in ice-poor soils

Frictional resistance is predominantly due to soil particles interlock force which increases with increasing normal stresses. Fractured ice crystals, moreover, contributes to the overall frictional resistance (Williams and Smith 1991). At lower temperatures, therefore, higher friction angles were recorded which could be due to a higher ice content. The smooth surface of steel piles would minimize the interlock force with sand particles which could yield lower frictional resistance at the pile-soil interface compared to the soil-soil interface in frozen soils. This explains the lower interface friction angles recorded at the pile-soil interface compared to the friction angles exhibited by the frozen sand at any given normal stress.

For design purpose, it would be useful to provide a correlation between the frictional resistance of the frozen soils and the frictional resistance that would be developed at the pile-soil interface. This correlation would be analogous to the one provided by the roughness factor “m” which correlates adfreeze strength to the cohesion strength of frozen soils. Therefore, by obtaining information about friction angle and cohesion strength of the frozen soil, the load carrying capacity of the piles can be accordingly estimated. For this reason, a frictional factor "n" similar to the

roughness factor “m” is introduced in this study to express the ratio between tan(δ) and tan ($\emptyset$) with respect to temperature. The frictional factor "n" versus temperature is presented in Table 4.1 and Figure 4.10. The tangent of friction angles ($\emptyset$) had a linear relationship with the tangent of interface friction angles (δ) with almost zero slope yielding an average frictional factor "n" of 0.75 at any given temperature between -10°C and -1.0°C. The frictional factor “n”, therefore, can be considered constant and given a value of 0.75 for the examined soil, pile material, and ground temperature range.

Therefore, the ultimate shaft resistance of steel piles in ice-poor soils can be theoretically correlated to the shear strength parameters of frozen soils through the modified roughness factor "m" and newly implemented frictional factor "n". The ultimate shaft capacity takes into account the combination of adfreeze strength and frictional resistance developed at the pile-soil interface and can be written as follow:

$$\tau_a = (0.86 - 0.02\,T)\,C + 0.75\,\sigma_n \tan(\emptyset) \qquad [4.2]$$

where: C and $\emptyset$ are shear strength parameters of the frozen ice-poor soil determined at field ground temperature, τ_a is ultimate shaft resistance of piles at the respected temperature, σ_n is horizontal stress acting on pile shaft, and T is the freezing temperature as a positive value.

4.5.3 Evolution of unfrozen water content and normal stress at pile-soil interface during freezing

Installation of pile foundations in frozen ground could induce an increase in horizontal stress at any depth along the pile shaft. This happens following to slurry freezing around piles installed in oversized holes, or by soil freeze-back occurrence after driving a pile directly in frozen ground or in a slightly undersized hole. Ladanyi and Theriault (1990) theoretically showed that the mobilized lateral pressure due to pile installation in ice-rich soils would dissipate within 24 hrs. falling to less

than 1% of the before-installation lateral pressure. Nevertheless, a rapid dissipation of the mobilized lateral pressure may not occur in frozen soils because of their extremely low permeability and long consolidation time that could be longer than the service life of the structure. Therefore, Ladanyi and Theriault (1990) suggested that lateral stresses around a pile in frozen ice-rich soil would unlikely fall below the total lateral stress in the ground. Subsequently they proposed that the ratio between total lateral stress acting on the pile shaft to the total vertical stress could vary from k_0 for dense frozen soils to 1 for ice-rich soils and crystalline ice.

The magnitude of horizontal stress acting on pile shaft from overburden pressure and/or slurry refreezing or soil freeze-back is still widely undefined. When an over-sized pre-drilling installation technique is used, horizontal stress from overburden pressure on pile shaft could be minimum and may not exceed 100 kPa in any other case (Ladanyi and Theriault 1990), However, induced horizontal stress from slurry refreezing or soil freeze-back may enhance the total normal stress.

Figure 11a shows the change in volumetric unfrozen water content (UWC) of the frozen sand, with respect to its initial UWC value of 0.40 cm^3/cm^3, at the pile-soil interface and within the soil following freezing. Unfrozen water content followed a typical trend of reduction corresponding to soil freezing below zero degree Celsius. The amount of UWC at a given freezing temperature, however, was always higher at the pile-soil interface compared to the UWC observed within the soil far from the pile. The difference in UWCs between the two locations increases slightly with decreasing temperature. As discussed earlier, this could be attributed to the quicker response to thermal change exhibited by the steel pile compared to frozen soils which could cause a faster freezing rate at the pile-soil interface. As a result, a greater inter-particles UWC volume

would be generated adjacent to the shear plane at pile-soil interface compared to the soil region farther from the interface.

The ration between the change in unfrozen water content at the pile-soil interface and in a region far from the pile are plotted against temperature in Figure 4.11b. On the same plot, the change in roughness factor “m” and the frictional factor “n” with temperature are also presented. The results showed that the ration between UWC at pile surface and within the soil increased as the temperature decreased referring to increasing the difference between UWC of the two locations as the temperature was reduced. These results explain the lower adfreeze strength of the pile-soil interface at any given temperature compared to the cohesion strength of frozen soil reported earlier. It also explains the lower roughness factor corresponding to lower exposure temperatures which could be attributed to the higher UWC ratio at lower temperature (Figure 4.11b). The frictional factor “n”, however, showed less sensitivity to temperature and UWC change as the friction contribution of frozen sand could be dominated by the interlock force between the soil particles with less contribution of interlock force within ice fraction. Thus, it shows constant value of 0.75 at any UWC and freezing temperature.

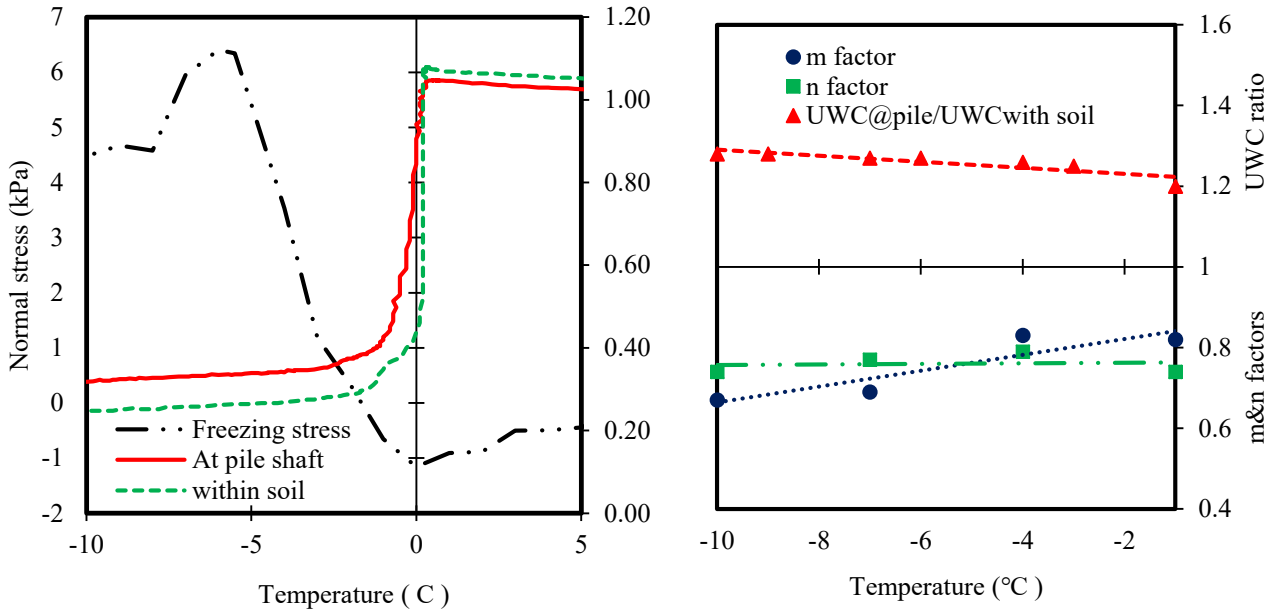

Figure 4. 11. (a) Unfrozen water content at pile shaft and within the soil, (b) variation of roughness factor and UWC ratio with temperature.

As the liquid water transforms to ice within the soil, the ice content increases, the unfrozen water content and permeability decrease, and frost heave develops. Figure 4.11a illustrates the variation of the exerted horizontal stress subjected to the pile shaft as a function of temperature and UWC. Before the freezing point, the horizontal stress experienced a slight reduction of about 1 kPa which could be attributed to soil consolidation around the pile. However, and as the temperature drops below zero-degree Celsius, the UWC decreases and horizontal stress dramatically builds up recording a maximum change of 7 kPa when the temperature reaches around -5.0°C. The increase in horizontal stress was most likely due to the contribution of the freezing induced stress following to soil freezing around the pile. As the freezing process progresses and the temperature drops below -5.0°C, the horizontal stress does not show further increase but rather experiences stress relaxation from 6 kPa to around 4.5 kPa and remained constant even when the temperature reached -15°C.

The increase in horizontal stress is mainly attributed to the volume expansion of liquid water as it transforms to ice. The increase in normal stress corresponded well to the reduction in unfrozen water content referring to a strong correlation between the two measurements. However, the contribution of freezing induced stress to the total horizontal stress was smaller than expected. The freezing induced normal stress in sand was smaller than those recorded in Leda clay which was around 84 kPa. This may be attributed to the large void space usually exists within the granular medium such as in sand, which would accommodate for most of the volume increase following to water freezing, thus, resulting in lower freezing induced normal stress. The observed freezing induced normal stress would be very small compared to normal stress from overburden pressure for a typical pile length in ice-poor soils. Therefore, the contribution of freezing induced normal stress in ice-poor soils maybe neglected as a conservative measure and Equation [4.2] could be used for estimating the ultimate adfreeze capacity of steel piles in frozen ice-poor soils.

4.5.4 Influence of pile loading rate on adfreeze strength under varying temperature exposure

It has been well documented that the adfreeze strength of piles in frozen soil increases as the strain rate increases. Parameswaran (1978), for example, showed that the peak yield adfreeze strength increased approximately linearly with increasing strain rate following a power-law trend on log-log scale and could be expressed as following:

$$\tau_a \sim i^m \qquad [4.3]$$

where, (i) is the strain rate and (m) is the strain exponent. The strain exponent from Parameswaran's (1978) experiment varied with the pile surface materials and was reported as 0.1035 for unpainted steel and 0.2161 for concrete piles. However, the dependence of ultimate strength of piles on strain rate in frozen soils has often been reported at a given freezing

temperature. Nevertheless, the influence of strain rate on ultimate capacity of piles may differ over a wide range of ground temperature due to the potential difference in unfrozen water content and change in viscus behavior of ice matrix. Williams and Smith (1991) suggested that frozen soil would exhibit higher strength when exposed to fast loading due to the undrained condition that would be respectively imposed on the frozen soil sample. Undrained condition associated with fast loading would limit the dissipation of the inter-particle unfrozen water content resulting in excess pore water pressure, thus, yielding a higher total shear strength of frozen soil. Xu et al. (2017), more recently, reported higher yield and peak stresses for frozen clay soil samples tested under faster strain rates attributing that to the different stress distribution in the test sample under different strain rates.

Figure 4.12a compares the ultimate adfreeze capacity of steel-pile interface determined under a fast shear rate of 0.0113 mm/min and a slow shear rate of 0.00208 mm/min The result shows that the adfreeze strength determined under fast loading was always greater than those measured under slow loading condition. This confirms the conclusion made by other researchers. Based on Xu et al. (2017)'s conclusion, the shear testing under slower strain rates would require longer testing time period which allows for more uniform stress distribution within the test samples causing the external load to be carried equally by the different matrices (i.e., ice, soil grains, and unfrozen water). As a result, soil samples tested under slower strain rates would deform uniformly and experience local failure, thus less likely to reach their peak stresses. In contrast, soil samples that are tested under higher strain rates would experience non-uniform stress distribution where the stresses are usually localized in parts of the sample and cause localized deformation. Therefore, only a portion of the sample carries most of load resulting in rapidly reaches its peak stress followed by brittleness failure occurrence. The non-uniform deformation would often limit the

development of the plastic deformation inside the sample and lead to the higher yield and peak stress under rapid strain rate condition.

To comprehend upon the role of temperature in controlling the effects of strain rate on the ultimate adfreeze strength of steel-soil interface, the ratio between ultimate adfreeze strength determined at the high strain rate and the ultimate adfreeze strength determined at the low strain rate is plotted against the freezing temperature and presented in Figure 4.12b. As noted, this ratio increased exponentially with increasing ground temperature varying from 1.6 at -10°C to 3.7 at -1.5°C. This refers to more pronounced effects of strain rate on ultimate adfreeze strength of pile foundations in frozen grounds that experience warm freezing temperature such as warm permafrost. This observation highlights the important role that the ground temperature plays in controlling the response of pile foundations under different loading type in frozen ground. The warmer frozen ground would perhaps contain higher unfrozen water content and lower ice content than the frozen grounds that exist at very cold temperature. The high quantity of unfrozen water in warm frozen ground would make a higher chance for the stress to be localized in the pore water than pore ice, therefore, resulting in greater excess pore water pressure under higher strain rates compared to the same sample tested under slower strain rates. As the test temperature decreases, ice content would respectively increase which would make the load to be more likely to be localized in ice pore. Because of its higher viscosity, crystalline ice is less sensitive to shear strain comparing to liquid water. Although, ice would carry greater load compared to liquid water, its load carrying characteristic would be less different under different strain rate at same level of temperature, thus yielding slight differences in load capacity if slow or high strain rates are applied. The short-term bearing capacity of pile foundations in frozen ground and under rapid loading condition may not only be due to interface adfreeze and frictional resistances but the contribution

of excess pore water pressure and stress localization too. Thereby, knowledge about long-term strength and creep behavior are always desired before designing pile foundations in frozen ground. Moreover, determining the design load of piles considering their ultimate load capacity at a given strain rate would require sufficient knowledge of the temperature regime and unfrozen water content of the surrounding soils for accurate estimation of load capacity and deformation prediction.

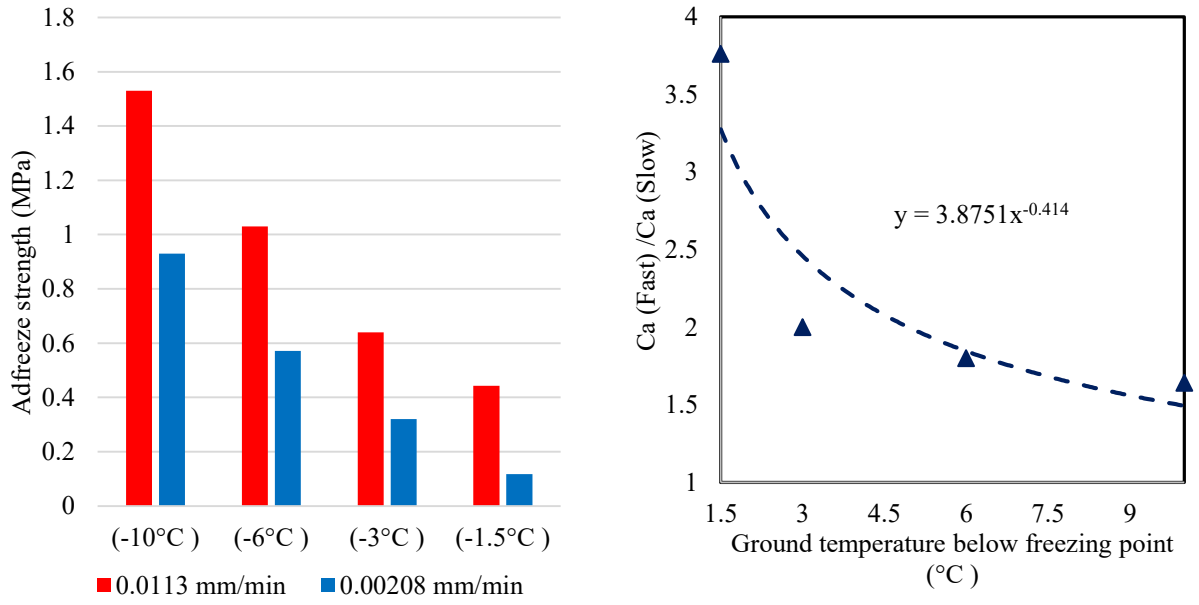

Figure 4. 12. (a) Adfreeze strength of steel-soil interface at different strain rates and temperatures, (b) Variation of the ration between undrained and drained adfreeze strength with freezing temperature

4.5.5 Comparison of ultimate capacities from interface element tests and model pile test

The pull-out capacity of the model steel pile embedded in the steel box was determined at -7°C and compared with those obtained from two steel-soil interface element tests for the purpose of validation and repeatability screening. The element tests showed very good repeatability exhibiting peak strengths of 1375 kPa 1310 kPa at the respective displacements of 1.26 mm 1.61

mm (Figure 4.13). The peak strength of the model pile under pull-out capacity agreed well with those determined from element tests recording 1175 kPa at an axial displacement of 1.32 mm. The slightly lower ultimate capacity from the model pile compared to the element tests could be attributed to the lower normal stress of 5 kPa subjected to the pile shaft in oppose to 25 kPa normal stress imposed on the element test samples. An ultimate capacity (Ca) of 1200 kPa was obtained from element tests at zero normal stress estimated based on Mohr-Coulomb lines as reported in Table 4.1. This value is very close to the ultimate capacity of the model pile as both were measured at a similar normal stress of 0 kPa and 5 kPa respectively. These results show the capability of the interface element tests in capturing the behavior of steel piles in ice-poor soils. The good repeatability observed from the element tests also supports the validity of the reported results in the current study.

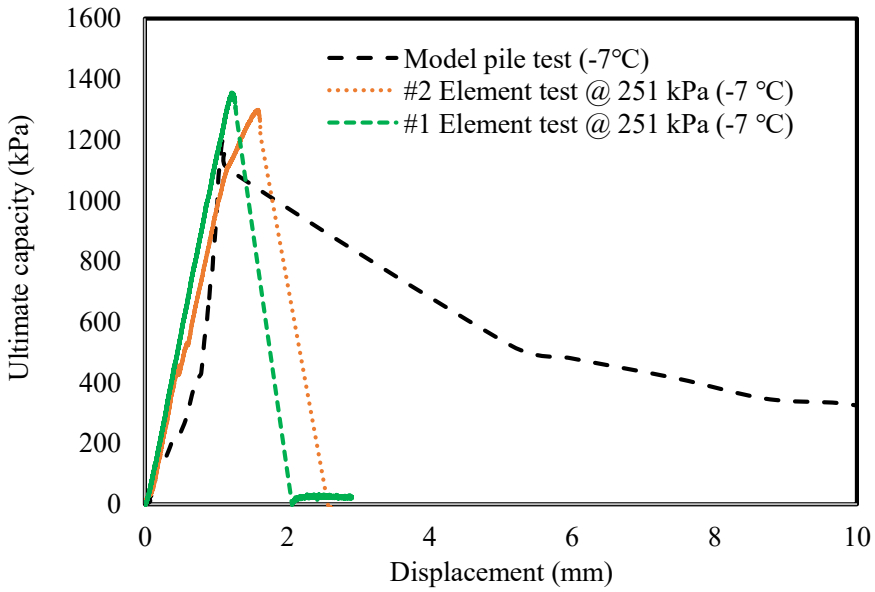

Figure 4. 13. Stress-displacement curves from model steel pile and steel-soil interface element tests

4.6 Conclusions

The current chapter reviewed the design approach used for pile foundations in ice-poor frozen ground. The ultimate shaft capacity of pile foundations in frozen sand is a resultant of adfreeze strength and frictional resistance developed at the pile-soil interface. A constant roughness factor of 0.7 was found to be reasonable to correlate the adfreeze strength of the steel pile shaft to the cohesion strength of the frozen sand with respect to ground temperature. A frictional factor "n" with a value of 0.75 was introduced to account for frictional resistance developed at the pile-soils interface based on the frictional resistance of the frozen soil with respect to ground temperature. A modified design approach was proposed for estimating ultimate shaft resistance of steel piles in ice-poor soils. The use of this equation should be limited for similar soil type, pile material, and thermal condition. The increase in normal stress subjected to the pile shaft in ice-poor soils was found to be minimal and can be neglected for conservative design load prediction.

Adfreeze strength of pile foundation can be significantly affected by the strain rate. Piles that are loaded under a rapid loading condition would most likely to exhibit greater adfreeze strength. The higher adfreeze strength could be attributed to the stress localization and possibly to the greater excess pore water pressure under faster strain rate. However, longer term adfreeze strength after this rapid loading condition may experience relaxation over the time due to the time-dependent behavior of frozen grounds.

The interface shear tests were shown to be capable of representing pile-soil interface strength behavior in the field and can be used to simulate the behavior of conventional steel piles in frozen ice-poor soils with acceptable degree of validity.

CHAPTER 5: LOAD TRANSFER OF PILE FOUNDATIONS IN FROZEN AND UNFROZEN SOFT CLAY

5.1 Introduction

Pile foundations are often used to support structures in many northern communities because of their sufficient load carrying capacity. Some of these piles are conventional such as timber, steel pipe and H-piles, precast and cast-in-place concrete piles, and others are recently proposed such as helical piles and thread par piles. The selection of pile type to support structural loads in cold regions is mainly governed by the permafrost conditions (i.e., warm permafrost or cold permafrost).

In frozen ground, the adfreeze strength developed during the frost formation along the pile shaft can significantly contribute to the pile capacity. Early studies have adopted a design approach based on the assessment of ultimate load capacity of piles related to the rupture of the adfreeze bond developed at the pile-frozen soil interface along the pile shaft (e.g., Crory and Reed 1965; Penner 1970, 1974; Penner and Irwin 1969; Penner and Gold 1971; Dalmatov et al. 1973). Although, piles have been shown to provide sufficient capacity when installed in frozen grounds, their performance could be severely degraded if the hosting frozen ground experienced warming. The adfreeze strength at the pile-frozen soils interface could encounter reduction if the frozen ground is exposed to warming, however, this reduction in pile capacity has not been quantified. Weaver and Morgenstern (1981) suggested that pile foundation design for frozen ground is mainly governed by time-dependent deformation (creep strain), however, the ultimate strength of pile foundations in frozen ground could be the key criteria particularly for frictional piles in ice-poor soils and frozen soils present at relatively warm temperatures.

Ground transformation from frozen to unfrozen condition is often accompanied with changes in the mechanical behavior of the ground materials. This change could accordingly influence the soil-structure interaction behavior. Pile foundation, as a structural element, interacts with the surrounding soil to develop its load capacity. The interface characteristics of piles in frozen soils, therefore, could be different from the interface characteristics of piles in unfrozen soils.

This chapter investigates load carrying capacity of five different pile foundations in frozen soft clay and evaluates the possible changes in pile capacity corresponding to the thawing action of frozen ground. In-situ pile load tests were conducted in frozen and unfrozen Leda clay and used to establish stress-displacement correlations to describe the load transfer of the test piles.

5.2 Site Preparation and Characteristics

The experimental program was conducted at the Canadian Geotechnical Research Site No. 1 located in Gloucester, Ontario. The site mainly consists of about 1.2 m top sandy silt overlaying deep layer of marine clay known as Leda clay. Leda clay was formed through marine deposition of the Champlain Sea, and now covers major parts of eastern Ontario and Quebec regions in Canada. The 1.2 m top soil was removed to reach the test level which will be called ground level from now on. Several in-situ tests were conducted to determine the geotechnical properties and ground temperature of the test soil. A 2-m deep thermocouple system was installed in the site to construct the temperature profile by recording temperature readings at intervals of 0.1-0.25 m (Figure 5.1). The undrained shear strength of the soil was determined by performing standard vane shear test in accordance to the field vane shear test procedure outlined in ASTM D2573 (2008). The undrained shear strength results showed strength reduction with depth moving from 35 kPa to 9 kPa at 0.25 m and 2.0 m depth respectively. The disturbed undrained shear strength was also determined and the results were presented in Figure 5.2.

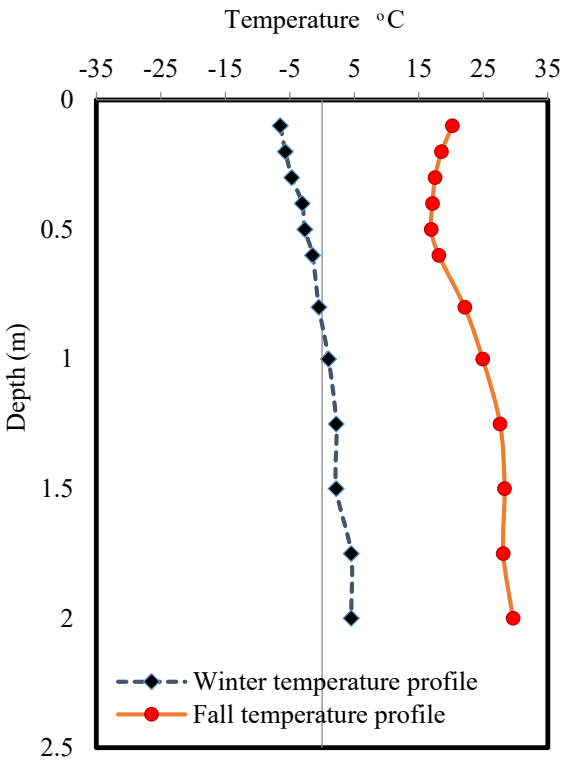

Figure 5. 1. Temperature profiles in winter and autumn seasons.

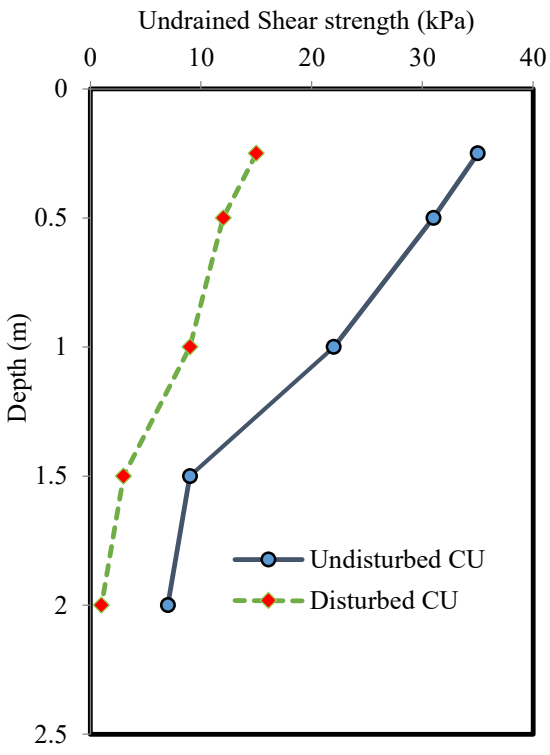

Figure 5. 2. Undisturbed and disturbed shear strength profiles for Leda clay.

5.3 Pile Characteristics and Configurations

Three model piles with different pile configurations namely circular section piles and single-helix helical piles were utilized in this study. The circular section piles were made of steel and reinforced concrete where the steel pile was an open-ended pipe pile with a wall thickness of 5 mm, outer diameter of 100 mm, and a height of 2.1 m. The precast reinforced concrete pile was a close-ended pile with 100 mm diameter and 2.1 m height, whereas the helical pile consists of 1.0 m open-ended circular shaft of 38.1 mm diameter and a single helix of 100 mm diameter located near the pile toe. Two circular shaft extensions each of 0.6 m height were connected to the helical pile to reach a total height of 2.2 m.

The test piles were equipped with 150 mm x 150 mm x 10 mm steel cap to facilitate pile driving, instrumentation, and testing (Figure 5.3). For steel pipe pile and helical piles, the cap was

aligned perpendicular to the pile central axis and then welded to the pile head. For precast concrete pile, the cap was first welded to the steel rebar, and then the concrete was casted where tight connection between the pile head and the steel cap was ensured. The pile caps were featured with 9.5 mm holes at the four corners. These holes were later used to attach another square plate which was featured at its center with high-strength threaded steel bar of 19 mm diameter and 1.5 m length to perform uplift pile load tests. All piles were inserted into the ground to a depth of 2.0 m from the ground surface and tested in frozen and unfrozen conditions under uplift pressure.

Other sets of single-helix helical piles were inserted to depths of 2.0 m, 1.0 m, and 0.25 m from the ground surface and tested under compression in frozen and unfrozen grounds to evaluate the effect of helix location on the load carrying performance of helical piles in frozen and unfrozen grounds.

Figure 5. 3. Pile configurations and driving setup.

5.4 Pile Installation

Circular section piles were driven into the ground using impact hammer driving technique. This was conducted by utilizing a 15.87 kg (35 lb) hammer falling from a distance of 0.5 m on the pile head using a pulley and drop hammer setup (Figure 5.3). The falling distance was maintained constant and hammering action was conducted manually at a rate of 10-15 blows per minute. The penetration rate of the pile tip varied with depth from 2-5 mm/blow along the upper 1.0 m depth. The penetration rate increased significantly to be as high as 10 mm/blow through the rest of the depth. Piles were driven up to 2.0 m depth and the cumulative blow count versus penetration depth of the steel pile is shown in Figure 5.4. The helical piles, on the other hand, were inserted into the

ground under a manual torque force applied at the pile head using a proper size steel wrench (Figure 5.5).

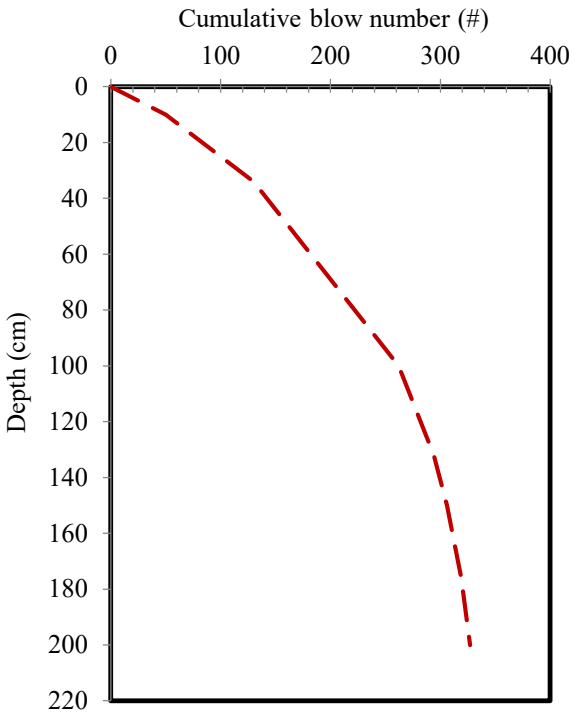

Figure 5. 4. Variation of cumulative blow count with depth.

Figure 5. 5. Helical pile installation.

5.5 Reaction Frame for Pile Load Testing

The reaction frame consisted of two reaction steel open-ended pipe piles, each of 150 mm diameter, 2.5 m length, and wall thickness of 5 mm. The reaction piles were connected to each other through two 300 mm x 50.8 mm x 3.65 m plywood reaction beams. The reaction beams were connected to the reaction piles using high-strength threaded steel bars of 19 mm (¾ inch) diameter. The threaded steel bars were passed through pre-drilled holes in the reaction beams and reaction piles, then, tightened carefully using steel nuts.

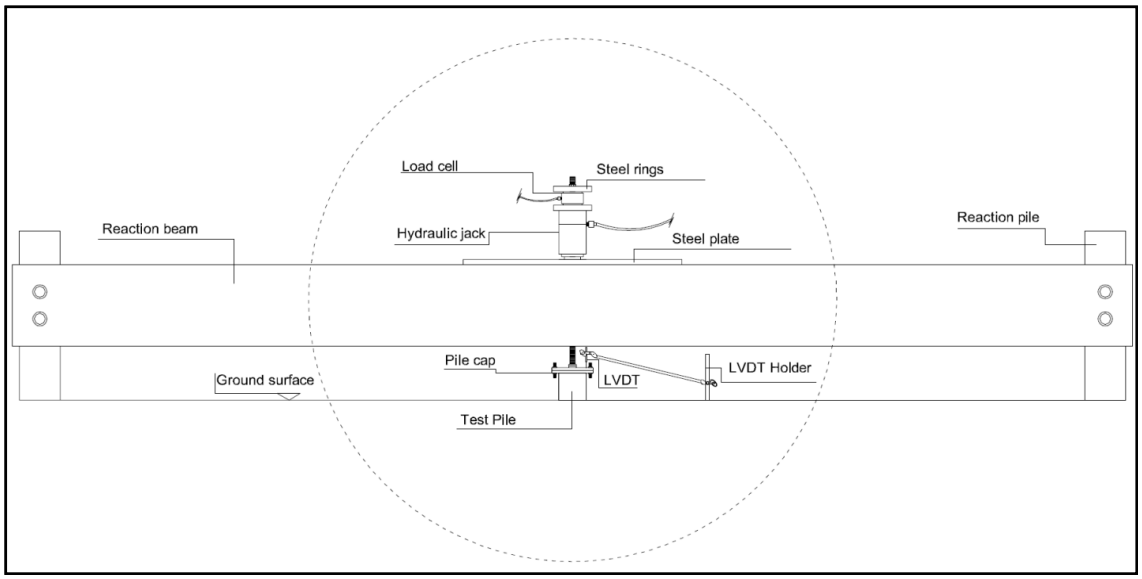

Figure 5. 6. Instrumentation and pile load test setup.

The reaction system has a theoretical capacity of approximately 3.0 times the capacity of the test piles. The reaction system was utilized to serve both pull-out and compression load testing. The load was applied using a 103 kPa (15 psi) manual hydraulic pump and a 100 kN hollow hydraulic jack. For pull-out test, the hydraulic jack was mounted on a 0.3 m x 0.4 m x 15 mm hollow steel plate situated on the edge of the reaction beams. The load cell was then positioned on top of the jack where the whole system was sealed by a circular steel ring tightened by a steel nut at the very top (Figure 5.6). The pull-out force was transmitted from the jack to the pile head through the 1.5-m high strength threaded steel bar, and the bar was connected to the pile cap through a steel square plate using four 6.35 mm (¼ inch) bolts (Figure 5.6). To perform compression tests, the hydraulic jack was positioned on the top of the pile cap to bear on the lower edges of the reaction beams through the steel plate. The load cell in this case was situated between the jack and the steel plate.

5.6 Instrumentations and Test Procedure

Both pull-out and compression tests were performed in accordance with ASTM D1143/D1134M (2007), following the Quick Test Method for single piles. The ultimate bearing capacity of the tested piles was estimated theoretically following the total stress analysis for cohesive soils. Uplift load was applied in increments of 10% of the theoretically estimated ultimate load capacity allowing 5 minutes' intervals between each loading step. Load measurements were facilitated utilizing a vibrating wire load cell. The test data was recorded electronically using a data acquisition system. The vertical pile displacement was recorded using Linear Variable Differential Transformers (LVDTs) with accuracy of ±0.01 mm and a maximum mechanical travel distance of 100 mm. The displacement sensor was mounted on a dial indicator holder attached to a circle-section steel reference beam. The reference beam was independently supported with two circle-

section steel columns positioned far enough from the reaction frame to eliminate the disturbance of displacement measurements during testing. The displacement transducer freely bears on the steel cap parallel to the vertical axis of the pile.

5.7 Results and Discussion

5.7.1 Temperature profile

Pile load tests and temperature measurements were conducted in Autumn season and Winter season respectively. Test piles were installed on September 20, 2014 and tested one month after the installation in order to account for pore water pressure dissipation (known also as pile set up effect) (Afshin and Rayhani, 2014; Hosseini and Rayhani, 2017). Ground temperature measured in the autumn shows a reduction from 20°C at 100 mm depth to 16.9°C at a half meter depth from ground surface. The temperature, then, increased reaching 29.6°C at 2.0 m depth from ground surface (Figure 5.1). The temperature change with time was tracked during Winter season until constant readings were observed and recorded on February 25, 2015. At a depth of 100 mm below ground surface, the temperature drops from 20°C in the Fall to -6.5°C in Winter. However, the Winter temperature profile shows a linear increase with depth intersecting the freezing point (0°C) at a depth of 0.85 m below ground surface and 4.5°C at depth of 2.0 m (Figure 5.1). Zero degree Celsius is the theoretical freezing point at which the phase change of water from liquid to solid occurs. Therefore, the portion of the ground that shows temperature equal or below freezing point was considered frozen. Although there is no permanent permafrost observed recently in Ottawa region, a seasonal freeze/thaw depth between 0.6-1.2 m (2-4 ft) is commonly encountered (Armstrong and Csathy 1963)

5.7.2 Theoretical estimation of bearing capacity of the test piles in unfrozen soft clay

In order to compare the experimental pull-out capacity with the theoretical capacity for piles tested in unfrozen condition, the theoretical capacity was calculated using total stress analysis for conventional circular-section piles and single-helix helical piles. For the uplift capacity for circular-section steel and concrete piles in unfrozen cohesive soil, Alpha method was used to determine the unit skin friction (CFEM, 2017; Meyerhof and Fellenius, 1985).

The pull-out capacity for the single-helix helical piles in unfrozen cohesive soil is a resultant of the plate bearing capacity Q_u and the skin frictions of the pile shaft Q_s. The equations used to estimate the theoretical pull-out capacity for helical pile in exam were derived by Tappenden and Sego (2007) based on the individual plate bearing failure mode. The plate bearing capacity in pull-out loading condition is obtained using equation [2.10] as follow:

$$Q_u = \frac{\pi(D^2 - d^2)}{4}(\mathrm{N_c C_u} + \gamma' H)$$

where: Nc is the bearing capacity factor for cohesive soil; Cu is the undrained shear strength (kPa); H is depth of helix below ground surface (m); D is the diameter of helix (m); d is the diameter of pile shaft (m). The bearing capacity factor for cohesive soil, Nc, is equal to 9 in compressive loading condition, but in uplift loading condition, Nc is to be determined from the equation [2.12] as following:

$$N_c = 1.2\left(\frac{H_1}{D_1}\right) \leq 9$$

The shaft resistance of helical piles installed in cohesive soils and exposed to either compressive or uplift loading was estimated from equation [2.11] as following:

$$Q_s = \pi . d . H_{eff} . \alpha . C_u$$

where: α is the adhesion factor and H_{eff} is effective shaft length which was estimated by Zhang (1999) as (H1-D1) where, H1 is the length of the pile shaft between the ground surface and the uppermost helix and D1 is the diameter of the helix.

A parametric study was conducted in laboratory using the interface direct shear tests to determine the adhesion factor α for the test soil. The test results showed α values equal to 0.4 for the steel-soil interface and 0.45 for the concrete-soil interface. Larger adhesion factor measured for concrete-soil interface could be attributed to the contribution of suction force resulted from the unsaturated concrete material. Using the measured α values and given that the average undrained shear strength is equal to 19 kPa (Figure 5.2), the theoretical pull-out capacity of 4700 N and 5400 N was estimated for the steel and concrete piles respectively, while the theoretical pull-out for the 2m-depth helical pile was about 2100 N (Figure 5.7).

5.7.3 Ultimate experimental pull-out capacity of the test piles in frozen and unfrozen soft clay

The load-displacement relationship was determined from pile load test results for piles in unfrozen and frozen ground (Figure 5.7). For piles in unfrozen soil, the maximum pull-out capacities were 4700 N and 5500 N for steel and concrete piles respectively. The corresponding displacement at failure varies from 0.8 mm for the steel pile to 1.3 mm for concrete pile (Figure 5.7a&b). The higher pull-out capacity for the concrete pile could be attributed to contribution of suction force generated from the concrete, as an unsaturated material, at the pile-soil interface (Giraldo and Rayhani, 2013). The single-helix helical pile recorded a maximum pull-out capacity of 1400 N at 1 mm displacement and tended to show strain hardening reaching a pull-out capacity of about 1600 N at the end of the test (Figure 5.7c).

The estimated theoretical capacity was in good agreement with the capacity measured for steel pile in the field, while the theoretical capacity was 14% less than the measured capacity for concrete pile. This could be attributed to the enhanced adhesion between the concrete pile and clay soil due to suction force applied from the unsaturated concrete material. For the single-helix helical pile, in contrast, the theoretical capacity was about 33% greater than the measured capacity. This difference might be attributed to the reduction in the undrained shear strength of the clay soils due to the disturbance occurred during the installation of helical piles, thus yielding lower measured capacity especially in pull-out loading condition. However, and based on the Canadian Foundation Engineering Manual (CFEM, 1978), the results from pile loading tests are considered more reliable as the actual pile capacity depends significantly on the geometry of the pile, the driving method, properties of clay, and time effects.

The pull-out tests in frozen ground were performed on the same piles that were subjected to pull-out testing in unfrozen ground, therefore, pile-soil interface disturbance may have occurred and could possibly affect the results of pile capacity in frozen ground. Ground heave following to freezing could have also mobilized the location of the pile with respect to the surrounding soil compared to the situation in unfrozen ground. However, the piles were left unloaded and free to heave with the ground during ground freezing aiming at minimizing the degree of pile-soil interface disturbance. The test results of steel and concrete piles in frozen soil showed a small yield stress at around 1000 N followed by continuous increase in the pull-out capacity with proportional increase in pile head displacement without exhibiting any signs of reaching an ultimate limit state. The performance of steel and concrete piles was quite similar up to a pile displacement of 2 mm and corresponding capacity of 7500 N. After this point, and at any given displacements, the steel pile exhibited higher capacity compared to the concrete pile until the test

was terminated when 5 mm displacement was reached (Figure 5.7a&b). The selection of 5 mm as limiting displacement was based on the 5% D failure criterion suggested by the Federal Highway Administration (FHWA) for driven piles. FHWA criterion is applicable if plunging of the shaft cannot be achieved, thus the failure load is considered to occur at a pile displacement of 5% the shaft diameter (Paikowsky 2004). In the current experiment, the corresponding pull-out capacities at termination (i.e., 5% D displacement) were 26,000 N and 24,000 N for the steel and concrete piles respectively. For the helical pile in frozen soil, the failure was observed at a maximum pull-out capacity of 4000 N and corresponding displacement of 1.5 mm. Compared to the pull-out capacity of steel and concrete pile, the capacity exhibited by the helical pile was significantly smaller. This was attributed to the absence of frozen soil at the helix location of the helical pile. The frozen soil profile, as it was interpreted from Figure 5.1, extended only to a depth of 0.85 m below the ground surface while the helix was driven to 2.0 m depth from the ground surface. The temperature recorded at this depth was 4.5°C indicating that the helix itself located in unfrozen soil layer. Therefore, the contribution of the adfreeze strength for helical pile was only limited to the upper 0.85 m of the pile shaft. Consequently, the pull-out capacity for helical pile in frozen soil recorded a slight increase compared to its capacity in unfrozen soil. The results may indicate that the load carrying capacity of the test piles in frozen ground was dominated by shear strength behavior of ice. Following to ground freezing, unfrozen water content would descend while ice content would increase and enhance pile load capacity due to the contribution of adfreeze strength. Adfreeze strength as reported in Chapter 3 & 4 depends on the roughness factor “m” and shear strength of frozen soil with respect to ground temperature. For an average ground temperature of -4℃ observed in the time of pile load testing, the cohesion strength and friction angle of the frozen ice-rich Leda clay would be 1120 kPa and 27.5° respectively as reported in Chapter 3. Using

Equation [3.7], the ultimate shaft capacity of the steel and concrete piles under an average overburden pressure of around 7.5 kPa can be determined as follow:

$$\tau_a = 0.54\,(4+1)^{0.215}\ 1120\ + 1.80\,(4+1)^{0.235}\ 0.0075\ \tan\ (27.5) = 0.86\,MPa$$

Given the frozen ground depth around the steel and concert piles of 0.85 m, the shaft area of the steel and concrete piles within the frozen portion was calculated as 0.267 m^2. The ultimate pull-out capacity of the steel and concrete piles could be then estimated as:

$$P = \tau_a * A = 860 * 0.267 = 230\ \text{kN}$$

The estimated ultimate pull-out capacity was significantly greater than the maximum pull-out load in filed which was around 25 kN. This indicates that the steel and concrete piles in this experiment were far from their ultimate pull-out load capacity under the subjected load in filed. Therefore, both piles experienced no failure and showed identical stress-displacement behaviors which reflected the behavior of the frozen soil. The greater capacity recorded for the tested piles in frozen ground may be correlated to the high compression and tensile strength of crystallin ice. In pull-out loading condition, tensile strength of ice would be the controlling factor, which was reported by Haynes, (1978) as 1.71 MPa at -0.1℃ and increasing to 3.16 MPa when the test temperature decreased to -54℃. The helical pile, in contrast, reached its ultimate limit state as its helix was below the frozen depth and only part of the shaft was within the frozen ground. Therefore, the surrounding soil could not sustain the applied pull-out load on the helical pile, thus, failure occurred.

The helix seems to be responsible for carrying the majority of the load applied on helical piles. The increase in pull-out capacity for helical pile could have been greater if the helix was within a frozen soil. The helical pile test results highlight the importance of ensuring the location

of the helix to be within strong soil layers in temperate region or within a permanent frozen soil in the cold region. In order to comprehend upon the effect of helix location on the load carrying capacity of helical piles in frozen ground, the next section was dedicated to compare pile load test results from three helical piles installed at three different depths and tested under compression loading.

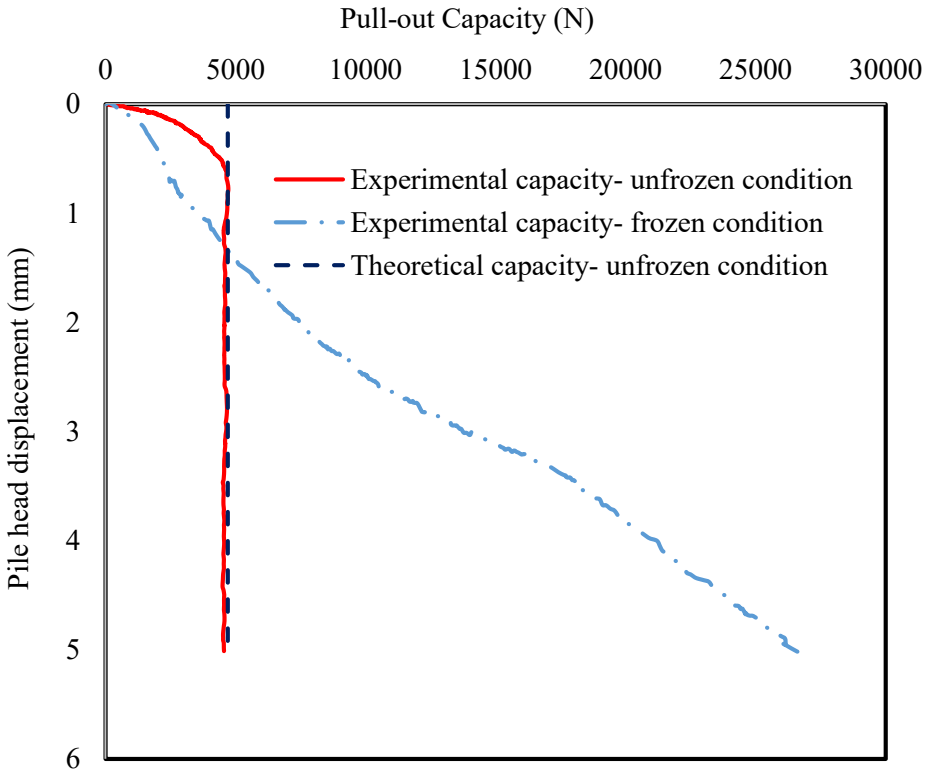

a. Steel pile

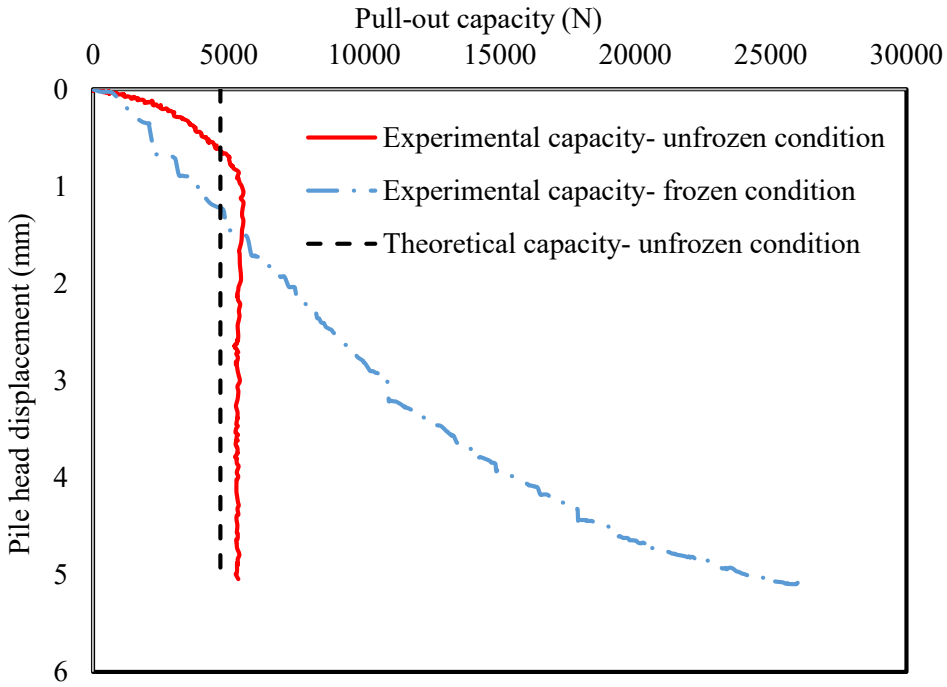

b. Concrete pile

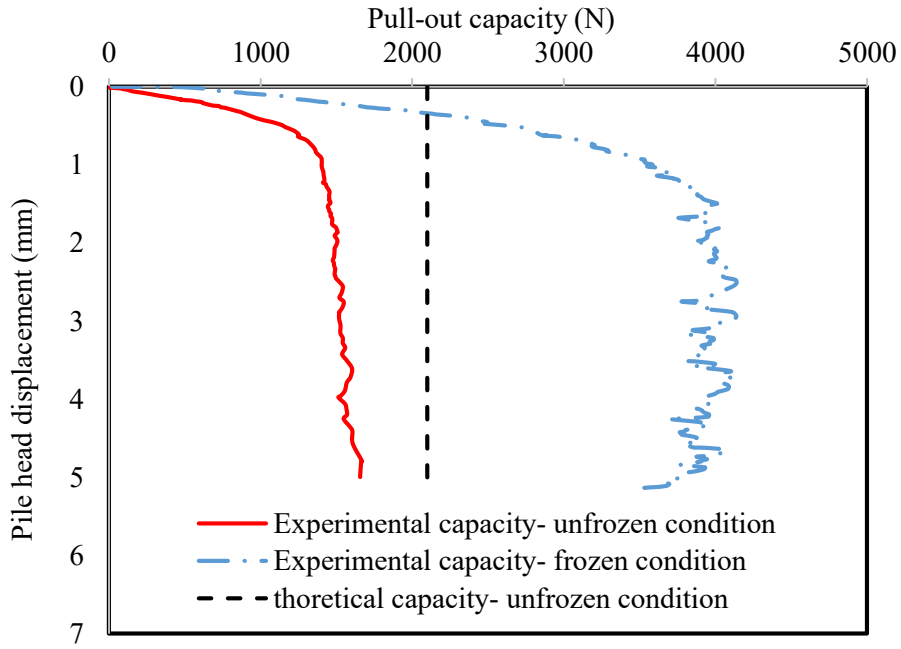

c. Helical pile

Figure 5. 7. Load-displacement relationships for test piles in frozen and unfrozen soils.

5.7.4 Effects of helix location on performance of helical piles in frozen grounds

Helical piles are distinguished by the number of helixes that are welded to their shaft to enhance their bearing capacity and accordingly maximize their ultimate load capacity by increasing the interaction area between the pile and the surrounding soil. High capacity helical piles commonly come in shaft diameters ranging between 100 to 320 mm and helix diameter of 2 to 3 times the shaft diameter. The bearing capacity of the helix could be responsible for up to 50% of the total load carrying capacity of helical piles. Therefore, it is significantly important to ensure the helix engagement in the pile resistance by positioning the helix at the right depth and in the proper soil layer. In the current study, three single-helix helical piles where inserted to depths of 2.0 m, 1.0 m, and 0.25 m from the ground surface in fall season and tested under compression in winter season to evaluate the effect of helix location on the carrying load performance of helical piles in frozen grounds.

The load-displacement curves from the three pile load tests performed in winter are plotted in Figure 5.8. The results show ultimate compression capacities of 3000 N and 4000 N for the helixes inserted to 1.0 m and 2.0 m depths from ground surface respectively. Higher ultimate capacity recorded for helical pile with the helix installed at 2.0 m can be attributed to the higher confining pressure and larger pile-soil interaction area compared to the one installed at 1.0 m depth. Controversially, the helical pile with helix installed at 0.25 m depth from ground surface exhibited an ultimate compression capacity of 13,000 N recording about 3 to 4 times greater capacity than the two former piles. By looking at the temperature profile recorded in winter season and showed in Figure 5.1, it is realized that the ground condition along the upper 0.85 m was frozen which resulted in an enhanced bearing capacity due to generation of adfreeze strength and higher bearing capacity of frozen ground, dissimilar to the portion of the ground below this point which remained

in its unfrozen condition. Since the helical pile that installed at 0.25 m depth was entirely within the frozen portion, its capacity accordingly became significantly higher due to high resistance of the soil located underneath the helix of this pile. This result highlights the important rule of helix in carrying a great portion of the load imposed on helical piles, and in order to maximize the helical pile performance, the helix should be positioned carefully. In frozen ground, the helix must be installed within the permanently frozen layers and should not be located within the active layer.

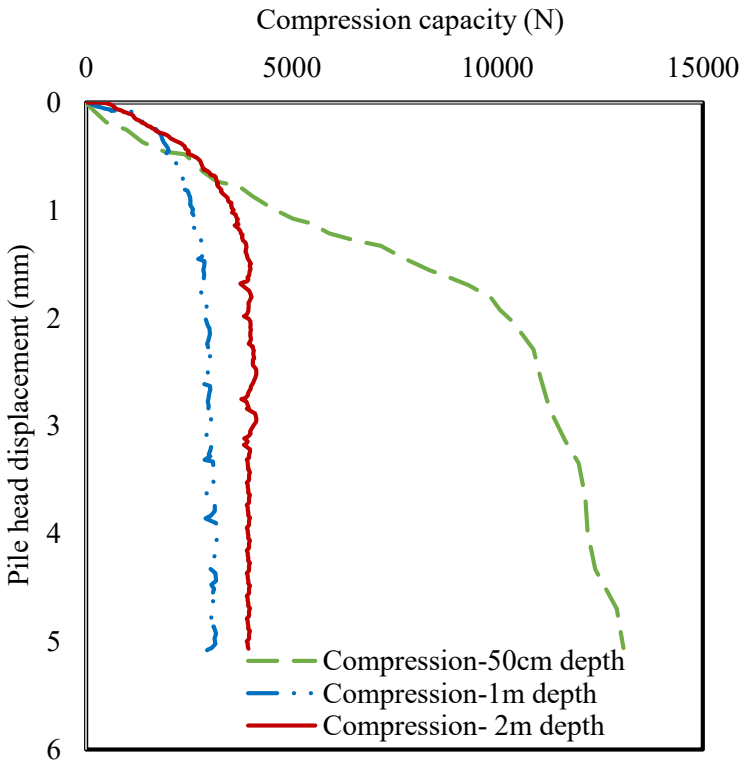

Figure 5. 8. Load-displacement curves for helical piles installed at different depths.

The experimental results also raised another issue that is related to the performance of piles in warming permafrost. The global warming has been reported to be associated with permafrost degrading in cold region. Based on the current results, a helical pile installed in frozen ground could lose 70% of its ultimate capacity if the ground experienced thawing. Global warming could

increase the ground temperature, increase the active layer thickness, and decrease the permanently frozen ground depth, and respectively decrease the shear strength of the soils and the ultimate capacity of the embedded pile foundations. Mini-helical piles used to support light structures in cold region are driven to relatively shallow depths slightly deeper than he depth of the active layer. If the anticipated permafrost degradation trend would happen, the depth of the active layer would simultaneously increase and reach the helix depth causing bearing capacity loss and respectively exaggerated deformation. Further discussion about the effect of ground thawing on ultimate capacity of pile foundations is presented in the following section.

5.7.5 The impact of thawing on the failure mode and carrying load capacity of piles in frozen soft clay

As the frozen soil is exposed to warming, its unfrozen water content increases and in turn leads to decreasing the ice content, reducing the cryosuction, and respectively decreasing the effective shear strength and the adfreeze strength (Williams & Smith, 1991). In the current study, the load–displacement relationships for the test piles in unfrozen Leda clay were typical, exhibiting elastic-perfectly plastic behavior over three distinct stages. The first stage was linear-elastic with sharp slope indicating high elastic modulus. The second stage was transitional showing nonlinear behavior where the displacement and load increments were considerably disproportional. The final stage was flat linear with slight slope for helical pile indicating strain hardening (Figure 5.8) and almost zero slope for steel and concrete piles indicating strain softening (Fig. 7a&b).

The stress-strain curves for steel, concrete and helical piles in frozen and unfrozen Leda clay were plotted on semi-logarithmic scale and illustrated in Figure 5.9. Utilizing semi-logarithmic scale enabled magnifying the correlation at the small stress region to compare the interface elastic modulus in different conditions. The behavior of the pile-soil interface in frozen

and unfrozen condition were almost identical yielding slightly higher elastic modulus for the pile-frozen soil interface. However, piles in frozen ground tended to exhibit disproportional stress versus strain showing higher load capacity at any given strain. As the temperature drops below freezing point in soil medium, the moisture content undergoes phase transformation from liquid to solid forming ice within the porous media of the soil. The shear strength of the frozen soil, therefore, would be dominated by ice behavior which usually exhibits higher shear strength, thus greater load carrying capacity of the piles compared to the unfrozen condition. The decrease in unfrozen water content and increase in the ice content may also increase the water potential within the soil around the pile and respectively enhance the suction force (cryosuction). Decreasing the unfrozen water content and increasing the suction force would also increase the effective shear strength of the soils, thus improve the load carrying capacity of the piles as the temperature decreases below the freezing point. However, the opposite case will happen if the soil experienced warming and undergo thawing action. The increase of the ground temperature will be accompanied with reduction in ice content and increase in unfrozen water content which would respectively decrease the cryosuction and the effective stress, thus reducing the carrying load capacity of the piles. At 0.05 percent strain, for example, the test piles in frozen Leda clay were still showing an increased capacity exhibiting stresses ranging from 15 kPa to 18 kPa at an average ground temperature of -5°C. Following to thawing, the piles show an average stress of 8 kPa at the same strain level of 0.05%, recording a reduction of about 2 times the load capacity of the same piles in frozen condition.

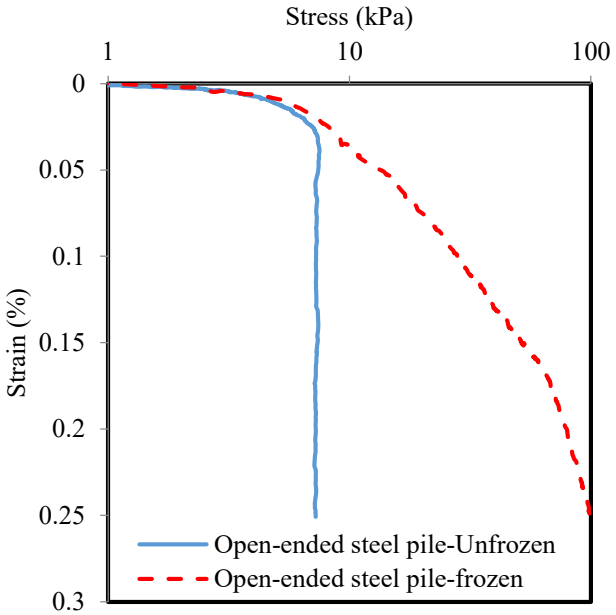

a. Stress-strain for steel

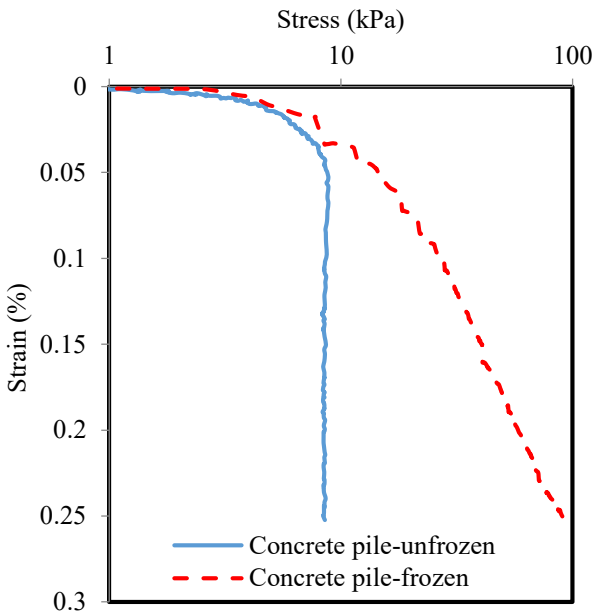

b. Stress-strain for concrete

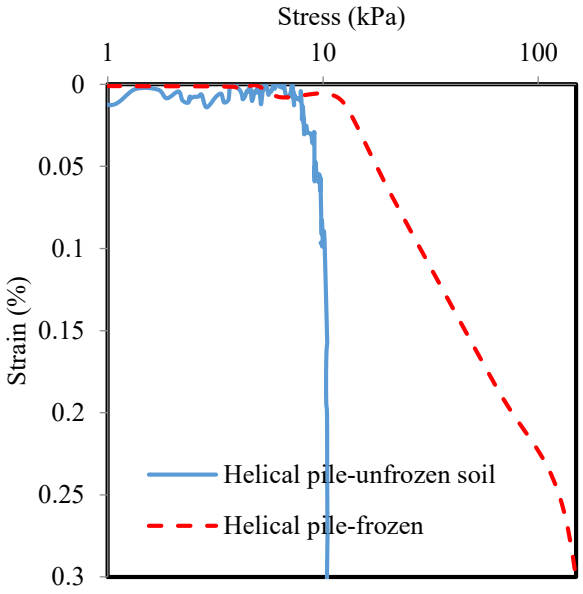

Stress-strain for helical pile in small strain region

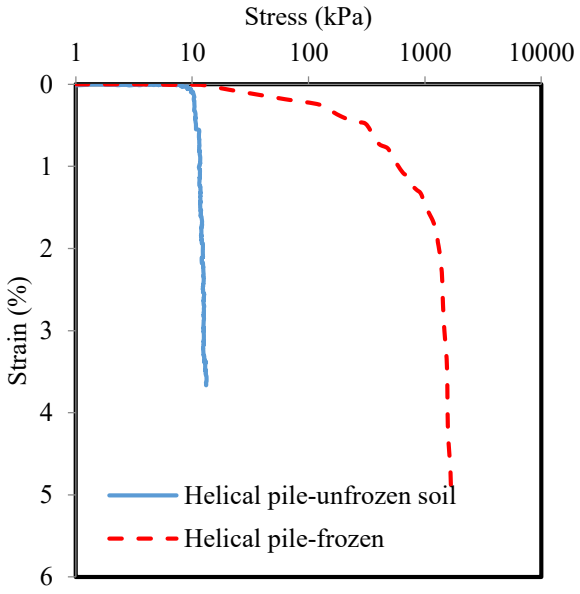

d. Stress-strain for helical pile in full strain region

Figure 5. 9. Stress-strain curves form pile in frozen and unfrozen ground.

To comprehend upon the effect of thawing on pile performance in warming frozen ground, the normalized pile capacity, expressed as the ratio between unit stresses in unfrozen Leda clay to the unit stresses in frozen soil, was correlated to the pile strain and plotted in Fig. 10. The correlation shows a drop of 20% in the pile capacity at the load onset when the ground experienced warming moving from an average of -5°C to thawing temperature. As the test proceeded and more load was applied, the piles in unfrozen soils exhibited greater reduction recording 90% less capacity compared to the piles in frozen soils at a strain of 0.25%. At this strain level, the piles in unfrozen soils have already reached their ultimate capacity while in the same soils at the frozen condition the piles still undergo a transition stage showing continuous stress gain. This highlights the significant loss in pile capacity when inclusive frozen ground degradation is encountered. The pile foundation that is designed to safely carry the computed allowable load in frozen ground at -5°C temperature could undergo severe deformation if an inclusive thawing is occurred since the pile capacity will drop by up to 90% based on the current experimental trend.

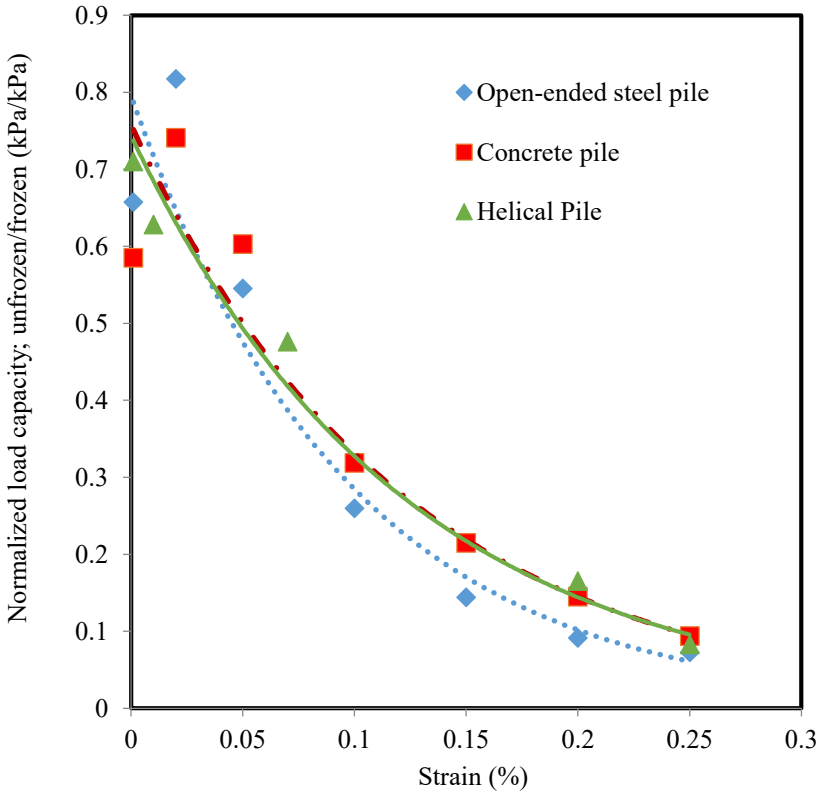

Figure 5. 10. Normalized pile capacity versus strain percentage.

Using the test data in Figure 5.10, a theoretical correlation could be developed to predict the unit stress of piles in unfrozen soil "τ_{cu}" utilizing the adfreeze strength of the piles in frozen soil "τ_a" at any given strain level "ε". The correlation is developed using exponential fitting parameters as follow:

$$\tau_{cu} = \tau_a * 0.7694 * e^{-9.24\varepsilon} \qquad [5.\ 1]$$

This equation can be used to predict the unit stress of pile foundations when the soil experienced warming from -5°C to complete thawing. Upon obtaining more experimental data at temperatures below and warmer than -5°C, the equation can then be modified with an incorporated temperature modulus to be used in predicting pile capacity at any given thermal boundary.

5.8 Conclusions

A series of pile load tests was conducted in unfrozen and frozen Leda clay to investigate the impact of frozen ground thawing on load transfer of circular section piles and single-helix helical piles in frozen soft marine clay (Leda clay). The stress-strain behavior of the circular section steel and concrete piles under pull-out loading condition in frozen Leda clay were comparable to the stress-strain behavior of helical pile under compression loading. The location of helix on helical piles was found to be crucial in defining the load carrying capacity of these piles in frozen ground. The helix must be positioned in permanently frozen layer to maximize the pile performance. A significant loss of helical pile capacity was recorded when the frost penetration depth did not reach the helix depth. This could degrade the performance of shallow depth helical piles used to support light structures in cold region if the active layer depth increases.

The piles designed to support structures in frozen Leda clay may generally lose more than 10 times their carrying load capacity if the frozen ground experienced inclusive thawing. This reflects the significant role of the thermal aspect in characterizing the performance of pile foundations in frozen soft clay. The thermal impact must be evaluated carefully and its effect should be directly included in any proposed formulation meant to estimate bearing capacity or creep response for piles in frozen ground. Finally, an analytical solution was proposed using the test data expressed in an exponential stress-strain correlation to predict the reduction in pile capacity corresponding to frozen ground thawing. The proposed equation could be more comprehensive in predicting pile capacity in frozen ground at different freezing temperatures if more test data are obtained and incorporated.

CHAPTER 6: LOAD TRANSFER AND CREEP BEHAVIOR OF CONVENTIONAL AND HELICAL PILES IN FROZEN GROUND

6.1 Introduction

Previous chapter demonstrated the effect of frozen ground warming on bearing capacity of different types of pile foundations. However, creep deformation may govern the failure criterion of pile foundations especially when installed in ice-rich frozen grounds. Although creep deformation for some types of pile foundations in frozen ground, such as smooth-shafted piles, is reasonably well-understood, other types of pile foundations, such as helical piles, lack clear design guidelines. Load transfer mechanism of helical piles installed in frozen ground is also widely unknown and required fundamental description. Furthermore, creep behavior and load transfer mechanisms of all types of pile foundations installed in frozen grounds that have freezing temperature close to the freezing point is not well-defined and requires comprehensive assessment.

To complement on the field work described in the previous chapter, the creep behavior and load carrying capacity in field for different types of pile foundations is investigated. this chapter is tackling the issue of load transfer mechanism and creep behavior of three model pile foundations installed in frozen ice-rich silt in Gloucester, Canada. Load transfer of these model piles under unfrozen condition is also presented and discussed.

The current field experiment is aimed at studying the performance of the test piles namely open-ended pipe pile, single helix helical pile and grouted shaft helical pile in ice-rich silt type of soil. The chapter provides comparison between the ultimate pull-out capacity and creep behavior of these piles under different creep stresses. It also compares the results obtained from this study with other pile creep and bearing capacity models for pile foundations in frozen ground. Creep

behavior and load transfer of the helical piles are carefully analyzed in an attempt to attain better understanding of their performance in frozen grounds.

6.2 Site Characteristics

Three test platforms were assembled at the Canadian Geotechnical Research Site #1, Gloucester, Ontario to carry out creep tests and pull-out bearing capacity tests on the three different pile types installed in the field. The site mainly constituted of 200 mm top soil formed of a mixture of gravel, sand and silt. The top soil is followed by 900 mm of sandy silt soil that overlays a 1000 mm of stiff silty clay layer followed by a deep profile of soft Leda clay. A roof structure was built over the piles to maintain snow-free surface at the pile locations during the winter season, thus, maximize the frost penetration depth. The three test piles were installed in the top one-meter soil layer. Representative soil samples were collected from this layer and underwent laboratory testing for geotechnical characterization. The particle size distribution analysis showed that the test soil was mainly sandy silt with zero clay fraction content (Figure 6.1). The liquid limit and plasticity index of the sandy silt soil were determined as 24% and 7% respectively. The natural water content of the soil was 21% while its bulk density was around 1.56 Mg/m3. The undrained shear strength for the sandy silt was determined at 50 kPa using the direct shear test technique following the quick loading approach.

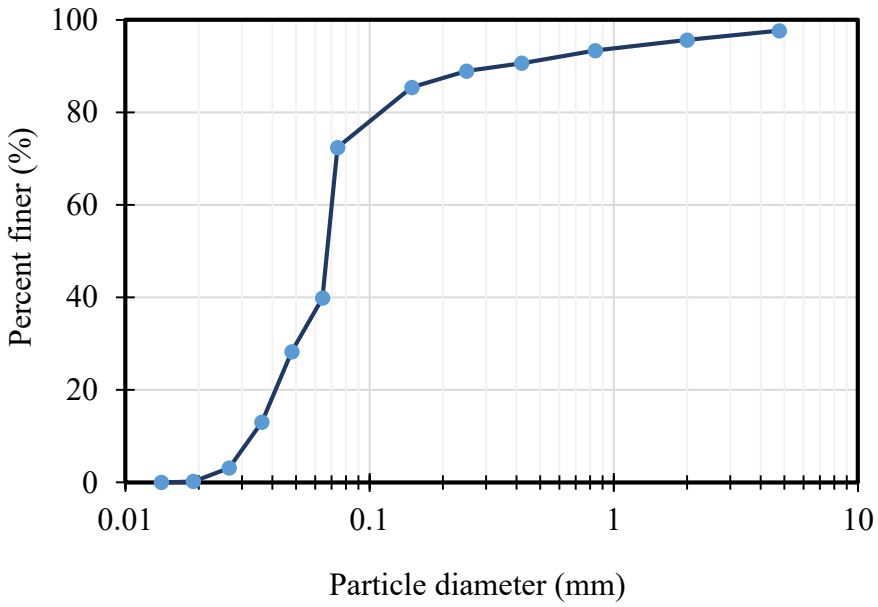

Figure 6. 1. Particle size distribution analysis of the test soil.

6.3 Pile Installation and Instrumentation

Three model piles with different geometries were examined in this study. The first pile was a steel open-ended pipe pile with a wall thickness of 5 mm, outer diameter of 100 mm, and height of 1500 mm. The second pile was a single-helix helical pile consisting of open-ended circular shaft of 38.1 mm diameter and a single helix of 100 mm diameter welded near the pile toe. The total length of the helical pile was 1000 mm. The third pile was a grouted shaft single-helix helical pile. It had similar geometry of the second pile but with the upper half of its embedded shaft grouted with concrete. The embedment depth for the open-ended pipe pile was 1000 mm while for the two helical piles was 600 mm. These embedment depths were adapted to ensure that the test piles are located within the seasonally frozen depth.

The steel open-ended pipe pile was driven to the targeted depth using impact hammer driving technique. This was conducted utilizing a 15.87 kg (35 lb) hammer falling from a distance of 500 mm on the pile head using a pulley and drop hammer setup. The falling distance was maintained constant and hammering action was conducted manually at a rate of 10-15 blows per

minute. The penetration rate of the pile tip varied with depth from 1 mm/blow along the upper 200 mm depth to 4 mm/blow through the rest of the depth. The helical piles, on the other hand, were inserted into the ground to the depth of 600 mm using a manual torque force applied at the pile head. For the grouted shaft helical pile, the ground was augured to a depth of 300 mm and a diameter of 100 mm prior to helical pile driving. The helical pile was then driven to the final depth of 600 mm. The shaft along the augured 300 mm depth was reinforced and grouted with concrete. The test location was also equipped with two copper-constantan thermocouple systems installed in the neighborhood of the test piles to monitor ground temperature in pile vicinity. The system designed to read the temperature in segments ranged from 100 to 200 mm along the embedment depth to obtain ground temperature profiles.

6.4 Testing Programs

6.4.1 Pile load testing in unfrozen ground

Test piles were installed in Fall 2017 and tested against pull-out loading after one month of their installations to determine their pull-out bearing capacity in unfrozen ground. A reaction frame was constructed in the field to facilitate pull-out testing. The reaction frame consisted of concrete blocks stacked on both sides of the piles and supported a steel reaction beam. The reaction beam was a prismatic-shaped steel truss designed to embrace a high strength pull-out steel rod and support a bearing plate, a hydraulic jack, and a load cell on top. A reference beam was built independent from the reaction frame to facilitate accurate pile displacement measurements during testing. The pull-out load was applied using a 103 kPa (15 psi) manual hydraulic pump and a 100 kN hollow hydraulic jack. The hydraulic jack was mounted on a 300 mm x 400 mm x 15 mm hollow steel bearing plate situated on the reaction beam. The load cell was then positioned on top of the jack and the whole system was restrained with a steel nut at the very top. The tension force

was transmitted from the jack to the pile head through the high strength threaded steel rod which was machined to connect to the pile heads.

The pull-out tests in unfrozen ground were performed in accordance with ASTM D1143/D1134M (2007), following the Quick Test Method for single piles. The ultimate pull-out capacity of the tested piles was estimated theoretically following the total stress analysis for cohesive soils. Uplift load was applied in increments of 10% of the theoretically estimated ultimate load capacity allowing 5 minutes' intervals between each loading step. Load measurements were facilitated utilizing a vibrating wire load cell. The test data was recorded electronically using a data acquisition system connected to a PC unit and all powered through an electrical generator. The vertical pile displacement was recorded using Linear Variable Differential Transformers (LVDTs) with accuracy of ±0.01 mm and a maximum mechanical travel distance of 100 mm. The displacement sensor was mounted on a dial indicator holder attached to the test piles while its free end restrained to the reference beam to track the upward movement of the test piles.

6.4.2 Pull-out loading and creep testing in frozen ground

Creep behavior and load carrying capacity of pile foundations in frozen grounds are mainly time dependents. Long-term observations, therefore, was aimed for capturing the true performance of test piles. However, using powered instrumentations in field was challenging due to the lack of long-term power sources in the test site. Alternatively, mechanical loading system and mechanical displacement indicators were adopted for this experiment. Three Lever systems were employed to mechanically apply the pull-out load on each of the three test piles (Figure 6.2). The lever system was aimed at leveraging the influence of an applied dead load at the effort end of the lever arm to generate sufficient pull-out loads at the resistance end of the lever arm at the pile head. The lever arms were rectangular steel hollow-section with a height of 100 mm, a width of 50 mm, and a wall

thickness of 5 mm. For the open-ended pipe pile, the lever arm was 3660 mm in length bearing on a solid steel roller in order to enable turning about a pivot support. The pivot support was a steel pipe column with 152.4 mm in diameter and 900 mm in height. The top of the column was equipped with a steel angle bed to facilitate the rotation of the steel roller and the lever arm. The bottom of the column was fixed to a 700 mm x 700 mm x 5 mm steel footing which supported the whole lever system (Figure 6.2). The resistance end of the lever arm and the pile head were both equipped with annular connectors to maintain perfect alignment between the loading axis and the vertical axis of the pile. This would minimize load eccentricity during all loading steps as the lever rotating and displacing the pile. The pull-out load was transmitted from the resistance end of the lever arm to the pile head via a heavy-duty steel chain which was fasten to the annular connectors at both sides.

The lever systems for the helical piles had a similar working mechanism but with 3250 mm length lever arms. The resistance end of the lever arm was machined to connect directly to the pile head through a ball joint connector again to eliminate any load eccentricity. The pivot column for the helical piles was 600 mm height and consisted of two steel channels designed to carry the solid steel roller in between and provide convenient bed for the lever arm to turn freely about the column. The column was fixed to a 300 mm x 400 mm x 5 mm steel footing to support the whole system (Figure 6.2).

The lever systems enabled elevating the dead load applied at the effort end by a ratio of 1:4.25 for the open-ended pipe pile and 1:2.25 for helical piles. The dead load was obtained by using several 30 kg-mass of concrete bricks. The effort ends of the levers were equipped with steel plates of 300 mm x 400 mm x 5 mm to carry the dead load. The pile displacement, on the other

hand, was measured by mechanical dial gauges with an accuracy of 0.005 mm. Two dial gauges were connected to each test pile to record the displacement from their both sides.

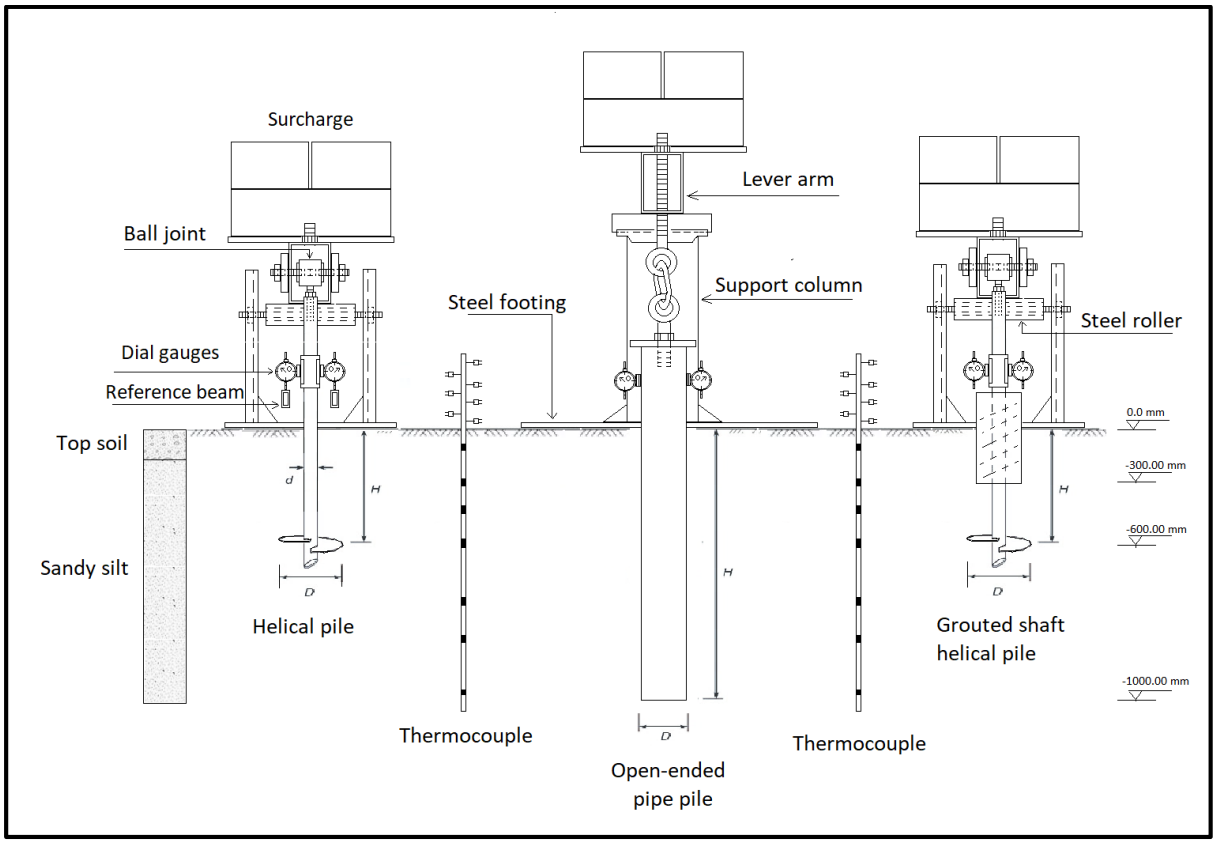

Figure 6. 2. Filed set up for pile load and pile creep testing.

Winter experiments began with creep testing started on February 13 and terminated on March 04, 2018. Piles where tested under different creep stresses including 50 kPa, 100 kPa and 140 kPa. During creep testing, ground temperature and creep displacement were measured and recorded on a daily basis. After creep testing, the test piles where left for sufficient time to re-establish their adfreeze bond before conducting pull-out load testing which was carried out between March 19 and March 20, 2018. The pull-out loading was conducted on steps where each loading step was equal to 10% of a theoretically estimated ultimate capacity using Equation 5 and cohesion strength for ice-rich silt reported by Vialov (1959). The load was applied through the lever system while the corresponding displacement was recorded when the displacement indicators reach a steady state.

6.5 Test Results

6.5.1 Pull-out capacity of test piles in unfrozen ground

Pull-out loading tests were conducted on the three test piles in Oct 23 and Oct 24, 2017. The ground was in the state of unfrozen as its temperature increased linearly from 5℃ at 100 mm depth to 15℃ at 1000 mm depth from ground surface. The load-displacement curves for the three tests were illustrated in (Figure 6.3). They showed three distinct stages: linear elastic stage with high stiffness, transitional curvilinear stage, and nearly linear rapid failure stage with small stiffness. The three test piles exhibited similar initial elastic stiffness, however, significantly different failure modes and load capacities. The failure signs usually observed somewhere near the beginning of the curvilinear stage. It is very important to adapt the right failure criterion that will locate the failure within this region. The failure of the open-ended steel pipe pile was clear when experienced plunging and dramatic displacement increase. It showed an ultimate pull-out capacity of 8000 N corresponding to a pile head displacement of 1.2 mm. However, the failure of helical piles, in particular the grouted shaft helical pile, was not easily identifiable. They showed smaller linear elastic stage followed by nonlinear disproportionally gained capacity with increased displacement. It is common in the helical pile industry to use a failure criterion equal to 5%D for helix diameters greater than 610 mm and 10%D for helix diameters less than 305 mm or at the plunging failure, whichever occurs first. However, Hanna and Carr (1971) reported that 20%D displacement was necessary to attain the ultimate capacity of a 38-mm diameter helical pile in sand. Moreover, Bhatnagar (1969) found that for a 75-mm diameter plate anchor in silty clay, a displacement equal to 50%D was needed to attain the ultimate capacity.

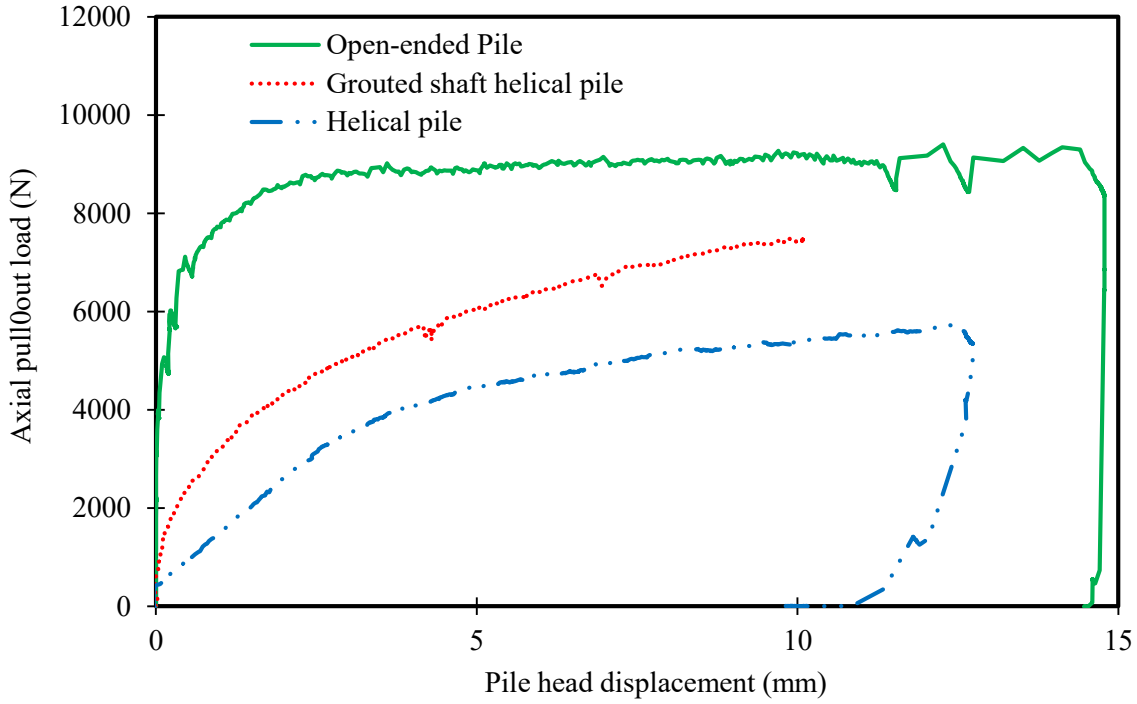

Figure 6. 3. Load-displacement curves for test piles in unfrozen condition.

The helical pile, in this study, showed very nonlinear load-displacement relationship compared to the open-ended pipe pile. Similar behavior has been reported by Bhatnagar (1969) and Ladanyi and Johnston (1974). The response of helical pile against pull-out loads was reported to be similar to those shown by deep circular footings which often achieved their ultimate capacity only after exhibiting a large displacement relevant to its diameter. The pull-out capacity of the test piles may not be taken explicitly for comparing the performance of the test piles without considering the interface area between the piles and the surrounding soil. The embedment areas of the test piles were 0.314 m^2 for open-ended pipe pile, 0.137 m^2 for grouted shaft helical pile, and 0.078 m^2 for non-grouted shaft helical pile. More accurate comparison, therefore, would be obtained from the stress analysis around the embedment areas.

6.5.2 Temperature profiles in Winter

Although there has been no permanent permafrost observed recently in Ottawa region, a seasonal freeze/thaw depth ranging from 800 mm to 1200 mm is commonly witnessed. In the current study, ground temperature was mainly below zero degree Celsius over the 800 mm depth during Winter experiment indicating frozen ground condition (Figure 6.4). Below this depth, ground temperature increased to above-zero degree Celsius in a couple of occasions. Figure 6.5 shows the fluctuation of ground temperature at depths over time. The daily temperature measurement has shown colder ground temperatures near the ground surface and gradual ground temperature increase with depth.

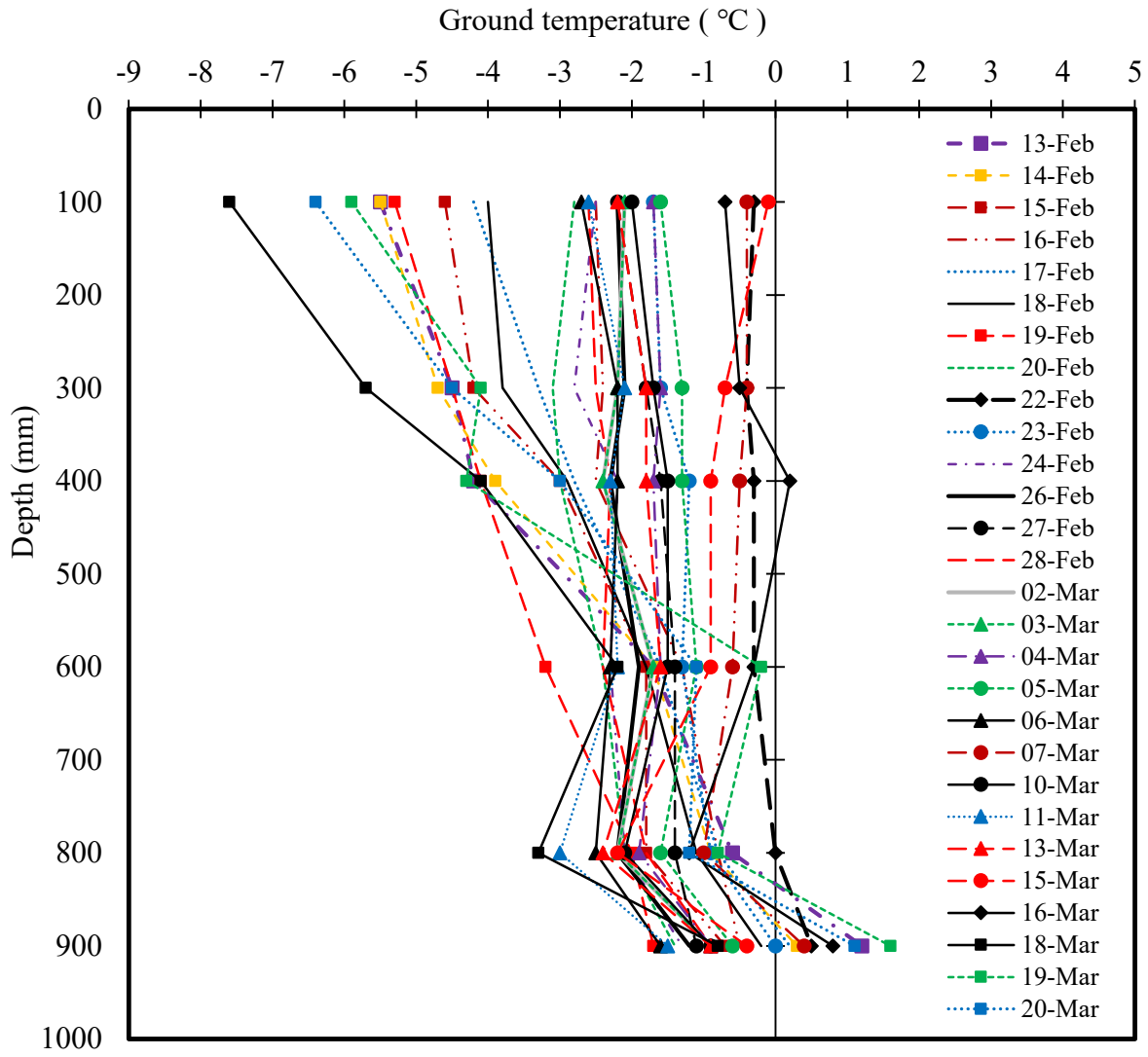

Figure 6. 4. Ground temperature versus depth.

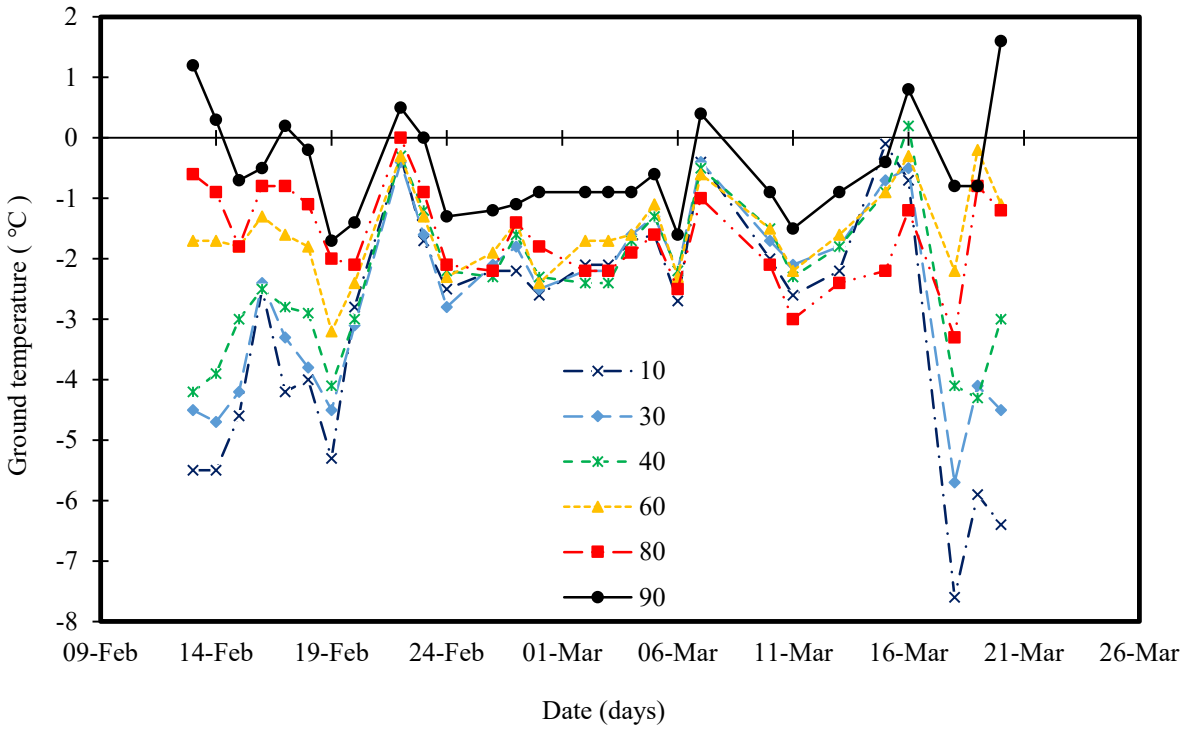

Figure 6. 5. Variation of ground temperature at depths over the test period.

The fluctuation of ground temperature from day-to-day measurement was larger near the ground surface moving between -8℃ to slightly colder than the freezing point. However, ground temperature at the very bottom fluctuated within a narrower range of -1.7℃ and +1.6℃. Ground temperature, in addition, was influenced directly by air temperature and usually responded to the change in air temperature in a matter of 24 to 48 hrs. The mechanical behavior of the piles, as a consequence, changed subsequently to the change in ground temperature.

6.5.3 Creep behavior of the test piles in frozen ground

When the ground temperature stabilized and frost depth reached the maximum expected penetration depth, the creep test was initiated. The test piles were subjected to an instantaneous shear stress of 50 kPa estimated based on each pile's embedment area. Taking into account the

maximum frost depth of 800 mm, the embedment area within the frozen ground was accordingly measured as 0.267 m2, 0.078 m^2, and 0.137 m^2 for the open-ended pipe pile, the helical pile, and the grouted shaft helical pile respectively. This, accordingly, corresponds to total loads of 13.35 kN, 3.9 kN and 6.85 kN to be imposed on the pile heads to reach the targeted creep stress. Considering the leverage ratios provided by the lever systems and the mass of the solid bricks, a brick quantity of 10.67, 5.89, and 10.34 were needed to apply the assumed uniformly distributed stress of 50 kPa on the embedment areas of the test piles. Only the exact number of the bricks were used where the fractions of the brick's quantity were then compensated by using steel weights. A similar calculation procedure was followed to determine the required dead loads needed to achieve the higher creep stresses of about 100 kPa and 140 kPa.

On February 13, 2018 the pile heads were subjected to the creep loads followed by frequent measurements of creep displacement and ground temperature over the test period. The average ground temperature along the 1000 mm depth and the normalized displacement (i.e., displacement divided by the piles' radii) are presented in Figure 6.6. The open-ended pipe pile showed a very small initial elastic displacement compared to 0.48 mm for the helical pile and 0.53 mm for grouted shaft helical pile. Under the creep stress of 50 kPa, the ground temperature seemed to have been the main driving factor for the pile creep displacement. There were two important occasions observed on Feb. 15 and between Feb. 19 and 22 where the air temperature significantly raised above the freezing point. The increase in air temperature recorded on Feb. 15 caused the average ground temperature to increase after 24hrs from -2.7℃ to -1.7℃ along the pipe pile shaft and from -3.4℃ to -2.1℃ along the helical piles' embedment depth. This resulted in an immediate displacement increase of 0.3 mm for the helical pile and 0.5 mm for the open-ended pipe pile. The second occasion, which occurred between Feb. 19 and Feb. 22, witnessed a very warm air

temperature recording +9℃. The warm air temperature elevated the ground temperature to be almost at the freezing point recording -0.1℃ along the pipe pile shaft and -0.3℃ along the helical pile embedment depth. This caused the open-ended pipe pile to undergo a tertiary creep and experience a slip failure showing a displacement of 250 mm which exceeded the range of displacement that the dial gauge could measure. However, the helical pile, unexpectedly, could withstand this warming action and bear the applied load without failure but with a significant displacement occurrence recording 1.497 mm. The test platform before and after the pipe pile failure are shown in Figure 6.7a&b respectively.

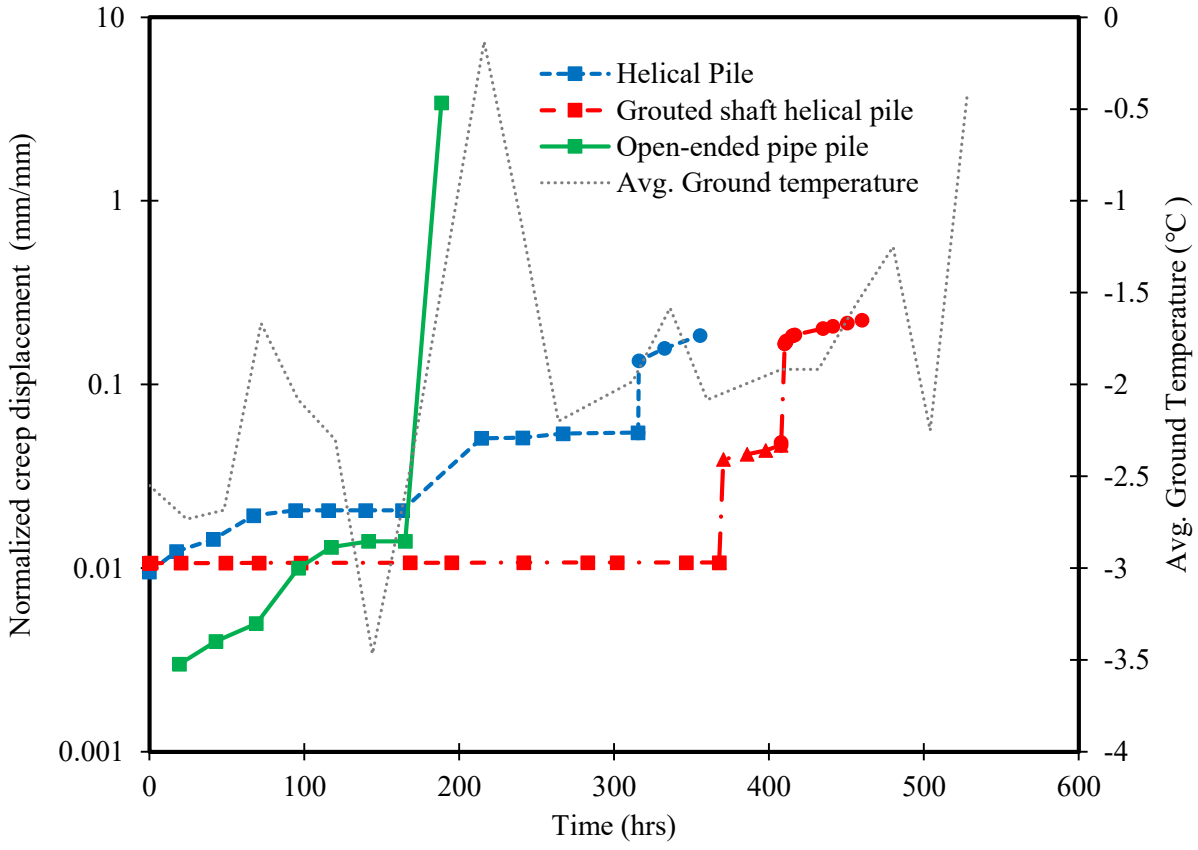

Figure 6. 6. Evolution of creep displacement with time and ground temperature under stress of 50 kPa (squared shape), 106 kPa (triangular shape) and 140 kPa (circular shape).

a. Feburary 14, before pipe pile failure

b. Feburary 22, after pipe pile failure

Figure 6. 7. Test platform before and after failure occurrence to the open-ended steel pipe pile.

The grouted shaft helical pile, in contrast, maintained a steady creep displacement during the same test period regardless to the fluctuation of the ground temperature. This could be attributed to the stronger bond between the grouted shaft and the surrounding soil that could have established during concrete casting. The pile showed a normalized creep rate of 3x10-07 hr-1 under the applied creep stress of 50 kPa.

The creep stress imposed on the helical pile was increased to 143 kPa on February 26. The pile experienced instantaneous displacement increase of 4 mm followed by a steady creep rate. The creep rate was unexpectedly fast, but, less sensitive to ground temperature fluctuations. After two days, the creep stress imposed on the grouted shaft helical pile was also increased to 106 kPa followed by another stress increase to a 140 kPa after another two days. At each loading step, the grouted shaft helical pile experienced instantaneous displacement increase recording 1.42 mm at 106 kPa and 6.14 mm at 140 kPa. Although the instantaneous displacement for grouted shaft pile was greater compared to the helical pile, its steady state creep rate was slower at all stages.

6.5.4 Pull-out capacity of test piles in frozen ground

After the termination of creep tests on March 05th, the test piles were left to gain sufficient adfreeze strength before the pull-out load test was performed on March 19 &20, 2018. This time was selected for testing based on the observation of the average ground temperature that showed relatively low levels during this time recording -2.5℃ along the pipe pile shaft and -3.5℃ along the helical pile depth. The load-displacement relationships for the piles in frozen ground exhibited similar trends of failure compared to those observed in unfrozen ground but with significantly stiffer elastic modulus and greater ultimate capacities (Figure 6.8). The open-ended pipe pile, for example, demonstrated an ultimate load capacity of 25000 N at 0.2 mm displacement compared to an ultimate capacity of 8000 N recorded at 1.2 mm displacement in unfrozen ground. This means about 3 times higher ultimate capacity and 6 times less displacement was needed to mobilize the pile when the surrounding soil became frozen at -2.5 C compared to the ground in unfrozen condition. The helical pile and grouted shaft helical pile in frozen medium mobilized under 12500 N and 18500 N after demonstrating larger displacements compared to the open-ended pipe pile recording 1.5 mm and 2 mm respectively. Their load capacity in unfrozen ground were around 2.5 times less recording 5400 N and 7400 N. As it was observed in unfrozen ground, the load-displacement curves for helical piles in frozen ground also needed to undergo relatively significant displacement before reaching their ultimate capacity showing some nonlinearity which was less intensive compared to their nonlinearity in unfrozen condition. Nonlinearity could be attributed to the load transfer mechanism of helical piles that is mainly governed by end bearing compared to shaft resistance load transfer mechanism for open-ended pipe pile that mobilizes after small displacement.

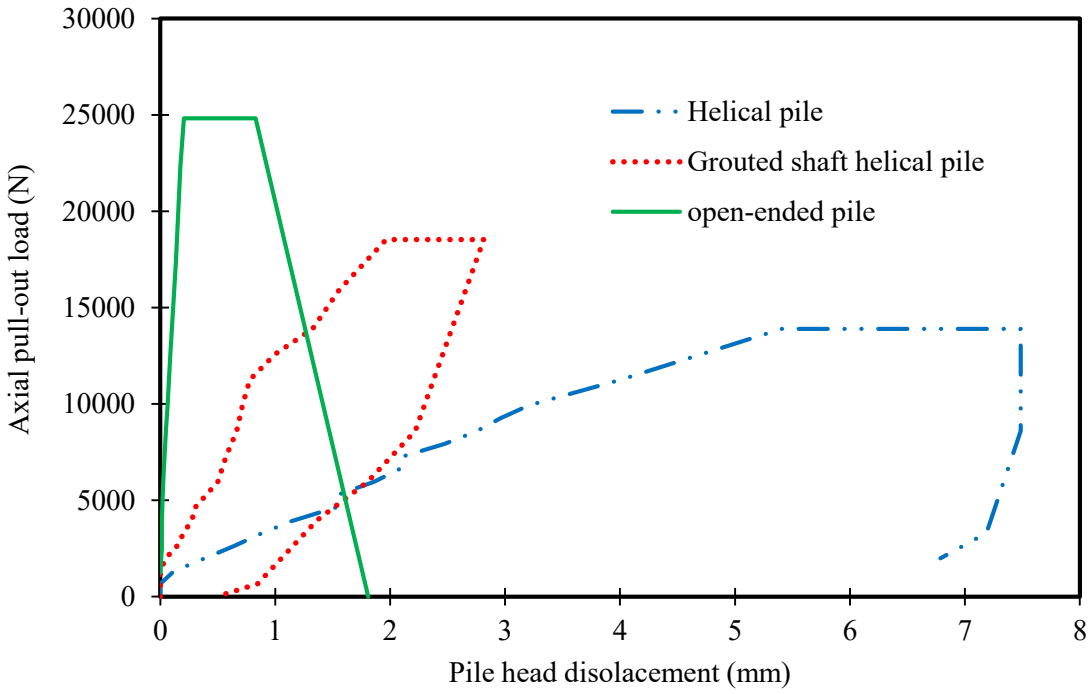

Figure 6. 8. Load-displacement curves for test piles in frozen condition.

After reaching its ultimate capacity, the open-ended pipe pile experienced accelerated displacement followed by a brittle failure resulted in a total loss in its load carrying capacity. A similar behavior was reported by many researchers including Ladanyi and Theriault (1990). The helical piles, on the other hand, were superior in this regard by maintaining their ultimate capacities even after undergoing significant displacement. This could distinguish helical piles over the conventional pipe piles or smooth-shafted piles for providing safer load carrying performance especially in warming permafrost regions where frozen grounds tend to degrade. Using helical piles in such condition could minimize the risk of catastrophic failures of superstructures in case of frozen ground degradation. However, the test piles have different geometries and are installed at different depths, therefore, a better comparison of their load carrying performance may be obtained from their stress-displacement curves rather than load-displacement curves.

6.6 Discussion

6.6.1 Load transfer mechanism of test piles in unfrozen ground

External load imposed on pile foundations is transmitted to the surrounding soil through different mechanisms including shaft friction and/or end bearing. This is dependent on other factors including load condition (e.g., pull-out or compression loading) and pile geometry such as open-ended pile, close-ended pile, and single-helix or multi-helix helical piles. Although the load transfer mechanism of the tested open-ended pipe pile under pull-out loading is likely happening through shaft friction, the mechanism of load transfer for helical piles may not be as easily determined. As mentioned earlier, two load transfer mechanisms could be exhibited by helical piles under external loading namely the Individual Plate Bearing (IPB) and Cylindrical Shear Model (CSM) (Figure 6.9). In this study, and to understand what load mechanism was experienced by the test piles in the field, their pull-out capacities were theoretically estimated using those different models and compared to the measured capacities. The model that gives closer prediction to the measured capacity would likely be the correct model and that can provide information about the load transfer mechanism of the subject pile. The theoretical pull-out capacity (Q_s) for the open-ended pipe pile was determined using the general equation for pile foundations in undrained condition as follow:

$$Q_s = \pi . D . \alpha . C_u . L \qquad [6.1]$$

where: Q_s is in kN; D is the shaft diameter (m); α is adhesion factor which was selected equal to 0.5 for pile-soil interface and 1.0 for soil-soil interface; and C_u is the undrained shear strength for the test soil = 50 kPa.

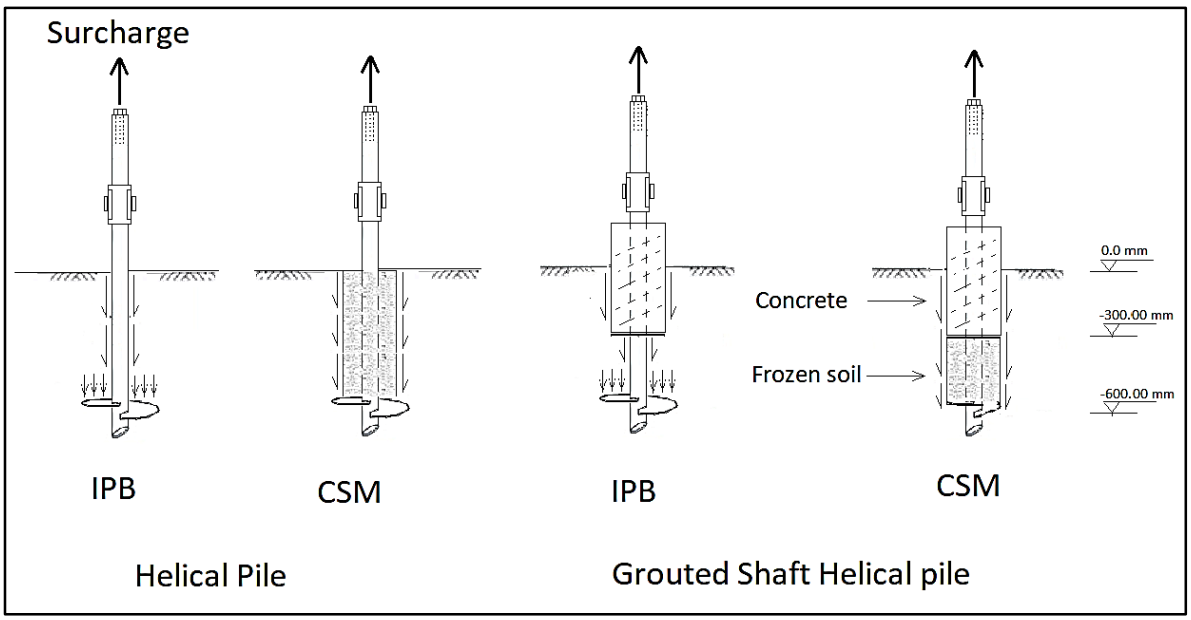

Figure 6. 9. Different load transfer mechanisms for helical piles.

For helical pile and grouted shaft helical pile, Equations [2.10] to [2.12] were used for the theoretical pull-out capacity estimation based on the IPB mechanism while Equation [2.13] was used for the CSM. The results are presented in Table 6.1 and illustrated in Figure 6.10. For comparison purpose, the test piles were considered fully mobilized at displacement equal to 10%D of the pile for the open-ended pipe pile and of the helix for the helical pile. The predicted capacity for the pipe pile using Equation [6.1] was 7 kN showing 20% less capacity than the measured capacity of 9 kN. The predicted capacity for the helical pile was 9.42 kN and 4.27 kN using the CSM and IPB models respectively compared to the 5.4 kN measured capacity. The results indicated that the ultimate capacity estimated by individual plate bearing (IPB) assumption had better agreement with the measured capacity with an error of 20% compared to 40% error when assuming CSM. This behavior was expected for single-helix helical pile which often gained its capacity through its plate bearing and its shaft friction rather than forming a confined soil cylinder in the absence of another helix.

Table 6. 1. Predicted pull-out capacity of the test piles in unfrozen soil for from different models.

Z (m)	H (m)	C_u (kPa)	Circumference (m)		Adhesion factor (α)		Pipe pile	Helix bearing (kN)	Grouted shaft helical pile		Non-grouted helical pile	
									Shaft capacity (kN)			
			PP & GSP	HP	SS	PS	Shaft capacity (kN)		CSM	IPM	CSM	IPM
1.0	0.30	50.0	0.31	0.12	1.00	0.50	7.850	2.48	2.36	2.36	9.42	1.79
	0.30								4.71	1.79		
Sublayer strength sum of individual pile elements (kN)								2.48		4.15		1.79
Ultimate pull-out capacity (kN)							7.85		7.07	6.63	9.42	4.27

PP: Pipe Pile; GSP: Grouted Shaft Helical Pile; HP: Helical Pile; SS: Soil-Soil Interface; PS: Pile-Soil Interface

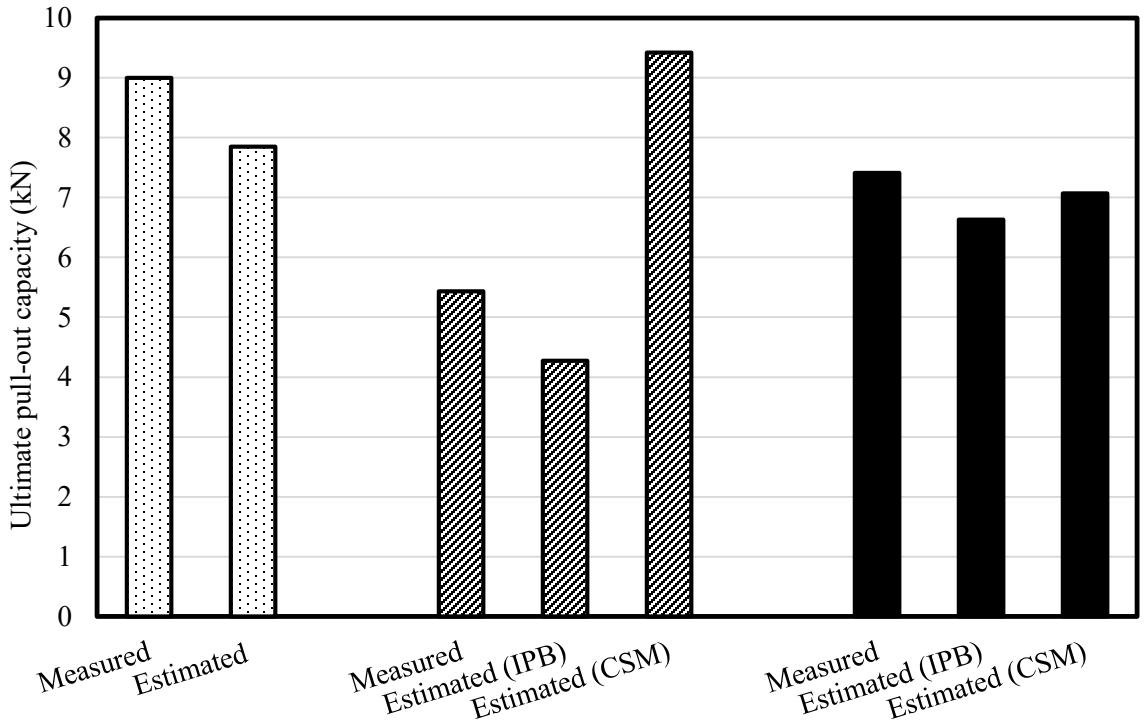

Figure 6. 10. Comparison between measured pile capacity in unfrozen soil with the predicted capacity from different models (dotted bars for PP; hatched bar for HP; solid bar for GSH).

The predicted capacities for grouted shaft helical pile were almost similar using both the CSM and IPB models recording 7 kN and 6.6 kN. However, the predicted capacity using the CSM assumption was closer to the measured capacity of 7.4 kN recording only 5% difference. The

bottom of the concrete body may have acted as an upper helix that formed a soil cylinder with lower principle helix, causing the behavior of grouted shaft helical pile to shift from being governed by individual plate bearing model to cylindrical shear model. The current observations have confirmed other researchers' findings that the performance of single-helix helical piles would mostly be governed by settlement. This can be inferred from its relatively large displacement occurrence that would be required before full mobilization is attained. Designing such piles, therefore, should be executed based on the allowable displacement of the superstructures instead of allowable bearing capacity of the pile. This behavior could be attributed to the load transfer mechanism of the single-helix helical piles which was mainly governed by their plate bearing. This was more pronounced for the used helical pile which had a helix diameter that was 2.6 times greater than its shaft diameter. End-bearing piles would often undergo larger displacement before being fully mobilized and reach their ultimate bearing capacity compared to frictional piles. This can be attributed to soil densification above the helix as the helix is displaced upward against the soil. The open-ended pipe pile, on the other hand, was a frictional pile that showed considerably larger pull-out bearing capacity at a relatively smaller displacement before mobilization and undergoing accelerated displacement. Such pile, in contrast, maybe designed based on bearing capacity considerations as its performance mainly governed by its load carrying capacity. This design hypothesis might be considered true when analyzing the load-displacement curve of the grouted shaft helical pile that seemed to have experienced transition performance from displacement-governed failure criterion to bearing capacity-governed failure criterion. Half the length of embedded shaft of this pile was increased in diameter by grouting. This seemed to have modified the load transfer mechanism of the pile to be governed by skin friction along the concrete body

and the soil cylinder formed in between the concrete and the lower helix. The design requirement for such pile, therefore, should meet both the displacement and bearing capacity considerations.

6.6.2 Load transfer mechanism of test piles in frozen ground

Load carrying capacity of pile foundations in frozen grounds is temperature dependent, therefore, understanding the thermal regime around the piles is important for understanding and predicting their load transfer mechanism. As the ground temperature in the current study varied with depth, it was necessary to divide the ground depth into sublayers and evaluate the interaction of each segment with the pile surface separately based on the temperature of each segment. Based on ground temperature observation, the ground was in frozen state along the 800 mm depth only, thus, this depth was only considered for the analysis. Determining the load carrying capacity using theoretical models and comparing the results with measured capacity in frozen ground would help to understand the load transfer mechanism of the test piles based on the assumptions made for each theoretical model.

The theoretically estimated ultimate capacity for the test piles are presented in Table 6.2 and Figure 6.11. The ultimate capacity for the open-ended pipe pile was estimated based on the frictional resistance of the pile shaft. The ground depth was divided into 5 sublayers based on the observed temperature. For each layer, the adfreeze strength of the pile-soil interface was calculated based on the temperature dependent cohesion strength of the ice-rich silt proposed by Vialov (1959). The pile-soil roughness factor "m" for steel and concrete was adopted from Weaver and Morgenstern (1981) as 0.6 while setting it equal to unity whenever soil-soil interface was encountered. The general equation for calculating the ultimate pull-out capacity for a frictional pile was applied as follow:

$$Q_u = \pi D \sum_{i=1}^{5} (0.6\ \mathrm{C_i} \Delta \mathrm{L_i}) \qquad [6.\ 2]$$

Adopting the Cylindrical Shear Model (CSM), the ultimate pull-out capacity was predicted for the helical and grouted shaft helical piles using modified formulations from the proposed equations by Tappenden and Sego (2007). The cohesion strength and the roughness factor "m" were used as mentioned above. The modified equation for helical pile [6.3] and for grouted shat helical pile [6.4] are written as follow:

$$Q_{cyl} = \pi D \sum_{i=1}^{5} (\mathrm{C_i} \Delta \mathrm{L_i}) \qquad [6.\ 3]$$

$$Q_{cyl} = \pi d [\sum_{i=1}^{2} (0.6\ \mathrm{C_i}\ \Delta \mathrm{L_i}) + \sum_{i=3}^{4} (\mathrm{C_i} \Delta \mathrm{L_i})] \qquad [6.\ 4]$$

When Individual Plate Bearing model was used, the ultimate pull-out capacity for the helical pile and the grouted shaft helical pile was predicted following modified formulations after Tappenden and Sego (2007). The shaft friction for helical and grouted shaft helical piles was estimated using the following equations:

$$Q_s = \pi D \sum_{i=1}^{4} (0.6\ \mathrm{C_i} \Delta \mathrm{L_i}) \qquad [6.\ 5]$$

$$Q_s = \pi d \left[\sum_{i=1}^{2} (0.6\ \mathrm{C_i}\ \Delta \mathrm{L_i}) + \sum_{i=3}^{4} (\mathrm{C_i} \Delta \mathrm{L_i}) \right] \qquad [6.\ 6]$$

The plate bearing for both piles was calculated based on the following equation

$$Q_b = \frac{\pi (D^2 - d^2)}{4} [N_c\ \mathrm{C_i} + \gamma'\ H] \qquad [6.\ 7]$$

where

$$N_c = 1.2 \left(\frac{H_1}{D_1} \right) \leq 9$$

Q_{cyl} = ultimate shaft capacity based on CSM

Q_s = shaft capacity based on IPB model

Q_b = plate bearing based on IPB model

H = depth of helix below ground surface (0.6 m)

D = diameter of helix, pipe pile and soil shaft in cylindrical shear model (0.1 m)

d = diameter of helical pile shaft (0.0381 m)

Nc = bearing capacity factor for cohesive soil which found to be 7.2 from on equation [9]

C_i = temperature-dependent cohesion strength (kPa) from Vialov (1959).

ΔL_i = thickness of the sublayer (m)

γ' = effective soil unit weight (15 kN/m3)

The predicted ultimate capacity of the open-ended pipe pile from Equation [6.2] was around 32 kN while the measured capacity in the field was 24.8 kN showing around 23% less capacity than predicted (see dotted bars in Figure 6.11). The smaller measured capacity could be attributed to the disturbance that happened to the pile-soil interface bond when the pile experienced slip failure during creep testing. The pile, therefore, may not have reconstituted sufficient adfreeze bond post to failure, thus exhibited a smaller capacity than what was predicted. On the other hand, the predicted ultimate capacity of the non-grouted helical pile agreed well with the measured value when the individual plate bearing model was assumed (see hatched bars). The predicted ultimate capacity was 15.76 kN compared to the measured capacity of 13.9 kN in the field. This difference in capacities falls within 12% error. Assuming the CSM assumption, in contrast, the predicted capacity was considerably higher than the measured capacity recording 47 kN. This indicates that the single-helix helical pile transferred its external load to the surrounding frozen soil through its helix bearing and its shaft friction following the IPB model assumptions. The good agreement

between measured and predicted capacitis of the helical pile in frozen ground indicated the applicability of the Tappenden and Sego (2007) models for predicting the design load for helical piles in both unfrozen and frozen ground.

The grouted helical pile, however, showed a measured capacity of 18.5 kN which was significantly smaller than the predicted capacity from both the IPB and CSM models (see solid bars). The predicted capacity from the two models were 28.3 kN and 33.6 kN respectively. Although the predicted capacities from the two models were significantly different from the measured capacities, they were comparable between each other. The smaller measured capacity for the grouted shaft helical pile could be attributed to the different time needed for the engagement of the shaft and the helix to the total capacity. As it was discussed before and reported by Bhatnagar (1969) that a displacement equal to 50%D was needed to attain the ultimate capacity for plate anchor in fine grained soil, the capacity attained by the concrete-soil interface would have been mobilized by the time the soil cylinder and the helix started to develop their capacity in the case of CSM. The contributed capacity gained from the concrete-soil interface was calculated to be 20.24 kN (Table 6.2), however, it would be mobilized at very small displacement similar to the displacement reported for steel-soil interface for the open-ended pipe pile. It was exhibited in chapter 5 that the concrete piles and steel piles would show identical load-displacement behavior with even smaller gained capacity by concrete pile at the load onset. Therefore, the 18.5 kN measured capacity could be resulted from the contribution of the concrete-soil interface only at the beginning. However, after further loading, the concrete-soil interface would be mobilized showing only a small residual strength, but the helix and the soil cylinder may then start contributing.

Table 6. 2. Predicted pull-out capacity of the test piles in frozen soil for from the modified formulations

Z (m)	H (m)	T (°C)	C_{al} (kPa) (Vialov, 1959)	Circumference (m)		Roughness factor		Pipe pile	Helix	Grouted shaft helical pile		Non-grouted helical pile	
				PP & GSP	HP	SS	PS	Shaft capacity (kN)	Plate bearing (kN)	CSM	IPM	CSM	IPM
										Shaft capacity (kN)			
0.10	0.10	-6.40	438.0	0.31	0.12	1.00	0.60	8.26		8.26	8.26	13.77	3.15
0.30	0.20	-4.50	318.0					11.97		11.98	11.98	19.96	4.56
0.40	0.10	-3.00	223.0					4.19		6.99	1.60	6.99	1.60
0.60	0.20	-1.10	102.0					3.842	4.99	6.40	1.46	6.40	1.46
0.80	0.20	-1.20	108.0					4.081					
Sublayer strength sum of individual pile elements (kN)									4.99		23.30		10.77
Ultimate pull-out capacity (kN)								32.35		33.63	28.29	47.12	15.76

PP: pipe Pile; GSP: Grouted Shaft Helical Pile; HP: Helical Pile; SS: Soil-Soil Interface; PS: Pile-Soil Interface

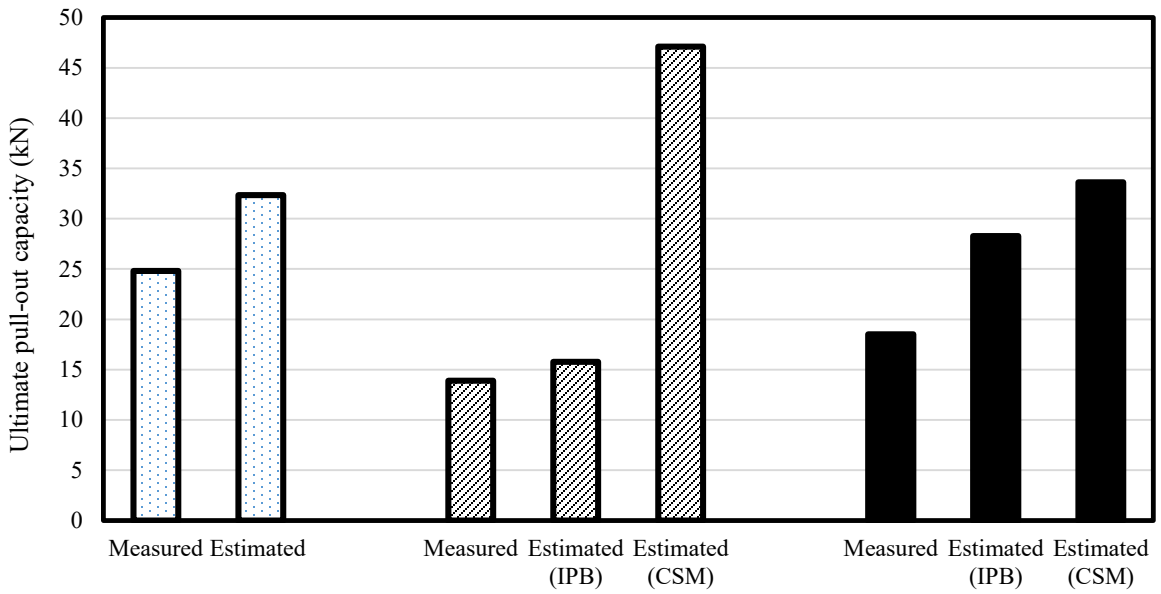

Figure 6. 11. Comparison between measured pile capacity in frozen soil with the predicted capacity from different models (dotted bars for PP; hatched bar for HP; solid bar for GSH).

The sum strength of 6.99 kN and 6.4 from the soil-soil interface and 4.99 kN form the helix would be fully engaged and resulted in a capacity of 18.38 kPa which was exactly similar to the measured capacity. In other words, the grouted shaft helical pile would not have its elements contributing to the ultimate capacity simultaneously rather they would work alternatively. This is an important finding through which a conclusion could be made that determining the design load for such piles must be considering either the concrete shaft friction or the soil cylinder friction and the plate bearing but not both.

The used models in this study showed acceptable capability of capturing the real behavior of the open-ended pipe pile and the helical pile. For helical pile, such finding would be very unique in the absence of previous theoretical approaches for predicting the design load for such pile type. The suggested load transfer mechanism of the grouted shaft helical pile could also be true; however, more investigation would be needed before a firm conclusion may be made.

Aside from their performance in unfrozen soil, the test piles in frozen soil exhibited identifiable yield points and ultimate load capacities. The open-ended pipe pile could not sustain its adfreeze bond, thus underwent brittle failure followed by zero residual strength. In contrast, helical piles could maintain their ultimate capacity even after large displacement. However, helical piles still needed to undergo large displacement before attaining their ultimate capacity compared to the open-ended pipe pile. By the time that the pipe pile reached its 100% ultimate capacity, only 10% of the ultimate capacity of helical pile was mobilized and 17% the ultimate capacity was recorded for the grouted shaft helical pile. This could be again attributed to the Individual Plate Bearing (IPB) model that governs the performance of single-helix helical piles in pull-out loading and multi-helix screw piles with an interhelix spacing ratio equal to or greater than 3.0 (CFEM 2006). The individual plate bearing for pull-out loading considers the bearing capacity above each helix in addition to skin friction along the section of pile shaft between the helix and the ground surface (Narasimha Rao et al. 1993; Mitsch and Clemence 1985). With a grouted shaft, helical pile tended to show transitional failure behavior toward frictional failure mode. The frozen soil between the concrete body and the helix may have formed soil shaft that interacted with the surrounding soil causing the grouted shaft helical pile to shift from Individual Plate Bearing model toward Cylindrical Shear Model (CSM). The ultimate pull-out capacity for cylindrical shear model was calculated as the skin friction acting along the cylinder of soil circumscribed between the top helix (the concrete based) and the bottom helix plus the skin friction acting along the cylinder of the concrete. It is very important to understand the governing failure mode of pile foundations in frozen ground before providing any solution that can predict the ultimate capacity of the piles in frozen medium.

6.6.3 Influence of shear stress on creep behavior of test piles

Pile creep in frozen ground is mainly driven by the applied stress and the ground temperature. Different analytical solutions were proposed to predict pile creep in frozen grounds by utilizing creep parameters

extracted from power low equations used to fit creep data of frozen soils. However, these solutions were mostly provided for smooth-shafted piles with limited studies on helical piles (e.g., Johnston & Ladanyi 1974). This section is devoted to discuss the effect of the applied stress on creep behavior of the test piles and compare their responses when exposed to identical boundary conditions. The average creep displacement (d) normalized by pile radii for open-ended pipe pile and helical radii for helical piles (a) are plotted versus time and illustrated in Figure 6.12a&b. Figure 6.12a presents the normalized creep displacement of the three piles under an applied stress of 50 kPa, while Figure 6.12b shows normalized creep displacement for the helical pile under 143 kPa and normalized creep displacement for the grouted shaft helical pile under 106 kPa and 140 kPa.

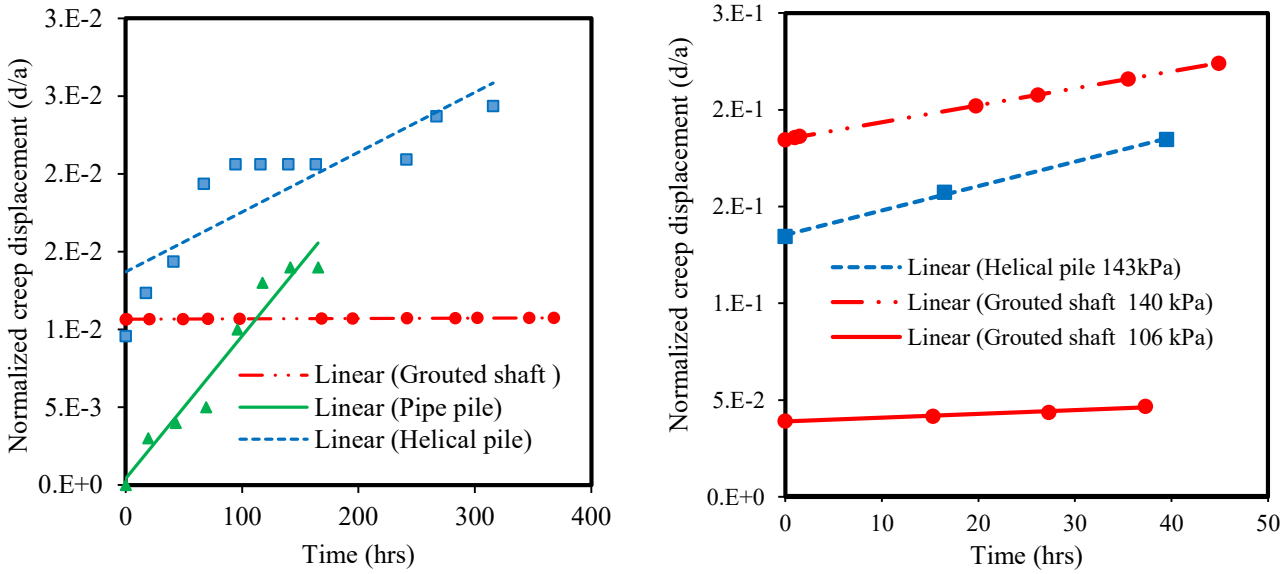

a) 50 kPa b) 106 kPa, 140 kPa and 143 kPa.

Figure 6. 12. Normalized creep displacement versus time under different creep stresses.

The creep displacement under 50 kPa was linearized to normalize for the effects of temperature fluctuation. The averaged creep rate may better represent the realistic behaviors of piles that may be installed at shallow depth in frozen grounds such as the piles used to support boardwalks, utilidors, fence posts, light posts, etc. These creep displacements were observed under an average ground temperature

ranged from -1.9℃ to -3.0℃ recorded along the embedment depths of the test piles. Under the applied stress of 50 kPa, the open-ended pipe pile showed the highest normalized creep rate of $9x10^{-5}$ h^{-1} followed by the helical pile and the least creep rate showed by the grouted shaft helical pile recording $4x10^{-5}$ h^{-1} and $3x10^{-7}$ h^{-1} respectively. When the applied stress increased to 106 kPa, the normalized creep rate for grouted shaft helical pile increased by around three orders of magnitudes recording $1.98x10^{-4}$ h^{-1}. The normalized creep rate was also increased for the grouted shaft helical pile when the applied stress increased to 140 kPa recording $8.77x10^{-4}$ h^{-1}. In contrast, the creep rate recorded for the helical pile was 1.26x10-3 h-1 under the applied stress of 143 kPa. The stress increase from 50 kPa to 143 kPa caused the normalized creep rate to increase by less than two orders of magnitudes for the helical pile compared to 3.5 orders of magnitudes increase of the normalized creep rate for the grouted shaft helical pile. In other words, the creep rate of grouted shaft helical pile was more sensitive to the stress change showing a higher trend of increase with stress compared to the helical pile.

The general practice in pile engineering in cold region is to show the correlation between the normalized creep rate and the applied stress for different ground temperatures in order to predict creep rate for piles with different diameters. This correlation was established and presented in Figure 6.13. Unfortunately, for open-ended pipe pile, only one data point could be obtained as the pile could be tested only under one stress level of 50 kPa.

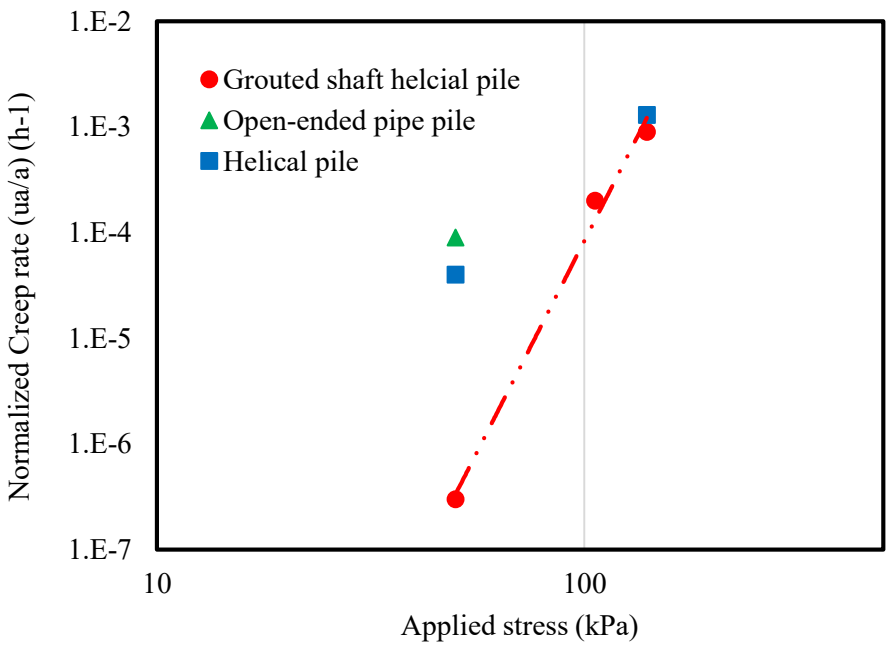

Figure 6. 13. Creep rates of the test piles at different creep stresses.

Two data points were obtained for the helical pile and three data points for the grouted shaft helical pile. Unfortunately, the obtained data from open-ended pipe pile and helical pile were not sufficient to establish a complete correlation. However, a power law equation could be obtained for the grouted shaft helical pile and presented as straight line in Figure 6.13. The trend line suggests that at small creep loading of 50 kPa the grouted shaft helical pile was superior compared to the other two piles by showing significantly smaller creep rate. When the creep loading increased to 106 kPa and 140 kPa, the creep rate of the grouted shaft helical pile increased significantly and became almost similar to the creep rate exhibited by the non-grouted helical pile in particular at 140 kPa. This behavior can be attributed to contribution of the concrete-soil interface strength within the small load-displacement region. This contribution would have been diminished as the concrete-soil interface strength was fully mobilized after significant creep displacement and, hence, the plate bearing and the soil-soil interface strength would start resisting the creep action. Therefore, the creep rate of the grouted shaft helical pile

started to show similar creep rate to the one exhibited by the non-grouted helical pile at the higher stress level as shown in Figure 6.13.

6.6.4 Ground temperature effects on creep behavior of pile foundations

From Figure 6.6, it is quite clear that the creep displacement was steadier and more uniform during the test period extended between February 24 and March 06 compared to the significantly fluctuated creep displacement experienced by the piles at earlier stages. When looking at temperature profile in Figure 6.5, it can be noted that the ground temperature prior to February 24 fluctuated significantly over time ranging between -5.5℃ and around zero-degree Celsius. Aiming at steadier thermal boundary around the test piles, the creep testing under 50 kPa was, therefore, prolonged to represent steady state creep rates. More stable ground temperature was observed between February 24 and 26 recording an average temperature of around -2.5℃. This enabled determining the steady state creep rate for the helical pile at $4.08x10^{-5}$ h^{-1} compared to a slower steady state creep rate of $3x10^{-7}$ h^{-1} observed for the grouted shaft helical pile under the same creep stress. Unfortunately, at this time, the open-ended pipe pile had been already failed and simultaneous steady state creep rate could not be obtained.

To comprehend upon the influence of temperature on creep displacement of the helical pile and the open-ended pipe pile, the changes in their creep rates versus average ground temperatures are plotted and presented in Figure 6.14a&b respectively. These data were extracted from the creep curves for the two piles in the test period extended from February 14 and 26, 2018.

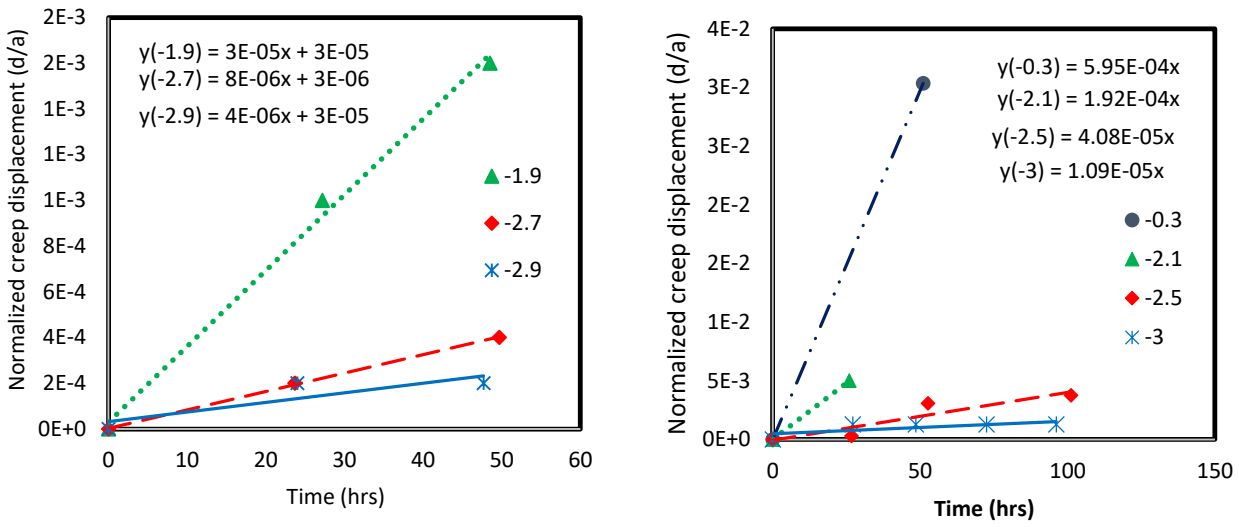

a) Open-ended pipe pile b) Non-grouted helical pile

Figure 6. 14. Variation of pile creep rates with ground temperature.

The creep rates for both piles increased as the temperature of the ground surrounding them raised up. The creep rate for the open-ended pipe pile increased by around an order of magnitude when the ground temperature increased from -2.9°C to -1.9°C recording $4x10^{-6}$ h^{-1} and $3x10^{-5}$ h^{-1} respectively. The creep rate for helical pile followed the same trend but with greater creep rate at any given temperature. Its creep rate also increased by an order of magnitude when the ground temperature increased from -3°C to -2.1°C recording $1.09x10^{-5}$ h^{-1} and $1.92x10^{-4}$ h^{-1} respectively. When the ground temperature approached the freezing point, the creep displacement for the helical pile experienced another half an order of magnitude increase recording $5.95x10^{-4}$ h^{-1}, whereas the creep rate for the open-ended pipe pile at the same thermal boundary accelerated significantly resulted in pile failure. These changes in creep rates for both the piles happened while the superimposed load on the pile head was constant (i.e., shear stress was at 50 kPa). This shear stress is considered relatively small compared to the stresses that the piles in frozen ground are designed for. However, the results showed that the pile stability may still be degraded even under such small stress due to ground warming. After February 26, although, the average ground temperature was warmer, it was steadier at around -2°C with negligible temperature fluctuation.

This would show the significant role that the ground temperature played in controlling the creep behaviors. These results highlight the significant creep displacement increase that the pile foundation in field can experience if the surrounding soil undergoes warming action. Pile foundation in cold region are generally designed based on the allowable creep displacement under a given stress assuming an isothermal boundary condition. However, considering the significant global warming impact and the increase in average air temperature around the globe, frozen grounds may not sustain a stable freezing temperature and, therefore, permafrost region have become degradation prone area. The observed annual air temperature around the globe has been fluctuating significantly moving between very warm to very cold condition from year to year (Smith et al., 2015& 2016). Although, the ground temperature may cool down again after a period of warming action following the typical trend of the global warming effects, the creep displacement, however, is not recoverable. In other words, pile foundations may undergo a higher creep rate than the design value if the ground experienced unexpected warming action. This may result in unpredicted superstructure settlement that will not be recovered even if the ground temperature cooled down in the following seasons. Therefore, it becomes very important to predict the range of freezing temperatures that the ground may experience along the life span of the superstructure and design accordingly to minimize the failure probabilities.

For creep stress of 50 kPa, the normalized creep rate-temperature relationship was established for the open-ended pipe pile and the non-grouted shaft helical pile (Figure 6.15). The creep rate within the reported range of temperature increased linearly as the ground temperature increased. This can be attributed to the increase in unfrozen water content and the reduction in the adfreeze bond between the pile and the frozen soil. The illustration in Figure 6.15 would be very useful for predicting the normalized creep rate for similar piles in similar frozen ground and under similar thermal boundary.

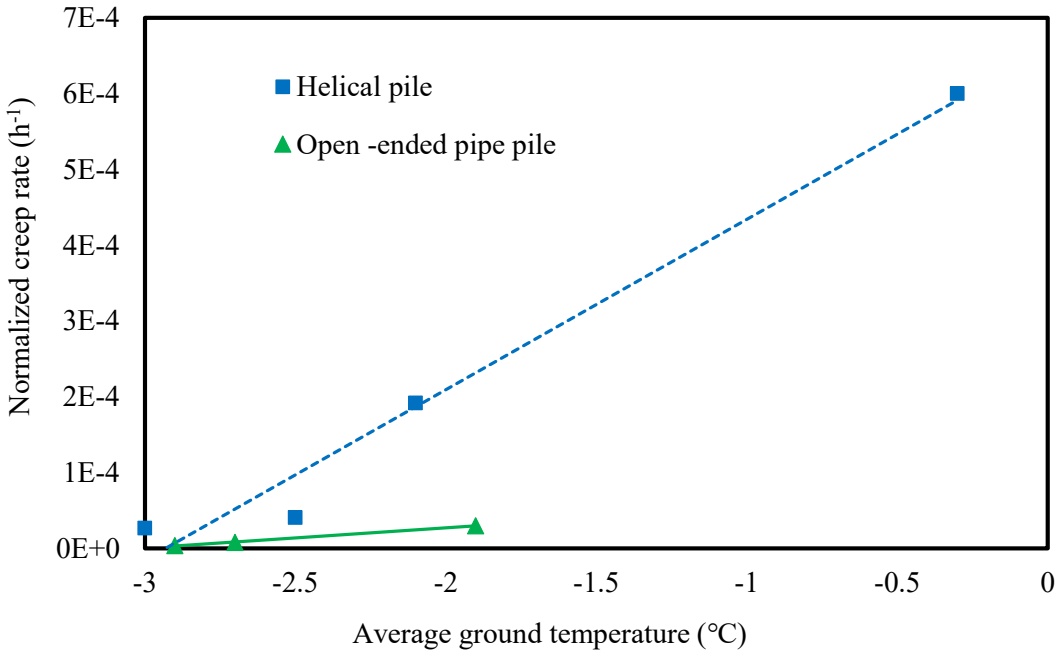

Figure 6. 15. Correlation between ground temperature and creep rate for open-ended pipe pile and non-grouted helical pile

6.6.5 Comparison with previous studies

The measured creep results for the open-ended pipe pile obtained from this study were compared with two different theoretical solutions provided by Nixon and McRoberts (1976) and Morgenstern et al. (1980) as illustrated in Figure 6.16. As most the theoretical solutions consider the average ground temperature in their data base, the reported creep rates in this study for all the test piles were reported for average ground temperatures too to enable meaningful comparison. The creep rate measured under 50 kPa and at an average ground temperature of -1.9°C was slightly higher than the values predicted by Nixon and McRoberts (1976). However, the measured creep rate under the same stress but at temperatures of -2.7C and -2.9C agreed well with the predicted values by Nixon and McRoberts (1976) when locating in between the predicted creep lines of -2.0°C and -5.0°C. The predicted creep rate by Morgenstren et al. (1980), however, was smaller than the measured creep at the same load and temperature conditions. This indicates that the pile creep model proposed by Nixon and McRoberts

(1976) is more capable for capturing the realistic creep behavior of the pipe pile in frozen ice-rich silt compared to the model proposed by Morgenstern et al. (1980).

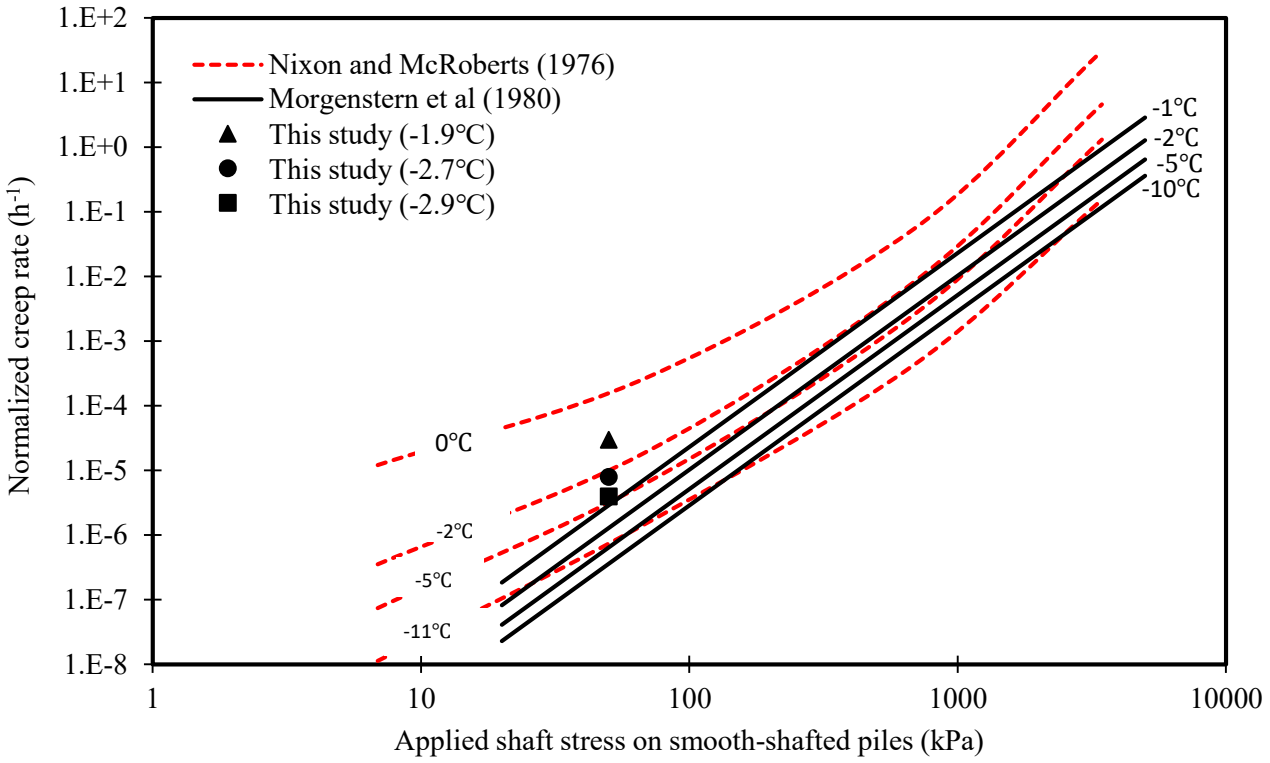

Figure 6. 16. Comparison between measured and predicted creep rates for open-ended pipe pile.

The measured creep rate for helical pile in this study was normalized by the helix diameter rather than the helix radii and projected on a graphical solution proposed by Johnston & Ladanyi (1974) in Figure 6.17. The normalized creep rate from the current study under 50 kPa and average ground temperature of -0.3℃ is located just along the middle line of Johnston & Ladanyi's (1974) curves. The normalized creep rates from this study at colder average ground temperatures is located beneath Johnston & Ladanyi's (1974) curves indicating lower creep rate as the average ground temperature dropped down.

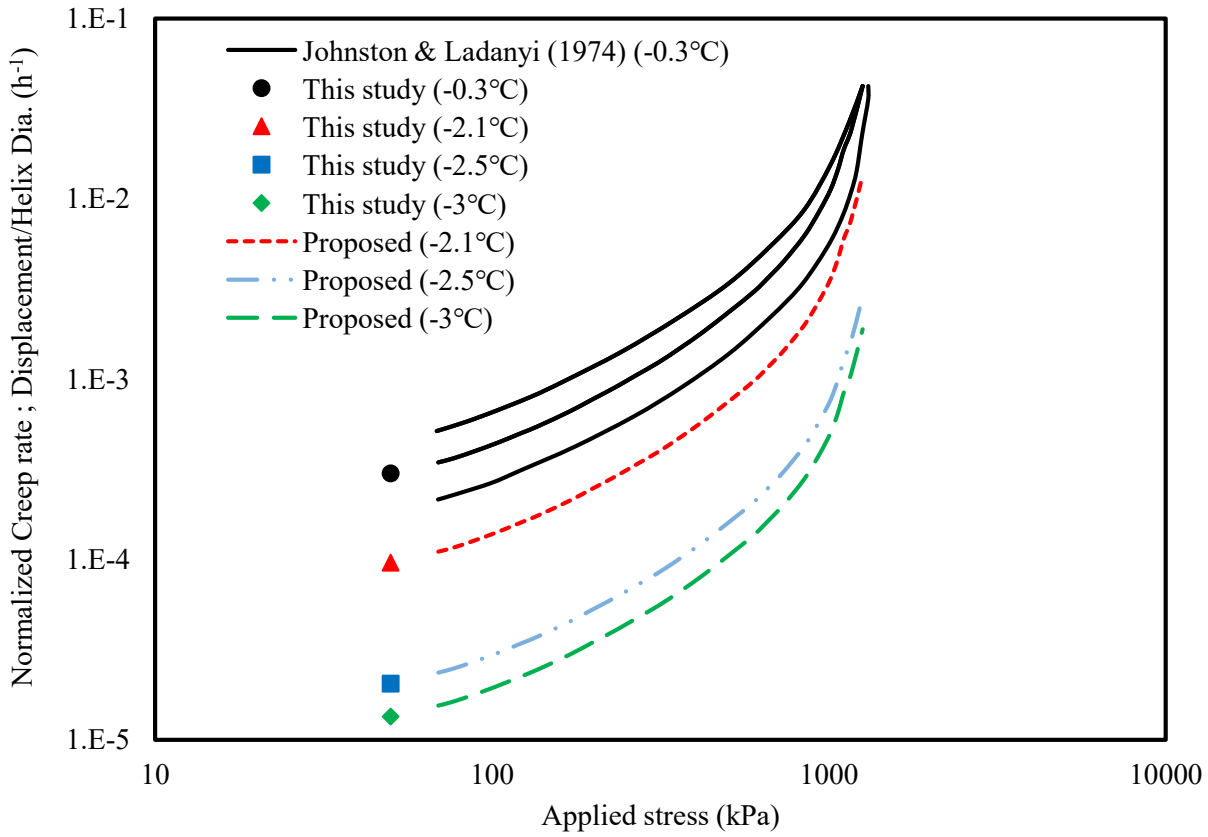

Figure 6. 17. Comparison between measured and predicted creep rates of the helical pile and proposed creep curves for different exposure temperatures.

The measured data points of the normalized creep rate from this study may be used to generate other curves parallel to Johnston & Ladanyi (1974) curves to predict normalized creep rate at various design load with respect to their temperature. It has been previously shown that the rate between the normalized creep rate and the applied stress stayed constant regardless of ground temperature. This rate could be obtained from the power law creep equation and known as stress exponent "n". The stress exponent was reported equal to 3 by Morgenstern et al. (1980) for their proposed linear relationship between normalized creep rate and the applied stress. Nixon and McRoberts (1976) reported that this relationship was nonlinear as the increase in creep rate tended to become faster at high stress level. Therefore, they proposed two stress exponents; n1 observed at low stress level and varied from 1.34 to

2.12 as the ground temperature decreased from 0℃ to -11℃ and n2 recorded for higher stress values and found to be constant and equal to 4. Similar nonlinearity could be inferred for the relationship shown by Johnston & Ladanyi (1974) and presented in Figure 6.17. Their helical piles also experienced higher acceleration rate at higher stress levels. When power law equations for their three creep curves were investigated, constant stress exponents of 1.07 and 4.06 were observed at the low and high stress levels respectively. Considering the hypothesis of constant stress exponent proposed by Morgenstern et al. (1980) over the whole stress region and by Nixon and McRoberts (1976) at high stress region, the stress exponent of Johnston & Ladanyi (1974) curves may be generalized to describe creep behavior at different ground temperatures. With the aid of the single measured data points from this study, the two stress exponents were used to establish other series of curves which is presented by dashed lines in Figure 6.17. Th proposed three curves, in addition to Johnston & Ladanyi's (1974) curves, can be used for predicting creep rate for single-helix helical piles for a given design load at temperatures of -0.3℃, -2.1℃, -2.5℃ and -3℃. Linear regression analysis for calculating the temperature-dependent creep parameters B1 and B2 for the test soil was conducted and the results are summarized in Table 6.3.

Table 6. 3. Creep parameters for predicting creep rate of helical piles in frozen silt.

Temperature (℃)	B_1 ($kPa^{-1} * hr^{-1}$)	n_1	B_2 ($kPa^{-1} * hr^{-1}$)	n_2
-0.3	1.00E-07	1.07	8.00E-15	4.06
-2.1	3.00E-08	1.07	3.00E-15	4.06
-2.5	7.00E-09	1.07	6.00E-16	4.06
-3	4.50E-09	1.07	4.00E-16	4.06

Using equation [2.20] proposed by Nixon and McRoberts (1976) and the summarized soil creep parameters in Table 6.3, the normalized creep rate can be readily predicted for a given design load, ground temperature and pile's helix diameter.

6.7 Conclusions

This chapter studied the performance of three different model piles including an open-ended pipe pile, a helical pile, and a grouted shaft helical pile in frozen and unfrozen silty soil. The test piles were evaluated under pull-out loading and creep loading and the following conclusions can be made:

1- The measured pull-out load capacity in unfrozen soil agreed well with the predicted capacities from the general equation for undrained condition for the open-ended pile and from design models proposed by Tappenden and Sego (2007) for helical piles in fine-grained soils.

2- Modified forms from Weaver and Morgenstern (1981) and Tappenden and Sego (2007) were used to predict pull-out capacity of the open-ended pipe pile and helical piles in the frozen ground. The predicted capacities compared well with the field measured capacities except for grouted shaft helical pile.

3- It was inferred that the concrete shaft and the steel helix of the grouted shaft helical pile engaged in resisting the external loading at different time, therefore, and at certain displacement, the concrete shaft friction would fail and only the helix and possibly the soil cylinder in (CSM) will remain resisting the load. Grouted shaft helical pile, therefore, must be designed as a single-helix helical pile to avoid an expected failure due to over estimated design load.

4- The pile creep model proposed by Nixon and McRoberts (1976) was capable of capturing the measured creep rate for the open-ended pipe pile at different temperatures unlike the model proposed by Morgenstern et al. (1980) which showed significantly smaller creep predictions.

5- The measured creep rate for the non-grouted helical pile showed an acceptable level of agreement with the predicted creep rate using Johnston & Ladanyi's (1974) creep model. The design chart proposed by Johnston & Ladanyi (1974) was improved by including another series of creep line that could be used for predicting creep rate for helical piles at wider range of ground temperatures.

6- Regression analysis was carried out to determine the creep parameters for the frozen silty soil in order to be used for predicting creep rate of helical piles in similar soils using the creep equation proposed by Nixon and McRoberts (1976).

CHAPTER 7: CREEP BEHAVIOR OF FROZEN LEDA CLAY UNDER COMBINED COMPRESSION STRESS AND THERMAL EXPOSURE

7.1 Introduction

Pile foundations installed in frost suitable soils (i.e., ice-rich soils) are often designed to satisfy settlement considerations, which depends on creep deformation of the frozen soil. The design load of a pile, therefore, is determined such that an allowable pile settlement over the lifespan of the superstructure is not exceeded. Soil structures and thermal regimes are two important parameters that control creep response of frozen soils, and thus, pile settlement. Different temperature-dependent analytical solutions for predicting pile settlement in frozen grounds were previously developed using temperature-dependent creep parameters of frozen soils. The creep parameters of ice-rich soils in those proposed models were mostly determined from creep data from crystalline ice, attributing that to the large ice content formed within ice-rich soils. However, the creep deformation response of ice-rich frozen soils may not be similar to pure ice given a certain state of an applied stress and temperature exposure. A detailed study was conducted by Eckardt (1982) to investigate creep behavior of frozen soils under tension and compression loading conditions. The study was performed using sand and clayey sandy silt at temperatures ranged from -40℃ to -5℃ and stresses from 0.5MPa to 10MPa. The author described dimensionless stress-strain behaviors using a power law that contains a temperature and time dependent modulus. However, the investigation did not consider temperatures warmer than -5℃ and lacked information about intact ice-rich frozen soils (intact cohesive soil) where the used clayey sandy silt contained less than 5% clay fractions. Moreover, creep behavior corresponding to stresses less than 0.5MPs were not addressed.

Although, researchers elaborated in developing theoretical approaches for designing pile foundations in frozen grounds, the creep data employed were either collected from tests conducted on

ice materials and/or limited to specific range of temperature. Studies enabling observation of creep deformation behaviors of frozen soils for broader temperature range and soil types are needed to produce temperature-dependent theoretical approaches that can better capture pile behaviors in various frozen ground conditions.

In this chapter, the creep behavior of a frozen ice-rich clay was studied under various working compression stresses and temperature exposures. Sets of uniaxial creep experiments were used to evaluate the creep behavior of undisturbed ice-rich Leda clay under combined effect of wide range of compression loads and freezing temperature levels. The tests were conducted in an environmental walk-in chamber using modified Oedometer apparatus to enable testing under controlled thermal boundary and stress condition. The tests were prolonged for sufficient time to capture a full representative creep curve.

7.2 Sampling and Physical Properties of the Test Soil

A marine soil known as Leda clay was used in this experiment to represent the ice-rich frozen materials. The clay soil was sampled intact from the Navan Landfill site in Ottawa, Ontario. The soil samples were collected as undisturbed samples in 200-liter steel barrels that were carefully pushed into the natural Leda clay forms using a backhoe (Figure 7.1). Before sampling, the bottoms of the barrels were drilled at their centres to generate holes which would enable the air to escape while pushing the barrels into the soil. The inside surface of the barrels was coated with a thin layer of wax followed by another layer of lubricant to facilitated soil sampling. The top 500 mm of the clay soil in the field was removed and the open sides of the barrels were then placed on the exposed clay soil. The barrels were then gently pushed into the soil using backhoe until the soil reached the bottoms of the barrels. The soil surrounding the barrels was then excavated and the barrels were lifted up and placed on their bases. After

sampling, the top of the clay sample was trimmed, waxed, and sealed with airtight plastic sheet followed by a steel led to ensure maintaining the natural water content of the collected samples. The barrels were then loaded on a truck using a loader and tightened enough to prevent falling or movement during transporting to the laboratory.

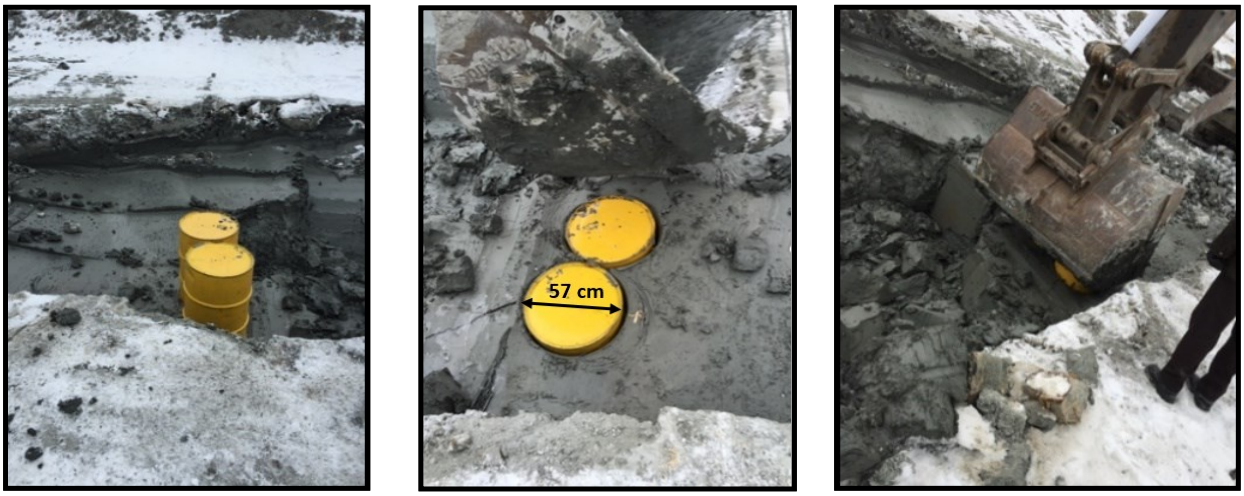

Figure 7. 1. Leda clay sampling at the Navan landfill in Ottawa.

The basic geotechnical properties of Leda clay including particle size distribution, Atterberg limits, bulk density, and the natural water content were examined (Table 7.1). Particle size distribution and clay contents of Leda clay were determined using sieve analysis and hydrometer tests in accordance with ASTM D422-63. The liquid limit of the soil was 51% while the plasticity index was 24% based on Atterberg limit test results (ASTM D4318-10). The average bulk density and water content of the test samples were 1.624 Mg/m^3 and 75% respectively. Hydraulic conductivity of the clay sample was also measured following the Falling Heading testing technique and using a Rigid-Wall mold (ASTM D5856-95, 2007) equipped with a rubber membrane to minimized side-wall leakage (Table 7.1).

Table 7. 1. Physical and hydraulic properties of the test soils.

Characteristic	USCS	$w_{i_{ave}}$ (%)	LL (%)	PI	$\rho_{b_{ave}}$ (Mg/m^3)	%clay	Activity	k (m/s)
Physical & hydraulic Properties	CH	75	51	24	1.624	71	0.34	5.9E-10

A chemical analysis was also performed on the extracted pore waters obtained by squeezing the soil samples under very high pressure. Cation concentrations including potassium, calcium, and magnesium ions were determined in the pore water (mg/l), while sodium concentration was measured based on acid extractable sodium ions (mg/kg). Cation exchange capacities (CEC) were determined and the results presented in Table 7.2.

A random X-ray powder diffraction analysis was carried out to determine the mineralogical composition of Leda clay. Semi-quantitative analysis was conducted on the X-ray results to measure the clay mineral components. The abundant clay mineral found in this Leda clay soil was illite comprising 83%. The remining mineral portion was kaolinite and chlorite with amounts of 11% and 6% respectively. The results indicated no evidence of having any expandable clay minerals (here defined as vermiculite, montmorillonite, or interlayered illite/ smectite) in the test soil (Table 7.2).

Table 7. 2. Chemical and mineralogical properties of the test soils.

Characteristic	Sodium (mg/kg)	Potassium (mg/l)	Calcium (mg/l)	Magnesium (mg/l)	(CEC)* meq/100 g	Illite	Chlorite	Kaolinite
Chemistry and Mineralogy	1700	15	83	40	18	83	6	11

*Cation exchange capacity.

7.3 Sample Preparation and Test Procedures

All test samples were obtained from Leda clay soil in the 200-liter steel barrels. Shelby tube sampler with an inner diameter of 69 mm was used for soil coring from the barrel. The soil was then extracted from Shelby tube using a mechanical extruder and trimmed to the desired dimensions (i.e., 50 mm by 100 mm) (Figure 7.2). After trimming, the clay samples were kept inside PVC columns that had similar dimensions to the clay samples. The PVC column are aimed at minimizing the loss of soil moisture before and during testing that. They also can provide some radial constrains to minimize the horizontal strain during freezing.

The experiment included five sets of uniaxial creep tests that were conducted in a temperature-controlled environmental chamber. Each experimental set consisted of three identical frozen soil samples, thus 15 samples in total. Each sample of the three was tested under different uniaxial compression stress using three Oedometer test frames while all three samples in the set were exposed to an identical temperature level. When one set of samples is terminated, the temperature of the environmental chamber is changed to the next desired temperature level and creep test is repeat again for another set of five frozen soil samples.

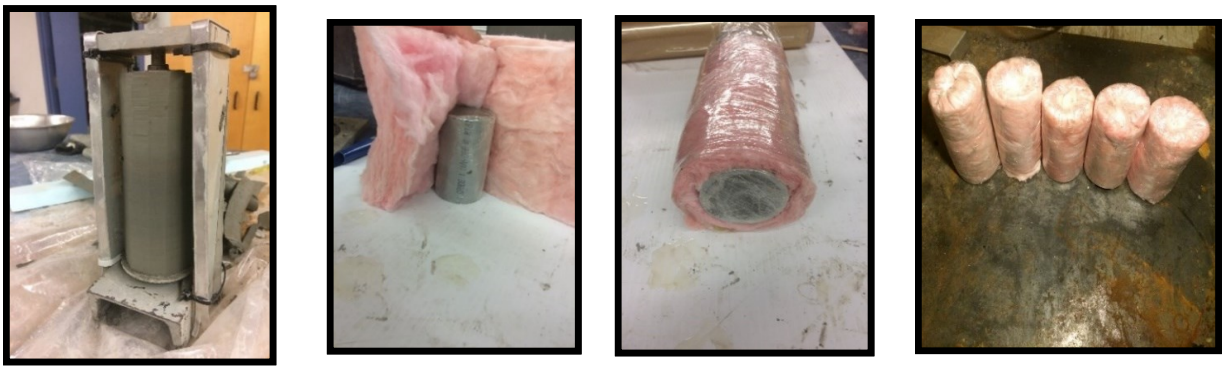

Figure 7. 2. Undisturbed Leda clay extraction and sample preparation.

Before exposed to freezing and in order to control freezing direction, the samples were surrounded by Fiberglass insulation materials on the top and sides to enhance 1D upward freezing action from the bottom of the sample aiming at generating realistic horizontal ice lenses. The test samples for each set were then placed in the environmental chamber under the desired temperature exposure. Five temperature levels were selected for this experiment including -1.0℃, -2.0℃, -4.0℃, -7.0℃, and -10℃. Upon reaching the thermal equilibrium, the insulation materials were removed and the samples were place in the oedometer test frames where each sample was exposed to a different static compression loads on top (Figure 7.3). The creep displacement of the test samples was automatically recorded through a serios of LVDTs to an accuracy of 0.001 mm. All test data were recorded on a data acquisition system and plotted subsequently using LabVIEW platform. Each Oedometer test frame was equipped with a mechanical dial gauge that used to take a periodic creep displacement reading over time to account for any unexpected Power outage. The Five different compression loads were selected to generate different compression stresses within a working range including 50kPa, 200kPa, 500kPa, 1000kPa, and 2000kPa. All creep tests were continued until a steady state creep rates (secondary creep rate) were observed.

Figure 7. 3. Oedometer devices utilized for uniaxial creep test.

7.4 Test Results

Summary of test conditions and the observed creep rates for each test sample is reported in Table 7.3. The correlation between creep displacement and compression stresses under different temperature exposures were plotted and presented in Figure 7.4. At the load onset, and under a given test temperature, the test samples exhibited primary creep strain that increased corresponding to the increase in the magnitude of the applied compression stresses. After a short period of a primary creep, all samples tended to show a non-linear transitional stage with a reduced creep rate. A linear steady state creep rate (secondary creep) was eventually observed where the axial strain consistently increased with time. Most of the test samples were believed to have reached a steady state creep rate condition especially after running some of the test for relatively long time. This was inferred from the proportional increase of creep displacement with time observed after the cessation of the transitional stage that was distinguished with disproportional increase of creep

displacement with time. The steady state creep rates were determined as the slope of the straight-line segments of the creep curves in Figure 7.4 and reported in Table 7.3.

Table 7. 3. Summary of test conditions and creep data of frozen ice-rich Leda clay samples.

Samples #	Temperature (℃)	Compression Stress (kPa)	Bulk Density (Mg/m^3)	Test duration (hrs.)	Creep rate ($year^{-1}$)
1	-1.0	50	1.626	144	0.103
2		500	1.620		0.3147
3		1000	1.623		0.5817
4	-2.0	50	1.618	624	0.0617
5		500	1.623		0.1862
6		1000	1.621		0.2231
7	-4.0	50	1.624	48	0.0096
8		200	1.619		0.045
9		2000	1.622		0.142
10	-7.0	50	1.621	240	0.0075
11		200	1.625		0.0147
12		1000	1.623		0.0567
13	-10.0	50	1.617	432	0.0043
14		200	1.621		0.0114
15		1000	1.626		0.0204

The test durations for the samples tested at -1.0℃, -2.0℃, -4.0℃, -7.0℃, and -10℃ were 6 days, 26 days, 2days, 10 days, and 18 days respectively. The short test period for the frozen samples tested at -4.0℃ happen due to some technical issues experienced with the environmental chamber that required to stop the test and carry out some maintenance. From the curves in Figure 7.4c, however, it could be inferred that the samples may have reached their steady state creep rates.

The magnitude of creep rates of the frozen soils influenced by the applied stress as well as the test temperatures. For the samples tested at -10℃, for example, the creep rates increased by an order of magnitude when the applied stress increased form 50kPa to 1000kPa recording $4.3x10^{-3}$ $year^{-1}$ and $2.04x10^{-2}$ $year^{-1}$ respectively. On the other hand, increasing the temperature from -10℃ to -1.0℃ while maintaining the applied stress at 50kPa resulted in about two order of magnitude creep rate increase recording $1.03x10^{-1}$ $year^{-1}$.

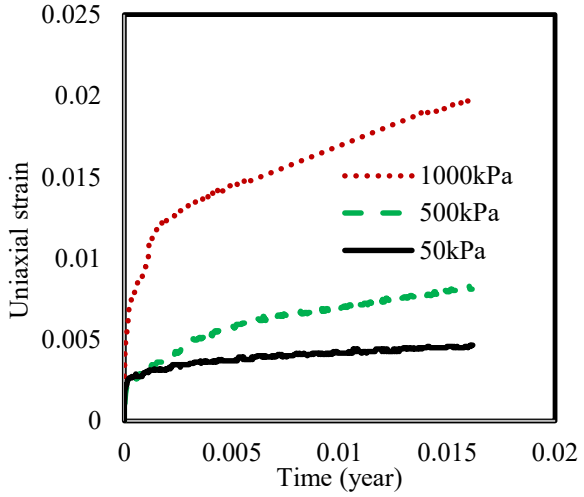

(a) −1.0℃

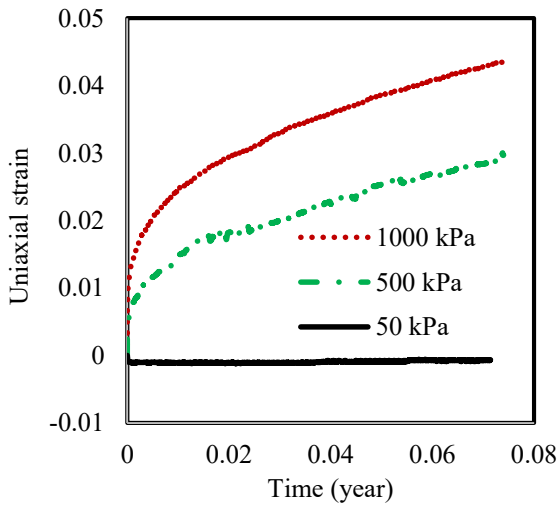

(b) -2.0℃

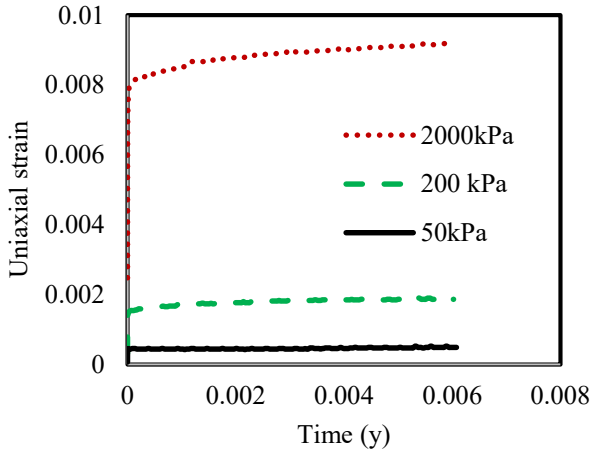

(c) -4.0℃

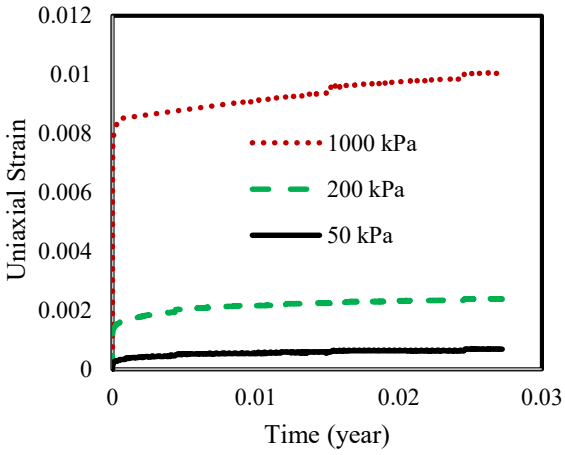

(d) -7.0℃

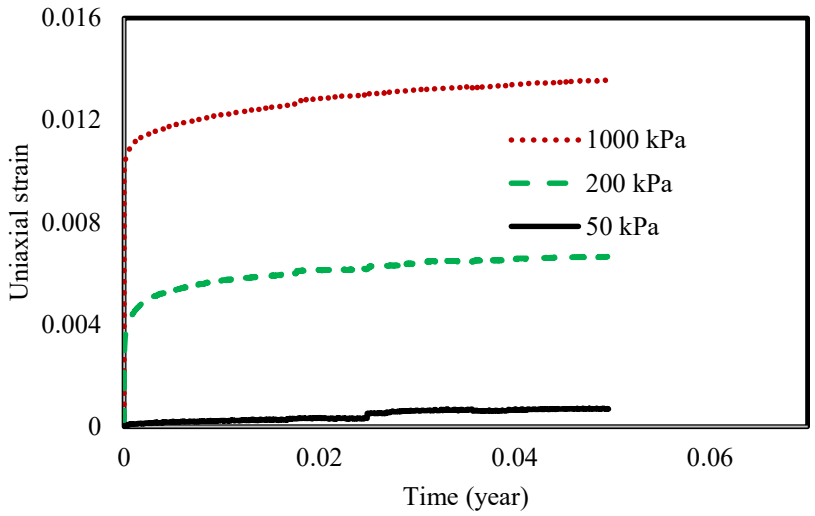

(e) -10.0℃

Figure 7. 4. Creep strain versus time relationships under different uniaxial creep stresses and temperature exposures.

7.5 Discussion

7.5.1 Creep behavior of ice-rich Leda clay

Leda clay is a cohesive soil that is able to intake and preserve significant amount of water because of its large specific surface area. Leda clay soils upon freezing, therefore, would contain a large content of ice and form ice-rich frozen material, which is resulted from the phase transformation of water content from liquid to solid. Therefore, the behavior of frozen Leda clay could be substantially influenced by the mechanical behavior of ice materiel that dominates its matrix. Crystalline ice has been reported to exhibit viscous response when it is exposed to loading. This behavior causes the material to undergo continues deformation over the time, known as creep, even under a small applied stress. Since the ice material dominates the matrix of frozen Leda clay, it could also control their overall deformation behaviors.

Performance of pile foundation installed in frozen Leda clay weather directly or backfilled with slurry could be influenced by the creep deformation behaviors of frozen Leda clay. Therefore, the common practice is to define the creep behavior of the surrounding soils by defining their creep parameters and used those parameters for predicting creep deformation of piles within the surrounding soils. Nixon and McRoberts (1976) and Morgenstern et al. (1980), for example, analyzed creep data from ice material and from limited quantity of ice-rich soils to obtain their creep parameters. Those creep parameters were later used for predicting creep deformation of piles in such frozen soils.

In order to obtain accurate creep parameters of a frozen soil, a steady sate creep rate under a constant load and stabile temperature has to be observed. Ladanyi (1972) stated that the initial elastic strain can be neglected as it is responsible for a small portion of deformation comparing to the larger creep deformation resulted over time during stead state creep. Therefore, and from the current experiment, steady state creep was extracted from the creep-time relationship in Figure 7.4 and respectively plotted against applied stress and presented in Figure 7.5. Similar to stress-strain results reported by Morgenstern et al. (1980), the stress-strain relationship for Leda clay on log-log scale is linear.

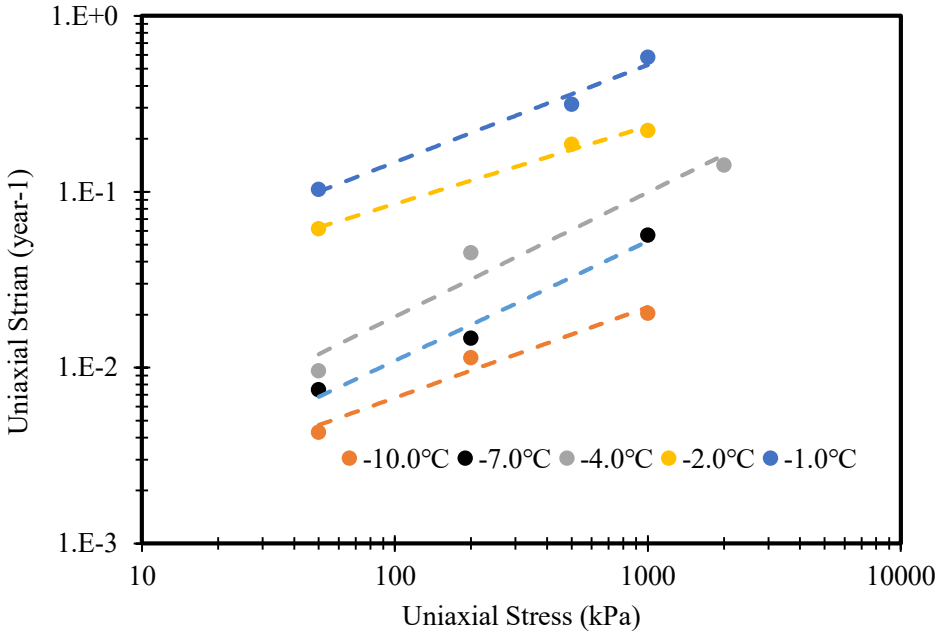

Figure 7. 5. Stress-strain relationship for frozen Leda clay under uniaxial compression loading.

Creep parameters of frozen Leda clay can be defined from the slop of those linear relationships and from the intersects with creep strain axis (Y-axis). The slope of the lines expresses the increase of creep strain as a function of stress increase and known as stress exponent "n". The intersects with Y-axis gives another creep constant known as "B". Before determining creep parameters from the raw data, a regression analysis was conducted on the stress-strain data to obtained more consistent and representative creep parameters. The results after modification are presented in Figure 7.6. The creep parameters for frozen Leda clay exposed to various freezing temperatures after rounds of regression analysis were obtained and also be summarized in Table 7.4

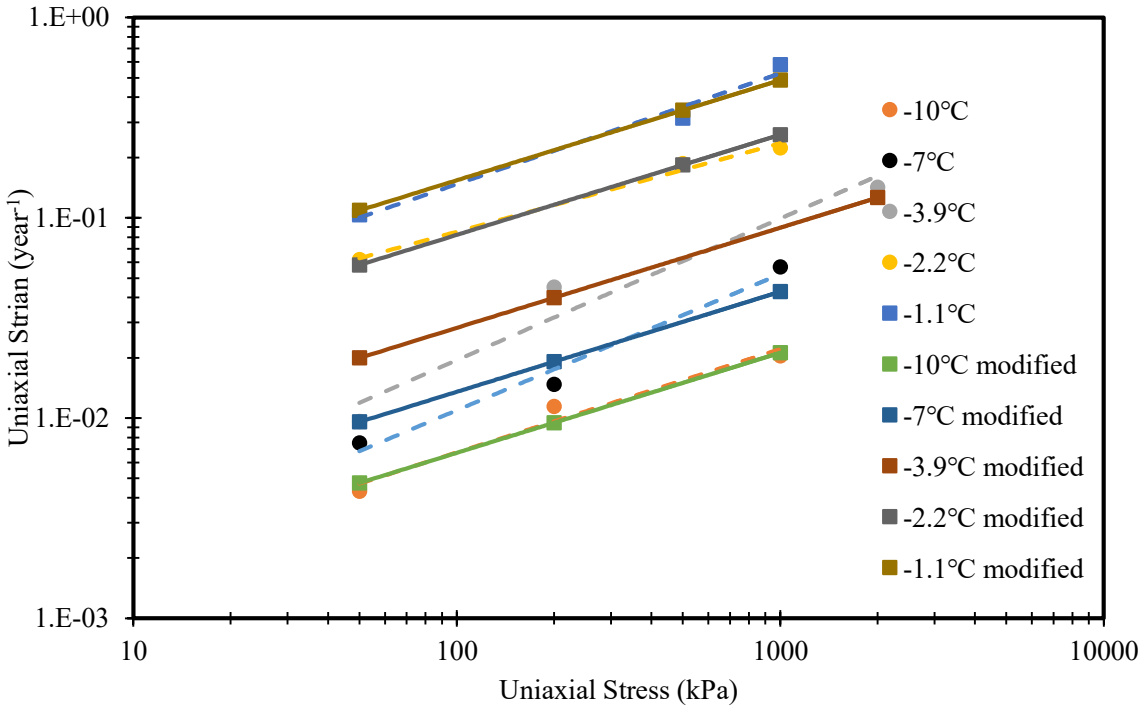

Figure 7. 6. Modified stress-strain relationship for frozen Leda clay under uniaxial compression loading.

Table 7. 4. Creep parameters for ice-rich Leda clay

Temperature (°C)	B (kPa^{-1}. $year^{-1}$)	n
-1.0	1.54E-02	0.5
-2.0	8.22E-03	0.5
-4.0	2.82E-03	0.5
-7.0	1.35E-03	0.5
-10.0	6.70E-04	0.5

The obtained stress exponent "n" in this study is constant regardless to the change in temperature exposure. Similar finding was reported by Morgenstern et al. (1980), however, the current stress exponent of 0.5 is significantly smaller than those reported by Morgenstern et al. (1980) and even Nixon and McRoberts (1976). Morgenstern et al. (1980) reported a constant stress

exponent of 3 at any given temperature levels, whereas, Nixon and McRoberts (1976) reported varying stress exponent from 1.34 to 2.12 at the low stress region but constant stress exponent of 4 at high stress region. The low value of stress exponent for frozen Leda clay refers to its stiffer structure and lower compressibility compared to the ice behavior reported by Nixon and McRoberts (1976). Morgenstern et al. (1980). This could be attributed the different structure between frozen Leda clay and crystalline ice.

7.5.2 Pile creep modeling in frozen Leda clay

It was discussed in details by many researchers (e.g., Vyalov 1959; Johnston and Ladanyi 1972; Nixon and McRoberts 1976) that the deformation of frozen ground around a pile shaft could be expressed as shearing of concentric cylinders. If the creep behavior of the frozen soil is characterized by the creep flow law proposed by Glen 1952 in equation [2.14], normalized pile velocity $\left(\frac{u_a}{a}\right)$, under constant tangential shear stress τ_a, and uniform constant ground temperature (T) can be determined from equation [2.21] proposed by Morgenstern et al. (1980) as follow:

$$\frac{u_a}{a} = \frac{3^{\frac{n+1}{2}}\ B\ \tau_a^n}{n-1}$$

where: u_a creep strain; a is the pile radius; n and B are creep parameters.

However, the stress exponent "n" observed in this study is smaller than the unity, therefore, using equation [2.21] proposed by Morgenstern et al. (1980) would result in negative predicted values of pile creep rate in frozen Leda clay. A modification, therefore, was needed to obtain a rational predictions of pile creep rates in such soil. A simple mathematical adjustment was implemented into the original equation by taking the absolute value of the denominator (n^{-1}) in equation [2.12]. This modification corrected for the negative sign convention and resulted in

positive values of the predicted pile creep rates. The modified form of Morgenstern et al. (1980) equation can be written as follow:

$$\frac{u_a}{a} = \frac{3^{\frac{n+1}{2}} \; B \; \tau_a^n}{|n-1|} \qquad [7.\ 1]$$

Using the modified equation and creep parameters for Leda clay reported in Table 7.4, pile creep can then be predicted for a given ground temperature, shaft stress, and pile radius. The predicted normalized pile creep for smooth-shafted pile foundation installed in frozen Leda clay, accordingly, is plotted in Figure 7.7. Pile creep predictions using Nixon and McRoberts (1976) model was also presented on the same graph for the purpose of comparison.

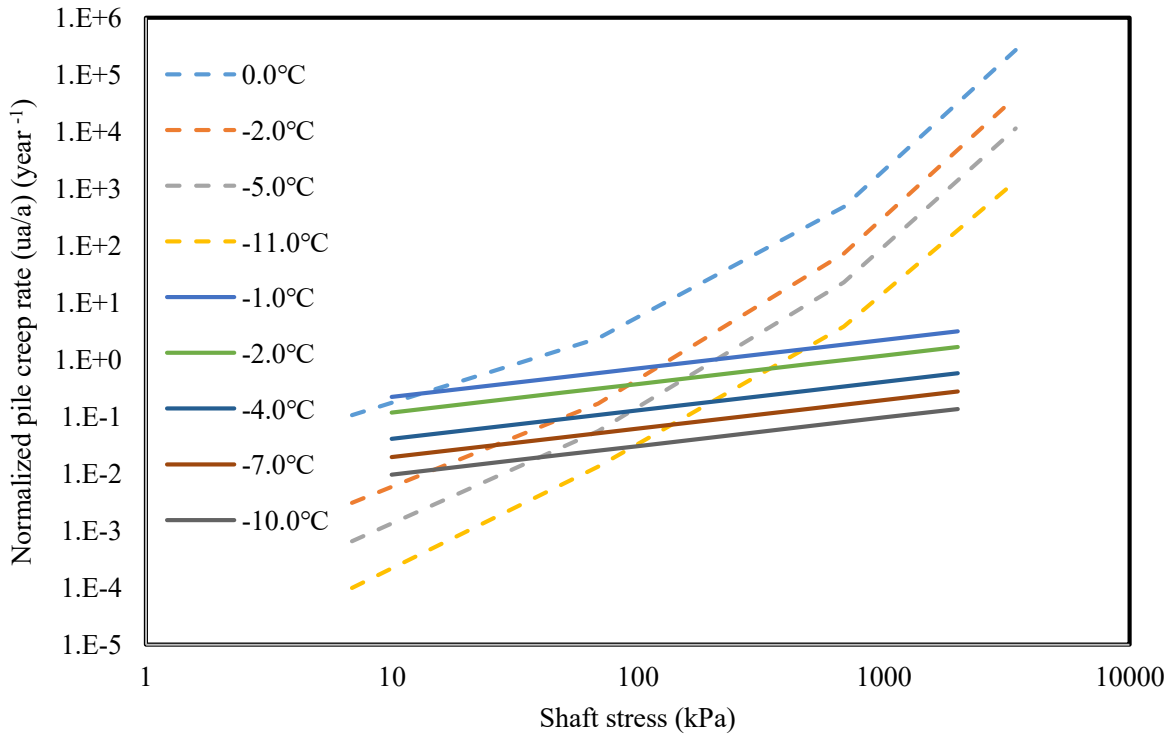

Figure 7. 7. Prediction of pile creep rate from the modified equation (solid lines) and from Nixon and McRoberts (1976) creep model (dashed lines).

It is clear that the predicted pile creep rates in frozen Leda clay using the modified equations are substantially different from those predicted using Nixon and McRoberts's (1976) creep model in ice-rich soils. The pile creep model proposed in this study provided more conservative creep prediction at the low stress region compared to Nixon and McRoberts's (1976) creep model. Since pile creep models are developed using creep parameters of the frozen soils, the difference in pile creep prediction, therefore, could be attributed to the difference in creep parameters of the modeled frozen soils. The difference in creep parameters observed in this study from the parameters reported in literature could be attributed to the difference in creep behaviors exhibited by frozen Leda clay as a realistic ice-rich frozen soil compared to the creep behavior of crystalline ice materials used by Nixon and McRoberts's (1976) and Morgenstern et al. (1980) and assumed to address the behaviors of frozen ice-rich soils. Frozen Leda clay contains soil particles, unfrozen water content, ice content and possibly air voids, thus, it is creep behavior, unsurprisingly, should be different than the creep of ice.

The proposed pile creep model in this study, however, still need to be validated with measured pile creep data from field in order to be used with more confidence. The next section provides comparison between the predicted pile creep data using this model and measured pile creep data from different sources in literature as well as from pile creep in field reported in chapter 6 of this study.

7.5.3 Pile creep modeling in frozen Leda clay

A review of previously reported field observations of pile creep in ice and ice-rich soils was conducted. The reviewed data were screened and the best representative ground condition in the reviewed data to the tested frozen Leda clay were selected for validation. Summary of the selected data is presented in Table 7.5.

Table 7. 5. Summary of pile creep data from field observations.

Source	Pile type	Pile Diameter (mm)	Soil type	Avg. ground Temp. (℃)	Shaft stress (kPa)	Creep rate ($year^{-1}$)
Valov (1959)	wood	35	Ice-rich silt	-0.4	100	1.5
Valov (1959)	wood	35	Ice	-0.4	55	1.1
					100	2.3
					60	1.5
Stehle (1970)	Steel H	304.8	Ice	-1.0	34	0.42
		76.2			31	0.32
Dokuchayev and Markin (1971)	concrete	400	Ice-rich silt	-1.0	170	0.96
This study	Steel pipe	100	Ice-rich silt	-1.9	50	0.26
				-2.7	50	0.070
				-2.9	50	0.035

The selected pile creep data were then plotted on the predicted pile creep from the proposed model in this study and all presented in Figure (7.8).

Creep data reported by Vyalov (1959) were measured for timber piles in ice and ice-rich silt at an average ground temperature of -0.4℃. These data plotted above the predicted pile creep rates model at ground temperature of -1.0℃. The stress exponent of Vyalov (1959) data points is found to be 0.7 from their trend line comparing to 0.5 for predicted creep lines reported in this study. This refers to good agreement between measured and predicted data from the proposed model.

Another set of data reported by Stehle (1970) and Dokuchayev and Markin (1971) for steel H-piles and concrete pile respectively. Piles were installed in ice at an average ground temperature of -1.0℃. These data plotted just on the predicted pile creep data at ground

temperature of -1.0℃ showing an outstanding agreement between measured and predicted data sets. The trend line of these data, moreover, overlapped the predicted creep line yielding a slightly larger stress exponent of 0.58.

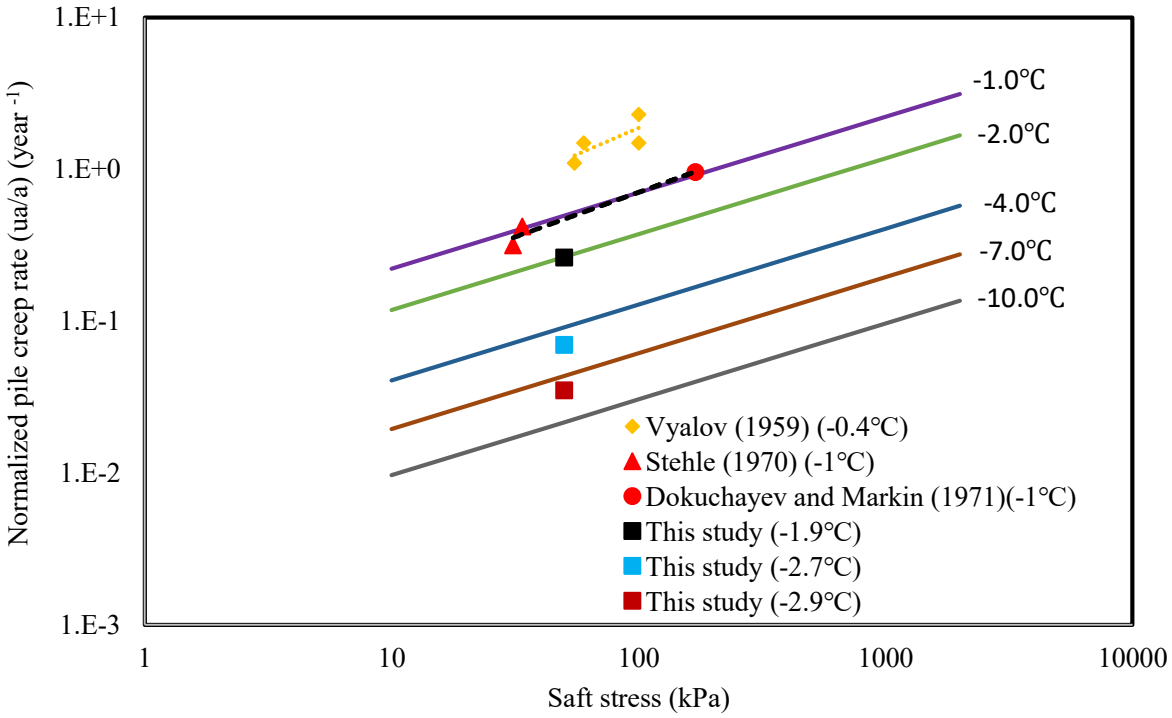

Figure 7. 8. Validation of the proposed pile creep model against measured pile creep data from this study and from literature.

Creep data for the steel pipe pile reported in chapter 6 of this study were also plotted on Figure 7.8. The measured pile creep at the average ground temperature of -1.9℃ located on the predicted pile creep line of -2.0℃. The measured pile creep data at ground temperature of -2.7℃ and -2.9℃, however, were off the predicted data by locating below the line of -4.0℃ and -7.0℃ respectively. The predicted data were conservative compared to the measured data at those two temperature levels. More field measurement of pile creep at temperature below -2.0℃ is required for better validation.

However, the current validation showed that the proposed pile creep model was capable of capturing most of the creep behaviors of piles in ice and ice-rich soils when ground temperature is at -2.0℃ or warmer. At colder temperature, the proposed creep model gives conservative pile creep prediction compared to the measured data.

4.1 Conclusion

An experimental program was conducted to investigate creep behavior of frozen Leda clay as an ice-rich soil at different freezing temperatures under uniaxial compression stresses. The stress-strain relationship on log-log scale was linear for all test temperatures showing constant stress exponent of 0.5. The resulted creep parameters for frozen Leda clay, however, were different from what have been previously reported in literature for ice and ice-rich soils. The difference may be attributed to the difference in creep behaviors between the real ice-rich Leda clay tested in this study compared to the crystalline ice tested to mimic ice-rich behavior in literature. A new pile creep model was proposed in this study and used to predict pile creep in ice-rich soils using creep parameters of frozen Leda clay. The predicted data using the proposed model were in a very good agreement with measured data at temperature of -2.0℃ or warmer. Predicted data at colder temperatures were conservative compared to the measured field data. More measured field data at temperature colder than -2.0℃ are desired to confirm the validity of the proposed pile creep model.

CHAPTER 8: CONCLUSIONS AND SUGGESTIONS

8.1 Introduction

Pile foundations are used as the main type of foundations for supporting structures and infrastructure systems in cold regions. They are aimed at transferring the carried loads to more thermally stable frozen layers to reduce the risk of failure at both sub and superstructures levels. Performance of pile foundations in frozen ground has been, therefore, intensely studied. However, their load carrying capacity and creep behavior were evaluated within not a broad enough range of temperatures, soil types, or/and loading rates. The current research work is dedicated to complement on previous research studies to overcome these limitations and minimize the uncertainties associated with predicted performance of pile foundations in frozen gourd.

8.2 Conclusions

8.2.1 Prediction of adfreeze strength of pile foundations in ice-rich and ice-poor soils

A comprehensive laboratory testing program was carried out to investigate strength behavior of frozen soils as well as adfreeze strength of steel-soil interface using ice-rich and ice-poor soil materials. The following conclusions could be drawn:

1- The ultimate shaft capacity of steel piles can be correlated to the shear strength of frozen soils using two surficial factors; roughness factor (m) and frictional factor (n).

2- The roughness factor “m” is found to vary with not only the pile materials (e.g., steel, concrete, timber), but also with ground temperature, soils type, and stress condition. In ice-rich soils, roughness factor decreases with increasing ground temperature reaching a minimum value of 0.54 at 0.0°C. In ice-poor soil, roughness factor was less sensitive to

temperature change and showed slight increase with increased ground temperature moving from 0.67 to 0.82 as temperature increased from −10.0°C to -1.0°C.

3- A frictional factor “n” representing the ratio between the frictional resistance of pile-soil interface to the frictional resistance of the frozen soil, is introduced in this study. For ice-rich soils, frictional factor decreases with increasing freezing temperature, but it is always greater than the unity and indicates a higher steel-soil frictional resistance at any given temperature compared to the frictional resistance of the frozen ice-rich soils. Frictional factor for steel piles in ice-poor soils, in contrast, is constant at 0.75 regardless to ground temperatures.
4- Steel piles in frozen ice-rich soil may exhibit larger load carrying capacity compared to those in frozen ice-poor soils. However, the pile capacity in both type of soils decreases linearly as the freezing temperature increases toward freezing point.
5- Empirical equations are provided for predicting shaft resistance of steel piles in frozen ground.

8.2.2 Effects of strain rates, development of unfrozen water content, and evolution of induced normal stress for pile foundations installed in frozen grounds

Frozen ground shows time-dependent behaviors which is expected to influence the shear strength and adfreeze strength of piles under different shear loading conditions. After pile installation in frozen ground, the surrounding soil/backfill would undergo refreezing which often be accompanied with decrease in unfrozen water content and increase in normal stress due to the freezing induced lateral pressure. The effect of strain rate on adfreeze strength was investigated. A physical model was also employed to investigate the phenomena of evolution of UWC and normal stress around the pile foundations and the following behaviors were observed:

1- Adfreeze strength of pile foundation can be significantly affected by the strain rate. Piles that are loaded under a rapid loading condition would most likely to exhibit greater adfreeze strength. The influence of changing shear rate was more pronounced for piles installed in ice-poor soil compared to those observed in ice-rich soil. The higher adfreeze strength could be attributed to the effect of stress localization under the higher strain rates and/or due to the excess pore water pressure. Rapid loading may enhance undrained condition which causes pore water pressure to bald up and contributes to a greater ultimate capacity of the pile. However, longer term adfreeze strength after this rapid loading condition may experience relaxation over the time due to the time-dependent behavior of frozen grounds.

2- Unfrozen water content followed a typical trend of reduction corresponding to soil freezing below zero degree Celsius in both ice-rich and ice-poor soils. The amount of UWC was generally greater near the pile shaft compared to the UWC observed farther from the pile. This could be attributed to the quicker response to thermal change exhibited by the steel pile compared to frozen soils which could cause a faster freezing rate at the pile-soil interface.

3- Before the freezing point, the normal stress experienced a slight reduction of about 7 kPa in ice-rich soil and 1 kPa in ice-poor soils which could be attributed to soil consolidation around the pile. However, and as the temperature drops below zero-degree Celsius, the UWC decreases and normal stress dramatically increases recording a maximum absolute value of 76 kPa in ice-rich soil when the temperature reaches around –10.0°C. As the temperature was further dropped, the increase in normal stress around the pile in ice-rich soil became nominal reaching and absolute maximum value of 84 kPa at -15°C. This

agreed well with the reduction trend of UWC which was at max up to -5.0°C followed by a slight declining corresponding to further temperature reduction. after 72 hrs. of observation, the induced normal stress maintained its value without experience any stress relaxation. The developed freezing normal stress, unlike to ice-rich soil, was found to be minimal in ice-poor soils recoding a maximum absolute value of 7 kPa. Induced normal stress in sand decreased after 3 days recording absolute value of 5.5 kPa. The lower value of induced normal stress and its relaxation in ice-poor soil comparing to ice-rich soil could be attributed to larger voids with the granular type of soil which can accommodate for the increase in ice volume following to freezing.

4- From the comparison between adfreeze strength obtained from interface element tests and from the model pile test, the interface element tests showed to be capable of representing pile-soil interface strength behavior for larger scale and can be used to simulate the behavior of conventional steel piles in frozen ice-rich and ice-poor soils with acceptable degree of validity.

8.2.3 Adfreeze strength and creep behavior of pile foundations from field observations

Various pile geometries including open-ended pipes pile, cylindrical concrete piles, helical piles, grouted shaft helical piles were tested in field to compare their strength and creep performance in frozen and unfrozen grounds. The behaviors of these model piles were evaluated under pull-out loading and creep loading and the following conclusions can be made:

1- Piles designed to support structures in frozen grounds may generally lose more than 90% of their carrying load capacity if the frozen ground experienced significant thawing action. This reflects the significant role of the thermal aspect in characterizing the performance of pile foundations in frozen grounds.

2- The location of helix on helical piles was found to be crucial in defining the load carrying capacity of these piles in frozen ground. The helix must be positioned in permanently frozen layer to maximize the end bearing and enhance the over all capacity of the helical piles.

3- The measured pull-out load capacity in unfrozen soil agreed well with the predicted capacities from the general equation for undrained condition for the open-ended piles and from design models proposed by Tappenden and Sego (2007) for helical piles in fine-grained soils.

4- Modified forms from Weaver and Morgenstern (1981) and Tappenden and Sego (2007) were used to predict pull-out capacity of the open-ended pipe pile and helical piles in the frozen ground. The predicted capacities compared well with the field measured capacities except for grouted shaft helical pile.

5- It was inferred that the concrete shaft and the steel helix of the grouted shaft helical pile engaged in resisting the external loading at different time, therefore, and at certain displacement, the concrete shaft friction would fail and only the helix and possibly the soil cylinder in cylindrical shear model will remain resisting the load. Grouted shaft helical pile, therefore, must be designed as a single-helix helical pile to avoid an expected failure due to over estimated design load.

6- The pile creep model proposed by Nixon and McRoberts (1976) was capable of capturing the measured creep rate for the open-ended pipe pile at different temperatures unlike the model proposed by Morgenstern et al. (1980) which showed significantly smaller creep predictions.

7- The measured creep rate for the non-grouted helical pile showed an acceptable level of agreement with the predicted creep rate using Johnston & Ladanyi's (1974) creep model. The design chart proposed by Johnston & Ladanyi (1974) was improved by including another series of creep line that could be used for predicting creep rate for helical piles at wider range of ground temperatures.
8- Regression analysis was carried out to determine the creep parameters for the frozen silty soil in order to be used for predicting creep rate of helical piles in similar soils using the creep equation proposed by Nixon and McRoberts (1976).

8.2.4 Creep modeling of frozen Leda clay and pile foundations ice-rich soils

The comprehensive testing programs performed in this study provided strong background for developing a testing program for investigating creep behaviors of frozen grounds as well as pile foundation in frozen grounds. Creep phenomenon is more important in frost susceptible soils such as ice-rich frozen grounds. Therefore, Leda clay, as an ice-rich soil, was selected to be tested for creep and using its creep parameters to develop pile creep model for piles in frozen ice-ich soils. The outcomes of this particular testing and analysis program can be summarized in the following bullets:

1- The obtained creep parameters for frozen Leda clay were different from what have been previously reported in literature for ice and ice-rich soils. The difference may be attributed to the difference in creep behaviors between the real ice-rich Leda clay tested in this study compared to the crystalline ice tested to mimic ice-rich behavior in literature.
2- Using creep parameters of Leda clay, a new pile creep model was proposed in this study and used to predict pile creep in ice-rich soils.

3- The predicted data using the proposed model were in a very good agreement with measured data at temperature of -2.0℃ or warmer.

4- Predicted pile creep data at colder temperatures using the proposed model were conservative compared to the measured field data. More measured field data at temperature colder than -2.0℃, therefore, are desired to confirm the validity of the proposed pile creep model to describe creep behavior of pile foundations over a wider temperature range.

8.3 Recommendations

The author worked to the best of his knowledge and put the most possible efforts to conduct this research and draw accurate and meaningful results and conclusions out of this study. However, rooms for improvement may always exist. The author wants to provide some recommendations such that other interested researchers can reproduce the similar testing programs taking into account these recommendations while performing any future research works. Some of these recommendations are highlighted and listed below.

1- The nature of this study and the limited availability of the key testing facility in this experiment which is the cold room enforced limiting the testing time of some of the testing programs. Some of the provided results, therefore, should be regarded as a short-term observation, and be dealt with based on that.

2- Adfreeze strength from element tests for ice-rich and ice-poor soils reported in this study must be taken considering the circumstances of the testing programs such as the shearing rates, soil type, testing temperature, and testing duration.

3- The interface element tests were aimed at evaluating the effect of surficial characteristic of the steel piles on adfreeze strength. The effect of testing duration was normalized when taking the ration between the strength of steel-soil interface to the strength of

frozen soils tested at similar shear rate. However, the reported strength of frozen soil and steel-soil interface must be considered as short-term behaviors. Long-term shear strength of frozen soils and adfreeze strength of piles may be obtain by elongating the test duration and reducing the shear rate to better capture the strength behavior of frozen soils and adfreeze strength of piles in field.

4- A comprehensive field instrumentations and testing programs are recommended for studying the mobilized normal stress around the pile following to freezing.

5- Large model pile creep test was aimed to be conducted for validation of the predicted pile creep data obtained from the proposed pile creep model. However, this test was not possible to be carried out due to the limited access to the cold room. Future testing program for evaluating pile creep behaviors under a controlled environment, therefore, is desired.

REFERENCES

A.B. Chance Co. (1996). Helical Pier Foundation System Technical Manual, Bulletin 01–96.

Afshin, A., and Rayhani, M.T. (2014). Evaluation of bearing capacity with time for small-scale piles driven into Leda clay. International Journal of Geotechnical Engineering, DOI: 10.1179/1939787914Y.

Andersland, O. B., and Alwahhab, M. R. M. (1982). Bond and slip of steel bars in frozen sand. In CRREL Proc. of the 3 d Intern. Symp. on Ground Freezing p 27-34(SEE N 83-15691 06-42).

Andersland, O. B., and Alwahhab, M. R. M. (1983). Lug behavior for model steel piles in frozen sand. Proceedings of the Fourth International Conference on Permafrost, Fairbanks, Alaska, Natl. Acad. Sci., 16–21.

Andersland, O. B., and Anderson, D. M. (1978). Geotechnical Engineering for Cold Regions, McGraw-Hill Book Co., Inc., New York, N.Y.

Andersland, O. B., and Ladanyi, B. (2004). Frozen ground engineering. John Wiley & Sons.

Armstrong, M. D., & Csathy, T. I. (1963). Frost design practice in Canada. Highway Research Record, (33).

ASTM D 4318. 2010. Standard Test Methods for Liquid Limit, Plastic Limit, and Plasticity Index of Soils. ASTM Int., West Conshohocken, PA, USA.

ASTM D2487-17, Standard Practice for Classification of Soils for Engineering Purposes (Unified Soil Classification System), ASTM International, West Conshohocken, PA, 2017,

ASTM D3080/D3080M-11. (2012). Standard Test Method for Direct Shear Test of Soils Under 494 Consolidated Drained Conditions, Annual Book of ASTM Standards, ASTM Int., 495 West Conshohocken, PA. ASTM D422-63. (2007).

ASTM D422-63. 2007. Standard Test Method for Particle-Size Analysis of Soils, Annual Book of 484 ASTM Standards, ASTM International, West Conshohocken, PA.

ASTM D5321-12. (2014). Standard test method for determining the shear strength of soil-geosynthetic and geosynthetic-geosynthetic interfaces by direct shear, ASTM Int., West Conshohocken, PA.

ASTM D5856-95, 2007. Standard Test Methods for Measurement of Hydraulic Conductivity of Porous Materials using a Rigid-Wall Compaction-Mold Permeameter. West Conshohocken, PA: ASTM International, doi: http:// dx.doi.org/10.1520/D5856-95R07.

ASTM D698, (2012). Standard Test Methods for Laboratory Compaction Characteristics of Soil Using Standard Effort (12 400 ft-lbf/ft3 (600 kN-m/m3), West Conshohocken, PA: ASTM International, DOI:10.1520/D0698-12.

ASTM. (2007). "Standard test methods for deep foundations under axial compressive load." ASTM International, D1143M-07., West Conshohocken, Pa.

ASTM. (2008). "Standard test method for field vane shear test in cohesive soil." ASTM International, D2573, West Conshohocken, Pa.

Barnes, P., Tabor, D., and Walker, J. C. F. (1971). The friction and creep of polycrystalline ice. Proceedings of the Royal Society of London, Series A, Vol. 324, pp. 127-155.

Benmokrane, B., and Ballivy, G. (1991). Five-year monitoring of load losses on prestressed cement-grouted rock anchors. Canadian Geotechnical Journal, 28(5), 668-677.

Bhatnagar, R. S. (1969). Pullout resistance of anchors in silty clay. M.Sc. thesis, Duke Univ. Sch. Eng., Durham, N.C., Soil Mech. Ser. No. 18.

Biggar, K. W., & Sego, D. C. (1993). Field pile load tests in saline permafrost. I. Test procedures and results. Can. Geotech. J., 30(1), 34-45.

Biggar, K. W., and Kong, V. (2001). An analysis of long-term pile load tests in permafrost from the Short-Range Radar site foundations. Canadian geotechnical journal, 38(3), 441-460.

Biggar, K. W., and Sego, D. C. (1990). The curing and strength characteristics of cold setting cement fondu grout. In Proceedings of 5th Canadian Permafrost Conference (pp. 349-56).

Brown, J. and Romanovsky, V.E., (2008). "Report from the International Permafrost Association: State of permafrost in the first decade of the 21st century." J. Permafrost and Periglacial Processes.

Budd, W. F. (1969). The dynamics of ice masses. Australian National Antarctic Research Expeditions Scientific Reports, Series A(IV), Glaciology Publ. No. 108. 216 p.

Bush, E., Etkin, D. A., Hayley, D., Hivon, E., Ladanyi, B., Lavender, B., and Smith, M. (1998). Climate change impacts on permafrost engineering design. Environment Canada, Environmental Adaptation Research Group, Downsview, Ontario.

Butkovich, T. R., and Landauer J. K. (1960). Creep of ice at low stresses. U.S. Army, Corps of Engineers, Snow, Ice, and Permafrost Research Establishment, Wilmette, IL. Research Report No. 72. 6 p

Butkovich, T. R., and Landauer, J. K. (1959). The flow law for ice. U.S. Army, Corps of Engineers, Snow, Ice, and Perma- frost Research Establishment, Wilmette, IL, Research Report No. 56. 7 p.

Canadian Geotechnical Society. Foundations Committee. (1978). "Canadian foundation engineering manual." Canadian geotechnical society.

CFEM. (2006). Canadian foundation engineering manual, 4th ed., Canadian Geotechnical Society, Richmond, British Columbia, Canada.

Colbeck S. C., and Evans, R. F. (1973). A flow law for temper- ate glacier ice. Journal of Glaciology, 12(64), pp. 71-86.

Crory, F. E. (1963). Pile foundations in permafrost. Proc. 1st Permafrost Int. Conf., Lafayette, Indiana, NAS-NRC Publ. No. 1287, pp. 467-472.

Crory, F. E. (1966). Pile foundations in permafrost. Proceedings of the First International Conference on Permafrost, (1963). Purdue Univ., W. Lafayette, Ind., Natl. Acad. Sci., 467–472.

Crory, F.E. and Reed, R.E. (1965). Measurement of frost heaving forces on piles. Cold Regions Res. and Eng. Lab. (CRREL), Technical Report, 145.

Cuthbertson-Black, Robert. (2001). The interaction between a flighted steel pipe pile and frozen sand.

Dalmatov, B.I., Karlov, V.D., Turenko, I.I., Ulitskiy, V.M. and Kharlab, V.D. (1973). Interaction of freezing heaving with foundations. Proc., 2nd Int. Conf. on Permafrost, Yakutsk, USSR Contribution, National Academy Press, Washington, DC, 1978, 572-576.

Eckardt, H. (1982). Creep tests with frozen soils under uniaxial tension and uniaxial compression. In Proceedings 4th Canadian Permafrost Conference (pp. 394-405).

Esch, D.C. and Osterkamp, T.E. (1990). Cold regions engineering: Climatic warming concerns for Alaska. J. of Cold Regions Eng. 4(1):6-14.

Fish, A. M. (1983). Comparison of USSR codes and US Army manual for design of foundations on permafrost. Cold Regions Science and Technology,8(1), 3-24.

Fossum, A. F. and Fredrich, J. T. (2000). Cap plasticity models and compactive and pliant prefailure deformation. Proc. of the 4th North American Rock Mechanics Symposium, NARMS2000, Seattle, Washington, 1169-1176.

Foster, M. L. (1986). Adfreeze strength of ice to steel pipe piles as a function of temperature. Proceedings of the Fourth International Conference on Cold Regions Engineering, Anchorage, Alaska, 11–20.

Foundation engineering for expansive soils, John Wiley & Sons, Inc., pp. 258-294

Frey, K. E., & McClelland, J. W. (2009). Impacts of permafrost degradation on arctic river biogeochemistry. Hydrological Processes: An International Journal, 23(1), 169-182.

Giraldo, J. and Rayhani, M. T., (2013). Influence of Fiber-reinforced Polymers on Pile–Soil Interface Strength in Clays, Advances in Civil Engineering Materials, Vol. 2, No. 1, 2013, pp. 1–17, doi:10.1520/ ACEM20120043. ISSN 2165-3984.

Glen, J. W. (1952). Experiments on the deformation of ice. Journal of Glaciology, 2(12), pp. 111-114.

Glen, J. W. (1955). The creep of polycrystalline ice. Proceedings of the Royal Society of London, Series A, Vol. 228, pp. 519- 538.

Hanna, T. H., and Carr, R. W. (1971). The loading behavior of plate anchors in normally and over consolidated sands. Proc. 4th Conf. Soil Mech., Budapest, Hung. pp. 589-600.

Haynes, F. D. (1978). Effect of temperature on the strength of snow-ice (No. CRREL-78-27). Cold Regions Research and Engineering Lab, Hanover, NH.

Haynes, F. D. (1978). Effect of temperature on the strength of snow-ice (No. CRREL-78-27).

He, P., Zhu, Y. and Cheng, G. (2000). Constitutive models of frozen soil. Can. Geotech. J., 37, 811-816.

Heydinger, A. G. (1987). Piles in permafrost. Journal of cold regions engineering, 1(2), 59-75.

Hosseini, M. A., & Rayhani, M. (2017). "Evolution of pile shaft capacity over time in marine soils." Int. J. of Geo-Eng.

Hult, J. A. H. (1966). Creep in engineering structures. Blaisdell Publishing Company, Waltham, MA. 115 p

IPCC in Climate Change. (2013). The Physical Science Basis. Contribution of Working Group I to the Fifth Assessment Report of the Intergovernmental Panel on Climate Change (eds Stocker, T. F. et al.) 1535 (Cambridge Univ. Press, 2013).

Johnson, G. H., and Ladanyi, B. (1972). Field tests of grouted rod anchors in permafrost. Can. Geotech. J., Nat. Res. Counc. Canada, 9(2), 176–194.

Johnson, J. B., & Buska, J. S. (1988). Measurement of frost heave forces on H-piles and pipe piles (No. CRREL-88-21). Cold Reg. Res. Eng. Lab, Hanover, NH.

Johnston, G. H. and Ladanyi, B., (1974) Field tests of deep power-installed screw anchors in permafrost: Canadian Geotechnical Journal, v. 11, No. 3, p. 348-358.

Johnston, G. H., & Ladanyi, B. (1972). Field tests of grouted rod anchors in permafrost. Canadian Geotechnical Journal, 9(2), 176-194.

Jones, S.J. (1982). The confined compressive strength of polycrystalline ice. J. of Glaciology, 28(98), 171-7.

Jorgenson, M. T., Shur, Y. L., & Pullman, E. R. (2006). Abrupt increase in permafrost degradation in Arctic Alaska. Geophysical Research Letters, 33(2).

Kitze, F.F. (1957). “Installation of piles in permafrost.”, Cold Reg. Res. Eng. Lab, Arctic construction and frost effects laboratory, Corps of Engineers, U.S. Army.

Ladanyi (1972) "In Situ Determination of Undrained Stress Strain Behavior of Sensitive Clays with the Pressure meter", Canadian Geotechnical Journal, Vol. 9; No. 3.

Ladanyi, B. (1972). An engineering theory of creep in frozen soils. Can. Geotech. J. 9(1), p. 63-80.

Ladanyi, B. (1995). Civil Engineering concerns of climate change in the Arctic. Transactions of the Royal Society of Canada, VI (VI): 7–19.

Ladanyi, B., & Johnston, G. H. (1974). Behavior of circular footings and plate anchors embedded in permafrost. Canadian Geotechnical Journal, 11(4), 531-553.

Ladanyi, B., & Theriault, A. (1990). A study of some factors affecting the adfreeze bond of piles in permafrost. In Proc. of Geotechnical Engineering Congress GSP (Vol. 27, pp. 213-224).

Ladanyi. B. (1988). Short- and long-term behavior of axially loaded bored piles in permafrost. Proc. of Int. Symp. Deep Found. on Bored and Auger Piles. Ghent. Belgium, 121-131.

Lai, Y., Long, J. and Chang, X. (2009). Yield criterion and elasto-plastic damage constitutive model for frozen sandy soil. Int. J. Plasticity, 25, 1177-1205.

Lawrence, D.M., & Slater, A.G. (2005). A projection of severe near-surface permafrost degradation during the 21st century. Geophysical Research Letters, 32(24).

Lee, M. Y., Fossum, A., Costiin, L. S., Bronowski, D. and Jung, J. (2002). Frozen Soil Material Testing and Constitutive Modeling. Sandia National Laboratories, Albuquerque, NM and Livermore, CA.

Li, D., Fan, J. and Wang, R. (2011). Research on visco-elastic-plastic creep model of artificially frozen soil under high confining pressures. Cold Regions Science and Technology, 65 (2), 219-225.

Linell, K. A., and Johnston, G. H. (1973). Engineering design and construction in permafrost regions: A review (pp. 553-575).

Linell, K. A., and Lobacz, E. F. (1980). Design and construction of foundations in areas of deep seasonal frost and permafrost. Special Report.No. 80-84, ADA 090324. U.S. Army Cold Regions Res. and Engrg. Lab., Hanover, N.H.

Maksimovg, H. (1967). Time of natural freezing around piles driven into permafrost. Osnovaniya Fundamenty I Mekhanika Gruntov, No. 3, pp. 12-14.

Meier, M. F. (1960). Mode of flow of the Saskatchewan Glacier, Alberta, Canada. U.S. Geological Survey, Professional Paper No. 351. 70 p.

Mellor, M., and Smith, J. B. (1967). Creep of snow and ice. In Physics of snow and ice. Edited by H. Oura. Institute of Low Temperature Science, Hokkaido University, Sapporo, Japan, Vol. 1, Part 2, pp. 843-855.

Mellor, M., and Testa, R. (1969a). Effect of temperature on the creep of ice. Journal of Glaciology, 8(52), pp. 131-145.

Mellor, M., and Testa, R. (1969b). Creep of ice under low stress. Journal of Glaciology, 8(52), pp. 147-152.

Meyerhof, G. G., & Fellenius, B. H. (1985). Canadian foundation engineering manual.

Mitsch, M.P. and Clemence, S.P. (1985). The uplift capacity of helix anchors in sand. Uplift capacity of anchor foundations in soil, ASCE, pp. 26-47.

Morgenstern, N. R., Roggensack, W. D., & Weaver, J. S. (1980). The behavior of friction piles in ice and ice-rich soils. Canadian Geotechnical Journal, 17(3), 405-415.

Moza, K. K., Katti, R. K., & Katti, D. R. (1987). Active pressure studies in saturated expansive soil. *In Proceedings of the Eighth Asian Regional Conference on Soil Mechanics and Foundation Engineering*, Kyoto, Japan (pp. 189-192).

Narasimha Rao, S., Prasad, Y.V.S.N., and Veeresh, C. (1993). Behavior of embedded model screw anchors in soft clays. Geotechnique, 43:605-614.

Nelson, J.D., Chao, K.C., Overton, D.D. and Nelson. E.J. (2o15). Soil treatment and moisture control

Ning, J. and Zhu, Z. (2007). Constitutive model of frozen soil with damage and numerical simulation of the coupled problem. Chinese Journal of Theoretical and Applied Mechanics, 39(1), 70-76.

Niu, Y., Miao, T., Zhang, C. and Zhang, J. (1998). Damage model of frozen soil under multiaxial state stress. Proc. of 7th International Conference on Permafrost, 811-814

Nixon, J. F. (1978). "Foundation design approaches in permafrost areas." Can. Geotech. J., 15(1), 96-112.

Nixon, J. F. (1988). "Pile load tests in saline permafrost at Clyde River, Northwest Territories." Can. Geotech. J., 25(1), 24-32.

Nixon, J. F., & McRoberts, E. C. (1976). A design approach for pile foundations in permafrost. Canadian Geotechnical Journal, 13(1), 40-57.

Nixon, J.F. (1978). Design approaches for foundations in permafrost areas. Canadian Geotechnical Journal, 15: 96-112.

Nixon, J.F. (1990a). Effect of climate warming on pile creep in permafrost. Journal of Cold Regions Engineering, 4(1): 67–73.

Nottingham, D. and Christopherson, A. B. (1983). “Driven piles in permafrost: state of the art.” Proceedings of the Fourth International Conference on Permafrost, Fairbanks, Alaska, 928–933.

Odquist, F. K. G. (1966). Mathematical theory of creep and creep rupture. Oxford Mathematical Monograph, Claren-' don Press, Oxford, England. 168 p.

Ofer, Z. (1981). Laboratory instrument for measuring lateral soil pressure and swelling pressure. *Geotechnical Testing Journal*, Vol.4, No.4, pp: 177-182.

Paikowsky, S.G. (2004). Load and resistance factor design (LRFD) for deep foundations (No. 507). Transportation Research Board.

Parameswaran, V. R. (1978). Adfreeze strength of frozen sand to model piles. Canadian geotechnical journal, 15(4), 494-500.

Parameswaran, V.R. (1979). Creep of model piles in frozen soil. Can. Geotech. J., Nat. Res. Counc. Canada, 16(1), 69–77.

Parameswaran, V.R. (1981). Adfreeze strength of model piles in ice. Can. Geotech. J., Nat. Res. Counc. Canada, 18(1), 8–16.

Parameswaran, V.R. (1982). Displacement of piles under dynamic loads in frozen soils (pp. 555-559). National Research Council Canada, Division of Building Research.

Parameswaran, VR (1987). "Adfreezing strength of ice to model piles." Can. Geotech. J., 24 (3), 446-452.

Paterson, W.S.B., and Savage, J.C. (1963). Measurements of the Athabasca Glacier relating to the flow law of ice. Journal of Geophysical Research, 68(15), pp. 4537-4543.

Penner, E. (1970). Frost heaving forces in Leda clay, Canadian Geotechnical Journal, 7(1), 8-16.

Penner, E. (1974). Uplift forces on foundations in frost heaving soils, Canadian Geotechnical Journal, 11, 323-338.

Penner, E. and Gold, L.W. (1971). Transfer of heaving forces by adfreezing to columns and foundation walls in frost susceptible soils, Canadian Geotechnical Journal, 8, 514-526.

Penner, E. and Irwin, W.W. (1969). Adfeezing of Leda clay to anchored footing columns, Canadian Geotechnical Journal, 6(3), 327-337.

Phukan, A. (1980). Design of deep foundations in discontinuous permafrost, ASCE Convention and Exposition, Portland, Oreg., 80–122, 1–21.

Phukan, A. (1985). Frozen Ground Engineering, Prentice-Hall, Inc., Englewood Cliffs, N.J. 07632.

Puppala, A. J., & Cerato, A. (2009). Heave distress problems in chemically-treated sulfate-laden materials. *Geo-Strata—Geo Institute of ASCE*, 10(2), 28.

Richards, B. G., & Kurzeme, M. (1973). Observations of Earth Pressures on a Retaining Wall at the Gouger Street Mail Exchange, *Adelaide* (No. Res Paper No. 220).

Rufiar, M., Mendoza, M. J., and Ibarra, E. (2011). Axial load capacity for an instrumented pile model: a review of alpha and beta methods. In Proceedings, Pan American CGS geotechnical conference, Toronto, Canada.

Saba, S., Barnichon, J. D., Cui, Y. J., Tang, A. M., & Delage, P. (2014). Microstructure and anisotropic swelling behavior of compacted bentonite/sand mixture. *Journal of Rock Mechanics* and Geotechnical Engineering, 6(2), 126-132.

Schreve, R.L. and Sharp, R.P. (1970). Internal Deformation and Thermal Anomalies in Lower Blue Glacier, Mount Olympus, Washington, D.C. Journal of Glaciology, 9(55), p. 65-86.

Sego, D. C., and L. B. Smith. (1989). Effect of backfill properties and surface treatment on the capacity of adfreeze pipe piles. Canadian Geotechnical Journal 26.4: 718-725.

Smith, E. A., McCarter, J. eds. (1997). Contested Arctic: Indigenous Peoples, Industrial States, and the Circumpolar Environment. University of Washington Press, Seattle, US.

Smith, S. L., A. G. Lewkowicz, C. Duchesne, and M. Ednie. (2015). Variability and change in permafrost thermal state in northern Canada. Paper 237. In GeoQuébec 2015 (Proceedings 68th Canadian Geotechnical Conference and 7th Canadian Conference on Permafrost). Québec. GeoQuébec 2015 Organizing Committee.

Smith, S. L., J. Chartrand, C. Duchesne, and M. Ednie. (2016). Report on 2015 field activities and collection of ground thermal and active layer data in the Mackenzie Corridor, Northwest Territories, Geological Survey of Canada Open File 8125.Tappenden, K. M., & Sego, D. C. (2007). Predicting the axial capacity of screw piles installed in Canadian soils. In the Canadian Geotechnical Society (CGS), OttawaGeo2007 Conference (pp. 1608-1615).Starr, J.L., and Paltineanu I.C. (2002). Methods for Measurement of Soil Water Content: Capacitance Devices. p. 463-474. In J.H.Dane, and G.C.Topp (ed.) Methods of Soil Analysis: Part 4 Physical Methods. Soil Science Society of America, Inc., Soil Science Society of America, Inc.

Sudhindra, C., & Moza, K. K. (1987). An approach for lateral pressure assessment in expansive soils. *In Proceedings. 6th intonational conference of expansive soils* (Vol. 1, pp. 67-70).

Tappenden, K. M., & Sego, D. C. (2007). Predicting the axial capacity of screw piles installed in Canadian soils. In Proceedings of the Canadian Geotechnical Society (CGS) Conference, OttawaGeo (pp. 1608-1615).

Thomas, H. P., & Luscher, V. (1980). Improvement of bearing capacity of pipe piles by corrugations. In Collection of Papers from a US Soviet Joint Seminar, Leningrad, USSR (pp. 229-234).

Thomas, R.H. (1971). Flow law for Antarctic ice shelves. Nature (London), Physical Science, 232, pp. 85-87. 1973a. The creep of ice shelves: theory. Journal of Glaciology, 12(64), pp. 45-53.

Thomas, R.H. (1973b). The creep of ice shelves: interpretation of observed behavior. Journal of Glaciology, 12(64), pp. 55- 70.

Ting, J. M., and Martin, R. T. (1979). Application of the Andrade equation to creep data for ice and frozen soil. Cold Regions Science and Technology, 1, pp. 29-36.

Ting, J.M. (1981). The creep of frozen sands: qualitative and 279 quantitative models - Final report II. U.S. Army Research Office, Res. Rep. N. R81-5.

U.S. Army/Air Force. (1967). Arctic and Subarctic Construction: Structure Conditions. Tech. Manual TM5-852-4/ AFM 88-19, chap. 4.

US Army Engineer School. (1985). Pile construction (FM 5-134). Field manual Head Quarters

Vialov, S. S. (1959). Rheological properties and bearing capacity of frozen soils, Transl. 74, US. Army CRREL, Hanover, N.H. 1965.

Vialovs, S. (1965). The strength and creep of frozen soils and calculations for ice-soil retaining structures. United States Army, Corps of Engineers, Cold Regions Research and Engineering Laboratory, Hanover, NH, Translation 76: 302.

Viggiani, G., Ando`, E., Takano, D., Santamarina, J., (2015). “Laboratory X-ray tomography: a valuable experimental tool for revealing processes in soils. Geotech. Test. J. 38 (1), 61−71.Voitkovskii, K.F. (1960). Mekhanicheskive svoystva Ida. (The mechanical properties of ice.) Moscow, Izd. AkademiiNauk. (English translation Air Force Cambridge Research Laboratories, Bedford, MA, AFCRL-62-838, AMS-T-R- #391.) 92 p.

Wang, J., Nishimura, S., & Tokoro, T. (2017). “Laboratory study and interpretation of mechanical behavior of frozen clay through state concept”. Soils Found., 57(2), 194-210.

Weaver, J. S., and Morgenstern, N. R. (1981). Pile design in permafrost. Canadian geotechnical journal, 18(3), 357-370.

Williams, P. J. (1986). Pipelines and permafrost: science in a cold climate (Vol. 10). McGill-Queen's Press-MQUP.

Williams, P. J., & Smith, M. W. (1991). The frozen earth: Fundamentals of geocryology. Cambridge, U.K.

Zhang, D. (1999). Predicting capacity of helical screw piles in Alberta soils. M.Sc. thesis, Department of Civil and Environmental Engineering, University of Alberta, Edmonton, Alberta.

Zhang, Y., and Michalowski, R. L. (2014). Thermal-Hydro-Mechanical Modeling of Frost Action in Frost-Susceptible Soils. In Soil Behavior and Geomechanics (pp. 735-744).

Zhu, Y. Zhang, J. Peng, W. Sheng, Z. and Miao, L. (1992). Constitutive relations of frozen soil in uniaxial compression. Journal of Glaciology and Geocryology, 14(3), 210-217.